March 2020

MODULATING NANOPARTICLE-PROTEIN INTERACTIONS THROUGH COVALENT OR NONCOVALENT APPROACH FOR BIOMEDICAL APPLICATIONS

Jingjing Gao

MODULATING NANOPARTICLE-PROTEIN INTERACTIONS THROUGH COVALENT OR NONCOVALENT APPROACH FOR BIOMEDICAL APPLICATIONS

A Dissertation Presented

by

JINGJING GAO

Submitted to the Graduate School of the
University of Massachusetts Amherst
In partial fulfillment of the requirements for the degree of

DOCTOR OF PHILOSOPHY

February 2020

Department of Chemistry

MODULATING NANOPARTICLE-PROTEIN INTERACTIONS THROUGH COVALENT OR NONCOVALENT APPROACH FOR BIOMEDICAL APPLICATIONS

A Dissertation Presented

by

JINGJING GAO

Approved as to style and content by:

_____
Sankaran Thayumanavan, Chair

_____
Richard Vachet, Member

_____
Min Chen, Member

_____
E. Bryan Coughlin, Member

_____
Ricardo Metz, Department Head
Department of Chemistry

DEDICATION

To my family

ACKNOWLEDGMENTS

I want to give sincere thanks to those who made this thesis possible.

First of all, I would like to thank my advisor Prof. Sankaran Thayumanavan for his immense support and guidance throughout the past five years. I enjoyed his style of managing the lab and his students. I learned a lot from him as a passionate scientist, a hard worker, a PI and a teacher. I really appreciate his efforts of training me to be a critical thinker, to solve a scientific problem, to present my science to broad audiences and to plan and prepare for my career. I feel very privileged to have him as my PI.

I would like to thank our group assistant Karen Hakala for going out of the way to help, support all of us and the selfless love she bestows upon all the Thai group members. She is so sweet and cares about us like a mother.

I would also like to thank my committee members, Prof. Richard Vachet, Prof. Min Chen and Prof. Bryan Coughlin, for their valuable inputs provided, especially during the prospectus, original research proposal and data defense. I want to thank them for their professional and prompt responses every time I reach out.

I am very grateful to my mentors, Dr. Jiaming Zhuang and Dr. Bo Zhao, for training me scientifically during my initial years and very useful discussions throughout the past five years. A special thank you to Dr. Meizhe Wang and Dr. Hui Wang for also mentoring me, providing constructive criticism and helpful inputs for my research.

I would like to express my gratitude to all my collaborators and colleagues, Jiaming Zhuang, Bo Zhao, Hui Wang, Meizhe Wang, Xiaochi Liu, Mahalia A. C. Serrano, Kingshuk Dutta, Peidong Wu, Ann Fernandez, Stephanie Le and Uyen (Jenny) Huynh. Their support,

constructive suggestions and valuable inputs have been a strong push for the research projects to be finished.

Thanks to the past and present members of the Sensing Subgroup, especially for their inputs during sub-group meetings. A big thank you to the UMass Chemistry staff Dennis Glick, J.M. Stowe, Kristina Knight, Robert Sabola and Ryan Feyrer for their support and assistance.

I would also like to thank Vikash Kumar, Wardah Ejaz, Piyachai Khomein, Manisha, Ann Fernandez, Priyaa Prysad, Kingshuk Dutta, Emil Samson, Peidong Wu, Bin Liu, Huan He, Hongxu Liu, Ruiling Wu, Ran Duan, Rui Huang, Qikun Yu and Miaowei Xu. They have brought incredible fun and joy and grad school wouldn't have been what it was without them.

I would like to thank my dearest friends Xiaoqiong Cao, Meizhe Wang, Chendi Niu, Chengfeng Ren who have stood by me as always, loved me the way I am. For the unconditional support and encouragement whenever I feel down and get confused.

None of this would have been possible without the love, support and encouragement from my family. You are my safe harbor when I sail away. You all are my motivation to work hard to chase my dream and never give up. I love you, each of you, as always.

ABSTRACT

MODULATING NANOPARTICLE-PROTEIN INTERACTIONS THROUGH COVALENT OR NONCOVALENT APPROACH FOR BIOMEDICAL APPLICATIONS

FEBRUARY 2020

JINGJING GAO

B.A., SOUTH CENTRAL UNIVERSITY FOR NATIONALITIES

M.A., SHANGHAI JIAO TONG UNIVERSITY

Ph.D., UNIVERSITY OF MASSACHUSETTS AMHERST

Directed by: Professor Sankaran Thayumanavan

Discoveries at the interface of chemistry, biology, and materials science has emerged as a powerful route to impact life science in this century. My research in the Thayumanavan group is focused on problems at this interface. A common theme of all the six projects is the use of modern synthetic organic chemistry to build interesting, novel macromolecules which are chemically rich, to study the molecular self-assembly behavior in solution and then translate to solve problems in biomedical area. By addressing the design challenge to prepare novel amphiphiles with desired functional groups, controlled molecular weight and the ability to respond to a broad range of stimuli, especially protein and enzyme, we have achieved the following aims that showed great potential for biomedical applications such as sensing, imaging and drug delivery: a) we have systematically studied the molecular weight effects and hydrophilic-hydrophobic balance effects on enzyme induced supramolecular disassembly, which could provide tunability over covalent and non-covalent guest molecules release kinetics. b) Other than single stimuli-responsive system, we outlined a simple and new strategy was outlined for amphiphilic nanoassemblies to

respond to a combination of intrinsic trigger protein and extrinsic trigger light in the logic gated fashion. c) Considering biomedical applications based on these nanoassemblies, we then try to solve the most critical step for nanomedicine, which is specific targeting. Unlike common strategies relying on complementary ligands, we showed a cellular AND gate for highly selective cell accumulation by covalently masking and unmasking ligands on block copolymer based nanogels, such an ability will facilitate tumor imaging and diagnostics; d) We then showed a self-immolative nanogel platform to deliver hydrophobic drugs, with accessible functional group present on the surface, this nanogel can be easily functionalized with various receptors for targeted delivery into cytosol and subcellular organelles; e) We designed a novel supramolecular approach that selectively transports water-soluble globular proteins from an aqueous phase to the water-pool of a reverse micelle in an apolar organic phase. Proteins can maintain functions after crossing an incompatible solvent interface, which opens new possibilities for application of supramolecular assemblies in sensing, diagnostics and catalysis. f) following these findings, we designed an enzyme nanoreactor for catalysis in apolar solvent and introduce crosslinks in the molecular assemblies, we will further try to control substrate permeability into the assembly to engineer unnatural selectivity in enzymes.

TABLE OF CONTENTS

Page

LIST OF TABLES

Page

LIST OF FIGURES

Page

LIST OF SCHEMES

Page

CHAPTER 1

INTRODUCTION

1.1 Supramolecular assembly

Amphiphilic molecules, ranging from small molecule surfactants, oligomers, dendrimers to higher molecular weight polymers, could aggregate in a self-organized fashion.[1-5] The self-assembled aggregates maintain an equilibrium with respecting monomers, could generate various morphologies such as micelles, vesicles, fibers and helical shape based on the molecule packing parameters (Figure 1.1).

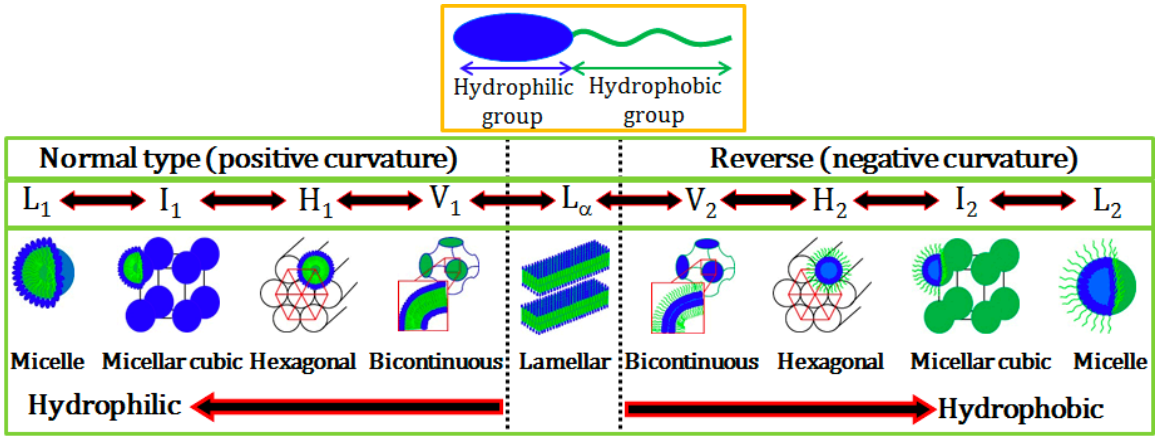

Figure 1.1 Self-assembled structures from amphiphilic molecules. Reproduced from ref. 3

The self-assembly process is usually driven by non-covalent interactions such as van der waals forces, pi-pi interactions, hydrogen-bonding, electrostatic interactions and hydrophobic effects.[6-7] These reversible interactions make self-assembly a dynamic process in response to environment cues. But amphiphiles must reach a certain concentration to form assemblies, which is called its critical aggregation concentration (CAC). Small molecular weight surfactants usually possess a relative high CAC value compare with higher molecular weight amphiphiles, due to its fast exchange with

corresponding aggregates. Surfactants have been often used as detergents, emulsifiers, foaming and anti-foaming agents. Self-assembled structures from higher molecular weight amphiphiles ten to be more thermodynamically stable, which could find interesting applications in a variety of areas such as sensing, drug delivery and diagnostics. Since amphiphilic molecules contain two distinctly different components: hydrophilic moiety and hydrophobic moiety, when they assemble in aqueous phase, the hydrophilic functional groups would present on the surface of the assemblies to form the primary interface with the solvent. Variations of the functional groups that would further induce changes in hydrophobic-hydrophilic balance of the assemblies could provide a lot of interesting applications. This thesis here will introduce different type of assemblies formed by dendrimers, oligomers and also polymers and potential applications.

1.2 Protein responsive supramolecular assemblies

Stimuli-responsive systems, which could respond to a certain environment stimulus, have raised particular interest in the past few decades because they can easily find use in a very broad range of applications.[8-10] For example, one could design supramolecular assemblies that is sensitive to pH change and yield a response in the form of guest molecule release. Various types of stimuli have been used as a trigger to induce the response of assemblies (Figure 1.2). In the context of biology, the triggers can be classified into two categories: extrinsic stimuli and intrinsic stimuli. Extrinsic stimuli include light, magnetic field, ultrasound, electric field and mechanical forces; intrinsic stimuli include pH, redox, temperature, nucleic acids, sugars, enzyme and protein. Current studies have reported a lot of advances in secondary imbalances such as pH, redox and temperature, however those are just secondary imbalances in biology. In the prospective of biomedicine, we are more

interested in developing protein or enzyme sensitive assemblies, because most of the pathological imbalances are directly caused by aberrant protein activity.

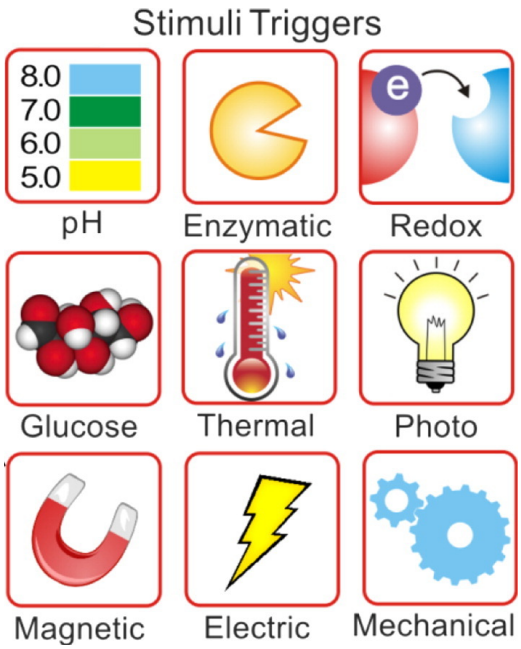

Figure 1.2 Various types of stimuli triggers. Reproduced from ref. 11. Copyright © 2014 Elsevier B.V. All rights reserved.

First, we targeted assemblies that are capable of responding to enzyme. Past few decades have witnessed considerable progress in the field of enzyme-responsive assemblies.[12-17] Typically these assemblies possess enzyme-reactive moieties in the form of labile linkages among the main or side chains of the molecular scaffold. Therefore, enzyme-catalyzed reactions induced chemical structural changes of the synthetic molecules could further lead to morphological transitions of these assemblies. We have shown several dendrimer amphiphiles that could undergo enzyme-induced disassembly by installing enzyme-responsive units onto the hydrophobic core of the micelle-like assemblies [15], we envisaged that the equilibrium between the unimeric state and the aggregate state must be involved in this process (Figure 1.3). We have been interested in investigating how the reaction kinetics and the ensuing change in the host-guest characteristics would be affected by

tuning unimer-aggregate equilibrium to alter the assemblies' accessibility to the enzyme. Moreover, we were interested in identifying as to how structural changes in host assemblies, induced by an enzyme, would affect rate of disassembly and kinetics of guest molecule release.

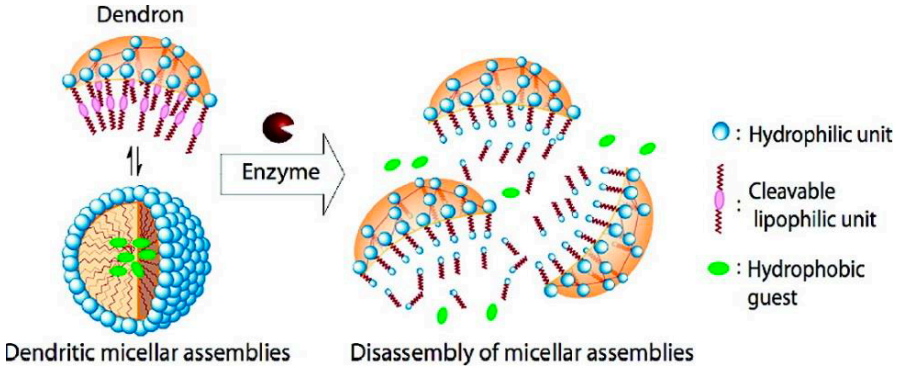

Figure 1.3 Schematic representation of enzyme-induced disassembly of dendritic micelles

While the enzyme-sensitive disassembly is dictated by a covalent and irreversible modification of the assemblies, supramolecular disassembly based on noncovalent interactions is also of great interest and a challenge, since a lot of disease-relevant proteins do not have known enzymatic activity. We envisaged that non-covalent binding between a ligand and protein could be utilized to develop a non-enzymatic protein responsive assembly. We designed a ligand-bearing amphiphilic dendron that formed stable assemblies but disassembled upon binding the target protein (Figure 5).[18] We hypothesized that the HLB of an assembly was significantly different from that of the protein−assembly complex, because the protein was rather large in molecular weight and was much more hydrophilic compared to the amphiphile. We actually found that ligand bearing assemblies were disrupted only by a target protein but not by other non-complementary proteins, indicated by the size decrease and guest molecule release.

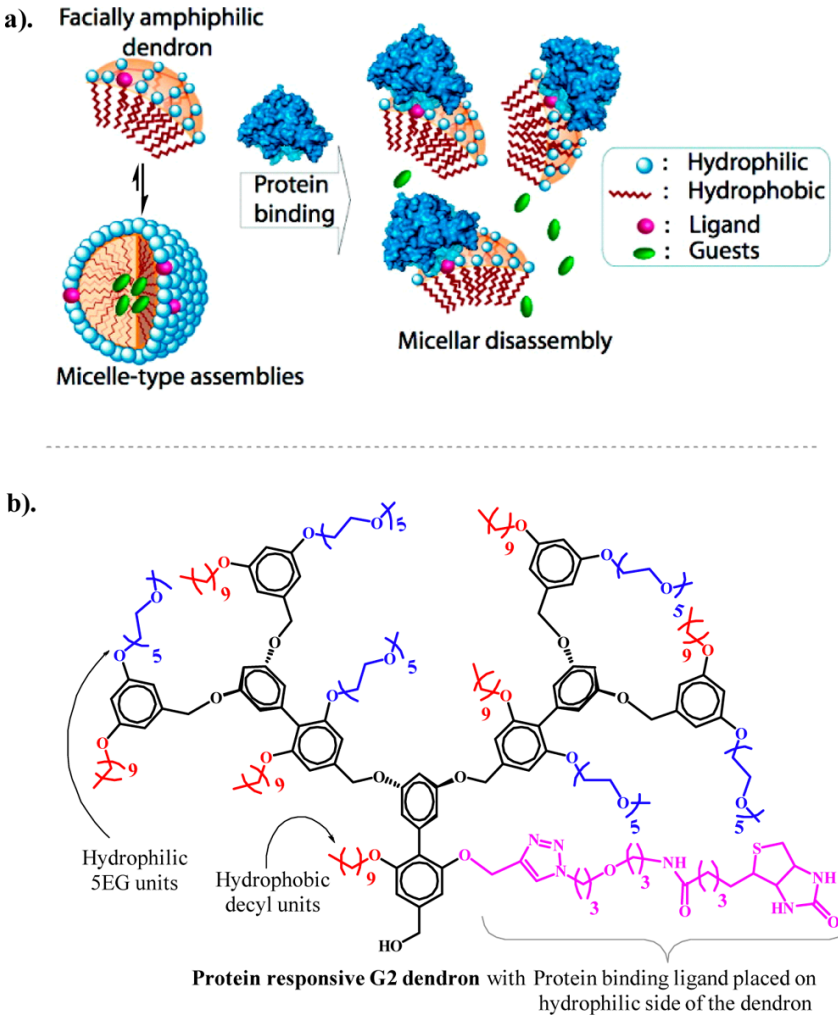

Figure 1.4 (a) Illustration of protein-induced disassembly; protein binds to the ligand present on the dendron's hydrophilic face, leading to the formation of an overall hydrophilic protein−dendron complex and micelle disassembly. (b) Structure of G2 dendron with enzyme responsive functional group

1.3 AND gated supramolecular disassembly

In addition to assemblies that can be triggered by a single stimulus, recent interests have been attracted by multiple stimuli-responsive systems, because they can provide enhanced selectivity in stimuli-responsiveness, which is critical in targeted delivery.[10] In engineering the combinations of these two triggers, we were inspired by the molecular logic gates proposed and studied over past couple of decades.[19-23] While there have been many reports on molecular logic gates involving small molecules, such gated strategies in nanoscale

assemblies are relatively limited, especially the 'AND gate'. We have introduced a dual protein stimuli-responsive AND gate design to amphiphilic dendrimers, where the system only responded to the concurrent presence of two different proteins (Figure 1.5).[24] A dendron molecule was designed containing an enzyme sensitive coumarin ester as the hydrophobic moiety and a protein-specific 2,4-DNP ligand as part of the hydrophilic PEG moiety. The release of the fluorescent umbelliferone from the coumarin ester cleavage due to the dual protein triggers was indeed found to be 26 times faster than that due to the enzyme alone.

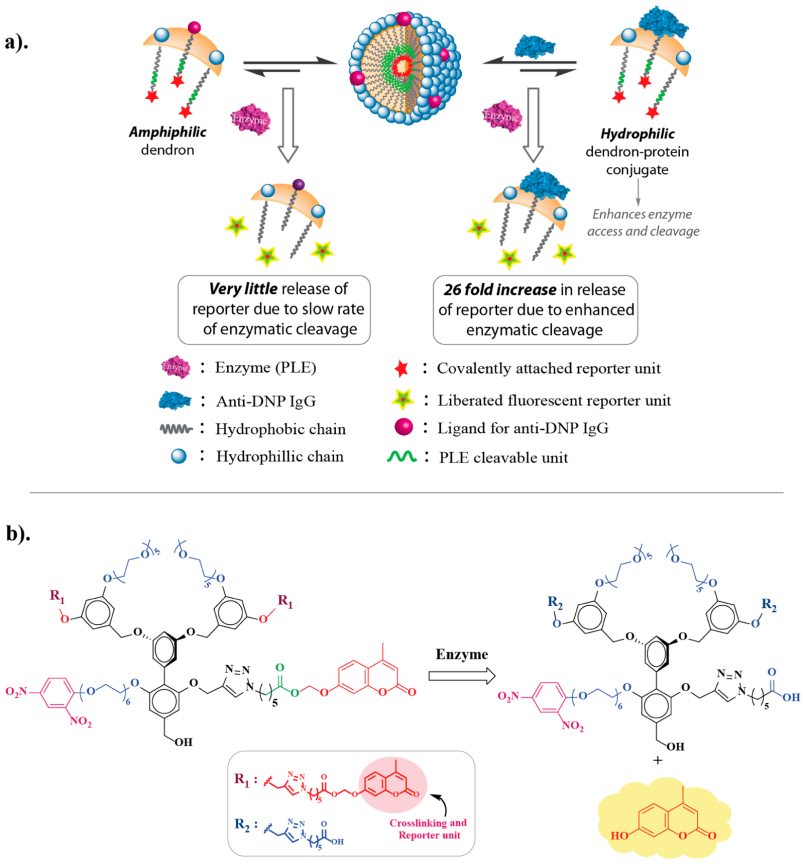

Figure 1.5 (a) Illustration of dual responsive system. (b) Enzyme induced change in the amphiphilic dendron accompanied by fluorophore release.[24]

1.4 Stimuli-responsive assemblies for targeting and drug delivery

Traditional routes of drug administration include systemic delivery, oral delivery and local injection, none of these methods are satisfying because they usually generate side effects due to drug degradation during circulation, undergo harsh environment and cause damage to surrounding tissues. To overcome these shortcomings, drug delivery system that can deliver the required dose of drugs to the specific disease site come into the stage. Our group has outlined the figure of merits for an ideal drug delivery system [25]: (a) it has to be nontoxic to human body; (b) it should be able to provide stable guest molecule encapsulation; (c) the delivery system could respond to certain stimuli so that the drug molecules can be released in presence of the trigger; (d) the carrier should be able to selectively accumulate at the disease site through either passive targeting or active targeting.

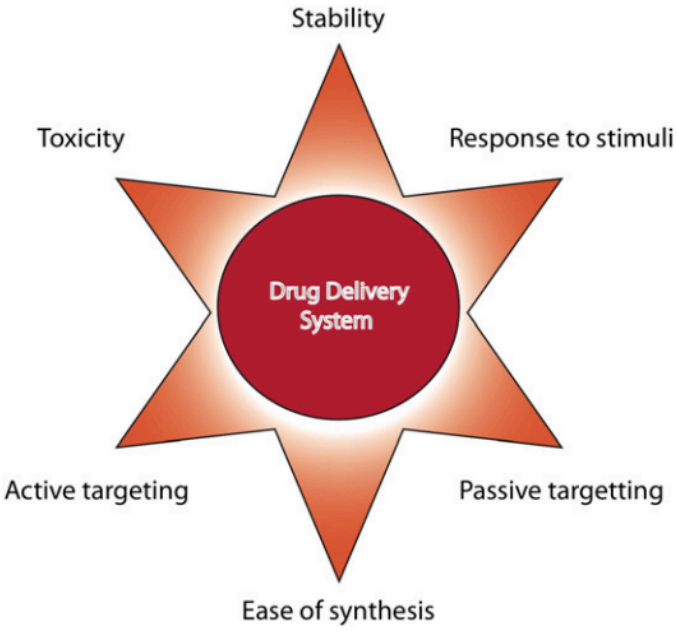

Figure 1.6 Figure of merits for an ideal drug delivery vehicle.[25]

Among these features, targeting specific disease cells is critical for a drug delivery system to be applicable in-vivo. It has been suggested that drug carriers with a size range of 10-200 nm may exhibit preferential accumulation in the context of tumors, mainly due to the extravasation of drug carriers into solid tumor tissues and prevent lymphatic drainage, the so-called enhanced permeation and retention (EPR) effect.[26-27] Drug carrier relying on this passive targeting has been clinically used and showed tumor accumulation, reduced clearance and reduced cardiotoxicity.[28-29]

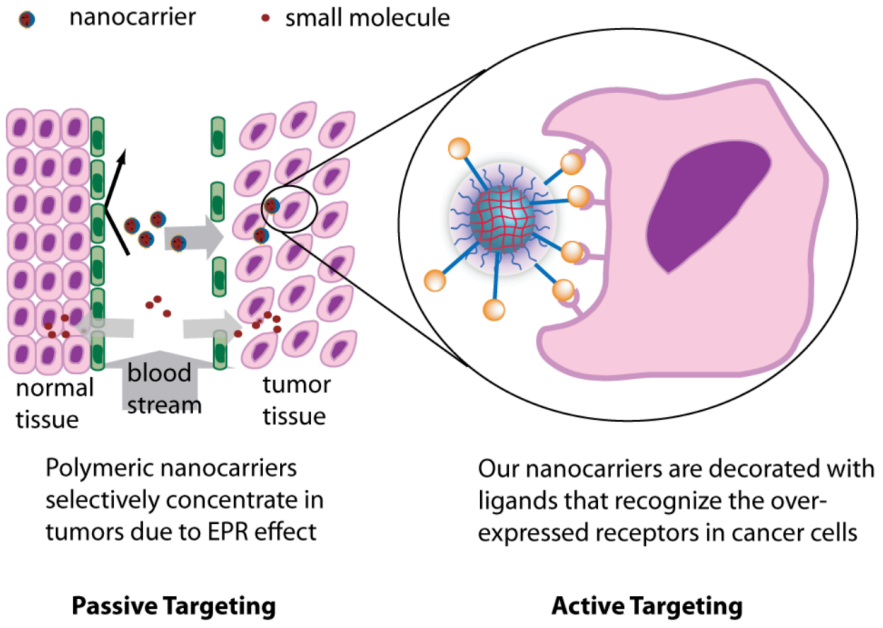

Figure 1.7 Cartoon representation of passive and active targeting mechanisms

On the contrary of passive targeting, active targeting rely on the specific binding to the cancer cell surfaces. By incorporation of specific ligands to the nanocarriers that are complementary to receptors overexpressed on tumor cell surface, these nanocarriers promises to target cancer cells more effectively than EPR effect alone. Cellular targets usually used in the active targeting strategy involve the targeting of cancer cells and tumour endothelium receptors including transferrin, folate, epidermal growth factor receptor,

vascular endothelial growth factor, αvβ3 integrins and the Vascular Cell Adhesion Molecule-1 (VCAM-1) or matrix metalloproteinases (MMP's).

The amphiphiles formed nanoassemblies we have introduced hold great potential for targeting and drug delivery because their container properties. Drugs could be non-covalently encapsulated by the nanoassembly and be protected from harsh environment. By installing stimuli-responsive functional groups, the drug molecules could be released in a controlled fashion. We have reported a nanogel system which contain a crosslinkable core and hydrophilic shell, which provide stable encapsulation of hydrophobic drug molecules.[30-31] The disulfide crosslink could lock the drug molecules and then release them at intracellular GSH concentration. Post-modification through disulfide exchange enable ligands decoration so the nanogels could be armed with active targeting capabilities.

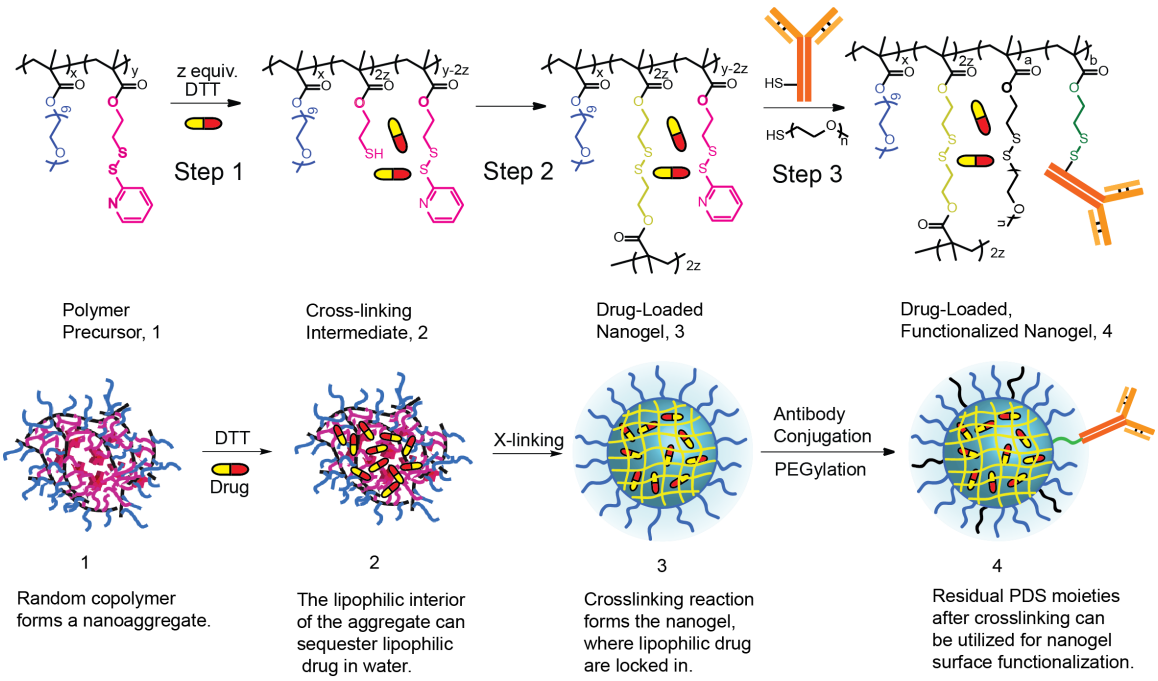

Figure 1.8 Nanogel design and preparation for target delivery.[30-31]

1.5 Thesis overview

This thesis will focus on design and synthesis of amphiphilic assemblies that hold great potential in areas such as sensing, cell targeting and drug delivery. In Chapter 2, we outlined a simple and new strategy to design amphiphilic nanoassemblies that could respond to a combination of intrinsic trigger protein and extrinsic trigger light in an logic gated (AND, OR, NOT) strategy, supramolecular disassembly and guest molecule release could then be achieved in a controlled fashion.

Chapter 3, we have systematically studied the molecular weight effects and hydrophilic-hydrophobic balance effects on enzyme induced supramolecular disassembly, which provide insights into the molecular design of enzyme-responsive systems.

Chapter 4, we have designed a self-immolative nanogel platform for hydrophobic drugs delivery, with accessible functional group present on the surface, this nanogel can be easily functionalized with various receptors for targeted delivery.

Chapter 5, we showed a novel approach for highly selective cell accumulation was designed by covalently masking and unmasking ligands on block copolymer based nanogels, such an ability will facilitate tumor imaging.

Chapter 6, we designed a novel supramolecular approach that selectively transports water-soluble globular proteins from an aqueous phase to the water-pool of a reverse micelle in an apolar organic phase. Proteins can maintain functions after crossing an incompatible solvent interface, which opens new possibilities for application of supramolecular assemblies in sensing, diagnostics and catalysis.

Chapter 6 showed the design of an enzyme nanoreactor for catalysis in apolar solvent and how to introduce crosslinks in the molecular assemblies, we will further try to control substrate permeability into the assembly to engineer unnatural selectivity in enzymes.

1.6 References

1. Evans, D. F.; Wennerstrom, H. The Colloidal Domain, 2nd ed.; *Wiley-VCH: New York*, **1999**.
2. Imamura, T. and Fukushima, K. *Coordination Chemistry Reviews*, **2000**, 198, pp.133-156.
3. Hill, J.P.; Shrestha, L.K.; Ishihara, S.; Ji, Q.; Ariga, K. *Molecules* **2014**, *19*, 8589-8609.
4. Raghupathi KR, Guo J, Munkhbat O, Rangadurai P, Thayumanavan S. *Acc Chem Res.* **2014**, 47, 2200–2211.
5. Ikkala, O., & ten Brinke, G. *Science*, **2002**, 295, 2407-2409.
6. Webber, M. J.; Appel, E. A.; Meijer, E. W.; Langer, R. *Nat. Mater.* **2015**, 15 (1), 13–26.
7. Stupp, S. I.; Palmer, L. C. *Chem. Mater.* **2014**, 26 (1), 507–518.
8. Theato, P., Sumerlin, B.S., O'Reilly, R.K. and Epps III, T.H., *Chem. Soc. Rev,* **2013**, 42(17), 7055-7056.
9. Blum, A. P.; Kammeyer, J. K.; Rush, A. M.; Callmann, C. E.; Hahn, M. E.; Gianneschi, N. C. *J. Am. Chem. Soc.* **2015**, 137(6), 2140-54.
10. Zhuang, J.; Gordon, M. R.; Ventura, J.; Li, L.; Thayumanavan, S. *Chem. Soc. Rev.* **2013**, 42 (17), 7421–7435.
11. Lu, Y., Sun, W. and Gu, Z., *J. Control. Release*, **2014**. 194, 1-19.
12. Feng, Z.; Han, X.; Wang, H.; Tang, T.; Xu, B. *Chem* **2019**, *5* (9), 2442–2449.
13. Zelzer, M.; Todd, S. J.; Hirst, A. R.; McDonald, T. O.; Ulijn, R. V. *Biomater. Sci.* **2013**, *1* (1), 11–39.

14. Harnoy, A. J.; Rosenbaum, I.; Tirosh, E.; Ebenstein, Y.; Shaharabani, R.; Beck, R.; Amir, R. J. *J. Am. Chem. Soc.* **2014**, *136* (21), 7531–7534.

15. Azagarsamy, M. A.; Sokkalingam, P.; Thayumanavan, S. *J. Am. Chem. Soc.* **2009**, *131* (40), 14184–14185.

16. Callmann, C. E.; Barback, C. V.; Thompson, M. P.; Hall, D. J.; Mattrey, R. F.; Gianneschi, N. C. *Adv. Mater.* **2015**, *27* (31), 4611–4615.

17. Li, Y.; Liu, G.; Wang, X.; Hu, J.; Liu, S. *Angew. Chemie Int. Ed.* **2016**, *55* (5), 1760–1764.

18. Azagarsamy, M. a.; Yesilyurt, V.; Thayumanavan, S. *J. Am. Chem. Soc.* **2010**, *132* (13), 4550–4551.

19. Andréasson, J.; Pischel, U. *Chem. Soc. Rev.* **2015**, *44* (5), 1053–1069.

20. De Silva, A. P.; Uchiyama, S. *Nat.Nanotech.* **2007**, 399–410.

21. Erbas-Cakmak, S.; Akkaya, E. U. *Angew. Chemie Int. Ed.* **2013**, *52* (43), 11364–11368.

22. Katz, E.; Privman, V. *Chem. Soc. Rev.* **2010**, 1835–1857.

23. Ikeda, M.; Tanida, T.; Yoshii, T.; Kurotani, K.; Onogi, S.; Urayama, K.; Hamachi, I. *Nat. Chem.* **2014**, *6* (6), 511–518.

24. Guo, J.; Zhuang, J.; Wang, F.; Raghupathi, K. R.;Thayumanavan, S. *J. Am. Chem. Soc*. **2014**, 136, 2220−2223.

25. Chacko, R.T. et al. *Adv. Drug. Deliv. Rev.,* **2012**, 64(9), 836-851

26. H. Maeda, J. Wu, T. Sawa, Y. Matsumura and K. Hori, *J. Controlled Release*, **2000,** 65, 271–284.

27. A. K. Iyer, G. Khaled, J. Fang and H. Maeda, *Drug Discovery Today*, **2006**, 11, 812–818.

28. A. Gabizon, R. Catane, B. Uziely, B. Kaufman, T. Safra, R. Cohen, F. Martin, A. Huang and Y. Barenholz, *Cancer Res.,* **1994**, 54, 987–992.

29. A. Gabizon, H. Shmeeda and Y. Barenholz, Clin. Pharmacokinet., **2003**, 42, 419–436

30. Ryu, J.-H.; Chacko, R. T.; Jiwpanich, S.; Bickerton, S.; Babu, R. P.; Thayumanavan, S. *J. Am. Chem. Soc.* **2010**, *132,* 17727-17235.

31. Ryu, J.-H.; Jiwpanich, S.; Chacko, R.; Bickerton, S.; Thayumanavan, S. Surface- *J. Am. Chem. Soc.* **2010**, *132* (24), 8246–8247.

CHAPTER 2

PHOTOACTIVATION OF LIGANDS FOR EXTRINSICALLY AND INTRINSICALLY TRIGGERED DISASSEMBLY OF AMPHIPHILIC NANOASSEMBLIES

Adapted with permission from Gao, J.; Liu, X.; Secinti, H.; Jiang, Z.; Munkhbat, O.; Xu, Y.; Guo, X.; Thayumanavan, S. Photoactivation of Ligands for Extrinsically and Intrinsically Triggered Disassembly of Amphiphilic Nanoassemblies. *Chem. Eur. J.* **2018**, 24, 1789-1794.

2.1 Introduction

Supramolecular nanoassemblies that predictably respond to an environmental change have been of interest due to their implications in areas that range from material science to biomedicine [1-5]. When designing molecular assemblies that have the potential to impact biomedicine, the input triggers can be classified into two main categories: extrinsic and intrinsic inputs.[6-10] Extrinsic triggers have the advantage of offering external spatiotemporal control over the change in the properties of a molecular assembly, e.g. shining light at a specific location and time to disrupt a supramolecular assembly. [11-22] On the other hand, intrinsic triggers are directly correlated with an aberrant biological condition and therefore have the opportunity to be selective, e.g. lower pH at the extracellular space of disease tissues.[23-27] Although both these systems present complementary advantages, the specificity offered by either of these systems by itself is insufficient. Therefore, a viable strategy would involve systems that would respond to a specific combination of extrinsic and intrinsic stimuli. We present a simple, new supramolecular approach that responds to a specific combination of extrinsic and intrinsic stimuli.

We use proteins as the intrinsic trigger in our studies here, although the often-targeted intrinsic triggers are pH, reducing conditions, and reactive oxygen species.[28-34] Proteins are challenging and interesting as inputs, because of their structural and functional fragility and because they are considered to be the primary cause of pathological imbalances in biology.[35-39] We use light as the extrinsic trigger in these studies. In engineering the combinations of these two triggers, we were inspired by the molecular logic gates proposed and studied over past couple of decades.[40-47] While there have been many reports on molecular logic gates involving small molecules,[48-54] such gated strategies in nanoscale assemblies are relatively limited.[55] We are particularly interested in developing systems that predictably respond to dual inputs, based on protein and light (Figure 2.1).

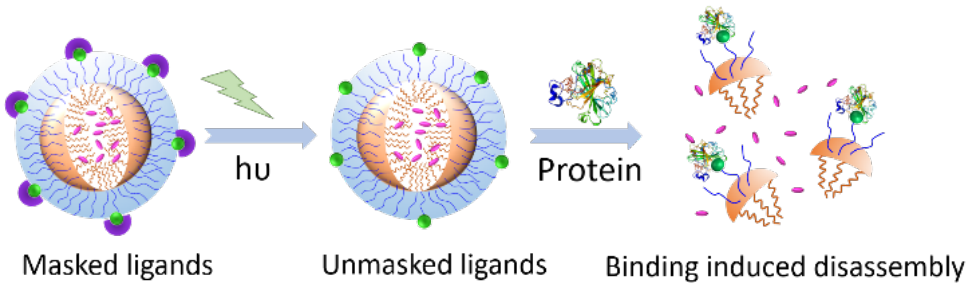

Figure 2.1 Schematic representation of protein and light responsive nanoassembly.

2.2 Results and discussion

2.2.1 Proof of concept on small molecules

First, we targeted the design of a molecular assembly that would respond only in the presence of a specific protein and light, but not in the presence of either of these inputs by themselves or in their absence. Such a system is interesting, as they offer the best opportunity to be specific, because it requires the concurrent presence of two different stimuli. For the protein, we used bovine carbonic anhydrase (bCA). Primary aryl

sulfonamides are well established ligands for this protein, where the active site zinc is known to be engaged with the sulfornamide moiety.[56-58] Examination of the structure of this binding interaction suggests that derivatizing the amino moiety of the sulfonamide group with an alkyl unit would cause this molecule to be not a good ligand for bCA. If such a substituent were to be removed in the presence of light, then the ligand is rendered activatable by light. Our design hypothesis is then that if such a functional group were to be then incorporated onto a protein-responsive assembly, then the assembly would respond only if there is both light and protein present, as shown in Figure 2.1.

Scheme 2.1 Photo-induced cleavage of compound 1 to expose sulphonamide ligand 2

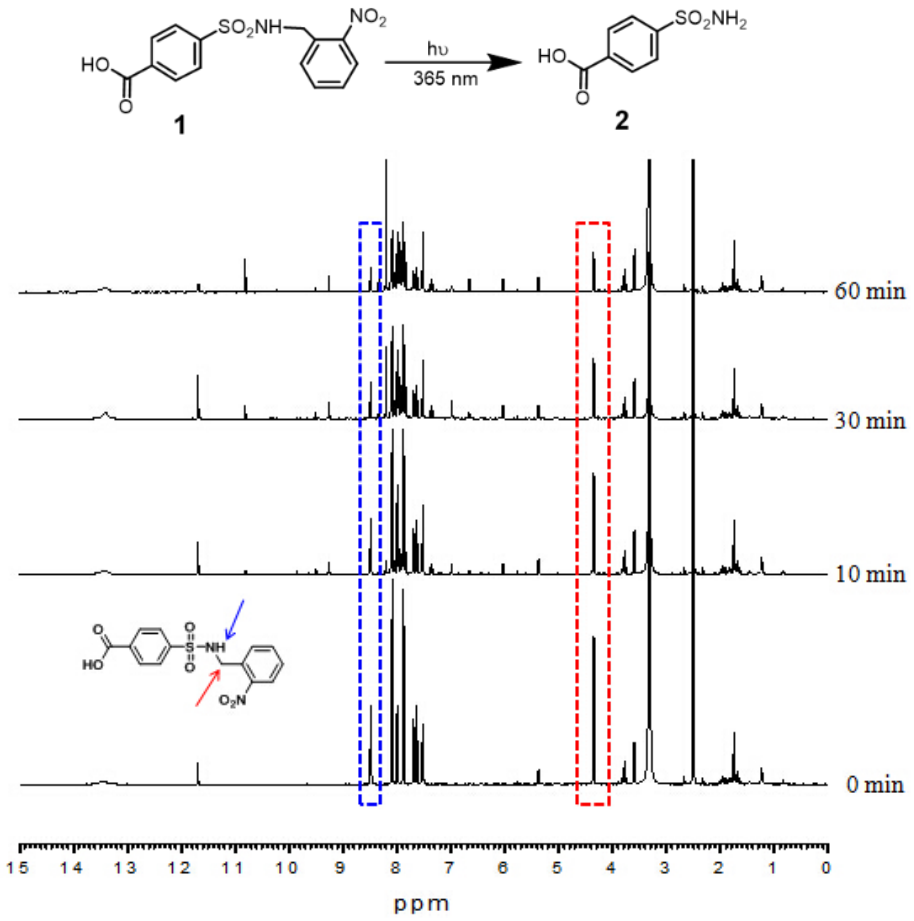

Figure 2.2 ^{1}H NMR spectra of compound **1** in D-DMSO at various UV irradiation periods. The gradual decrease of peaks at 8.49 and 4.36 ppm, which is corresponding to imino and methylene group, indicated the photo-cleavage of o-nitrobenzyl group.

To test this hypothesis, we first tested whether small molecule sulfonamide ligand can be protected by an o-nitrobenzyl moiety, which can then be released in the presence of light. Accordingly, we synthesized the molecule **1** and evaluated the possibility of deprotection of the nitrobenzyl moiety due to light irradiation at 365 nm (Figure 2.1). Indeed, ^{1}H NMR and LC-MS studies showed that the sulfonamide ligand was fully liberated to afford the sulfonamide ligand **2**, in response to UV irradiation (Figure 2.2, 2.3). We also tested molecules **1** and **2** as the ligands for bCA using a 5-(Dimethylamino)-1-naphthalenesulfonamide (DNSA) in a competitive displacement assay, the fluorescence emission at 460 nm formed by DNSA-bCA complex indicates whether DNSA is replaced.[11] Our studies showed that when the ligand was masked in **1**, it did not competitively remove DNSA, while the photo-cleaved product **2** was able to displace DNSA at a molar ratio of 1:1 for bCA and DNSA (Figure 2.4).

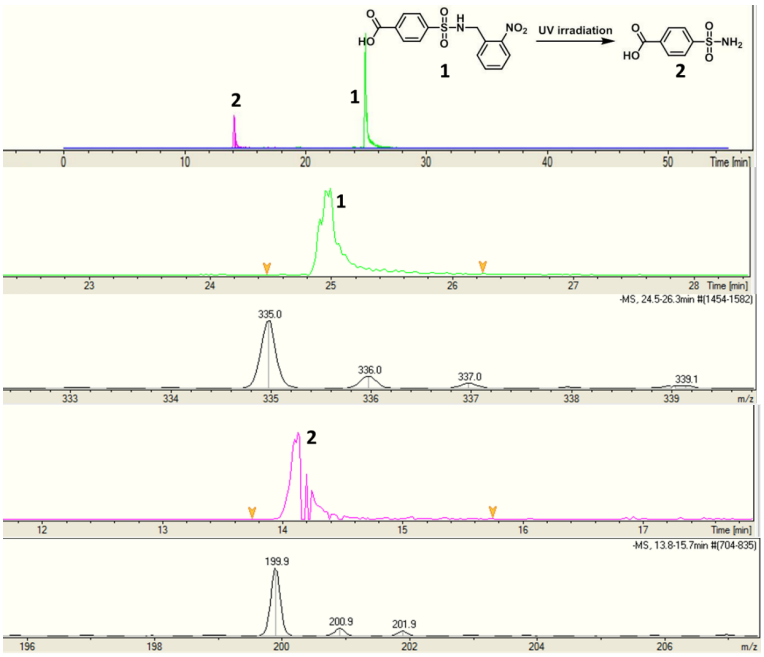

Figure 2.3 LC-ESI-MS results of compound **1** upon UV irradiation. Green peak (m/z = 335.0) is corresponding to compound 1. Pink peak (m/z = 200.0) is corresponding to compound **2**: 4-carboxylbenzene-sulfonamide. This result indicated that sulfonamide is generated after UV irradiation.

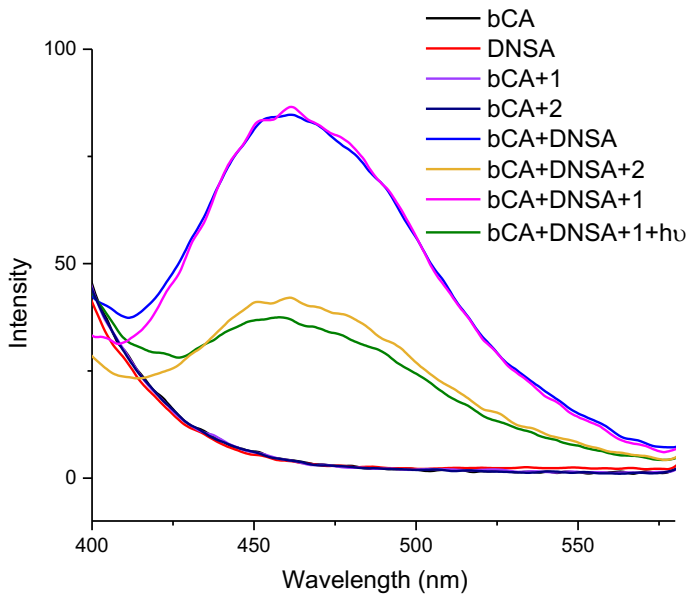

Figure 2.4 Emission spectra of bCA, DNSA, bCA-DNSA complex, bCA-**2** complex, CA-**1** complex irradiated by UV, competitive binding between 2 and DNSA.

2.2.2 Protein AND light gated disassembly and guest release

To generate a nanoassembly that would predictably respond only to the concurrent presence of light irradiation and the protein, we took the structural components of molecule **1** and install it into an amphiphilic dendrimer. The molecular structure that potentially serves this purpose is shown in Figure 2.5b as 3. The facially amphiphilic trimer contains an alkyl chain as the hydrophobic moiety and an oligoethylene glycol (OEG) chain as the hydrophilic moiety in each of the repeat units. The key functional group, N-(o-nitrobenzyl) benzene sulfonamide, is clicked on to the central unit on the hydrophilic face of the amphiphile using the Huisgen cycloaddition reaction. This amphiphile is known to aggregate to form nanoassemblies, which could then disassemble in response to a ligand-protein binding because of the change in the hydrophilic-lipophilic balance (HLB) upon protein binding. We also hypothesized that this nanoassembly would disassemble only in response to both light and protein, but not to just one of these two inputs. When the

assembly is irradiated with light, the sulfonamide moiety would be liberated; this change however would not be sufficient to change the HLB of the assembly. Similarly, since the ligand moiety is masked, it would be unavailable for the binding-induced disassembly in response to the protein. However, in the presence of both light and the protein, the nanoassembly should disassemble as the light would unmask the ligand, binding of which to the protein would cause a significant change in the HLB of the amphiphile.

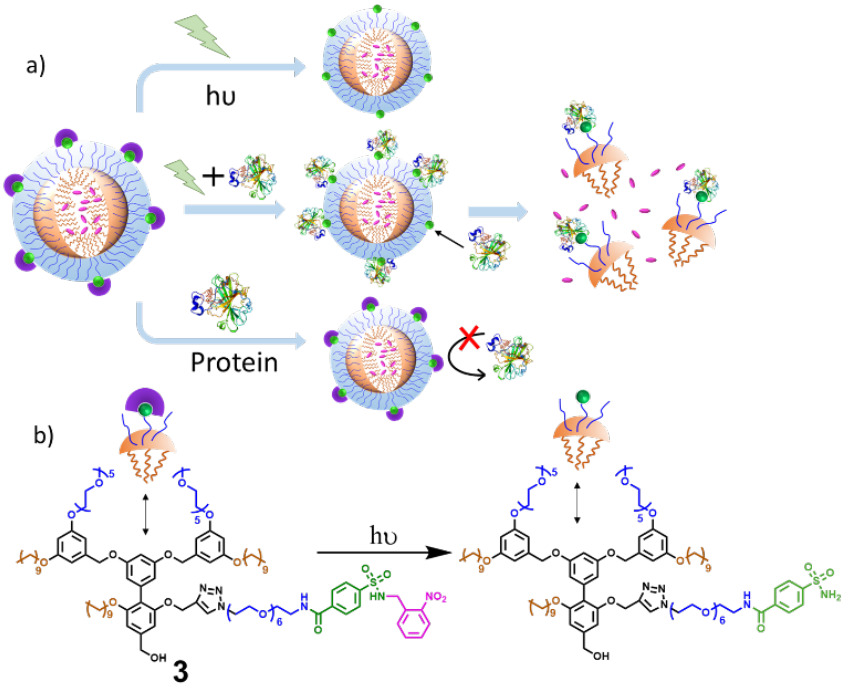

Figure 2.5. (a) Schematic representation of protein AND light gated disassembly and guest release, (b) Molecular structure of 3.

Prior to testing this hypothesis, we characterized the nanoassembly, formed from molecule 3. Synthetic details and the molecular characterization are shown in the SI. Since 3 contains, the nanoassembly formed would be an amphiphilic assembly, the critical aggregation concentration (CAC) can be estimated using the possibility of incorporating a hydrophobic molecule within the interiors of the assembly. The CAC for 3 was found to be ~36 μM. To assess the size of the nanoassembly formed, an aqueous solution of 3 was assessed using dynamic light scattering (DLS), at a concentration above its CAC (50 μM). The

amphiphilic nanoassembly was found to have an apprarent hydrodynamic diameter of >120 nm (Figure 2.6a). The spherical morphology of the assembly was ascertained using transmission electron microscopy (TEM) (Figure 2.6c) and atomic force microscopy (AFM) (Figure 2.7). Size from TEM images showed that the observed aggregates are

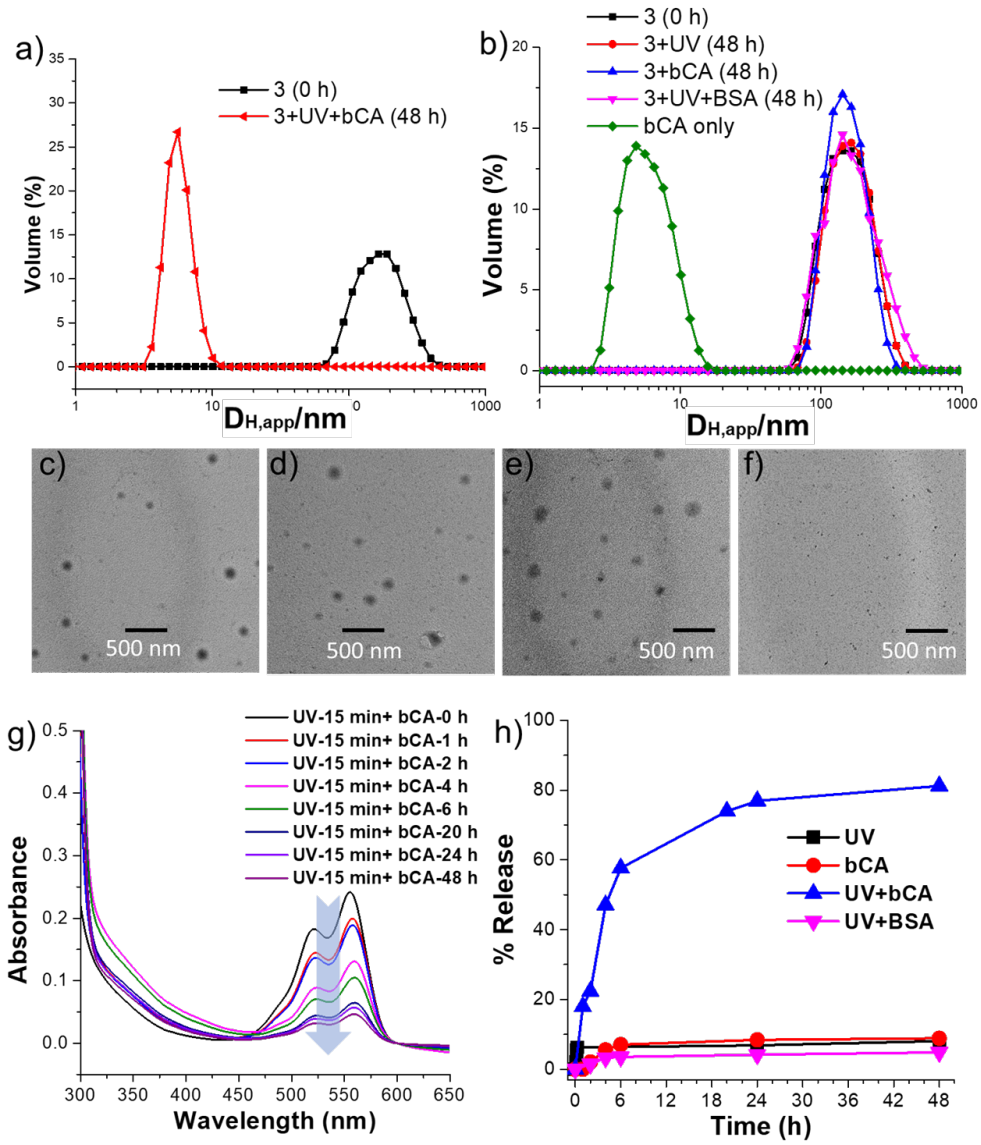

Figure 2.6 (a) Apparent hydrodynamic diameter($D_{H,\,app}$) of nanoassembly formed by **3** (50 μM) determined by one-angle dynamic light scattering, and **3** in presence of bCA and UV after 48h, (b) $D_{H,\,app}$ of nanoassembly **3** in presence of UV, bCA, UV and BSA, TEM images of **3** (50 μM) in presense of (c) no inputs, (d) UV light, (e) bCA, (f) bCA and UV light, (g) DiI release from 50 μM **3** solution in response to UV and bCA, (h) Plot of % release of DiI.

slightly lower than those from DLS, this difference is likely due to the shrinkage of the particles in the dry state or due to overestimation of the size of the particles in DLS as it also includes hydration shells around the particles.

Next, to test our hypothesis that the nanoassembly from **3** would be sensitive to the concurrent presence of both light and proteins, we treated a 50 μM solution of **3** with 365 nm light irradiation for 15 minutes and 60 μM bCA. We were gratified to find that the size of the assembly reduced from >120 nm to <10 nm (Figure 2.6a). To fully test whether this is indeed a response to the combination of these two inputs, effects of the light irradiation and the presence of bCA were tested independently. In both these cases, there was no discernible change in the size of the assembly, compared to the assembly of **3** itself (Figure 2.6b). The size change in the presence of both stimuli, and lack thereof in the presence of either of these stimuli, were also confirmed by TEM (Figure 2.6c-f) and AFM (Figure 2.7). These results provided the first indicator that the system is only responsive to the presence of both stimuli.

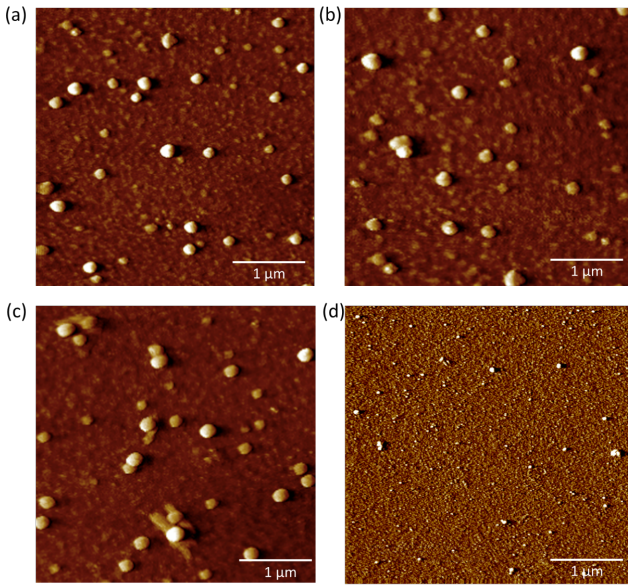

Figure 2.7 AFM images of **3** (50 μM) supramolecular micellar structures in aqueous solution in presence of (a) no inputs, (b) bCA, (c) UV light, (d) bCA and UV light.

To test these findings further, we utilized the host-guest properties of the nanoassembly. Since **3** forms amphiphilic aggregates with a hydrophobic interior in the aqueous phase, it can function as a nanocontainer to host water-insoluble guest molecules. We envisaged that by taking advantage of this container-like feature and employing AND logic inputs to the nanoassemblies, we will be able to regulate the guest release profile. Here, we use 1,1'-dioctadecyl-3,3,3'3'-tetramethyl-indocarbocyanine perchlorate (DiI), as the guest molecule to be entrapped inside the hydrophobic interior of **3**. Encapsulation of DiI in this assembly was found to be quite stable with time, where there was a <10% change in the characteristic absorption of DiI over 48 hours (Figure 2.6h). Similarly, when the 50 μM solution of **3** was irradiated with light at 365 nm or when it was treated with 60 μM concentration of bCA,the change in absorption peak was small and indistinguishable from the assembly in the absence of any stimulus (Figure 2.6h). Interestingly however, a rather dramatic decrease in DiI absorption was observed in the presence of both light and bCA, where ~60% of the guest molecules were released from the assembly in ~6 hours and >80% of the molecules were released in 48 hours (Figure 2.6g, h). These data are all consistent with our hypothesis that our nanoassembly is programmed to respond only in the presence of both stimuli. However, it is important to show that the presumed disassembly and guest release is indeed due to specific protein-ligand binding. To test the specificity of the protein-ligand binding, we applied UV irradiation and bovine serum albumin (BSA), a protein that has no specific interaction with sulfonamide, as the simultaneous inputs to investigate the size transformation and guest release. Indeed, there was neither any change in the size of the nanoassembly nor was there any discernible guest release over 48 h. These results further validate that the assembly is specific in response to bCA.

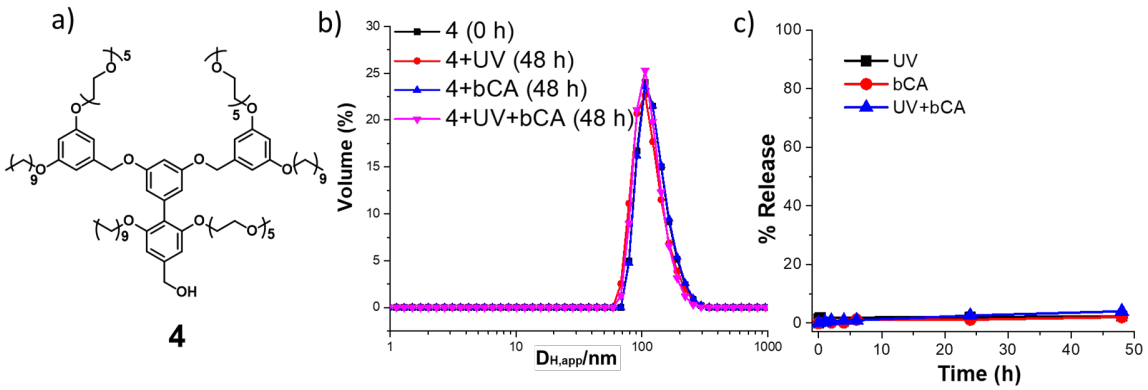

Figure 2.8. (a) Molecular structure of **4**, (b) $D_{H,\,app}$ of **4** nanoassembly (concentration of **4** = 50 μM); (c) Plot of % release of DiI from 50 μM **4** solution.

Also, we were interested in another control experiment, where we utilize a structurally related amphiphile forms a similar nanoassembly, but lacks the features that respond to light or to the specific protein. In this case, we prepared the trimeric amphiphile, **4**, in which every unit contains both hydrophobic alkyl chains and hydrophilic PEG moieties without any light sensitive moieties or protein-binding ligand functionalities. This molecule, too, forms a similarly sized nanoassembly in aqueous phase. Similar to the methods above, we studied the effects of individual and concurrent orthogonal inputs of UV light and bCA protein. No size transition or discernible guest release were observed, independent of whether a single input, no input, or both inputs were applied (Figure 2.8b and c). These results validate that the introduction of N-(o-nitrobenzyl) benzene sulfonamide ligand is critical for realizing the observed AND-gated disassembly and guest release.

2.2.3 Protein OR light gated disassembly and guest release

In dual responsive logic-gated systems, the next challenge in designing nanoscopic systems involves the OR gate, where a nanoassembly can respond to either of the inputs. To address this design challenge, we designed and synthesized the amphiphile **5**, shown in Figure 2.9. This molecule contains a sulfonamide moiety in the middle repeat unit on the hydrophilic face of the amphiphile, similar to **3**, but the bCA-ligand is present here in its unmasked

form. At the two terminal units, the hydrophobic decyl chain is linked to the trimeric scaffold using a photo-responsive o-nitrobenyzl ester linker. Synthetic details and are shown in the SI. We envisage here that when **5** is exposed to UV light, photo-induced cleavage of the nitrobenzyl ester will disconnect the long hydrophobic chain from the amphiphilic oligomer, while concurrently generating a carboxylic acid moiety. This transformation should render the entire oligomer much more hydrophilic, thus triggering disassembly. On the other hand, when treated with bCA, the already unmasked and available sulfonamide ligand should bind to the protein efficiently, causing a change in the HLB of the amphiphile to result in disassembly.

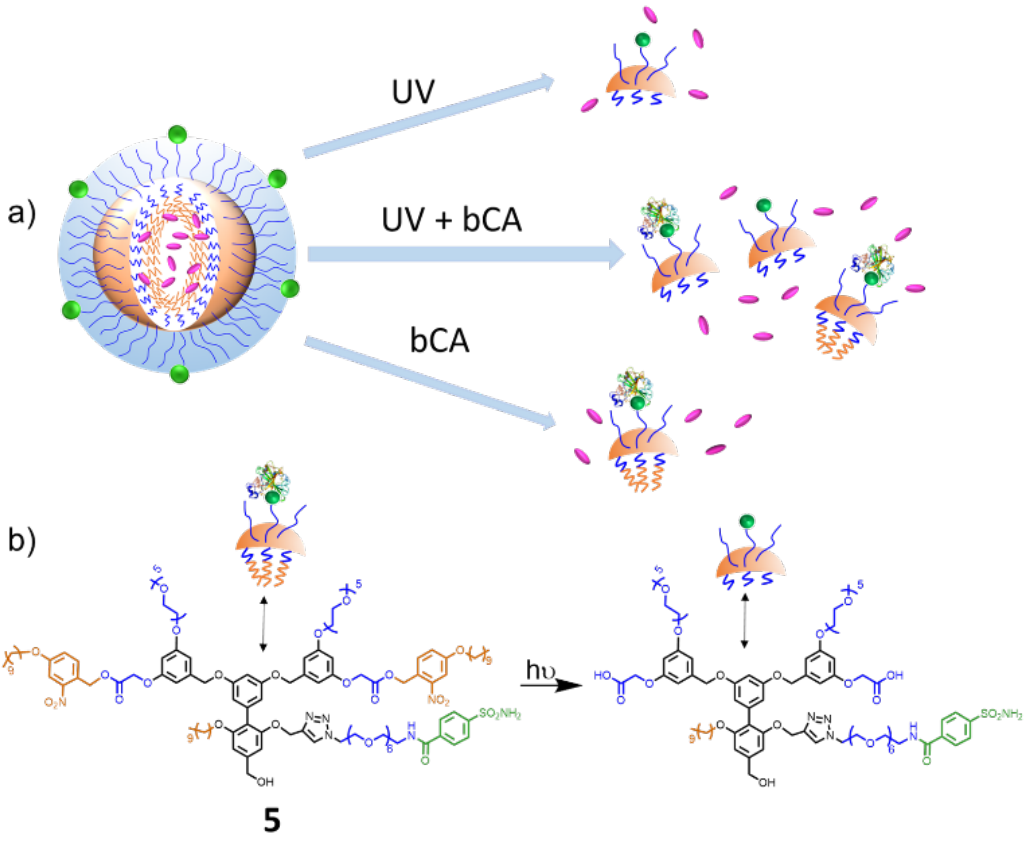

Figure 2.9. (a) Schematic representation of OR logic gated disassembly and guest release, (b) Molecular structure of **5**.

To test these design hypotheses, the size transformation of a solution of **5** was evaluated using DLS. As shown in Figure 1.10e, either UV light or the bCA protein inputs induce a size change in the nanoassembly from ~150 nm to ~10 nm. TEM images of **D2** before and after applying one or both inputs further confirm the disassembly event (Figure 2.10a-d). We also tested the host-guest properties of the assembly in the presence of these stimuli. Indeed, the DiI guest encapsulated in the D2 nanoassembly was released, when exposed to the bCA protein or the UV irradiation (Figure 2.10f). Note that the extent of molecular release with the protein binding is smaller than that of unmasked **3**. This is expected, because the overall hydrophobicity of the interior of the assembly from **5** is significantly higher than that from **3**, because of the introduction of additional aromatic units in the two of the three hydrophobic units. In fact, aromatic-aromatic interactions have been shown to have a substantial effect on the stability of encapsulation of molecules in these nanoassemblies.[12] Removal of these hydrophobic units, followed by treatment with the protein brings the guest release profile, comparable to that found with the unmasked **3**.

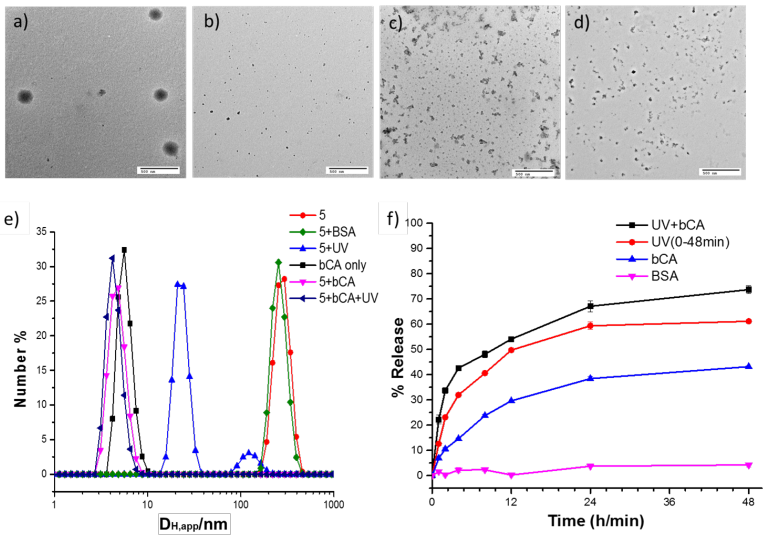

Figure 2.10. TEM images of **5** (50 μM) in presense of (a) no inputs, (b) UV light, (c) bCA, (d) bCA and UV light; (e) $D_{H,\,app}$ of **5** nanoassembly in response to UV and bCA, (f) Plot of % release of DiI.

2.3 Summary

To summarize, we have demonstrated a set of amphiphilic supramolecular assemblies that can disassemble in the presence of an extrinsic physical stimulus (light) and an intrinsic biological stimulus (protein). Since these nanoassemblies are capable of sequestering hydrophobic guest molecules, the host-guest properties of the assemblies are also compromised in the presence of these inputs. We outline molecular designs that can respond to the presence of either one or both of these stimuli, as well as that would respond only to the concurrent presence of both stimuli. The latter system was developed by caging a protein-specific ligand with a photo-protecting group that masks the ligand from being available for protein binding and thus preventing binding-induced disassembly. Therefore, the nanoassembly requires the concurrent presence of both light and the specific protein for programmed disassembly. In the former scenario, where the nanoassembly responds to either of the inputs, the disassembly was achieved by strategically placing the light-responsive moieties and the protein-responsive moiety in two different parts of the amphiphilic building block. As controlled responses to the concurrent presence of two different stimuli present the possibility of substantially increasing specificity in responses, the design insights provided here will find use in the design of novel protein-responsive drug delivery and controlled-release systems.

2.4 Experimental procedures

2.4.1 Materials and general methods

All the reagents were from commercial source and used as received. ^{1}H NMR and ^{13}C NMR spectra were recorded on a Bruker DPX-400 MHz NMR spectrometer using the residual proton resonance of the solvent as the internal standard. All molecules without

characterization data mentioned below were synthesized through well-established synthesis procedures previously reported by our group. [59-61] UV-vis absorption spectra were obtained by a Carry 100 Scan spectrometer. Fluorescence spectra were recorded on a PerkinElmer LS 55 spectrofluorimeter. Mass spectrometric data were collected by Capillary LC (Thermo Dionex Ultimate 3000)-ESI-MS (Bruker AmaZon quadrupole ion trap).

Dynamic Light Scattering (DLS) Study: For the DLS measurements, 2 μmol of **3**, **4** or **5** was dissolved in 10 mL PBS buffer (pH 7.4, 10 mM) and stirred at 4 ^{o}C for overnight and then stored in room temperature as 200 μM stock solution. Then these oligomeric amphiphile solutions were diluted to 50 μM with PBS buffer and filtered using hydrophilic membrane (pore size 0.450 μm) before experiment was performed. The diluted samples were treated with UV irradiation (Black Ray UV lamp, 365 nm, 115 V ~ 60 Hz); bCA; UV irradiation followed the addition of bCA or UV irradiation followed the addition of BSA. The sizes of each solution were recorded overtime by a Malvern Nanozetasizer ZS90 with a 637-nm laser source with non-invasive backscattering technology detected at 173^{o} using disposable sizing cuvette. Standard operating procedures (SOP) are set up including following parameters: the sample was equilibrated for 120 s at 25 ^{o}C before each measurement; the sizes were reported as the hydrodynamic diameter (D_H) and each measurement average 16 runs were repeated three times; the data was automatically analyzed by the zetasizer software through Mie model which then give the view of count rate, correlation function, intensity particle size distribution (PSD), volume PSD and Number PSD after each measurement.

Transmission Electron Microscope (TEM) Study: The same sample for DLS measurement was dropped onto carbon-coated copper grid. The grid was dried by slow evaporation in air, and then dry separately in a vacuum overnight. Images were recorded on a JEOL-2000FX electron microscopy operated at 200 kV and at a nominal magnification of 5000X. At least 10 locations on the TEM grid were examined. The assembly diameter was calculated using ImageJ software.

Atomic force microscopy (AFM): AFM images were taken using a Brucker Dimensions 3000 Scanning Probe Microscope under tapping mode. Silicon wafers [Cemat Silicon S.A., (111)-oriented] were pre-cleaned by sonication in ethanol and acetone for 20 min, respectively. Then the wafers were dried with Ar flow and treated with UV-O3 for 15 min. For AFM measurement, the oligomers at a concentration of 50 μM was drop-cast onto the corresponding substrate.

DiI encapsulation: 50 μM oligomeric amphiphile solutions in PBS buffer were stirred at room temperature and DiI stock solution (1 mg/mL in acetone, 5 wt% to **3**, **4 or 5**) was added in each solution. The solutions were stirred for 8 h in room temperature, open to the atmosphere allowing the organic solvent to evaporate, and then filtered through hydrophilic membranes with pore size of 0.45 μm to remove unencapsulated DiI.

Guest release study: DiI-encapsulated oligomeric amphiphile solutions (50 μM) were treated with 15 min UV irradiation; 60 μM bCA; 15 min UV irradiation followed the addition of 60 μM bCA or 15 min UV irradiation followed the addition of 60 μM BSA. The absorption spectra of DiI were recorded overtime. The % release of DiI was calculated by using the following equations:

% Release of DiI = $(I_t-I_0)/I_t*100$

I_0 =the highest absorbance of DiI; I_t = the highest absorbance of DiI at each time point

Calculation of critical aggregation concentration (CAC): A stock solution (1 mM) of **3/4/5** micelle was prepared was diluted into various solutions of different concentrations. The concentration range of polymer was maintained from 0.1 mM to 0.001 mM. Nile Red was encapsulated to the micelle by adding 10 µL of Nile Red stock solution (20 µM in acetone). All the micelle solutions were kept uncapped overnight to evaporate the acetone. Then emission spectrum was recorded for each solution and emission maxima of each spectrum were plotted as a function of the concentration of **3/4/5**. The inflection point of the plot was taken as CAC of polymer **3/4/5**.

2.4.2 Synthesis and characterization

Scheme 2.2. Synthetic protocol of masked ligand

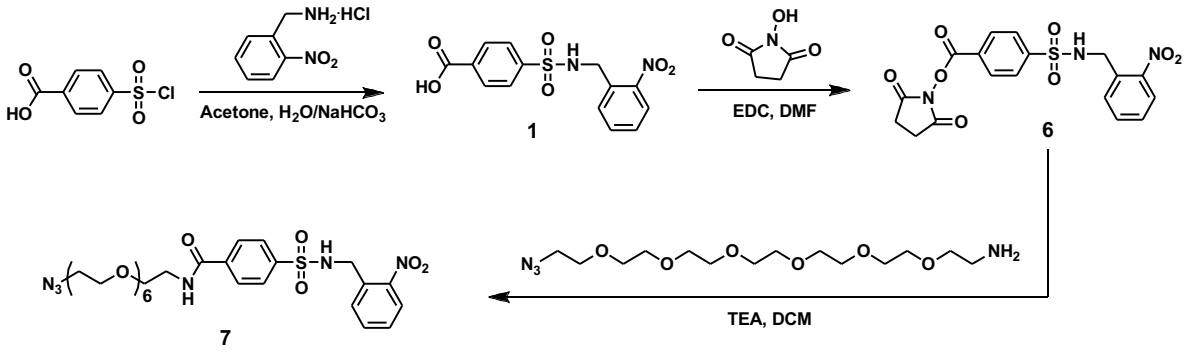

Synthesis of compound 1: 4-(Chlorosulfonyl) benzoic acid (2.2 g, 10 mmol) was taken into a round bottomed flask along with 2-Nitrobenzylamine hydrochloride (1.89 g, 10 mmol) and dissolved in the co-solvent of acetone (100 mL) and H_2O (25 mL). $NaHCO_3$ (1.68 g, 20 mmol) in H_2O was then added to the reaction mixture. The solution was stirred for overnight, concentrated, followed with the addition of 100 mL H_2O. The residue was extracted with 3×200 mL ethyl acetate, the organic phase was combined, concentrated and

purified by combiflash using DCM/methanol as eluant. The product was eluted at a polarity of 11% methanol in DCM and obtained as a light yellow solid. Yield: 27%. ^{1}H NMR (400 MHz, DMSO-*d6*, TMS): δ (ppm) = 8.49 (t, 1H), 8.08 (d, 2H), 7.97 (d, 1H), 7.69 (t, 1H), 7.63 (d, 1H), 7.52 (t, 1H), 4.36 (d, 2H).

Synthesis of compound 6: Compound **1** (268 mg, 0.8 mmol) and N-Hydroxysuccinimide (138 mg, 0.96 mmol) were dissolved in DMF (15 mL), followed with the addition of EDC·HCl (184 mg, 1.2 mmol). The solution was allowed to stir in room temperature for overnight. The reaction mixture was mixed with 50 mL DCM and washed with 3×30 mL H_2O, 3×30 mL saturated $NaHCO_3$ solution and 3×30 mL brine. The organic layer was collected and dried over anhydrous Na_2SO_4, concentrated and purified by combiflash using hexanes/ethyl acetate as eluant. The product was eluted at polarity of 50% ethyl acetate in hexanes and obtained as a light yellow solid. Yield: 88%. ^{1}H NMR (400 MHz, $CDCl_3$, TMS): δ (ppm) = 8.19 (d, 2H), 8.00 (d, 1H), 7.91 (d, 2H), 7.56 (m, 2H), 7.44 (t, 1H), 4.48 (d, 2H), 2.93 (s, 4H).

Synthesis of compound 7: Compound 2 (260 mg, 0.6 mmol) and triethylamine (112 μL，0.8 mmol) were dissolved in 10 mL DCM and stirred. O-(2-Aminoethyl)-O'-(2-azidoethyl) pentaethylene glycol (175 mg, 0.5 mmol) was dissolved in 5 mL DCM and added to the reaction mixture dropwise with the help of an addition funnel. The reaction was allowed to go on for overnight at room temperature, after which it was washed with 2×10 mL H_2O and 2×10 mL brine. The DCM layer was then dried over Na_2SO_4, concentrated and purified by combiflash using hexanes/ethyl acetate as eluant. The product was eluted at a polarity of 100% ethyl acetate and obtained as amber liquid. Yield: 78%.^{1}H NMR (400 MHz, $CDCl_3$, TMS): δ (ppm) = 7.98 (d, 1H), 7.92 (d, 2H), 7.87 (d,

2H), 7.60 (d, 2H), 7.47 (m, 1H), 7.15 (s, 1H), 5.66 (t, 1H), 4.44 (d, 2H), 3.70-3.59 (m, 26H), 3.36 (m, 2H).

General procedure for click reaction： The mixture of dendritic acetylene compound (1.0 eq), azide (2 eq for 1 acetylene group), $CuSO4{\cdot}5H_2O$ (0.5 equiv.) and sodium ascorbate (0.5 eq.) in THF/H_2O (1:1) solvent mixture was heated at 50 ^oC for 24 h. The reaction progress was monitored by TLC. After completion of the reaction, the reaction mixture was partitioned between ethyl acetate and saturated aqueous NH_4Cl solution. The aqueous layer was extracted twice with ethyl acetate and the combined organic layer was dried over Na_2SO_4 and evaporated to dryness. The crude product was purified by silica gel column chromatography.

Synthesis of 3: Synthetic protocol of **3** is outlined in scheme 2.3.

Scheme 2.3. Synthetic protocol of targeted oligomer 3

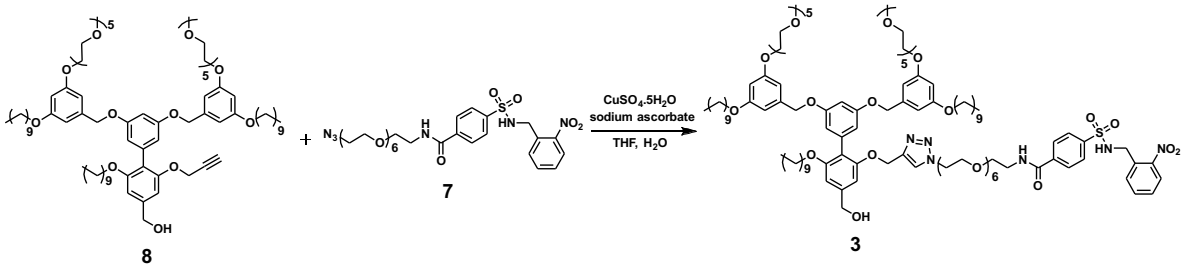

8 7 3

Synthesis of D1 (compound 5): Compound **8** was synthesized according to our previous report[1]. According to general procedure for click reaction, compound **8** (50 mg, 35 μmol) was treated with azide **7** (47 mg, 70 μmol) to give 52 mg of **3**. Yield: 72%. NMR (400 MHz, $CDCl_3$) δ 7.96 (t, 3H), 7.82 (d, 2H), 7.71 (br, 1H), 7.59 (d, 2H), 7.54 (m, 1H), 7.40 (t, 1H), 6.32 (s, 1H), 6.61 (m, 8H), 6.39 (t, 1H), 6.17 (t, 1H), 5.15 (s, 2H), 4.89 (s, 4H), 4.66 (s, 2H), 4.41 (m, 4H), 4.09 (t, 4H), 3.90-3.36 (m, 68H), 3.36 (s, 6H), 1.76-1.18 (m,

48H), 0.95-0.80 (m, 9H); ^{13}C NMR (400 MHz, $CDCl_3$) δ 166.0, 160.4, 160.0, 159.0, 157.2, 156.3, 147.9, 142.6, 142.4, 139.4, 138.4, 135.8, 134.0, 132.5, 131.6, 128.9, 128.2, 126.9, 125.0, 119.3, 110.3, 106.2, 105.8, 104.8, 104.7, 100.9, 100.7, 71.9, 70.7, 70.6, 70.5, 70.5, 70.4, 70.4, 70.3, 69.7, 67.9, 67.4, 65.0, 59.0, 53.4, 50.3, 44.8, 40.1, 31.9, 29.7, 29.6, 29.5, 29.4, 29.3, 29.3, 29.3, 26.1, 26.0, 25.6, 22.7, 22.4, 14.1; ESI-TOF m/z 1067.4 $[M+2Na]^{2+}$: Calculated: 1067.32, found: 1067.4 $[M]^{+}$+Na: Calculated: 2111.64, found: 2112.0.

Synthesis of D2: Synthetic protocol of **5** is outlined in scheme 2.4:

Scheme 2.4. Synthetic protocol of targeted dendrimer D2

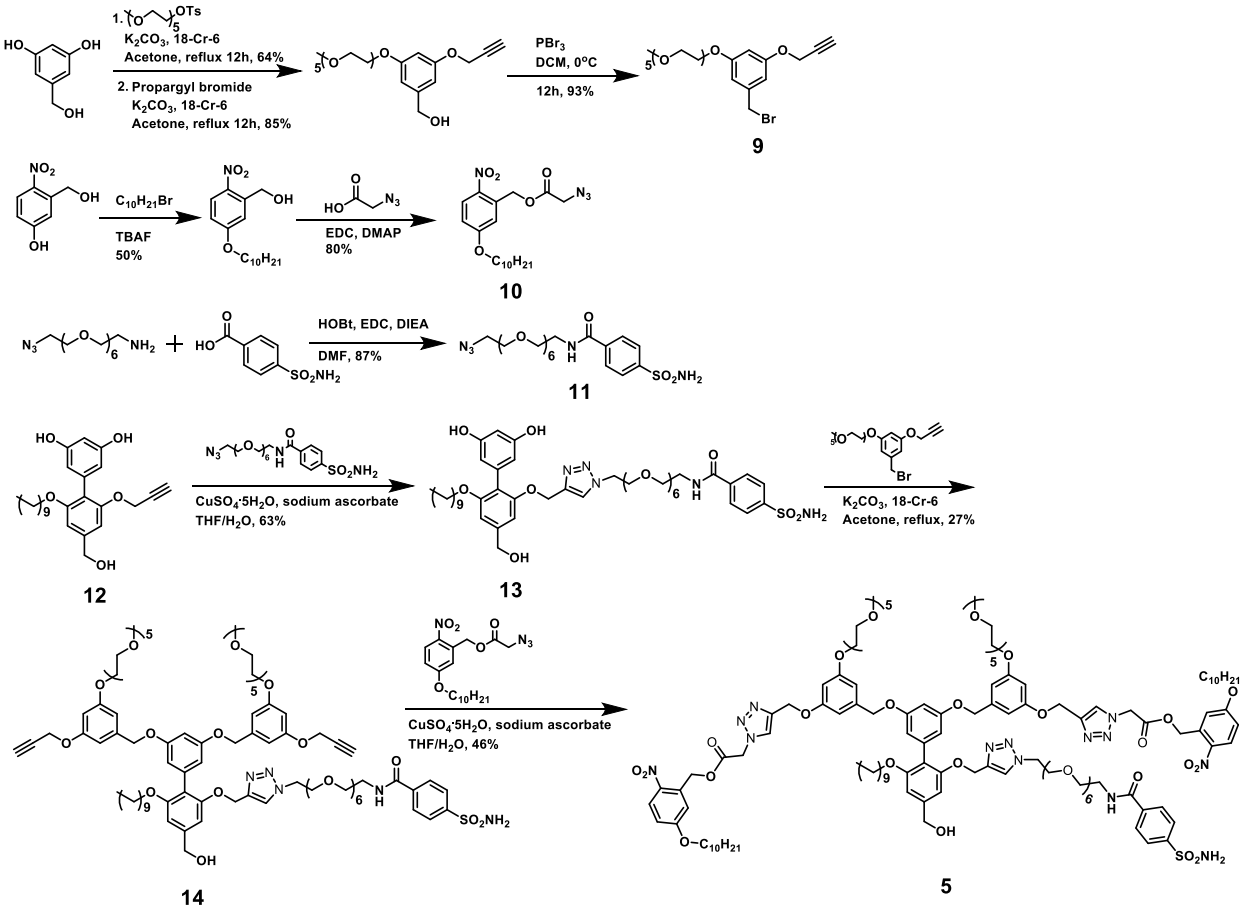

Synthesis of compound 11: EDC·HCl (328 mg, 1.68 mmol) and N, N-diisopropylethylamine (0.60 ml, 3.36 mmol) were added to a solution O-(2-Aminoethyl)-

O'-(2-azidoethyl) pentaethylene glycol (500 mg, 1.4 mmol) and 4-carboxybenzenesulfonamide (287 mg, 1.4 mmol) and HOBt (262 mg, 1.68 mmol) in dimethylformamide (5 ml) and stirred for 24 hours at room temperature under nitrogen. The solvent was removed in vacuo and the residue purified by column chromatography on silica gel eluting with dichloromethane:methanol (95:5) (by volume) to give compound **11** as a colorless oil. Yield 87%. ^{1}H NMR ($CDCl_3$, 400 MHz) δ 7.77-7.84 (m, 4H), 7.56 (s, 1H), 6.24 (s, 1H), 3.36-3.73 (m, 24H). ESI-MS m/z calcd for $[M+Na]^+$: 556.21; found: 556.3718.

Synthesis of compound 13: Compound **12** was prepared following our previously reported procedure[1]. According to general procedure for click reaction, compound **12** (400 mg, 0.94 mmol) was treated with azide **11** (600 mg, 1.18 mmol) to give 560 mg of **13**. Yield: 63%. ^{1}H NMR ($CDCl_3$, 400 MHz) δ 7.91 (br s, 1H), 7.77 (m, 4H), 7.56 (s, 1H), 6.7 (s, 1H), 6.58 (s, 1H), 6.30 (m, 3H), 6.10 (br s, 1H), 4.64 (s, 2H), 4.53 (s, 2H), 4.46 (t, 2H), 4.21 (s, 4H), 3.93 (m, 4H), 3.78-3.83 (m, 6H), 3.52-3.73 (m, 50H), 3.35 (s, 6H), 1.55 (m, 2H), 1.2-1.4 (m, 14H), 0.88(m, 3H). ESI-MS m/z calcd for $[M+Na]^+$: 959.45; found: 982.4715.

Synthesis of compound 14: Compound **10** (280 mg, 0.29 mmol), K_2CO_3 (121 mg, 0.87 mmol), 18-crown-6 (38 mg, 0.145 mmol) and compound **9** (305 mg, 0.638 mmol) were mixed together in anhydrous acetone (50 mL) and refluxed for 12 h under argon. After slowly cooling the reaction to room temperature and evaporating the solvent, the resultant mixture was dissolved in ethyl acetate and washed with water. The combined organic layers were dried over Na_2SO_4, concentrated under reduced pressure and the crude mixture was purified by silica gel chromatography with MeOH/ethyl acetate (6:94 v/v) to give compound **14** (135 mg, 27%). ^{1}H NMR ($CDCl_3$, 400 MHz) δ 7.94 (d, 2H), 7.79 (d, 2H),

7.56 (br s, 1H), 7.53 (s, 1H), 6.72 (s, 1H), 6.63 (s, 1H), 6.17~6.39 (m, 9H), 5.08 (s, 2H), 4.64 (s, 2H), 4.53 (s, 2H), 4.46 (t, 2H), 4.21 (s, 4H), 3.93 (m, 4H), 3.78-3.83 (m, 6H), 3.52-3.73 (m, 50H), 3.35 (s, 6H), 1.55 (m, 2H), 1.2-1.4 (m, 14H), 0.88(m, 3H). ESI-MS m/z calcd for $C_{89}H_{129}N_5O_{28}SNa$ [M+Na] : 1770.85; found: 1771.5027, $[M+2Na]^{2+}$ 896.7148.

Synthesis of 5：According to general procedure for click reaction, compound **14** (100 mg, 56 μmol) was treated with azide **10** (66 mg, 168 μmol) to give 66 mg of **5**. Yield: 46%. ^{1}H NMR ($CDCl_3$, 400 MHz) δ 8.15 (d, 2H), 7.94 (d, 2H), 7.89 (s, 2H), 7.79 (d, 2H), 7.53 (s, 1H), 7.48 (br s, 1H), 6.94 (m, 4H), 6.72 (s, 1H), 6.62 (s, 1H), 6.17~6.37 (m, 9H), 5.60 (s, 4H), 5.48 (s, 4H), 5.02 (d, 6H), 4.63 (s, 2H), 4.4 (t, 2H), 4.15 (s, 4H), 4.02 (t, 6H), 3.91 (m, 4H), 3.81 (m, 8H), 3.51-3.7 (m, 50H), 3.35 (s, 6H), 1.8 (m, 4H), 1.55 (m, 2H), 1.46 (m, 4H), 1.2-1.5 (m, 38H), 0.88 (m, 9H); ^{13}C NMR ($CDCl_3$, 100 MHz) δ 166.2, 165.95, 163.70, 159.97, 159.15,157.16, 156.75, 156.35, 144.49, 144.10, 142.8, 139.82, 138.27, 137.91, 136.06, 133.82, 128.37, 128.18, 127.08, 125.00, 124.05, 119.64, 114.67, 113.76, 110.49, 107.54, 107.37, 104.95, 104.86, 101.77, 101.31, 71.89, 70.68, 70.54, 70.45, 70.38, 70.30, 70.04, 69.79, 69.56, 69.30, 69.15, 68.79, 67.42, 65.06, 64.92, 63.57, 61.64, 58.99, 55.99, 53.44, 51.25, 50.77, 50.18, 40.09, 31.89, 29.70, 29.59, 29.35, 29.31, 29.09, 28.98, 25.93, 22.68, 14.13. ESI-MS m/z calcd for $C_{127}H_{185}N_{13}O_{38}SNa$ $[M+Na]^+$: 2555.26; found: 2555.9831.

2.5 References

1. J. Zhuang, M. R. Gordon, J. Ventura, L. Li, S. Thayumanavan, *Chem. Soc. Rev.* **2013**, 42, 7421-7435.
2. S. M. Lee, S. T. Nguyen, *Macromolecules* **2013**, 46, 9169-9180.
3. X. Hu, Y. Zhang, Z. Xie, X. Jing, A. Bellotti, Z. Gu, *Biomacromolecules* **2017**, 18, 649-673.
4. A. P. Blum, J. K. Kammeyer, A. M. Rush, C. E. Callmann, M. E. Hahn, N. C. Gianneschi*, J. Am. Chem. Soc.***2015**, 137, 2140-2154.
5. G. Yu, K. Jie, F. Huang*, Chem. Rev.* **2015**, 115, 7240-7303.
6. V. P. Torchilin, *J. Controlled Release* **2001**, 73, 137-172.
7. E. Soussan, S. Cassel, M. Blanzat, I. Rico-Lattes, *Angew. Chem., Int. Ed.* **2009**, 48, 274-288.
8. K. R. Raghupathi, J. Guo, O. Munkhbat, P. Rangadurai, S. Thayumanavan, *Acc. Chem. Res*. **2014**, 47, 2200-2211.
9. J. D. Hartgerink, E. Beniash, S. I. Stupp, *Science* **2001**, 294, 1684-1688.
10. H. Cabral, N. Nishiyama, K. Kataoka*, Acc. Chem. Res*. **2011**, 44, 999-1008.
11. N. K. Mal, M. Fujiwara, Y. Tanaka, *Nature* **2003,** 421, 350.
12. A. P. Goodwin, J. L. Mynar, Y. Ma, G. R. Fleming, J. M. Fréchet, *J. Am. Chem. Soc.* **2005**, 127, 9952-9953.
13. D. P. Ferris, Y.-L. Zhao, N. M. Khashab, H. A. Khatib, J. F. Stoddart, J. I. Zink, *J. Am. Chem. Soc.* **2009**, 131, 1686-1688.
14. V. Yesilyurt, R. Ramireddy, S. Thayumanavan, *Angew. Chem., Int. Ed.* **2011**, 50, 3038-3042

15. M. Karimi, P. Sahandi Zangabad, S. Baghaee-Ravari, M. Ghazadeh, H. Mirshekari, M. R. Hamblin, *J. Am. Chem. Soc*. **2017**, 139, 4584-4610.

16. G. Yu, W. Yu, Z. Mao, C. Gao, F. Huang, *Small*, **2015**, 11, 919-925.

17. R. J. Amir, N. Pessah, M. Shamis, D. Shabat, *Angew. Chemie* **2003**, 115, 4632-4637.

18. R. J. Amir, D. Shabat, *Chem. Commun.* **2004**, 1614-1615.

19. M. A. Kostiainen, D. K. Smith, O. Ikkala, *Angew. Chemie Int. Ed.* **2007**, 46, 7600–7604.

20. M. A. Kostiainen, J. Kotimaa, M.-L. Laukkanen, G. M. Pavan, *Chem.-A Eur. J.* **2010,** 16, 6912-6918.

21. A. Nazemi, T. B. Schon, E. R. Gillies, *Org. Lett.* **2013**, 15, 1830-1833.

22. A. Nazemi, E. R. Gillies, *Chem. Commun.* **2014**, 50, 11122-11125.

23. E. R. Gillies, T. B. Jonsson, J. M. Fréchet, *J. Am. Chem. Soc.* **2004**, 126, 11936-11943.

24. J. Du, Y. Tang, A. L. Lewis, S. P. Armes, *J. Am. Chem. Soc.* **2005**, 127, 17982-17983.

25. Y. Li, W. Du, G. Sun, K. L. Wooley, *Macromolecules* **2008**, 41, 6605-6607.

26. H. S. Peng, J. A. Stolwijk, L. N. Sun, J. Wegener, O. S. Wolfbeis, *Angew. Chem., Int. Ed.* **2010**, 122, 4342-4345.

27. Y. Li, T. Zhao, C. Wang, Z. Lin, G. Huang, B. D. Sumer, J. Gao, *Nat. Commun.* **2016**, 7, 13214.

28. T. Chen, Y. Hu, Y. Cen, X. Chu, Y. Lu, *J. Am. Chem. Soc.* **2013**, 135, 11595-11602.

29. Y. Yao, Y. Wang, F. Huang, *Chem. Sci*., **2014**, 4312-4316.

30. Z. Deng, Y. Qian, Y. Yu, G. Liu, J. Hu, G. Zhang, S. Liu, *J. Am. Chem. Soc* 2016, 138, 10452-10466.

31. A. Napoli, M. Valentini, N. Tirelli, M. Muller, J. A. Hubbell, *Nat. Mater.* **2004**, 3, 183.

32. C. Li, J. Madsen, S. P. Armes, A.L. Lewis, *Angew. Chem., Int. Ed*. **2006**, 45, 3510-3513.

33. J. Ryu, R.T. Chacko, S. Jiwpanich, S. Bickerton, R.P. Babu, S. Thayumanavan, *J. Am. Chem. Soc.* **2010**, 132, 17227-17235.

34. W. C. de Vries, D. Grill, M. Tesch, A. Ricker, H. Nüsse, J. Klingauf, A. Studer, V. Gerke, B. J. Ravoo*, Angew. Chem., Int. Ed.* **2017**, 56, 9603-9607.

35. T. K. Chaudhuri, S. Paul, *FEBS J.* **2006**, 273, 1331-1349.

36. C. A. Ross, M.A. Poirier*, Nat. Med.* **2004**, 10, S10-S17.

37. F. Chiti, C. M. Dobson, *Annu. Rev. Biochem.* 2006, 75, 333-366.

38. C.M. Dobson, *Nature* **2002**, 418, 729-730.

39. Y. Takaoka, T. Sakamoto, S. Tsukiji, M. Narazaki, T. Matsuda, H. Tochio, M. Shirakawa, I. Hamachi, *Nat. Chem.* **2009**, 1, 557-561.

40. De Silva P. A., Gunaratne N. H. Q., McCoy C. P., *Nature* **1993**, 364, 42-44.

41. Aviram A., *J. Am. Chem. Soc*. **1988**, 110, 5687-5692.

42. De Silva A. P., *Nat. Mater.* **2005**, 4(1), 15.

43. De Silva A. P., Uchiyama, S. *Nat. Nanotech.* **2007**, 2(7), 399-410.

44. C. P. Collier, E. W. Wong, M. Belohradský, F. M. Raymo, J. F. Stoddart, P. J. Kuekes, R. S. Williams, J. R. Heath, *Science,* **1999**, 285, 391-394.

45. S. Kou, H.N. Lee, D. van Noort, K.E.E. Swamy, S.H. Kim, J.H. Soh, S. Park, *Angew. Chem., Int. Ed.* **2008**, 47, 872-876.c

46. S. Erbas-Cakmak, E.U. Akkaya, *Angew. Chem., Int. Ed.* **2013**, 52, 11364-11368.

47. D. Margulies, G. Melman, C.E. Felder, R. Arad-Yellin, A. Shanzer, *J. Am. Chem. Soc.* **2004**, 126, 15400-15401.

48. De Silva A. P., James M. R., McKinney B. O. F., Pears D. A., Weir S. M., *Nat. Mater*. **200**6, 5, 787.

49. Margulies D., Hamilton A. D., *J. Am. Chem. Soc.* **2009**, 131, 9142.

50. Chen J., Fang Z., Lie P., Zeng L., *Anal Chem.* **2012**, 84, 6321.

51. Nikitin, M. P., Shipunova, V. O., Deyev, S. M., & Nikitin, P. I. *Nat. Nanotech,* **2014**, 9, 716-722.

52. M. You, L. Peng, N. Shao, L. Zhang, L. Qiu, C. Cui, W. Tan, *J. Am. Chem. Soc.* **2014**, 136, 1256-1259.

53. V. M. Krishnamurthy, G. K. Kaufman, A. R. Urbach, I. Gitlin, K. L. Gudiksen,D. B. Weibel, G. M. Whitesides, *Chem. Rev.* **2008**, 108, 946- 1051.

54. V. Alterio, A. Di Fiore, K. D'Ambrosio, C. T. Supuran, G. De Simone, *Chem. Rev.* **2012**, 112, 4421-4468.

55. H. N. Li, Y. X. Ci, *Analytica chimica acta* **1995**, 317, 353-357.

56. O. Munkhbat, M. Garzoni, K. R. Raghupathi, G. M. Pavan, S. Thayumanavan, *Langmuir*, **2016**, 32, 2874-2881.

57. C. Tanford, C. 2nd ed.; *J. Wiley and Sons: New York*, **1980**.

58. J. N. Israelachvili, D. J. Mitchell, B. W. Ninham, *J. Chem. Soc*., Faraday Trans. **1976**, 72, 1525−1568.

59. Azagarsamy, M. A.; Yesilyurt, V.; Thayumanavan, S. *J. Am. Chem. Soc.* **2010**, *132*, 4550-4551.

60. Yesilyurt, V., Ramireddy, R., Thayumanavan, S. *Angewandte Chemie International Edition*, **2011**, 50(13), 3038-3042.

61. Aathimanikandan, S. V.; Savariar, E. N.; Thayumanavan, S. *J. Am. Chem. Soc.* **2005**, 127, 14922-14929

CHAPTER 3

TUNABLE ENZYME RESPONSES IN AMPHIPHILIC NANOASSEMBLIES THROUGH ALTERATIONS IN UNIMER-AGGREGATE EQUILIBRIUM

Adapted with permission from Gao, J.; Wang, Hui.; Zhuang, J.; Thayumanavan, S. Tunable enzyme responses in amphiphilic nanoassemblies through alterations in unimer-aggregate equilibrium. *Chem. Sci.,* **2019**, 10, 3018-3024.

3.1 Introduction

Enzymes, as one of the most essential macromolecules in living organisms, are known to catalyse more than 5000 biochemical reactions efficiently and serve a variety of functions in biological processes. [1] Therefore, dysregulation of enzymatic activities has been associated with many human pathologies. [2-4] In this context, introducing enzymes as stimuli to trigger specific responses in artificial supramolecular assemblies have been of interest, as these have potential in areas such as activity profile based biological imaging and drug delivery. [5-13] A promising design strategy that leads to such materials involves covalent incorporation of substrate functionalities in self-assembling molecules, such as amphiphilic macromolecules, where the specific catalytic actions of an enzyme covalently modify the substrate moiety. If it were to be designed such that the product of this enzymatic reaction exhibits distinctly different self-assembly features, compared to the substrate, then there exists a unique opportunity for programmable changes in the nanostructures and their host-guest properties.

Many supramolecular systems including polymeric nanoparticles, hydrogels, silica nanoparticles and gold nanoparticles have displayed adaptive behaviors toward enzymes. [14-23] Tunability in kinetics of the enzymatic response still remains a challenge, as it is

mainly influenced by two factors: accessibility of enzyme to substrate moiety and degree of difference in the host-guest properties between the reactant and product assemblies. In the case of amphiphilic assemblies, our group and others have shown that enzymatic activation usually occurs at unimeric state, where substrate is more accessible to enzyme

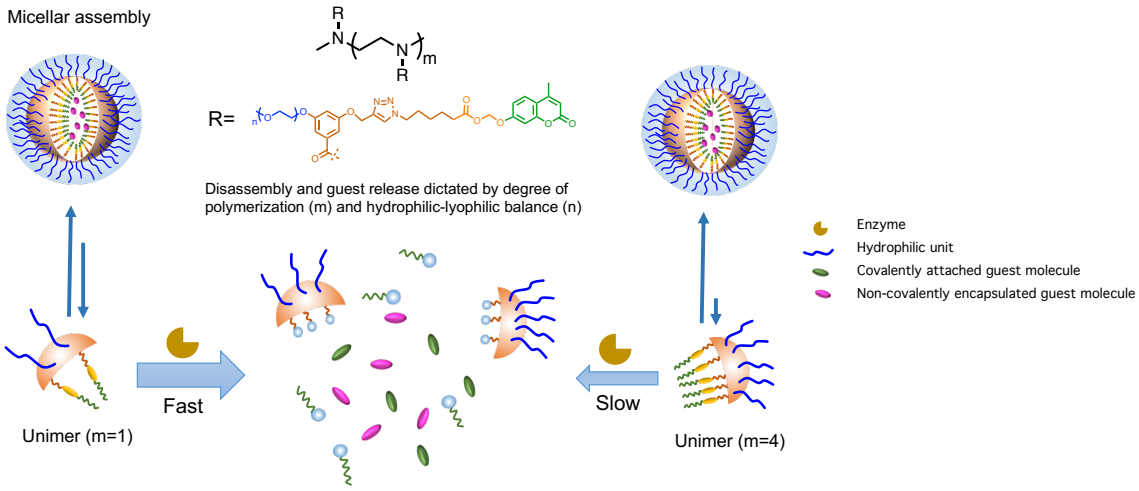

Figure 3.1 Schematic representation of enzyme-induced disassembly and guest release from varied oligomeric assemblies.

than their assembled micellar form.[24,25] Following these findings, we have been interested in investigating how the reaction kinetics and the ensuing change in the host-guest characteristics would be affected by tuning unimer-aggregate equilibrium to alter the assemblies' accessibility to the enzyme. Moreover, we were interested in identifying as to how structural changes in host assemblies, induced by an enzyme, would affect rate of disassembly and kinetics of guest molecule release. We envisaged that oligomeric amphiphiles would be an ideal choice to address this question, because: (*i*) these molecules have critical aggregation concentrations (CACs) that are quite low and compare very well with amphiphilic polymers; (*ii*) despite the fact that they do exhibit a low CAC, unlike polymers, these are amenable to a well-defined structure–property relationship study as the degree of oligomerization can be precise. Here we report a new modular design of

oligomeric amphiphiles with which a precise control over degree of polymerization (DP) and functional group placements in the scaffolds can be achieved (Figure 3.1). These oligomers are expected to self-assemble in aqueous phase and host hydrophobic guests at their interiors. By varying the DP and hydrophilic moieties of host molecules, we explore the molecular features that underlie the kinetics of enzymatic response in these supramolecular assemblies.

3.2 Results and discussion

3.2.1 Oligomer design and synthesis

Since enzymatic activation usually occurs at the unimeric state, where the substrate is more accessible to enzyme than their assembled micellar form, we envisaged that shifting the equilibrium between the unimer and the assembled state would provide an opportunity to alter the enzymatic reaction rate. Degree of polymerization is one of the key factors that can alter this equilibrium[26-29] and thus change the accessibility of an enzyme to its substrate. To test this possibility, it is critical that all the designed amphiphiles possess the same hydrophilic-lipophilic balance (HLB). For this purpose, a series of oligomeric amphiphiles from dimer (**2-EG5**) to pentamer (**5-EG5**), have been synthesized (Scheme 3.1). To further evaluate the effects of DP on the enzymatic response, a polymer **P-EG5** with ~14 repeating units was also synthesized. In these amphiphiles, penta-ethylene glycol (EG5) monomethyl ether moieties are installed as the hydrophilic functionality, while alkylated coumarin moieties are used as the hydrophobic units. Both these units are attached to the meta-positions of a benzoyl building block, which are then attached to well-defined oligoamines to generate amphiphiles with different degrees of oligomerization. In all these systems, the coumarin moiety is chosen as the covalently-appended model guest molecule. In order to

release this guest molecule in the presence of an enzyme, we use an acetal-ester linkage to connect the coumarin to the oligomer. The esterase-induced cleavage of the carboxylate moiety would create a hemi-acetal coumarin, which is hydrolytically unstable. This hemi-acetal therefore rapidly hydrolyzes further to generate a highly fluorescent, 4-methylumbelliferone. In addition to releasing this covalently attached molecule, this transformation also replaces an aryl moiety on the hydrophobic side of these amphiphiles with a carboxylic acid moiety. This change results in a significant

Scheme 3.1. Molecular structures of oligomers: legends of each oligomer indicate increased degree of polymerization from **2-EG5** to **P-EG5**, **EG5** indicates oligomers with five ethyleneglycol units, **EG8** indicates oligomers with eight ethyleneglycol units as hydrophilic moiety.

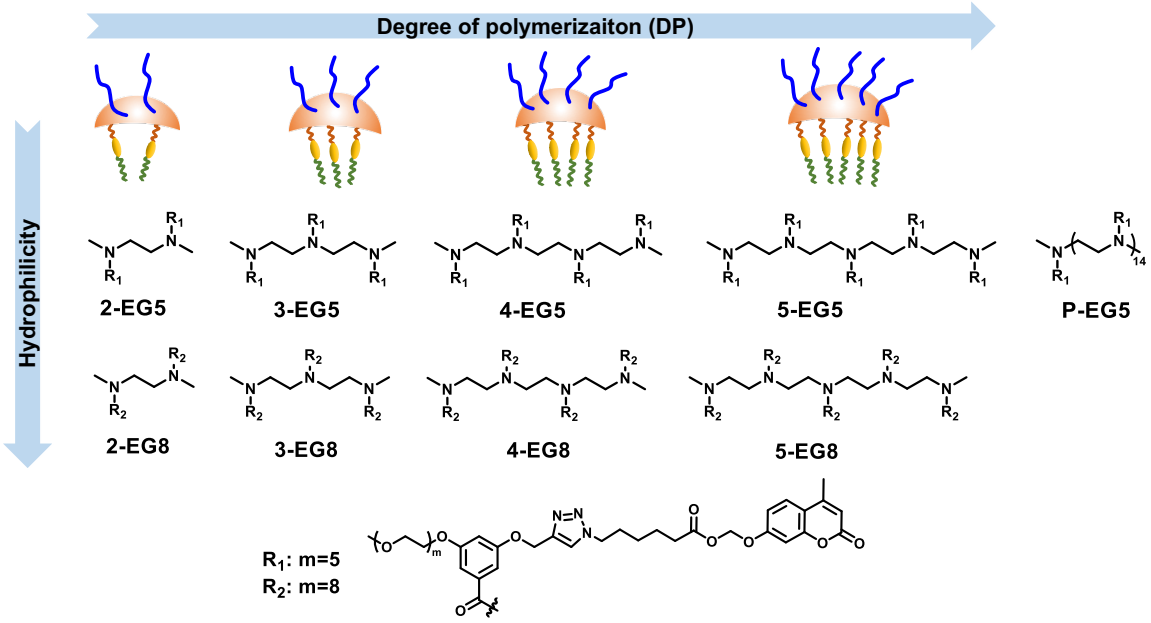

Scheme 3.2. Synthesis route of oligomers exemplified using **3-EG5**

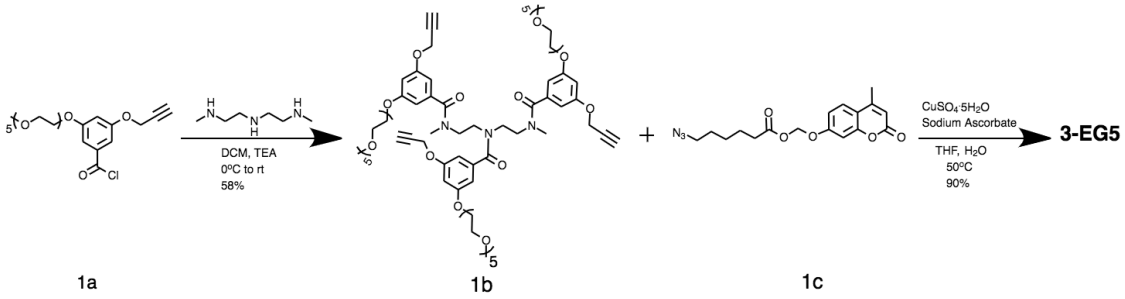

change in the HLB of the amphiphile. Note that this series of amphiphiles share all the common structural features including backbone, hydrophobic and hydrophilic functionalities; the only variation within this series of amphiphiles is DP. Therefore, this investigation allows us to inquire about the impact of this DP upon self-assembly and enzyme induced disassembly events.

In addition to DP, HLB of oligomers is another factor that impact the unimer-aggregate equilibrium. To test this possibility, with the same oligomer series above, we simply increased the length of the oligoethyleneglycol chain length from five to eight units. Thus, we synthesized four more oligomers **2-EG8, 3- EG8, 4- EG8,** and **5- EG8** (Scheme 3.1). We hypothesized that the increase in hydrophilicity upon going from penta-ethylene glycol monomethyl ether (EG5) to octa-ethylene glycol (EG8) monomethyl ether would increase the dynamics of the unimer-aggregate equilibrium, which will then increase the availability of the substrate moiety for the enzymes. In this study, we also test this hypothesis.

The amphiphilic oligomers were designed in such a way that they can be synthesized in a modular fashion, providing facile access to vary the number of repeating units and functional group placement. The synthetic routes for the target oligomers are exemplified by the synthesis of trimer **3-EG5** in Scheme 3.2. The 3,5-disubstituted-benzoyl chloride molecule **1a** was reacted with N,N"-dimethyl diethylenetriamine under basic conditions to generate the substituted oligoamine scaffold **1b**. This molecule now contains the pentaethyleneglycol hydrophilic unit and the alkyne moiety to anchor the hydrophobic unit. The hydrophobic and fluorogenic enzyme substrate was then attached at all three repeat units of the oligomer using the Huisgen 1,3-dipolar cycloaddition reaction, the so-called "click" chemistry[14], to yield the desired oligomer **3-EG5** (Scheme 3.2).

3.2.2 Nanoassembly preparation and characterization

We first investigated whether these oligomeric amphiphiles would form aggregates in aqueous phase, since they contain both hydrophobic and hydrophilic moieties. If self-assembly occurs, the interior of these assemblies would have the capability to non-covalently encapsulate hydrophobic molecules. To test this, the oligomers were directly dissolved in phosphate buffer and non-covalent incorporation of a solvatochromic dye, Nile Red, within these assemblies was attempted. We found that at lower concentrations of oligomers, the emission intensity of Nile Red was quite low. However, once the concentration of the oligomers reached a certain point, a rather sharp increase in emission intensity was observed. This onset point is taken to be the onset of hydrophobicity-driven aggregation, which is estimated to be the critical aggregation concentration (CAC) of these oligomers. As shown in Table 2.1, with DP increasing from 1 to 13, the CAC values of these oligomers vary from 75 μM to 0.58 μM (Figure 3.2). In general, oligomers with higher DP tend to aggregate at lower concentrations, despite the fact that the HLB of all

Table 3.1. Summary of oligomer assembly characterizations including critical aggregation concentration and assembly size.

Oligomer	m	n	M_w (kDa)	CAC (μM)	Size (nm)
2-EG5	1	5	1594	66	240
3-EG5	2	5	2392	7.8	192
4-EG5	3	5	3189	2.0	310
5-EG5	4	5	3986	0.74	184
P-EG5	13	5	11162	0.58	97
2-EG8	1	8	1858	75	208
3-EG8	2	8	2789	8.3	127
4-EG8	3	8	3716	3.8	202
5-EG8	4	8	4647	0.95	125

these oligomers are identical. At same DP, the systems with longer ethylene glycol chains as hydrophilic moiety exhibited higher CAC values.

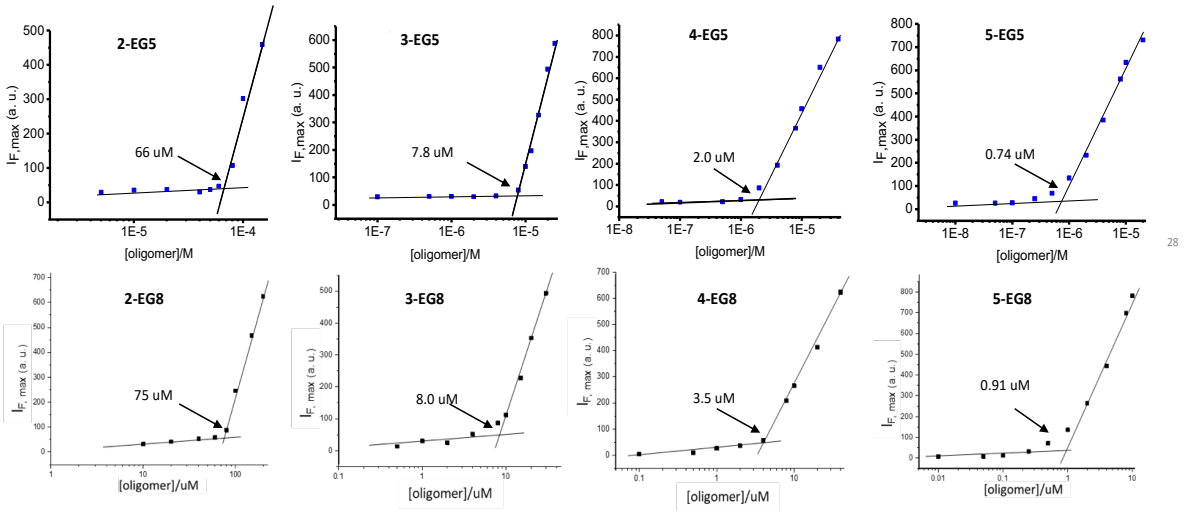

Figure 3.2 Critical aggregation concentration (CAC) of oligomeric assemblies.

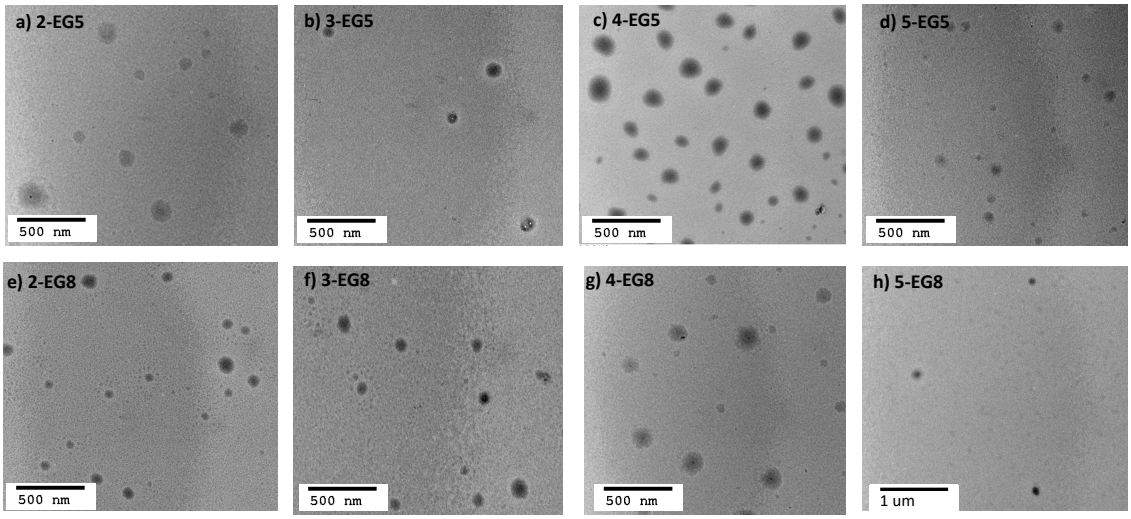

Figure 3.3 TEM images of oligomeric assemblies.

The solution phase sizes of these nanoassemblies were then measured by dynamic light scattering (DLS) at a concentration above their CACs. We observed an average hydrodynamic diameter ranging from ~100-300 nm for these assemblies (Table 3.1). The spherical morphology and size of these assemblies were further ascertained using transmission electron microscopy (TEM), as shown in Figure 3.3.

3.2.3 Covalently attached guest molecule release in presence of enzyme

Note that we hypothesized that if the HLB of the oligomers were kept constant, then higher DP oligomeric amphiphiles would be hydrolyzed by enzyme at a slower rate than their lower DP counterparts. To test this, we first measured the enzymatic cleavage rates of all oligomers. Since the enzymatic reaction releases the fluorescent byproduct, 4-methylumbelliferone, we were able to monitor the cleavage rates spectroscopically. For an accurate comparison, it is necessary that all these oligomer solutions are not only prepared at concentrations above their respective CACs, but also contain the same concentration of the substrate functionalities, regardless of their DP. To meet these two criteria, we prepared oligomer solutions that contain 200 μM enzyme substrates (based on coumarin), *i.e.* 100 μM dimer, 66.7 μM trimer, 50 μM tetramer, and 40 μM pentamer, and then treated with 60 nM esterase. As shown in Figure 3.4, a clear trend of the enzymatic reaction rate was observed for these oligomers with PEG as hydrophilic moieties, amphiphile **2-EG5** exhibited the fastest enzymatic rate over 48 hours, systematically followed by **3-EG5**, **4-EG5** and **5- EG5**. Moreover, when the same concentrations of enzyme and the substrate were used in the case of the 14-mer **P-EG5**, the molecular weight of which is comparable to polymers, little hydrolysis was observed from the emission spectra. These results are consistent with our hypothesis that the higher DP would result in slower enzymatic reaction rate, which in turn provides a convenient handle to tune reaction rates of enzymes and the resultant release of the covalently bound molecules.

When same experiments were performed with the second series of oligomers (the EG8 series) that contain longer ethylene glycol chains as the hydrophilic group, a similar trend was indeed observed, *i.e.* hydrolysis rate decreases for oligomers with higher DP. These

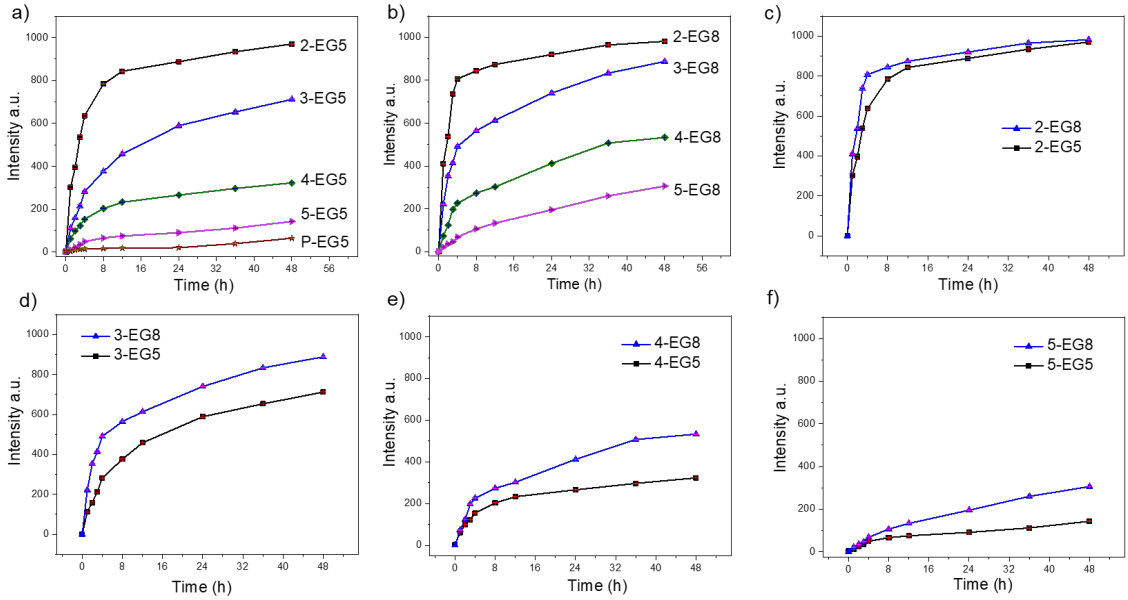

Figure 3.4. Enzymatic hydrolysis of oligomeric assemblies based on coumarin release a) oligomer assemblies with EG5 as hydrophilic moiety, b) oligomer assemblies with EG8 as hydrophilic moiety, enzymatic hydrolysis comparison between oligomer-EG5 and corresponding oligomer-EG8 c) - f).

results again confirmed our hypothesis that amphiphiles with higher DP are less accessible to enzyme and thus more stable compared with oligomers with lower DP. Meanwhile, comparison of the two series of oligomers also allows us to evaluate HLB effects on the enzymatic hydrolysis rates of these oligomers. Note that the basis for our hypothesis that the degree of oligomerization would causes slower reaction rate is that the dynamics of the unimer-aggregate equilibrium would be slower at higher DP. The results above support this hypothesis. If this were true, then it should also follow that if the hydrophilicity of these oligomers changes, the dynamics of the unimer-aggregate equilibrium would also be affected, which would in turn alter the sensitivity of these oligomers to enzyme. To test this idea, we compared the hydrolysis rates of EG5 oligomers and EG8 oligomers under the same experimental conditions. Interestingly, we observed that the cleavage rate of the covalently attached molecules from **2-EG5** and **2-EG8** were very similar (Figure 3.4c).

However, when the DP increases to trimeric or higher, **n-EG8** oligomers with longer ethylene glycol chains indeed consistently exhibited faster cleavage, compared to their corresponding **n-EG5** oligomers with shorter PEG chains (Figure 3.4d-f). These results suggest that lowering hydrophilicity of oligomers will make them more stable in presence of esterase. This is reasonably expected, because increase in hydrophilicity is expected to increase the dynamics in the unimer-aggregate equilibrium, which facilitates enzyme's access to its substrate functionalities. We attribute the lack of significant difference between **2-EG5** and **2-EG8** assemblies to the fact that these low order oligomers are already sufficiently dynamic, such that there is no significant advantage to increasing the hydrophilicity of the oligomeric amphiphile from EG5 to EG8.

3.2.4 Non-covalent guest molecule release in presence of enzyme

Next, we were interested in evaluating the effect of the enzyme-induced change in the HLB of the amphiphiles upon their host characteristics for hydrohobic guest molecules. We were especially interested in identifying whether this anticipated molecular release event will follow a DP- and hydrophilicity- dependent trend observed in the covalent modification of the amphiphile. To test these, we encapsulated a hydrophobic fluorophore, 1,1'-dioctadecyl-3,3,3',3'-tetramethylindocarbocyanine (DiI), into these assemblies. The DiI-encapsulated oligomeric assemblies were treated with the esterase and the molecular release was assessed by fluorescence change. A change in fluorescence is anticipated in this case, because DiI molecule is insoluble in aqueous solutions and therefore precipitates out of solution, upon release from the hydrophobic pockets of these amphiphilic assemblies. As with the experiments above, the concentration of esterase and the substrate

functionalities in the oligomers were maintained for appropriate comparison of the relative rates of molecular release.

Indeed, we found that the guest release depends on the DP of oligomers at constant HLB of the molecule, *i.e.* within the same oligomer series (EG5 or EG8 series). That is, assemblies from higher order oligomers exhibit the ability to more stably encapsulate the guest molecules and responds to the enzyme much more slowly, compared to the lower order oligomers (Figure 3.5). Also, assemblies with longer ethylene glycol chains can release guest molecules much faster at the same time range (Figure 3.5, 3.6). These results show that a precise control over the release kinetics of non-covalently encapsulated guest molecules can also be achieved by tuning the molecular structures.

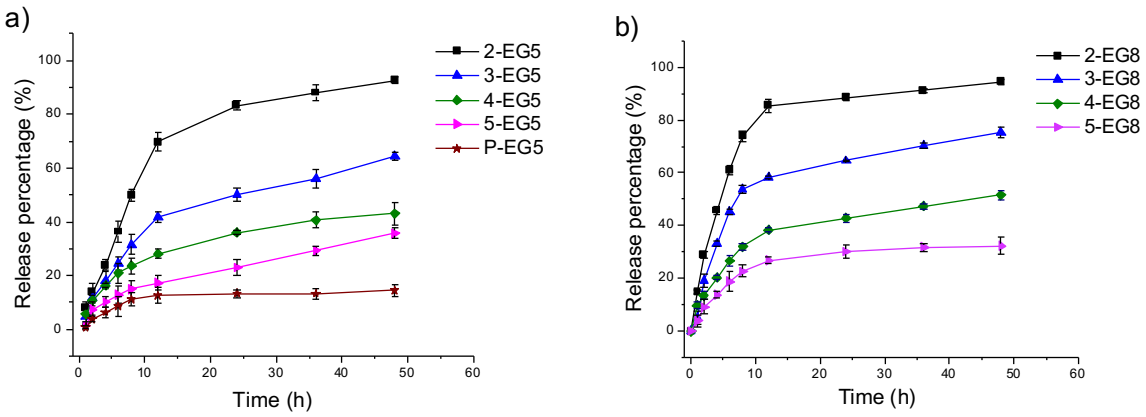

Figure 3.5. Non-covalent guest (DiI) release from nanoassemblies.

Comparison of data for the covalent molecular release based on the enzymatic cleavage of the substrate functionalities and the release of the non-covalently bound guest molecules revealed that the latter process lags behind the former process. The potential reason behind this difference is that the enzymatic cleavage of the covalently attached guest molecules happens first, which is followed by the loss in capability of the amphiphilic assemblies to hold the guest molecules to cause molecular release. In this scenario, the intermediate states

of the aggregated assemblies generated by the enzymatic reaction (*e.g.* only one of the coumarin moieties cleaved in a pentameric amphiphile) also can bind to guest molecules, but their relative ability to act as a host might be lower. This process in conjunction with the need for a critical concentration of DiI to cause its precipitation likely manifests itself as the lag in the non-covalent guest release, relative to the covalent modification of the oligomers by the enzyme.

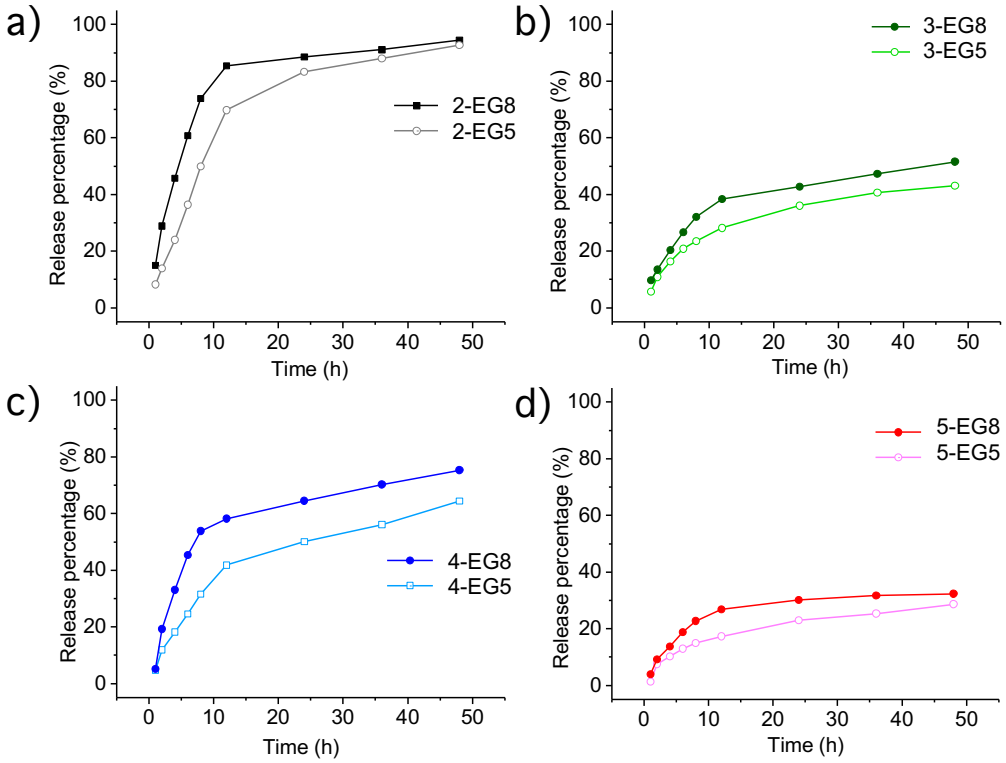

Figure 3.6. Comparison of non-covalent guest release kinetics between oligomer-PEG and oligomer-OEG.

3.2.5 Assembly size transformation in response to enzyme

Since the enzymatic cleavage of hydrophobic groups seems to be the primary reason for assemblies to lose their stability and capability to hold guest molecules, it is likely that this enzyme reaction induces morphological changes of the aggregated assemblies. To test this

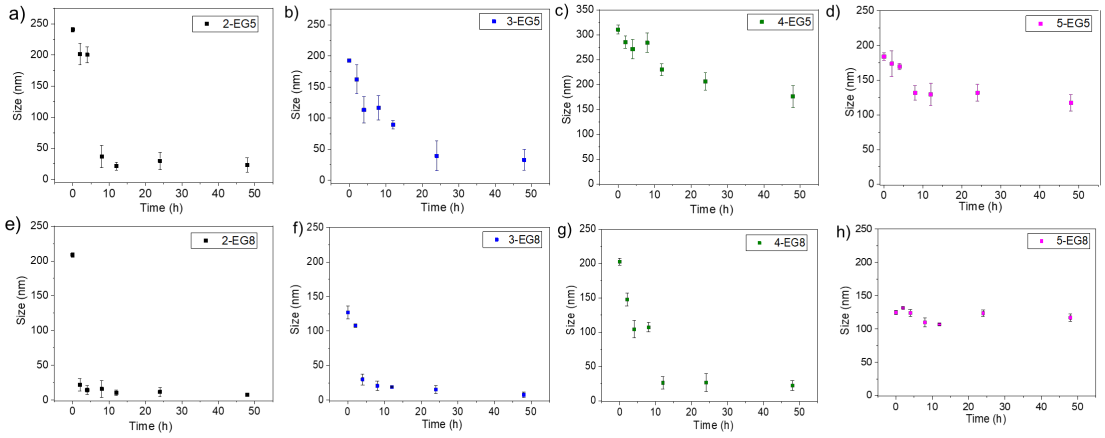

Figure 3.7. Size evolution of assemblies in presence of esterase in 48 hours.

possibility, we monitored the temporal evolution of the size of these assemblies by DLS. We found that the size of assemblies change immediately after esterase was introduced to these systems. As shown in Figure 3.7, both **2-EG5** and **3-EG5** completely disassembled in presence of enzyme: the size of assembly **2-EG5** sharply decreased from ~240 nm to ~20 nm, while assembly **3-EG5** formed a ~35 nm assembly from an initial size of ~220 nm in 48 hours, this size change was also confirmed by TEM images which showed clear spherical structures initially but little visible aggregates after 48 hours of enzymatic reactions. However, the size of oligomers **4-EG5** and **5-EG5** remained relatively unchanged over the same timeframe. Furthermore, a similar trend of assembly size change was observed for **n-EG8** oligomers with longer EG chains at same experimental conditions. While **4-EG8** and **5-EG8** were rather more stable in presence of enzyme, both **2-EG8** and **3-EG8** completely disassembled in presence of enzyme at a faster rate compared with corresponding n-EG5 oligomers, respectively. These results suggested that enzymatic cleavage can induce the disassembly process. Also, both DP and HLB variations of oligomeric amphiphiles can alter the disassembly kinetics, which correlate well with the

guest release profiles of both covalently bound and non-covalently bound hydrophobic molecules.

3.3 Summary

To summarize, two series of oligomeric amphiphiles were prepared to evaluate the possibility of tuning enzyme-induced changes in their self-assembly properties and host-guest characteristics. We have shown that: (*i*) when the degree of oligomerization increases in the amphiphiles, the enzymatic reaction rate decreases. This offers a straightforward opportunity to tune the release kinetics of covalently-appended guest molecules. (*ii*) This reaction kinetics can also be tuned by varying the hydrophilic-lipophilic balance of the self-assembling substrate molecule itself, where increase hydrophilicity accelerates the molecular release rates. (*iii*) In the assemblies where the enzyme-induced alteration in HLB occurs at a reasonable rate, *i.e.* in lower order oligomers, a significant change in size and morphology of the assemblies were also observed. (*iv*) Non-covalently bound guest molecules can also be released from these amphiphilic assemblies in response to the enzyme-induced alteration in HLB, the trends of which closely follows those observed in the release of the covalently bound guest molecules. The trends in the enzymatic reaction rates and the change in the host-guest characteristics can be understood by correlating structural variations to change in the dynamics of unimer-aggregate equilibrium. Factors that lead to faster unimer-aggregate equilibrium dynamics lead to faster enzymatic response. Overall, this study provides two simple and straightforward approaches to altering enzyme-induced changes in amphiphilic assemblies, which in turn offer tunability in the release kinetics of covalently and non-covalently bound guest molecules from these assemblies. The findings presented here could provide a basis for designing enzyme

responsive materials with controlled release capabilities in materials and biomedical applications.

3.4 Experimental procedures

3.4.1 General Methods

All the reagents were from commercial source and used as received. ^{1}H NMR and ^{13}C NMR spectra were recorded on a Bruker DPX-400 MHz NMR spectrometer using the residual proton resonance of the solvent as the internal standard. All molecules without characterization data mentioned below were synthesized through well-established synthesis procedures previously reported by our group.[30-32] UV-vis absorption spectra were obtained by a Carry 100 Scan spectrometer. Fluorescence spectra were recorded on a PerkinElmer LS 55 spectrofluorimeter. Mass spectrometric data were collected by Capillary LC (Thermo Dionex Ultimate 3000)-ESI-MS (Bruker AmaZon quadrupole ion trap).

For the DLS measurements, the sizes of each solution were recorded overtime by a Malvern Nanozetasizer ZS90 with a 637-nm laser source with non-invasive backscattering technology detected at 173^{o} using disposable sizing cuvette.

The same sample for DLS measurement was dropped onto carbon-coated copper grid. The grid was dried by slow evaporation in air, and then dry separately in a vacuum overnight. Images were recorded on a JEOL-2000FX electron microscopy operated at 200 kV and at a nominal magnification of 5000X. At least 10 locations on the TEM grid were examined.

A stock solution (1 mM) of oligomer micelle was prepared was diluted into various solutions of different concentrations. The concentration range of polymer was maintained

from 0.2 mM to 0.001 mM. Nile Red was encapsulated to the micelle by adding 10 μL of Nile Red stock solution (20 μM in acetone). All the micelle solutions were kept uncapped overnight to evaporate the acetone. Then emission spectrum was recorded for each solution and emission maxima of each spectrum were plotted as a function of the concentration of each oligomer. The inflection point of the plot was taken as CAC of each oligomer.

For DiI encapsulation, oligomeric amphiphile solutions in phosphate buffer were stirred at room temperature and DiI stock solution (1 mg/mL in acetone, 5 wt% to oligomers) was added in each solution. The solutions were stirred for 8 h in room temperature, open to the atmosphere allowing the organic solvent to evaporate, and then filtered through hydrophilic membranes with pore size of 0.45 μm to remove unencapsulated DiI.

For guest release study, DiI-encapsulated oligomeric amphiphile solutions (50 μM) were treated with esterase. The absorption spectra of DiI were recorded overtime.

The % release of DiI was calculated by using the following equations:

% Release of DiI = $(I_t-I_0)/I_t*100$

Where I_0 =the highest absorbance of DiI

I_t = the highest absorbance of DiI at each time point

3.4.2. Synthetic procedures

General procedures for synthesis of molecule **b**: Oligoamine (1 eq.) was dissolved in dry tetrahydrofuran (THF), trienthylamine (2 eq. for 1 amine group) was added to the solution and stirred for 15 minutes at 0°C. A solution of benzoyl chloride molecule **1a** (1.2eq for one amine group) in THF was added to the mixture dropwise and then stirred at room temperature overnight. Solvent was evaporated and then redissolved in dichloromethane,

then washed with water for three times. The organic layer was dried over Na_2SO_4 and evaporated to dryness. The crude product was purified by silica gel column chromatography.

General procedures for synthesis oligomers: The mixture of oligomeric acetylene compound **b** (1.0 eq.), azide **1c** (2 eq. for 1 acetylene group), $CuSO_4{\cdot}5H_2O$ (0.5 eq.) and sodium ascorbate (0.5 eq.) in THF/H_2O (1:1) solvent mixture was heated at 50 ^oC for 24 h. The reaction progress was monitored by TLC. After completion of the reaction, the reaction mixture was partitioned between ethyl acetate and saturated aqueous NH_4Cl solution. The aqueous layer was extracted twice with ethyl acetate and the combined organic layer was dried over Na_2SO_4 and evaporated to dryness. The crude product was purified by silica gel column chromatography.

3.4.3 Characterizations for oligomers

2-EG5: Yield: 94%. ^{1}H NMR (400 MHz, $CDCl_3$, TMS): δ (ppm) 7.63 (s, 2H), 7.55 (d, J = 8.8 Hz, 2H), 6.99-6.94 (m, 4H), 6.59-6.55 (m, 6H), 6.17 (s, 2H), 5.80 (s, 4H), 5.15 (s, 2H), 5.01 (s, 2H), 4.27 (t, J = 5 Hz, 4H), 4.01-3.54 (m, 40H), 3.36 (s, 6H), 3.05 (s, 4H), 2.41-2.35 (m,10H), 1.89 (m, 4H), 1.63 (m,8H), 1.33 (m, 4H). ^{13}C NMR (100 MHz, $CDCl_3$) δ (ppm) 171.98, 171.36, 160.92, 159.43, 154.89, 152.37, 138.18, 125.92, 115.18, 113.18, 112.95, 105.89, 105.53, 103.38, 84.70, 71.91, 70.73, 70.56, 70.54, 70.48, 69.52, 67.63, 61.82, 59.01, 44.51, 37.92, 33.68, 29.79, 25.86, 23.90, 18.70. MALDI-ToF m/z 1618.593 ($C_{80}H_{106}N_8O_{26}$+Na^+ requires 1617.738).

3-EG5: Yield: 90%. ^{1}H NMR (400 MHz, $CDCl_3$, TMS): δ (ppm) 7.69-7.64 (m, 3H), 7.55 (d, J = 8.8 Hz, 3H), 6.98-6.94 (m, 6H), 6.56-6.52 (m, 9H), 6.17 (s, 3H), 5.80 (s, 6H), 5.18-4.92 (m, 6H), 4.31-4.27 (m, 6H), 4.12-3.52 (m, 62H), 3.36 (s, 9H), 3.05-2.99 (d, J = 13.6

Hz, 3H), 2.65 (s, 3H), 2.40-2.38 (m, 15H), 1.89 (m, 6H), 1.63 (m, 12H), 1.33 (m, 6H). ^{13}C NMR (100 MHz, $CDCl_3$) δ (ppm) 171.97, 160.90, 160.03, 159.87, 159.40, 159.23, 154.84, 152.42, 137.67, 125.93, 115.15, 113.16, 112.88, 105.51, 103.34, 84.67, 71.86, 70.68, 70.50, 70.43, 69.47, 67.71, 61.91, 58.97, 50.33, 33.65, 29.74, 25.84, 23.87, 18.68. MALDI-ToF m/z 2414.982 ($C_{120}H_{158}N_{12}O_{39}$+$Na^+$ requires 2414.107).

4-EG5: Yield: 76%. ^{1}H NMR (400 MHz, $CDCl_3$, TMS): δ (ppm) 7.72 (m, 4H), 7.55 (d, *J* = 4.4 Hz, 4H), 7.01-6.94 (m, 8H), 6.59-6.53 (m, 12H), 6.19 (s, 4H), 5.80 (s, 8H), 5.31-5.02 (m, 8H), 4.32 (m, 8H), 4.13-3.54 (m, 80H), 3.37 (s, 12H), 3.05 (m, 4H), 2.64 (m, 3H)2.42-2.39 (m,20H), 1.89 (m, 8H), 1.71 (m, 16H), 1.33 (m, 8H). ^{13}C NMR (100 MHz, $CDCl_3$) δ (ppm) 171.99, 160.91, 159.86, 154.86, 152.41, 125.93, 115.16, 113.16, 112.90, 103.36, 103.17, 84.68, 71.88, 70.68, 70.59, 69.48, 67.59, 58.99, 50.07, 33.87, 29.80, 25.83, 23.89, 18.69. MALDI-ToF m/z 3211.185 ($C_{160}H_{210}N_{16}O_{52}$+$Na^+$ requires 3210.476).

5-EG5: Yield: 78%. ^{1}H NMR (400 MHz, $CDCl_3$, TMS): δ (ppm) 7.73 (m, 5H), 7.53 (d, *J* = 4.2 Hz, 5H), 6.97-6.94 (m, 10H), 6.52 (m, 15H), 6.16 (s, 5H), 5.80 (s, 10H), 5.29-4.95 (m, 10H), 4.29 (m, 10H), 4.13-3.54 (m, 128H), 3.37 (s, 15H), 2.96(m, 4H), 2.61 (m, 4H), 2.39-2.36 (m,25H), 1.89 (m, 10H), 1.68 (m, 20H), 1.34 (m, 10H). ^{13}C NMR (100 MHz, $CDCl_3$) δ (ppm) 171.99, 160.90, 160.05, 159.42, 154.85, 152.42, 137.73, 125.96, 115.15, 113.16, 112.89, 105.85, 103.37, 84.75, 71.88, 70.50, 69.50, 67.72, 58.99, 33.68, 29.67, 25.99, 23.89, 18.71. MALDI-ToF m/z 4007.328 ($C_{200}H_{262}N_{20}O_{65}$+$Na^+$ requires 4006.845).

P-EG5: Yield: 80%. ^{1}H NMR (400 MHz, $CDCl_3$, TMS): δ (ppm) 7.71, 7.53, 6.94, 6.45, 6.13, 5.78, 5.07, 4.91, 4.25, 3.60-3.33, 2.38, 1.83, 1.62, 1.31. ^{13}C NMR (100 MHz, $CDCl_3$) δ (ppm) 172.02, 160.87, 159.98, 159.44, 154.83, 152.50, 137.69, 126.04, 115.12, 113.10,

112.83, 105.15, 103.38, 84.71, 71.87, 70.46, 70.45, 62.32, 67.57, 58.97, 49.92, 33.66, 29.82, 25.83, 23.89, 18.69. THF GPC: Mw 12 kDa, PDI 1.08.

2-EG8: Yield: 92%. ^{1}H NMR (400 MHz, $CDCl_3$, TMS): δ (ppm) 7.63 (s, 2H), 7.54 (d, *J* = 4.4 Hz, 2H), 6.95 (m, 4H), 6.59-6.52 (m, 6H), 6.17 (s, 2H), 5.80 (s, 4H), 5.15 (s, 2H), 5.01 (s, 2H), 4.28 (t, J = 3.6 Hz, 4H), 4.11-3.53 (m, 60H), 3.36 (s, 6H), 3.05 (s, 3H), 2.71(s, 2H), 2.41-2.37 (m,10H), 1.89 (m, 4H), 1.69 (m, 8H), 1.33 (m, 4H). ^{13}C NMR (100 MHz, $CDCl_3$) δ (ppm) 171.98, 160.92, 159.91, 159.42, 154.87, 152.39, 138.16, 125.92, 123.11, 115.17, 113.17, 112.92, 105.86, 105.51, 103.36, 103.21, 84.67, 71.90, 70.70, 70.52, 70.46, 69. 50, 67.60, 61.96, 59.01, 49.99, 33.67, 29.84, 29.68, 25.80, 23.89, 18.69. MALDI-ToF m/z 1882. 356 ($C_{92}H_{130}N_8O_{32}$+Na^+ requires 1881.879).

3-EG8: Yield:69%. ^{1}H NMR (400 MHz, $CDCl_3$, TMS):δ (ppm) 7.69-7.67 (m, 3H), 7.55 (d, *J* = 4.4 Hz, 3H), 6.98-6.95 (m, 6H), 6.56-6.51 (m, 9H), 6.17 (s, 3H), 5.80 (s, 6H), 5.18-4.92 (m, 6H), 4.29 (m, 6H), 4.12-3.52 (m, 98H), 3.36 (s, 9H), 3.05-2.99 (d, J = 13.2 Hz, 3H), 2.65 (s, 3H), 2.40-2.35 (m, 15H), 1.89 (m, 6H), 1.63 (m, 12H), 1.34 (m, 6H).^{13}C NMR (100 MHz, $CDCl_3$) δ (ppm) 171.96, 160.90, 160.04, 159.40, 154.84, 152.41, 137.91, 125.93, 115.15, 113.16, 112.88, 105.86, 103.34, 84.67, 71.87, 70.68, 70.49, 69.48, 67.69, 61.86, 58.98, 50.23, 33.65, 29.76, 25.82, 23.87, 18.68. MALDI-ToF m/z 2810.593 ($C_{138}H_{194}N_{12}O_{48}$+$Na^+$ requires 2810.342).

4-EG8: Yield: 77%. ^{1}H NMR (400 MHz, $CDCl_3$, TMS): δ (ppm) 7.69 (m, 4H), 7.53-7.51 (d, *J* = 4.2 Hz, 4H), 6.96-6.93 (m, 8H), 6.53-6.50 (m, 12H), 6.15 (s, 4H), 5.79 (s, 8H), 5.01-4.95 (m, 8H), 4.27 (m, 8H), 4.13-3.54 (m, 120H), 3.36 (s, 12H), 2.97 (s, 3H), 2.71-2.58 (m, 3H), 2.39-2.34 (m, 20H), 1.89 (m, 8H), 1.65 (m, 16H), 1.33 (m, 8H). ^{13}C NMR (100 MHz, $CDCl_3$) δ (ppm) 172.07, 160.86, 160.05, 159.86, 154.85, 152.40, 137.67, 125.95, 115.14,

113.14, 112.88, 105.48, 103.35, 84.69, 71.88, 70.68, 70.50, 69.50, 67.71, 59.00, 53.51, 46.06, 33.91, 29.66, 26.06, 25.88, 18.69. MALDI-ToF m/z 3738.234 ($C_{184}H_{258}N_{16}O_{64}$+$Na^+$ requires 3738.788).

5-EG8: Yield: 82%. ^{1}H NMR (400 MHz, $CDCl_3$, TMS): δ (ppm) 7.73 (m, 5H), 7.55-7.53 (d, *J* = 4.2 Hz, 5H), 7.00-6.95 (m, 10H), 6.51 (m, 15H), 6.16 (s, 5H), 5.80 (s, 10H), 5.19-4.96 (m, 10H), 4.29 (m, 10H), 4.08-3.51 (m, 166H), 3.36 (s, 15H), 2.96(m, 3H), 2.61 (m, 3H), 2.40 (m,25H), 1.88 (m, 10H), 1.65 (m, 20H), 1.31 (m, 10H). ^{13}C NMR (100 MHz, $CDCl_3$) δ (ppm) 172.01, 160.92, 160.07, 159.44, 154.87, 152.43, 125.97, 115.17, 113.18, 112.91, 106.20, 103.39, 84.75, 71.90, 70.52, 69.52, 67.61, 59.02, 33.70, 29.69, 25.95, 23.91, 18.73. MALDI-ToF m/z 4667.821. ($C_{230}H_{322}N_{20}O_{80}$+$Na^+$ requires 4667.235).

3.5 References

1. I. Schomburg, A. Chang, S. Placzek, C. Söhngen, M. Rother, M. Lang, C. Munaretto, S. Ulas, M. Stelzer, A. Grote, M. Scheer and D. Schomburg, *Nucleic Acids Res.*, 2013, **41**, D764–D772.
2. S. M. Dhanasekaran, T. R. Barrette, D. Ghosh, R. Shah, S. Varambally, K. Kurachi, K. J. Pienta, M. A. Rubin and A. M. Chinnaiyan, *Nature*, 2001, **412**, 822.
3. P. Imming, C. Sinning and A. Meyer, *Nat. Rev. Drug Discov.*, 2006, **5**, 821.
4. H. Sato, T. Takino, Y. Okada, J. Cao, A. Shinagawa, E. Yamamoto and M. Seiki, *Nature*, 1994, **370**, 61.
5. J. Zhou, G. Yu and F. Huang, *Chem. Soc. Rev.*, 2017, **46**, 7021–7053.
6. X. Ma and Y. Zhao, *Chem. Rev.*, 2015, **115**, 7794–7839.
7. L. You, D. Zha and E. V Anslyn, *Chem. Rev.*, 2015, **115**, 7840–7892.
8. Y. Wang, K. Zhou, G. Huang, C. Hensley, X. Huang, X. Ma, T. Zhao, B. D. Sumer, R. J. DeBerardinis and J. Gao, *Nat. Mater.*, 2013, **13**, 204.
9. D.-E. Lee, H. Koo, I.-C. Sun, J. H. Ryu, K. Kim and I. C. Kwon, *Chem. Soc. Rev.*, 2012, **41**, 2656–2672.
10. A. P. Blum, J. K. Kammeyer, A. M. Rush, C. E. Callmann, M. E. Hahn and N. C. Gianneschi, *J. Am. Chem. Soc.*, 2015, **137**, 2140–2154.
11. M. Molina, M. Asadian-Birjand, J. Balach, J. Bergueiro, E. Miceli and M. Calderón, *Chem. Soc. Rev.*, 2015, **44**, 6161–6186.
12. J. Gao, B. Zhao, M. Wang, M. A. C. Serrano, J. Zhuang, M. Ray, V. M. Rotello, R. W. Vachet and S. Thayumanavan, *J. Am. Chem. Soc.*, 2018, **140**, 2421–2425.
13. M. Zelzer, S. J. Todd, A. R. Hirst, T. O. McDonald and R. V Ulijn, *Biomater. Sci.*,

2013, **1**, 11–39.

14. A. B. Lowe, *Polymer (Guildf).*, 2014, **55**, 5517–5549.
15. L. M. Randolph, M.-P. Chien and N. C. Gianneschi, *Chem. Sci.*, 2012, **3**, 1363–1380.
16. S. Mura, J. Nicolas and P. Couvreur, *Nat. Mater.*, 2013, **12**, 991.
17. S. Goggins, B. J. Marsh, A. T. Lubben and C. G. Frost, *Chem. Sci.*, 2015, **6**, 4978–4985.
18. A. Bernardos, E. Aznar, M. D. Marcos, R. Mart\'\inez-Máñez, F. Sancenón, J. Soto, J. M. Barat and P. Amorós, *Angew. Chemie*, 2009, **121**, 5998–6001.
19. X. Xu, M. S. Han and C. A. Mirkin, *Angew. Chemie*, 2007, **119**, 3538–3540.
20. Y. Xiao, F. Patolsky, E. Katz, J. F. Hainfeld and I. Willner, *Science (80-.).*, 2003, **299**, 1877–1881.
21. J.-H. Kang, D. Asai, J.-H. Kim, T. Mori, R. Toita, T. Tomiyama, Y. Asami, J. Oishi, Y. T. Sato, T. Niidome and others, *J. Am. Chem. Soc.*, 2008, **130**, 14906–14907.
22. R. V Ulijn, *J. Mater. Chem.*, 2006, **16**, 2217–2225.
23. Y. Li, G. Liu, X. Wang, J. Hu and S. Liu, *Angew. Chemie Int. Ed.*, 2016, **55**, 1760–1764.
24. A. J. Harnoy, I. Rosenbaum, E. Tirosh, Y. Ebenstein, R. Shaharabani, R. Beck and R. J. Amir, *J. Am. Chem. Soc.*, 2014, **136**, 7531–7534.
25. M. A. Azagarsamy, P. Sokkalingam and S. Thayumanavan, *J. Am. Chem. Soc.*, 2009, **131**, 14184–14185.
26. C. J. Hawker, K. L. Wooley and J. M. J. Frechet, *J. Chem. Soc. Perkin Trans. 1*, 1993, 1287–1297.
27. G. Fleischer, *J. Phys. Chem.*, 1993, **97**, 517–521.

28. G. R. Newkome, C. N. Moorefield, G. R. Baker, A. L. Johnson and R. K. Behera, *Angew. Chemie Int. Ed. English*, 1991, **30**, 1176–1178.

29. E. N. Savariar, S. V Aathimanikandan and S. Thayumanavan, *J. Am. Chem. Soc.*, 2006, **128**, 16224–16230.

30. F. Wang, A. Klaikherd and S. Thayumanavan, *J. Am. Chem. Soc.*, 2011, **133**, 13496–13503.

31. K. R. Raghupathi, U. Sridhar, K. Byrne, K. Raghupathi and S. Thayumanavan, *J. Am. Chem. Soc.*, 2015, **137**, 5308–5311.

32. K. R. Raghupathi, M. A. Azagarsamy and S. Thayumanavan, *Chem. Eur. J.*, 2011, **17**, 11752–11760.

CHAPTER 4

PERIPHERY FUNCTIONALIZABLE SELF-IMMOLATIVE NANOGEL FOR TARGET DELIVERY INTO CYTOSOL AND SUBCELLULAR ORGANELLES

4.1 Introduction

Nanoparticles as drug delivery vehicles have displayed huge potential to combat the implications that are always associated with traditional drug administration methods[1-2], such as fast clearance, poor solubility and off target effects. By delivering the exact dose of therapeutic drugs to a specific disease site, nanoparticles could level up the therapeutic efficiency and safety.[3-6] To date, various materials include dendrimers, polymers, gold nanoparticle, silica nanoparticle and liposome have been exploited towards either improving cargo loading efficiency, targeting capability or controlling the drug release.[7-14] Current challenges in this emerging field involve the design of nanoparticles displaying multiple features, and in particular, converging all these merits into one simple platform without compromising synthetic ease and attractive features. Self-immolative polymers provided an opportunity for programmed fragmentation and triggered release from peripheral functional groups, which could promote advanced drug delivery but require extensive synthesis.[15-20] Previously our group have introduced an emulsion-free method to prepare crosslinked nanogels which can sequester hydrophobic guest molecules in aqueous media and release them in response to a biologically relevant stimulus.[21-23] However, the post-functionalization through disulfide-exchange offers limited efficiency and could induce loss of encapsulation stability due to the cleavage of hydrophobic functional groups.

We envisaged that a periphery functionalizable self-immolative nanogel platform would be an ideal system for targeted drug delivery into cytosol or subcellular organelles (Figure

4.1). The primary requirements for this platform to meet are: 1) ease of synthesis, 2) high drug loading capacity, 3) fast triggerable release, 4) facile post-functionalization, 5) targeting capability. We hypothesized that incorporation of cross-linkable hydrophobic units in an amphiphilic polymer, with triggerable self-immolative feature, would generate nanoassemblies with capabilities to hold guest molecules and release them in response to an environmental stimulus. Meanwhile, introducing a reactive handle on the surface of nanogels would provide easy access to install various ligands for targeted delivery.

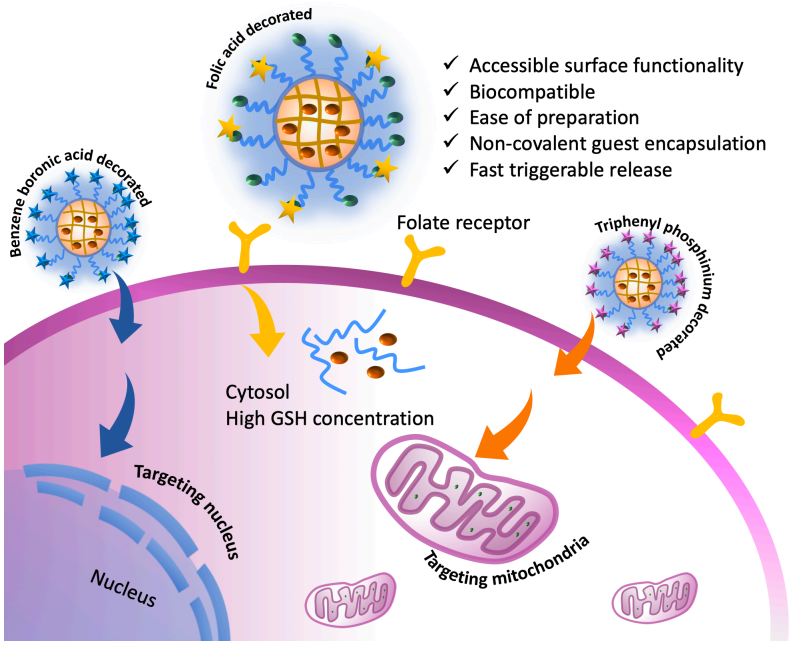

Figure 4.1. Illustration of functionalized nanogel for targeted delivery into cytosol and subcellular organelles.

4.2 Results and discussion

4.2.1 Molecular design and synthesis

To this end, an amphiphilic block copolymer **P1** that satisfies all the above requirements is synthesized through RAFT polymerization, which contains amine terminated polyethyleneglycol (PEG_{5000}) as the hydrophilic moiety and carbonate bridged pyridyl disulfide (PDS) as the hydrophobic moiety (Scheme 4.1). Polymers with varied repeating

units of PDS were synthesized for optimizaiton of drug loading (table 4.1). The key premise of this molecular design here is that once this polymer self-assembles, it will generate nanoparticles with a functionalizable surface with amine as the reactive handle, and a hydrophobic core that is crosslinkable and responsive to highly reductive intracellular environment. The cleavage of disulfide will further cleave the carbonate to make the polymer completely hydrophilic, which will benefit the payload release.

Scheme 4.1 Functional nanogel preparation illustration (a) and reaction scheme for polymer synthesis (b) and mechanism for redox triggered decrosslinking and self-immolation.

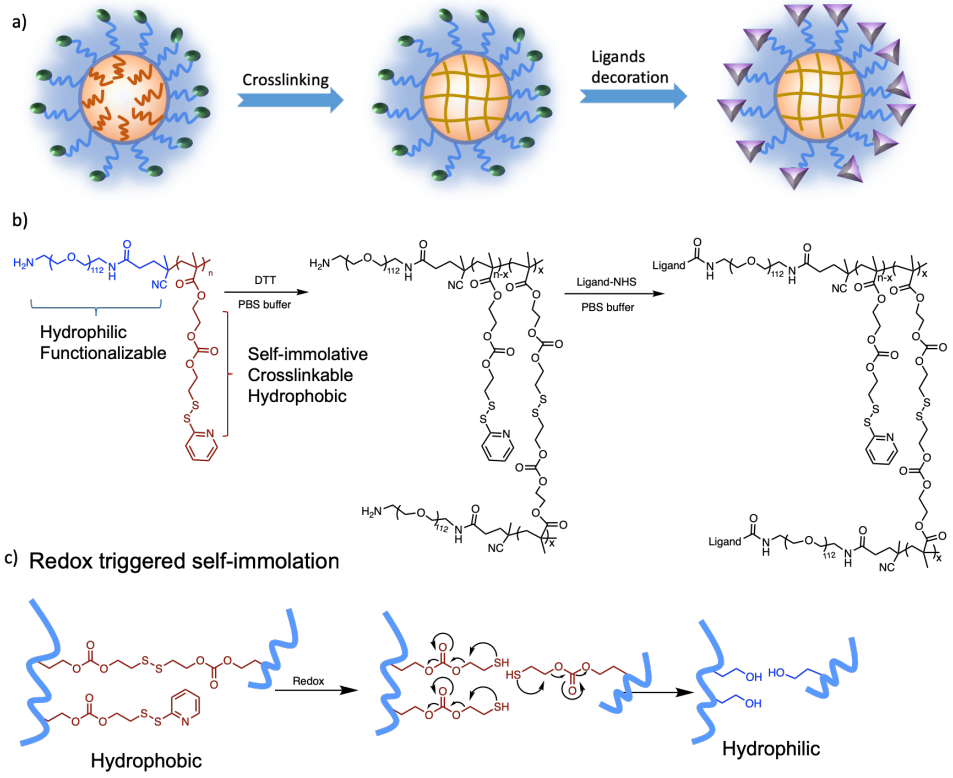

Table 4.1 Characterization data of polymers synthesized

PEG:PDS Ratio	Mn (kDa)	Mw (kDa)	Đ
1:10	11.1	12.7	1.15
1:20	13.6	13.9	1.02
1:30	13.1	15	1.14

4.2.2 Nanogel preparation and characterization

To test our design, polymer **P1** was distributed in phosphate buffer (10 mM, pH 7.4), nanoassemblies with a size ~105 nm was observed from dynamic light scattering (DLS) shown in Figure 4.2a. Following this step, addition of dithiothreitol (DTT) would induce the crosslinking of the nanoparticle core through cleavage of PDS groups and results in the formation of nanogels, the crosslinking density can be quantitatively determined by the pyridothione released. Size of the crosslinked nanogels is similar to the initial nanoaggregates (Figure 4.2a), the spherical morphology was also confirmed by transmission electron microscopy (TEM) as shown in Figure 4.2c. It is noteworthy that free thiol generated after PDS cleavage could potentially trigger the polymer self-immolation, which competes with the crosslinking reaction. After monitoring the crosslinking reaction with varied amount of DTT using NMR, we figured out that self-immolation of the polymer proceeded only when excess DTT (higher than 0.5 equivalence of PDS group) is present

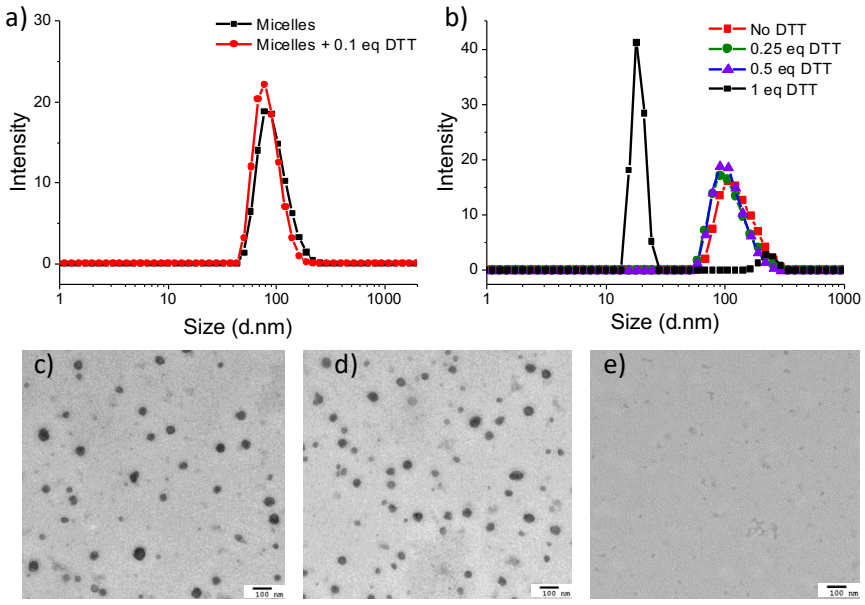

Figure 4.2. a) DLS profile of micelles before and after crosslinking by DTT, b) DLS profile of micelles treated with varied amount of DTT, TEM images of nanogels treated with varied amount of DTT c) 0.25 eq, d) 0.5 eq, e) 1eq, scale bar 100nm.

(Figure 4.3). This is further confirmed by monitoring the size of these assemblies with different concentration of DTT, as shown in figure 4.2b-e, deficient amount of DTT (less than 0.5 eq. of PDS group) resulted in a crosslinked nanogel that is similar in size to the micelles, while excess DTT would degrade the assemblies. The findings here equipped the nanogel with interesting features such as proper size, crosslinkable core and triggerable degradation.

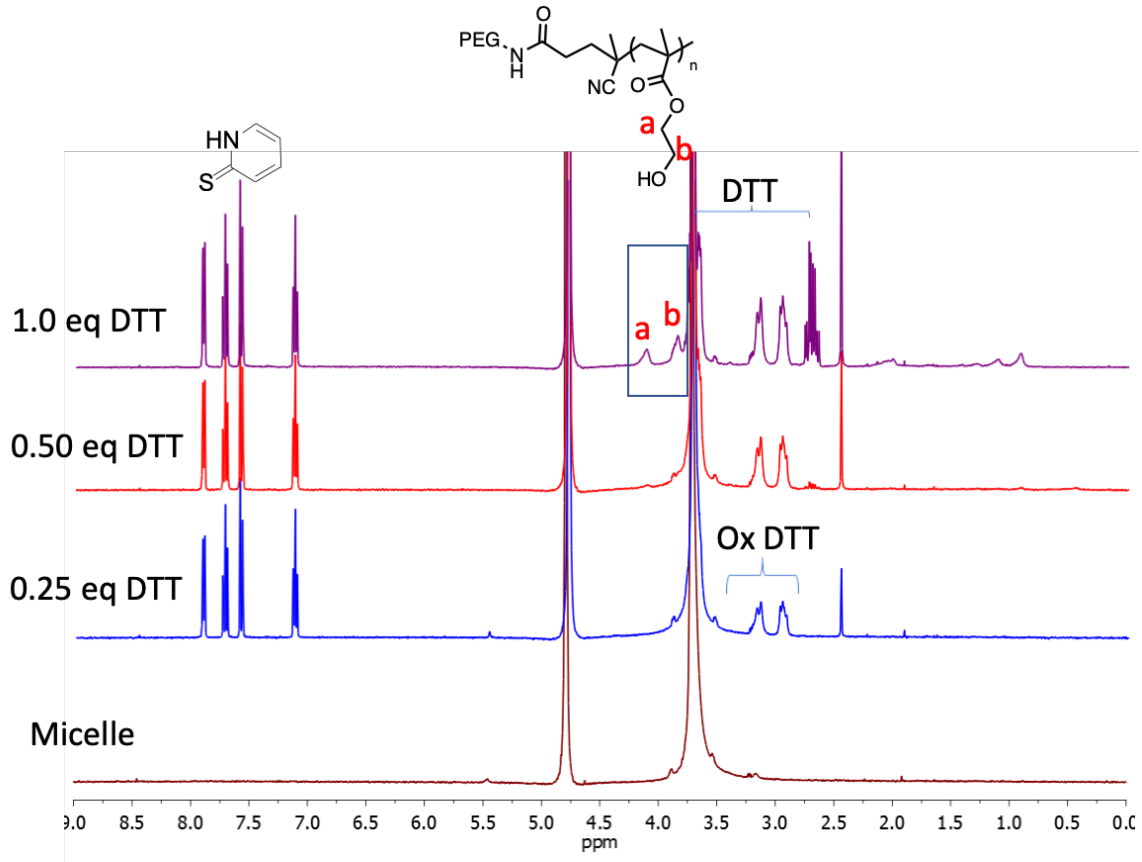

Figure 4.3. NMR of micelle solution in presence of different amount of DTT, peak a and b indicates the self-immolated polymer, which was only observed when excess amount of DTT (more than 0.5 eq.)was added.

We anticipated the amine functional group located at the terminus of hydrophilic PEG chain would present at the surface of the nanogel, which could provide free access to for independent post functionalization. This possibility was tested by adding fluoresceinamine,

an amine reactive fluorescent molecule, to the nanogel solution. Since fluoresceinamine itself is non-fluorescent in buffer, the strong emission peak generated from the nanogel solution suggested the successful covalent labeling reaction (Figure 4.4a). Surface zeta potential change from positive to negative also confirmed this post-modification event (Figure 4.4b).

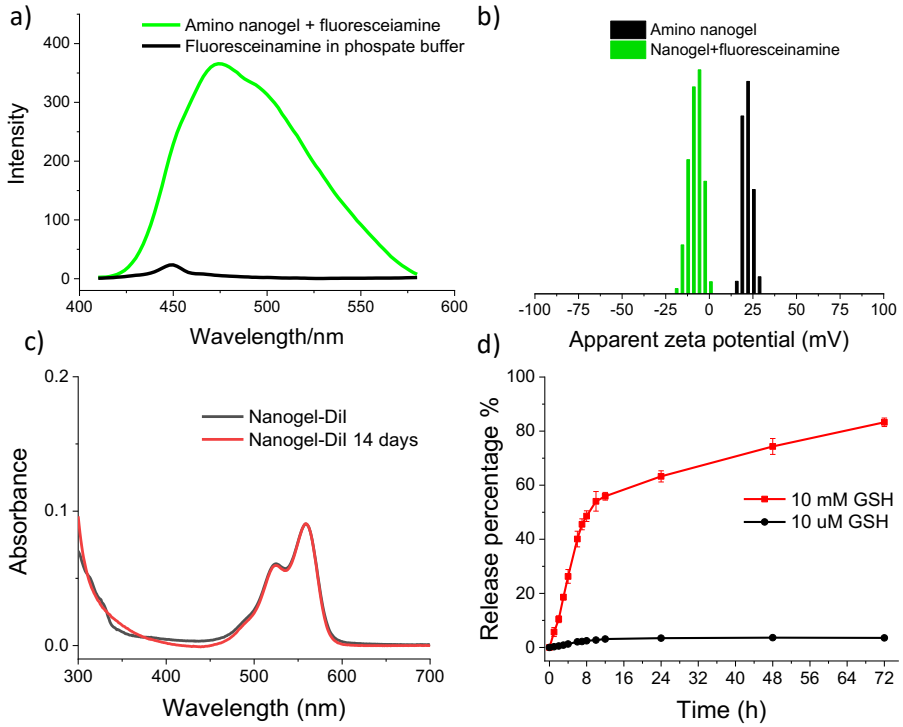

Figure 4.4 a) Emission spectrum of nanogel treated with fluoresceinamine, b) Zeta potential of nanogel before and after reaction with fluoresceinamine, c) Absorption of encapsulated DiI in nanogel for 1 day and 14 days, d) DiI release from the nanogel in presence of 10 mM/10 uM GSH.

The capability of encapsulating guest molecules was firstly evaluated with 1,1'-dioctadecyl-3,3,3'3'-tetramethyl-indocarbocyanine perchlorate (DiI). Encapsulation of DiI achieved over 96% loading efficiency and was found to be extremely stable in the crosslinked nanogel within two weeks, indicated by the characteristic absorption of DiI (Figure 4.4c). We are then interested to see whether the trapped guest molecules can be

released efficiently in response to a biologically relevant stimulus. We expected that glutathione (GSH), with millimolar concentration level in cytosol, would cleave the disulfide crosslinking and induce the release guest molecules. High concentration of GSH will also facilitate the self-immolation of the carbonate bond and result in huge decrease of the hydrophobicity of the nanogel, which could further promote the guest release. To test this, we treated the dye-loaded nanogel solutions with different concentrations of GSH (10 μM and10 mM, correspond to extra- and intra-cellular level GSH concentrations) and investigated their release profiles by tracing the decrease of the hydrophobic dye's absorption caused by its insolubility in aqueous media. The nanogel was able to hold most of the guest molecules at low GSH concentration, but at high GSH concentration, 83% of loaded cargo was released in 72 hours, which is much more efficient compare with previous reported system (Figure 4.4d).[21,24] Followed by these observations, two different chemotherapy drugs, paclitaxel (PTX) and doxorubicin (DOX), were encapsulated in the nanogel. By modifying the drug feeding ratio from 10 wt% to 30 wt%, crosslinking density from 10% to 30% and hydrophobic repeating units of polymer from 10 to 20, 24.3 wt % and 6.5 wt % loading capacity were achieved for PTX and DOX using polymer P1 with 20% crosslinking, respectively (Table 4.2).

Table 4.2. Optimization of drug loading capacity.

	Variations			Result: loading capacity	
Trial #	a. X-linking 10%, 20%, 30%	b. Drug feeding 10%, 20%, 30%	c. PEG:PDS ratio 1：10, 1：20	Doxorubicin	Paclitaxel
1	a1	b1	c1	2.9±0.13%	6.3±0.1%
2	a1	b2	c1	4.8±0.08%	10.2±0.21%
3	a1	b3	c1	5.5±0.12%	22.3±0.13%
4	a1	b1	c2	3.1±0.05%	6.2±0.08%
5	a1	b2	c2	4.4±0.11%	13.7±0.13%
6	a1	b3	c2	4.9±0.09%	23.7±0.12%
7	a2	b3	c1	6.5±0.07%	24.3±0.15%
8	a3	b3	c1	5.1±0.14%	21.1±0.22%

4.2.3 Cytosolic drug delivery

These nanogels themselves are nontoxic to cells such as 293T and MDA-MB-231 cells even at high concentrations, which provides the opportunity to act as drug delivery system (Figure 4.5). With these exciting features of this nanogel system, we are interested to explore the capability of this nanogel to deliver chemotherapeutic drugs into cytosol or even subcellular organelles in cancer cell lines. Folate receptors have been known to be overexpressed in malignant tumors[25-27], which hold potential for folate-based tumor imaging and drug delivery.[25,28] We envisaged that decoration the nanogel with folic acid could enhance the nanogel uptake in folate positive cells (Figure 4.6a). To test this, folic acid decorated nanogel (FA-Nanogel) was labeled with Cy3 dye to monitor cellular uptake in folate positive breast cancer cell MDA-MB-231 and folate negative cell HepG2. After 3 hours incubation, significant red fluorescence was observed in MDA-MB-231 cells using confocal laser scanning microscopy (CLSM), but limited fluorescence signal was found in HepG 2 cells, indicating folic acid could enhance the uptake towards FR positive cells (Figure 4.6b,c). Next, we evaluated cell viabilities of MDA-MB-231 cells with nanogels using MTT assay. Empty nanogels were barely toxic even at high concentrations, but the PTX loaded nanogel lower cell viabilities by 40% and FA-nanogel was found to be more efficient to induce cell death, suggesting PTX has been delivered into the cells efficiently.

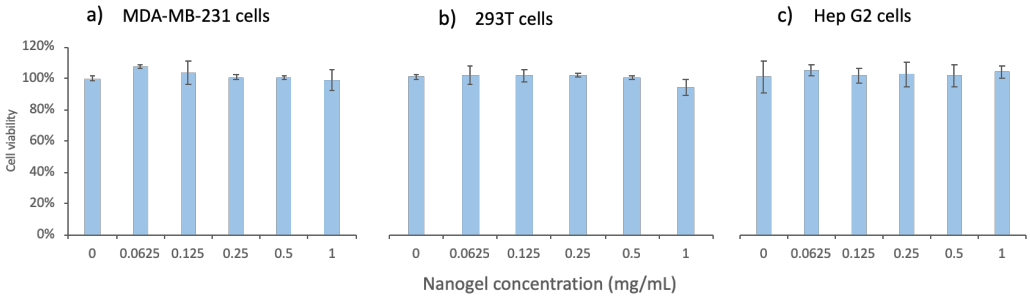

Figure 4.5. Cell viability of control nanogels at varied concentrations.

Notably, increasing the folic acid content on nanogel from 25% to 100% (molar ratio to PEG chain) also resulted in a decrease in cell viability (Figure 4.6d).

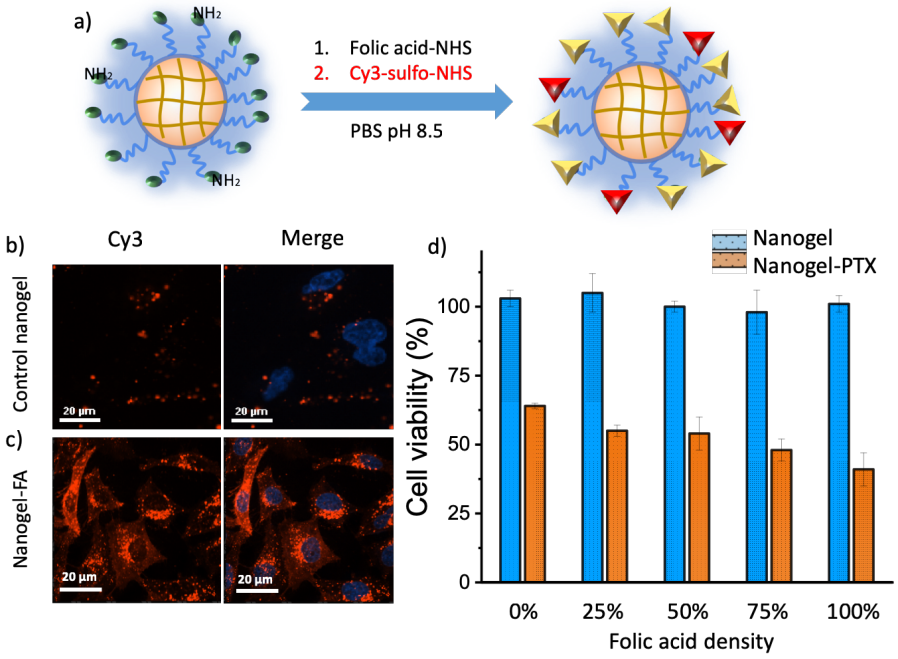

Figure 4.6. Efficient cytosolic delivery into MDA-MB-231 cells using folic acid functionalized nanogel. a) Functionalization of nanogel with Cy3 and folic acid, b) cellular uptake of control nanogel (b) and folic acid functionalized nanogel (c) after 3 h incubation (red, cy3-nanogel; blue, heochst). c) Cell viability of empty nanogel and PTX loaded nanogel with varied folic acid content from 0 to 100% (eq. per PEG chain).

4.2.4 Targeted drug delivery into mitochondria

To test the versatility of our system, we were interested in the potential of this strategy for subcellular organelle targeting. Mitochondria, as key regulators of cell apoptosis, necrosis and autophagy, has been an attractive drug target.[29-31] PTX has been shown to act on mitochondria triggering apoptosis but normally only a fraction of drug molecules is available to mitochondria due to multiple interactions with other cell compartments,[32,33] the drug efficiency would be significantly improved if it can be specifically delivered into the mitochondria. To this end, triphenyl phosphinium (TPP)[31,34], a molecular motif

targeting mitochondria, was decorated on the surface of nanogels (Figure 4.7a). Mitochondria localization of TPP-nanogel was then assessed in MDA-MB-231 cells using CLSM. Colocalization of the red dots (from the Cy3-TPP-nanogel) and green dots (from mitotracker green) as shown in figure 4.7c suggested the nanogels accumulated in the mitochondria. In vitro cytotoxicity of PTX loaded TPP nanogel was then evaluated in MDA-MB-231 cells. Control nanogels was indeed nontoxic, but when treated the cells with PTX loaded nanogel, the cell viability decreased to 66%. Additionally, with TPP decoration from 25% to 100% (molar ratio to PEG chain), the therapeutic effect of PTX could be significantly enhanced, as suggested by the cell viability decrease from 57% to 31% (Figure 4.7d).

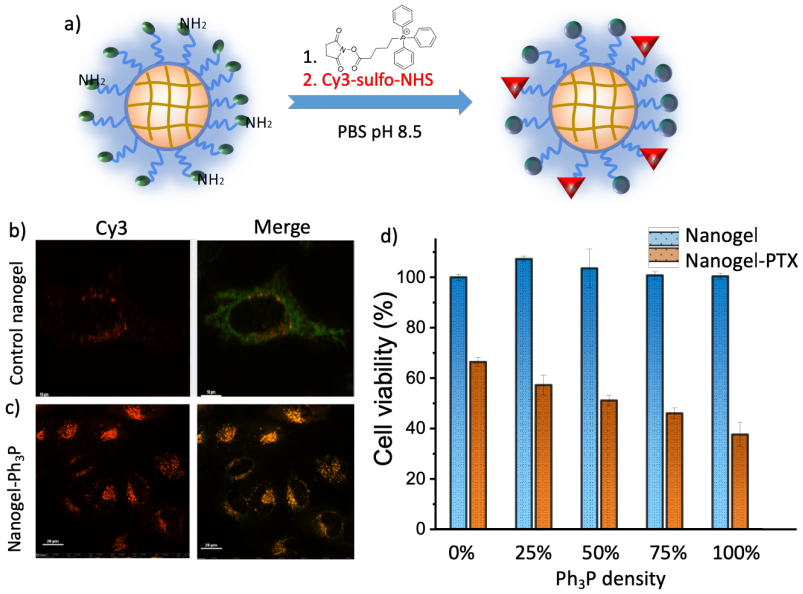

Figure 4.7. Targeted delivery into mitochondria in MDA-MB-231 cells using triphenyl phosphinium functionalized nanogel. a) Functionalization of nanogel with Cy3 and TPP, b) cellular uptake of control nanogel (b) and folic acid functionalized nanogel (c) after 3 h incubation (red, cy3-nanogel; green, mitotracker; orange, merged two channels). c) Cell viability of empty nanogel and PTX loaded nanogel with varied TPP content from 0 to 100% (eq. per PEG chain).

4.2.5 Targeted drug delivery into nucleus

To further validate the applicability, we loaded our nanogel with another chemotherapy drug DOX and then functionalized the nanogel with benzene boronic acid (BB) (Figure 4.8.a), aiming to target cell nucleus, where the drug could maximize its efficiency.[35-38] For this purpose, Cy3 labelled BB nanogel was firstly applied to MDA-MB-231 cells to monitor their cellular uptake. After 3 hours incubation, we were excited to see significant red fluorescence in the nucleus site of the cell, which perfectly colocalize with the nucleus stain (Figure 4.8.c). Moreover, the BB functionalized DOX nanogel induced 81% cell death, which is much more effective than DOX-nanogel without targeting ligands (Figure 4.8.d).

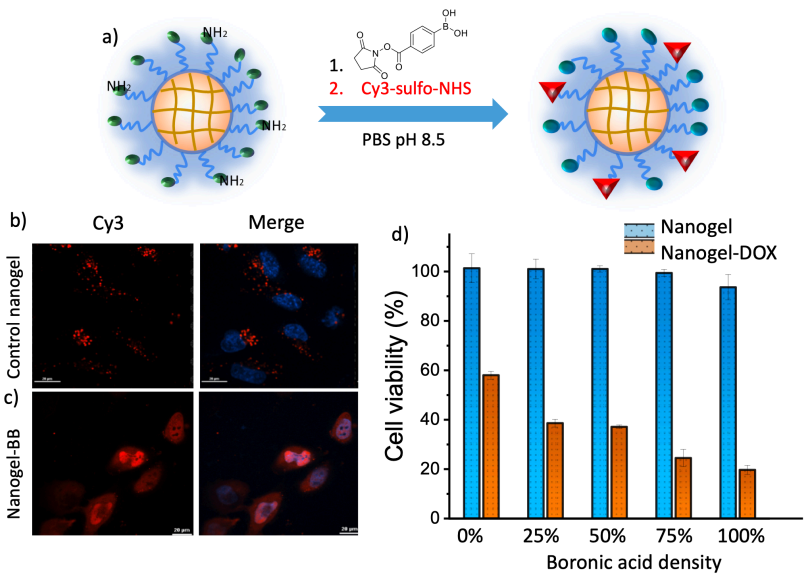

Figure 4.8. Targeted delivery into nucleus in MDA-MB-231 cells using benzene boronic acid functionalized nanogel. a) Functionalization of nanogel with Cy3 and BB; Cellular uptake of control nanogel (b) and BB functionalized nanogel (c) after 3 h incubation (red, Cy3-nanogel; blue, hoechst; pink, merged two channels. d) Cell viability of empty nanogel and DOX loaded nanogel with varied boronic acid content from 0 to 100% (eq. per PEG).

4.3 Summary

To summarize, we have developed a functional self-immolative nanogel system for the encapsulation of chemotherapy drugs and the delivery of them into the cytosol and subcellular organelles such as nucleus and mitochondria of cancer cells. This approach perfectly meets all the requirements of an ideal drug delivery system by the following facts (i) it takes very simple steps to prepare; (ii) therapeutic drugs are encapsulated with high fidelity, i.e., high loading capacity and high stability (iii) the cargo is non-covalently encapsulated without any modification; (iv) guest molecules can be released efficiently in response to a target intracellular environment; (v) triggered polymer self-immolation transforms the polymer from being amphiphilic to completely hydrophilic, which favors the complete drug release; (vi) the nanogels can be easily and independently functionalized with targeting ligands at the surface; and (vi) drug loaded nanogel can induce efficient cell apoptosis. With all these exciting features installed in one nanogel system that is easy to prepare, we believe it will serve as a potent drug delivery platform for a broad range of small molecules and hold great potential for translational clinical research.

4.4 Experimental Procedures

4.4.1. General Methods

All the reagents were from commercial source and used as received. ^{1}H NMR and ^{13}C NMR spectra were recorded on a Bruker DPX-400 MHz NMR spectrometer using the residual proton resonance of the solvent as the internal standard. All molecules without characterization data mentioned below were synthesized through well-established synthesis procedures previously reported by our group.[39] Molecular weight of the polymers was measured by gel permeation chromatography (GPC, Agilent) using a PMMA standard

with a refractive index detector. THF was used as eluent with a flow rate of 1mL/min. UV-vis absorption spectra were obtained by a Carry 100 Scan spectrometer. Fluorescence spectra were recorded on a PerkinElmer LS 55 spectrofluorimeter. Dynamic Light Scattering (DLS) data were recorded by a Malvern Nanozetasizer ZS90 with a 637-nm laser source with non-invasive backscattering technology detected at 173^{o} using disposable sizing cuvette. For Transmission Electron Microscope (TEM) Study: The same sample for DLS measurement was dropped onto carbon-coated copper grid. The grid was dried by slow evaporation in air, and then dry separately in a vacuum overnight. Images were recorded on a JEOL-2000FX electron microscopy operated at 200 kV and at a nominal magnification of 5000X. At least 10 locations on the TEM grid were examined.

4.4.2. Polymer synthesis

Scheme 4.2 Synthesis route for polymer P1

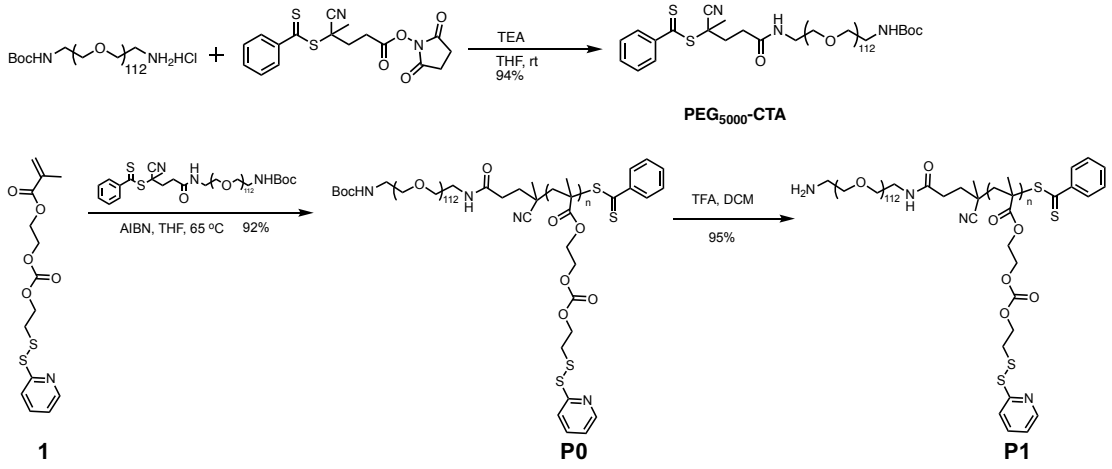

Synthesis of monomer 1: 2-hydroxylethylmathacrylate (1.3 g, 0.01 mol) was dissolved in dry THF and then phosgene (15% wt in toluene) (1 eq.) was added dropwise and kept at room temperature for 3 hours, solvent was removed and then redissolved in dichloromethane under ice bath, a mixture of triethylamine (2.02 g, 0.02 mol) and 2-

hydroxylethyl-2-pyridyl disulfide (1.87 g, 0.01mol) in DCM was added dropwise, the reaction mixture was then stirred at room temperature overnight. Solvent was removed and redissolved in ethylacetate, the organic phase was then washed by $NaHCO_3$ solution and brine. The organic layer was then evaporated to dryness and purified by silica gel column chromatography (0-30% ethyl acetate in hexanes) to afford 2.3 g (67% yield) of **1**. ^{1}H NMR (400 MHz, $CDCl_3$) δ 8.47-8.49 (d, *J* = 8 Hz, 7.6 Hz, 2H), δ 7.61-7.68 (m, 2H), δ 7.08-7.12 (m, 1H), δ 6.14 (s, 1H), δ 5.60 (s, 1H), δ 4.37-4.43 (m, 4H), δ 3.06-3.10 (t, *J* = 6.6 Hz, 2H), δ 1.94 (s, 3H). ^{13}C NMR (100 MHz, $CDCl_3$) δ 167.2, 159.6, 154.8, 149.9, 137.1, 135.9, 126.4, 121.1, 120.1, 65.9, 65.7, 62.4, 37.1, 18.4. ESI-MS (expected: $[m+H]^+$= 344.0548, obtained: $[m+Na]^+$= 366.0685)

Synthesis of chain transfer reagent (PEG5000-cta) : To a solution of O-(2-Aminoethyl)-O′-[2-(Boc-amino)ethyl]decaethylene glycol (0.5 g, 0.1 mmol) and triethylamine (0.0612 g, 0.6 mmol) in DCM was added 4-Cyano-4-(phenylcarbonothioylthio)pentanoic acid N-succinimidyl ester (0.18 g, 0.5 mmol) solution, the mixture was kept stirring overnight at room temperature. Solvent was removed then dialyzed against DCM/MeOH to get purified PEG-CTA. (0.51 g, 94% yield). ^{1}H NMR (400 MHz, $CDCl_3$) δ 7.89-7.91 (d, J = 8.0 Hz 1H), δ 7.54-7.57 (t, J = 7.2 Hz, 7.6 Hz, 1H), δ 7.37-7.41 (t, J = 8 Hz, 7.6 Hz, 2H), δ 6.37 (s, 1H), δ 5.03 (s, 1H), δ 3.30-3.81 (m, 454H), δ 2.41-2.69 (m, 4H), δ 1.93 (s, 3H), δ 1.43 (s, 9H). ^{13}C NMR (100 MHz, $CDCl_3$) δ 170.4, 144.6, 132.9, 128.6, 126.7, 118.7, 70.6, 70.2, 69.7, 50.8, 46.1, 40.6, 39.5, 34.2, 31.6, 28.4, 24.1. GPC (THF): 6.4 kDa, Đ= 1.02.

Synthesis of polymer P0: A solution of **1** (103 mg, 0.3 mmol), PEG-CTA (150 mg, 0.03 mmol) and AIBN (0.984 mg, 0.006 mmol), in THF (400 uL) was degassed by three freeze-

pump-thaw cycles before being sealed off under argon protection and vaccum. After 6 h at 65 °C, the polymerization media was diluted in dichloromethane and condensed using rotavap, precipitated in diethyl ether for 3 times to remove unreacted monomers. The precipitate was collected and dried under vacuum to yield 233 mg (92% yield) of **P0**. GPC (THF): Mn= 9.2 K Da, Đ= 1.02. ^{1}H NMR (400MHz, $CDCl_3$) δ 8.45, 7.66, 7.09, 4.17-4.39, 3.45-3.81, 3.08, 1.55-1.96, 1.43, 0.85-1.20. ^{13}C NMR (100 MHz, $CDCl_3$) δ 159.4, 154.6, 149.8, 137.2, 121.0, 119.9, 70.5, 70.2, 65.6, 62.4, 53.4, 36.9, 29.7, 28.4. From ^{1}H NMR, integration of f and d provided the molar ratio of PEG/PDS.

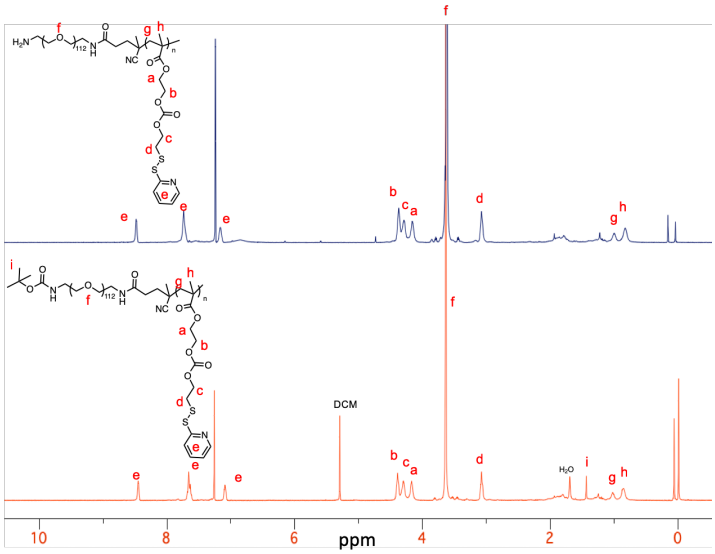

Figure 4.9. NMR spectrum of polymer P0 and P1

Synthesis of polymer P1: P0 was dissolved in DCM/TFA (1mL/1mL) mixture and stirred overnight at room temperature. The solvent was evaporated and redissolved in DCM, the solution was then dialyzed against DCM/MeOH to get purified P1 (95% yield). GPC (THF): Mn= 9.2 K Da, Đ= 1.05. 1H NMR (400MHz, $CDCl_3$) δ 8.50, 7.76, 7.18, 4.18-4.39, 3.45-3.87, 3.09, 1.75-1.96, 0.85,1.02. ^{13}C NMR (100 MHz, $CDCl_3$) δ 160.0, 159.3, 155.2,150.4,

138.5, 138.1, 122.2, 121.8, 120.8, 71.0, 70.6, 66.3, 63.2, 40.8, 37.6, 30.4. Disapperance of peak i at 1.43 ppm confirmed the successful deprotection.

4.4.3 Competition between crosslinking and self-immolation

Scheme 4.3 Mechanism of crosslinking and self-immolation induced by DTT

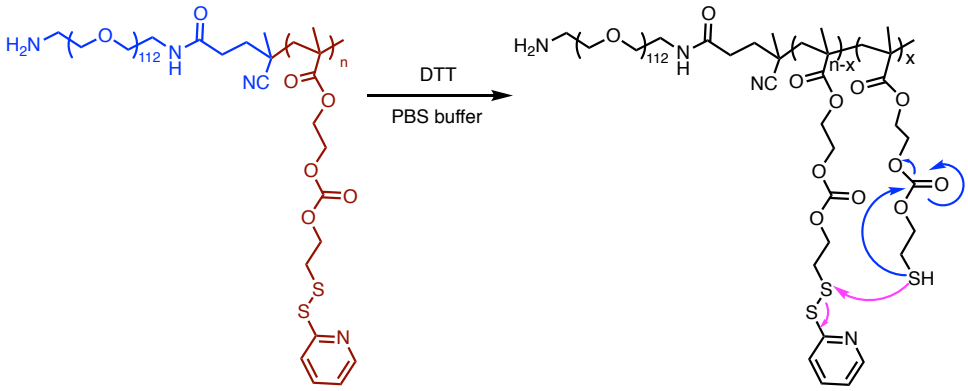

4.4.4. Nanogel preparation

(a) Control nanogel: Deionized water was added to the polymer (5 mg/mL) solution in THF (100 uL) and stirred overnight to allow THF to evaporate. Nanogels were achieved by chemically cross-linking this equilibrium assembly of the polymer at 25 °C using a calculated amount of DTT for 4 h as reducing agent as previously reported.[40,41] Cross-linking was determined by calculating the amount of byproduct 2-pyridinethione using its molar extinction coefficient (8.08×10^3 M^{-1} cm^{-1} at 343 nm) by UV–vis spectroscopy. The size and zeta potential of these nanogel samples were then measured by dynamic light scattering at 0.2 mg/ml.

(b) Guest encapsulation: Polymer solutions in deionized water were stirred at room temperature and DiI/PTX/DOX stock solution (15 mg/mL in acetone) was added according to designated feeding ratio from 10% to 30%. The solutions were stirred for 8 h in room temperature and calculated amount of DTT was then added to crosslink the micelles to

generate guest encapsualted nanogel. The solution was then purified by dialysis against water for 3 days.

Standard curve of DOX was determined using absoprtion at 510 nm of a set DOX samples at varied concentration (Figure 4.10.a). The amount of encapsulated DOX in nanogel was then calculated from the standard curve. To determine the amount of encapsulated PTX, 1mg/ml nanogel-PTX solution was first treated with GSH to release the drug, the mixture was lyophilized and then redissolved in THF for GPC measurement using the UV detector at 220 nm. The loaded PTX amount can be then calculated from the standard curve, which was obtained by measuring PTX peak area at different concentrations using GPC (THF). (Figure 4.10.b).

To achieve the maximum drug loading capacity, we have optimized the crosslinking density, drug feeding ratio and polymer hydrophobicity. Nanogel with 20% crosslinking, 30% drug feeding ratio and PEG:PDS ratio at 1:10 showed the highest drug loading capacity, this condition was used for the following cell culture experiments. The encapsulation efficiency (EE) and loading capacity (LC) were calculated based on the following formulas:

EE, % = Absorption of loaded drug/absorption of initial feeded drug ×100%

LC, % = Amount of "encapsulated" drug / amount of polymer ×100%

(c) Ligands modification: Nanogel formed by **P1** can be functionalized with Cy3/folic acid/triphenylphosphinium/benzene boronic acid by reacting with corresponding NHS ester in PBS buffer pH 8.5, functionalized nanogel was then purified through dialysis against deionized water. To vary the ligand density, mix polymer **P0** and **P1** with calculated amount and prepare nanogel following the same protocol as described in a) and b).

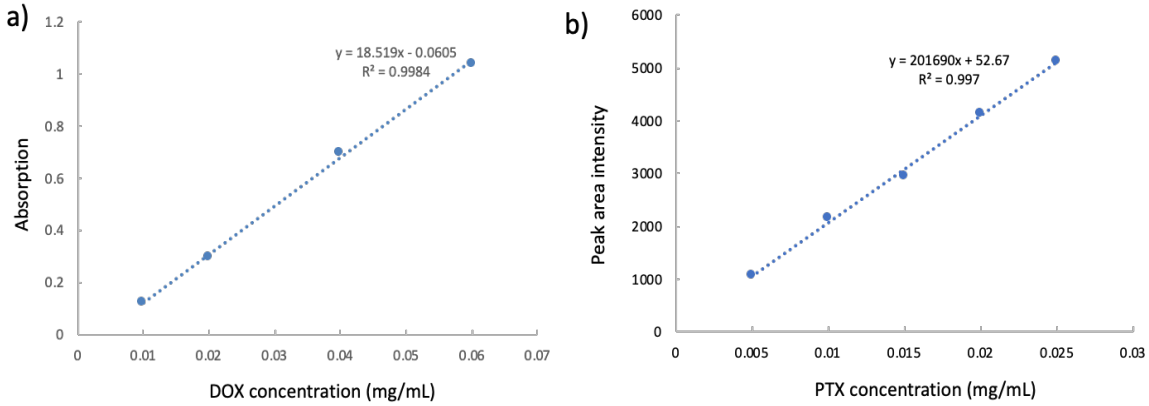

Figure 4.10. Standard curve of a) DOX based on absorption, b) PTX based on GPC peak area.

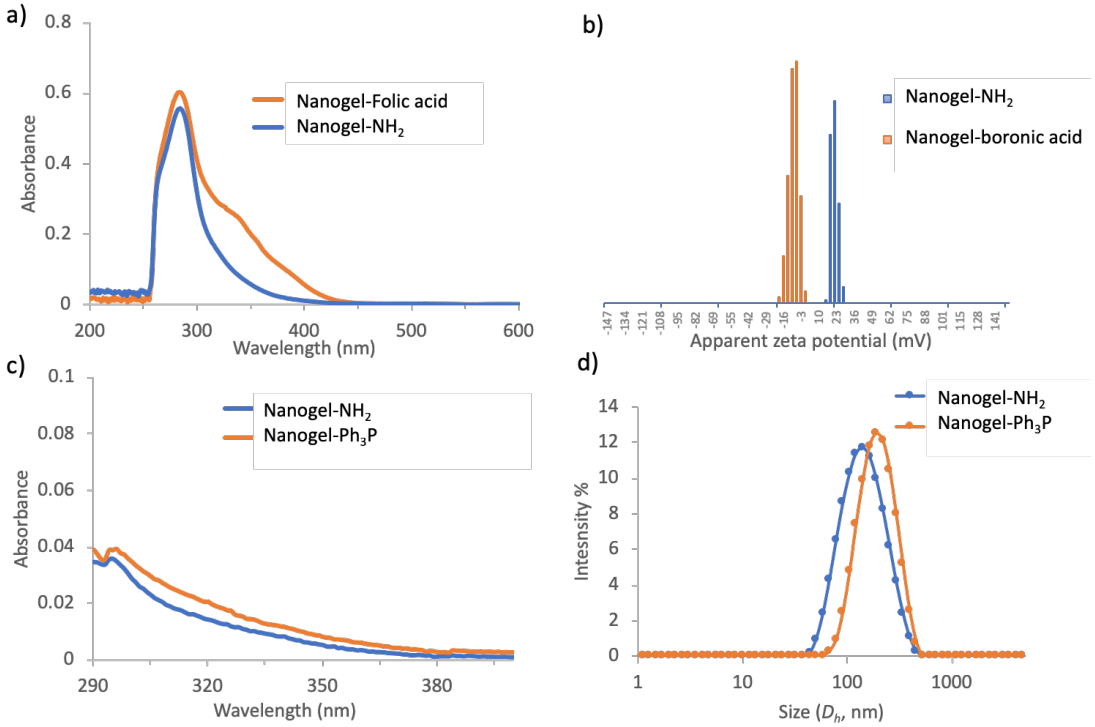

Figure 4.11. Characterization of ligand decorated nanogels: a) absorption at 345 nm suggested folic acid attachment, b) Boronic acid modification shifted the nanogel charge from positive to negative; absorption increase at 290 nm (c) and nanogel size increase (d) confirmed the Ph_3P modification.

4.4.5. Cell Culture

A human breast cancer cell line MDA-MB-231and human liver carcinoma cells Hep G2 and healthy T293 kidney cell line were grown in DMEM supplemented with 10% (FBS), 1% l-glutamine, and 1% antibiotic-antimycotic (comprised of 100 units/mL penicillin and 100 µg/mL of streptomycin). All cells were grown at 5% CO_2 and 37 °C. Digestion of cells for culture was performed according to protocols from ATCC.

(a) Cell viability assay: Cells were seeded on flat-bottom 96-well tissue culture plates at a density of 5000 cells/well and rested for 24 h at 37 °C in 5% CO_2. After overnight incubation, the culture medium was removed, and cells were treated with empty or drug loaded nanogel samples at different concentrations in complete medium for 48 h. After treatments, cells were washed and medium was replaced with 3-(4,5-dimethylthiazol-2-yl) 2,5-diphenyltetrazolium solution (MTT) (prepared as 0.5 mg/mL in medium) and further incubated for 3–4 h at 37 °C. Remove 75 ul of medium and add 50 uL DMSO to each well and incubate for another 10 mins. Purple color formation was observed and recorded using a plate reader at 540 nm.

(b) Confocal imaging: Cells were seeded at 30–50% confluency (~10,400 cells/cm^2) in 4-chamber 35 mm glass bottom dishes and incubated overnight at 37 °C in 5% CO_2 before performing uptake. Culture media was removed, and cells were washed with PBS one time before adding new culture media containing Cy3-labeled nanogels diluted to 0.1 mg/mL in DMEM (10× , diluted to 1× with PBS). Samples were incubated for 2 h. Nuclear staining (NucBlue, 80 µL/mL of media) and mitotracker green was added in the final 30 min of incubation. Medium was removed from cells, which were washed with PBS three times; then, live cell imaging buffer was added for confocal imaging. Assessment of Cy3-

conjugated nanogel intracellular uptake was recorded using 560 nm laser, and nuclear stain was detecting using a 405 nm wavelength laser, mitotracker green was detected using a 488 nm wavelength laser. Confocal microscopy was performed on a Nikon Yokogawa spinning disk confocal microscope equipped with 40× oil or 60× oil objectives and an Andor EMCCD camera. Co-localization of blue (hoechst) and red (cy5) channels was studied to check the nuclei of cells.

4.5 References

1. M. W. Tibbitt, J. E. Dahlman, R. Langer, *J. Am. Chem. Soc.* **2016**, *138*, 704–717.
2. J. Shi, O. C. Farokhzad. et al, *Nat. Rev. Cancer* **2017**, *17*, 20–37.
3. E. Blanco, H. Shen, M. Ferrari, *Nat. Biotechnol.* **2015**, *33*, 941–951.
4. R. Langer, others, *NATURE-LONDON*- **1998**, 5–10.
5. M. J. Akhtar, S. Kumar. et al, *Clin. Chim. Acta* **2014**, *436*, 78–92.
6. S. Gelperina, K. Kisich, M. D. Iseman, L. Heifets, *Am. J. Respir. Crit. Care Med.***2005**, *172*, 1487–1490.
7. R. T. Chacko, J. Ventura, J. Zhuang, S. Thayumanavan, *Adv. Drug Deliv. Rev.* **2012**, *64*, 836–851.
8. B. SHI, M. Zheng, T. Jiang, W. Yang, Y. Zou, H. Wu, X. Liu, K. McDonald, D. Ling, J. Shi, et al., *Angew. Chemie Int. Ed.* **2019**.
9. G. Liu, X. Wang, J. Hu, G. Zhang, S. Liu, *J. Am. Chem. Soc.* **2014**, *136*, 7492–7497.
10. M. You, L. Peng, N. Shao, L. Zhang, L. Qiu, C. Cui, W. Tan, *J. Am. Chem. Soc.* **2014**, *136*, 1256–1259.
11. I. I. Slowing, J. L. Vivero-Escoto, C.-W. Wu, V. S.-Y. Lin, *Adv. Drug Deliv. Rev.* **2008**, *60*, 1278–1288.
12. E. R. Gillies, J. M. J. Frechet, *Drug Discov. Today* **2005**, *10*, 35–43.
13. P. Ghosh, G. Han, M. De, C. K. Kim, V. M. Rotello, *Adv. Drug Deliv. Rev.* **2008**, *60*, 1307–1315.
14. Z. Yang, M. Lin, C. Ren, J. Liu, L. Dai, Y. Shi, J. Gao, H. Shen, J. Zhan, Y. Cai, *J. Am. Chem. Soc.* **2017**, *139*, 2876–2879.
15. A. Sagi, R. Weinstain, N. Karton, D. Shabat, *J. Am. Chem. Soc.* **2008**, *130*, 5434–5435.

16. R. V Kolakowski, K. T. Haelsig, K. K. Emmerton, C. I. Leiske, J. B. Miyamoto, J. H. Cochran, R. P. Lyon, P. D. Senter, S. C. Jeffrey, *Angew. Chemie Int. Ed.* **2016**, *55*, 7948–7951.

17. G. I. Peterson, M. B. Larsen, A. J. Boydston, *Macromolecules* **2012**, *45*, 7317–7328.

18. X. Tan, B. B. Li, X. Lu, F. Jia, C. Santori, P. Menon, H. Li, B. Zhang, J. J. Zhao, K. Zhang, *J. Am. Chem. Soc.* **2015**, *137*, 6112–6115.

19. G. Liu, G. Zhang, J. Hu, X. Wang, M. Zhu, S. Liu, *J. Am. Chem. Soc.* **2015**, *137*, 11645–11655.

20. K. M. Mahoney, P. P. Goswami, A. H. Winter, *J. Org. Chem.* **2013**, *78*, 702–705.

21. J.-H. Ryu, R. T. Chacko, S. Jiwpanich, S. Bickerton, R. P. Babu, S. Thayumanavan, *J. Am. Chem. Soc.* **2010**, *3*, 2–10.

22. J. Zhuang, S. Jiwpanich, V. D. Deepak, S. Thayumanavan, *ACS Macro Lett.* **2012**, *1*, 175–179.

23. M. Canakci, F. Anson, M. R. Gordon, R. W. Vachet, A. Fernandez, S. Thayumanavan, C. Homyak, K. Singh, B. Zhao, *Biomacromolecules* **2018**, *19*, 860–871.

24. J.-H. Ryu, S. Jiwpanich, R. Chacko, S. Bickerton, S. Thayumanavan, *J. Am. Chem. Soc.* **2010**, *132*, 8246–8247.

25. K. R. Kalli, A. L. Oberg, G. L. Keeney, T. J. H. Christianson, P. S. Low, K. L. Knutson, L. C. Hartmann, *Gynecol. Oncol.* **2008**, *108*, 619–626.

26. C.-O. Evans, P. Reddy, D. J. Brat, E. B. O'Neill, B. Craige, V. L. Stevens, N. M. Oyesiku, *Cancer Res.* **2003**, *63*, 4218–4224.

27. S. D. Weitman, A. G. Weinberg, L. R. Coney, V. R. Zurawski, D. S. Jennings, B. A. Kamen, *Cancer Res.* **1992**, *52*, 6708–6711.

28. J. A. Ledermann, S. Canevari, T. Thigpen, *Ann. Oncol.* **2015**, *26*, 2034–2043.

29. G. Appiah Kubi, Z. Qian, S. Amiar, A. Sahni, R. V Stahelin, D. Pei, *Angew. Chemie* **2018**, *130*, 17429–17434.

30. S. Schmitt, H. Zischka, *Dtsch. Zeitschrift fur Onkol.* **2018**, *50*, 124–130.

31. Z. Wang, W. Guo, X. Kuang, S. Hou, H. Liu, *Asian J. Pharm. Sci.* **2017**, *12*, 498–508.

32. N. André, D. Braguer, G. Brasseur, A. Gonçalves, D. Lemesle-Meunier, S. Guise, M. A. Jordan, C. Briand, *Cancer Res.* **2000**, *60*, 5349–5353.

33. K. Miller, M. Wang, J. Gralow, M. Dickler, M. Cobleigh, E. A. Perez, T. Shenkier, D. Cella, N. E. Davidson, *N. Engl. J. Med.* **2007**, *357*, 2666–2676.

34. S. Fulda, L. Galluzzi, G. Kroemer, *Nat. Rev. Drug Discov.* **2010**, *9*, 447.

35. S. Zhang, X. Liu, T. Bawa-Khalfe, L.-S. Lu, Y. L. Lyu, L. F. Liu, E. T. H. Yeh, *Nat. Med.* **2012**, *18*, 1639.

36. R. Tang, M. Wang, M. Ray, Y. Jiang, Z. Jiang, Q. Xu, V. M. Rotello, *J. Am. Chem. Soc.* **2017**, *139*, 8547–8551.

37. G. A. Ellis, M. J. Palte, R. T. Raines, *J. Am. Chem. Soc.* **2012**, *134*, 3631–3634.

38. L. Lu, W. Chen, J. Liu, Y. Wang, C. Jiang, B. Yu, Z. Sun, *Angew. Chemie Int. Ed.* **2019.**

39. J.-H. Ryu, R. T. Chacko, S. Jiwpanich, S. Bickerton, R. P. Babu, S. Thayumanavan, *J. Am. Chem. Soc.* **2010**, 3, 2–10.

40. J.-H. Ryu, S. Jiwpanich, R. Chacko, S. Bickerton, S. Thayumanavan, *J. Am. Chem. Soc*. **2010,** 132, 8246–8247.

41. M. Canakci, F. Anson, M. R. Gordon, R. W. Vachet, A. Fernandez, S. Thayumanavan, C. Homyak, K. Singh, B. Zhao, *Biomacromolecules,***2018**, 19, 860–871.

CHAPTER 5

CELL REGULATED NANOGEL ACCUMULATION IN TARGET CELLS

5.1 Introduction

Off-target accumulation of nanoparticles, especially for in vivo tumor imaging and therapeutics, is one of the major hurdles preventing nanoparticles from being successfully translated and commercialized for biomedical application. Thus, tremendous efforts have been taken to develop the capability of on-target accumulation. These attempts mainly focus on optimizing the so-called enhanced permeation and retention (**EPR**) effect and on introducing ligand-receptor interactions for active targeting. Though certain nanoscopic objects seem to have the capability of enhancing accumulation in tumor tissues due to EPR effect, attributed to defective tumor vasculature and impaired lymphatic drainage, their effectiveness in nanomedicine is significantly impeded by the inherent heterogeneity of tumors.[1-6] Alternatively, active targeting where complementary ligands are incorporated onto nanocarriers to recognize receptors overexpressed in tumor cells has been explored for selective tumor localization.[7-10] However, presence of low level of receptors in off-target locations can still accumulate ligand-decorated nanocarriers, which gives poor selectivity gain and hampers the efficacy of active targeting in vivo.

To enhance the selectivity of active targeting, ligand masking strategies in which ligands are masked and availabilities are only revealed in response to disease microenvironment until they reach targets have been developed. But current strategies developed for ligand unmasking are primarily focused on using secondary imbalances in disease including escalated acidity, redox potential and external stimuli such as ultraviolet light that does not have the penetration depth to be useful.[11-17] A more effective approach

involves the primary imbalance in the disease microenvironments - enzymes to trigger ligand exposure.[18-23] Past approaches in this regard involves noncovalent, steric protection of ligand with enzyme-cleavable bulky groups (*e.g.* PEG) that decrease the accessibility of ligand to bind with receptors. These approaches require extensive engineering but also have limited targeting capability due to the slow cleavage kinetics.

Here, we propose a cellular AND gate to utilize cell itself to regulate cell-nanoparticle interactions and achieve highly selective targeting (Figure 5.1). Alkali phosphatase (ALP) and carbonic anhydrase IX (CA IX) are two disease-relevant enzymes overexpressed on cell surface.[24-27] Nanogels are firstly designed in such a way that they will only accumulate in specific disease cells which overexpress both these two types of enzyme, which is termed as 'single cellular AND gate'. If each enzyme is presented on different cell type, the uptake of nanoparticles into the CA IX overexpressed cells could be greatly promoted by cells overexpress ALP which could reveal the cell interactive functionalities on the nanoparticles, this is termed as 'intercellular AND gate' (Figure 5.2). Since enzymes are considered to be the primary cause of pathological imbalances in biology, these dual enzymes based cellular AND gated nanoparticle uptake would open up more possibilities for tumor imaging, diagnosis and targeted delivery.

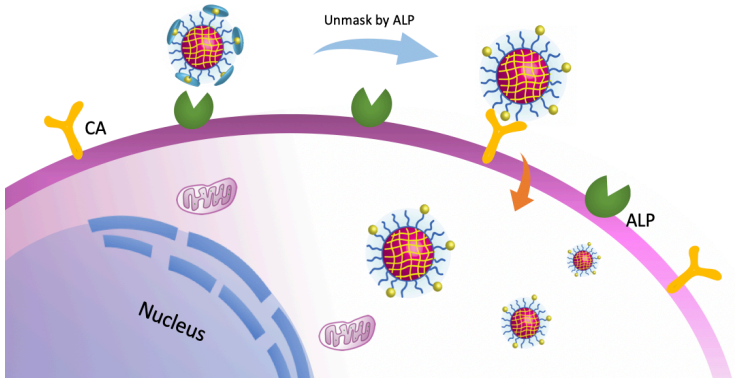

Figure 5.1 Schematic representation of single cellular AND gated nanogel uptake

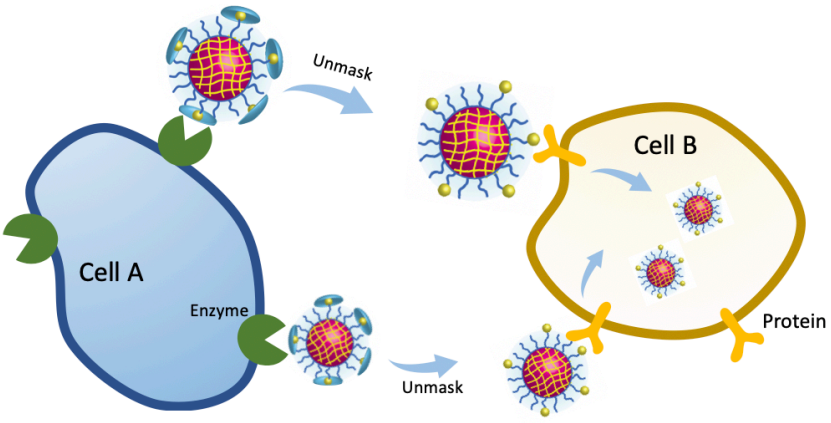

Figure 5.2 Schematic representation of intercellular AND gated nanogel uptake

5.2 Results and discussion

5.2.1 Design and synthesis

Our molecular design involves covalently mask binding motif for CA IX on nanogel with alkaline phosphatase (ALP) substrates through a self-immolative linkage to suppress nanoparticle cell interaction and cellular accumulation. Since cell membrane interactive functionalities are covalently masked, their availability for cell interaction will be completely eliminated. We hypothesize that ALP overexpressed cells will cleave the readily accessible substrate on nanogel surface to rapidly liberate the sulphonamide ligands for interaction with CA IX overexpressed cells. Thus, concurrent presence of ALP and CA IX on one cell type would generate a cellular AND gate to achieve specific and rapid cellular accumulation.

The molecular design strategy is shown in Fig. 5.3. The nanogels will be synthesized from a block copolymer that is composed of three components, crosslinkable hydrophobic coumarin methacrylate block, a polyethylene glycol block providing hydrophilicity to

drive the self-assembly of nanogel, and a phenylsulphonamide, masked with a self-immolative phosphate substrate, was attached to chain end of the block polymer backbone.

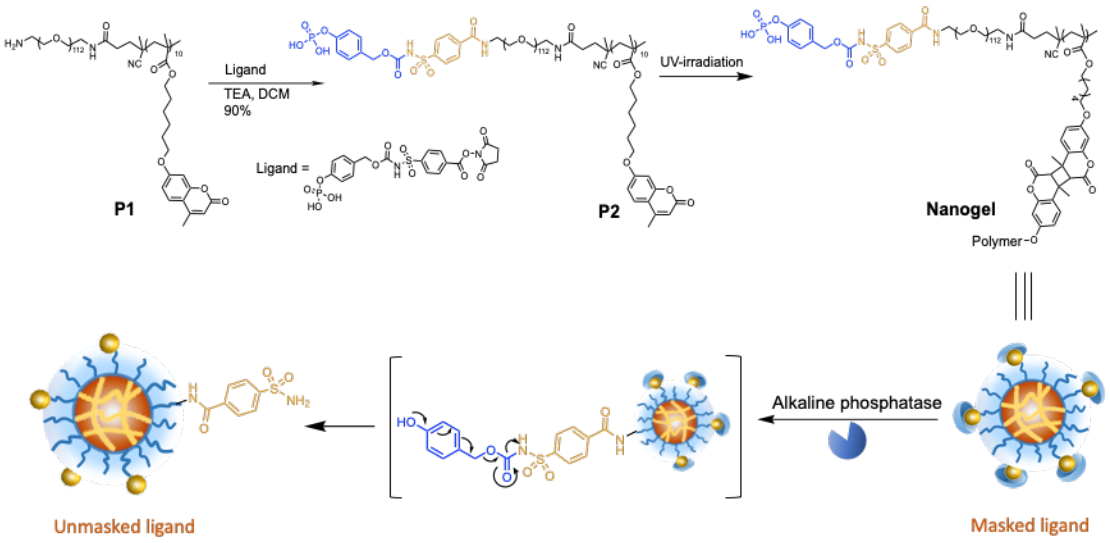

Figure 5.3 Chemical structures of polymeric nanogel and ALP induced exposure of sulfonamide ligands

5.2.2 Nanogel preparation and characterization

Due to the amphiphilic nature of polymer **P2**, we attempted to prepare nanoassemblies by distributing **P2** in water. The nanoassembly formed was found to have an apparent hydrodynamic diameter of >120 nm (Figure 5.4) using dynamic light scattering (DLS). The hydrophobic core of the nanoassembly was constituted of coumarin moieties, which are known to dimerize under UV irradiation (>350 nm).[28-29] When expose the nanoassemblies to UV light, dimerization of coumarin would crosslink the hydrophobic interior and stabilize the nanoassemblies to generate nanogels. Decrease of UV absorption of coumarin moieties supported this crosslinking process (Figure 5.4c). Crosslinking density can be easily tuned by varying the time of UV exposure. We also noticed that the

crosslinked nanogel have a similar size to the nanoassemblies before crosslinking (Figure 5.4 b).

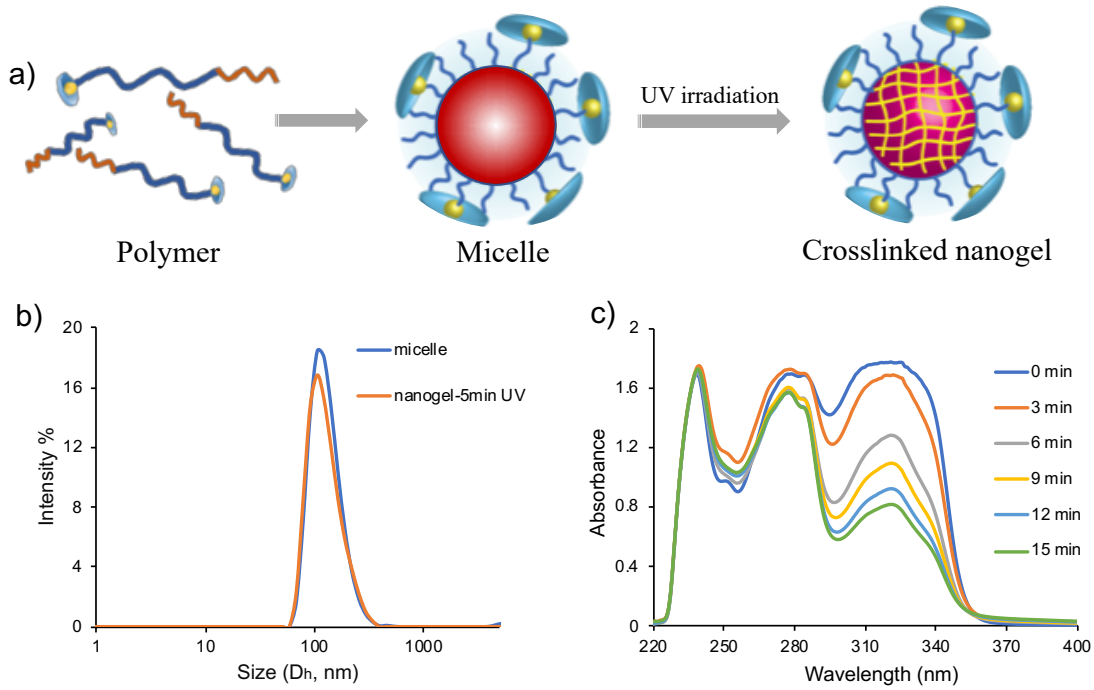

Figure 5.4 a) Preparation of nanogel; b) DLS profile of micelle and crosslinked nanogel; c) UV induced crosslinking of micelles.

5.2.3 Competitive binding assay

Our design hypothesis is that the polymeric nanogel will not be capable of binding to target enzyme carbonic anhydrase until the presence of ALP covalently cleave the phosphotase mask to reveal the sulfonamide ligands. To test this hypothesis, we tested whether proposed nanogel as the ligands can bind to bCA using a competitive displacement assay where 5-(Dimethylamino)-1-naphthalenesulfonamide (DNSA) is used as the initial ligand, the fluorescence emission at 460 nm formed by DNSA-bCA complex indicates whether DNSA is replaced (Figure 5.5a). Our studies showed that when the ligands on the nanogel were masked by the phosphate moiety, it did not competitively remove DNSA, suggested by the little change of fluorescence intensity before and after nanogel was added.

However, when added ALP to this system, significant fluorescent signal decrease was observed over 30 minutes, indicating the unmasked nanogel was able to displace DNSA (Figure 5.5b).

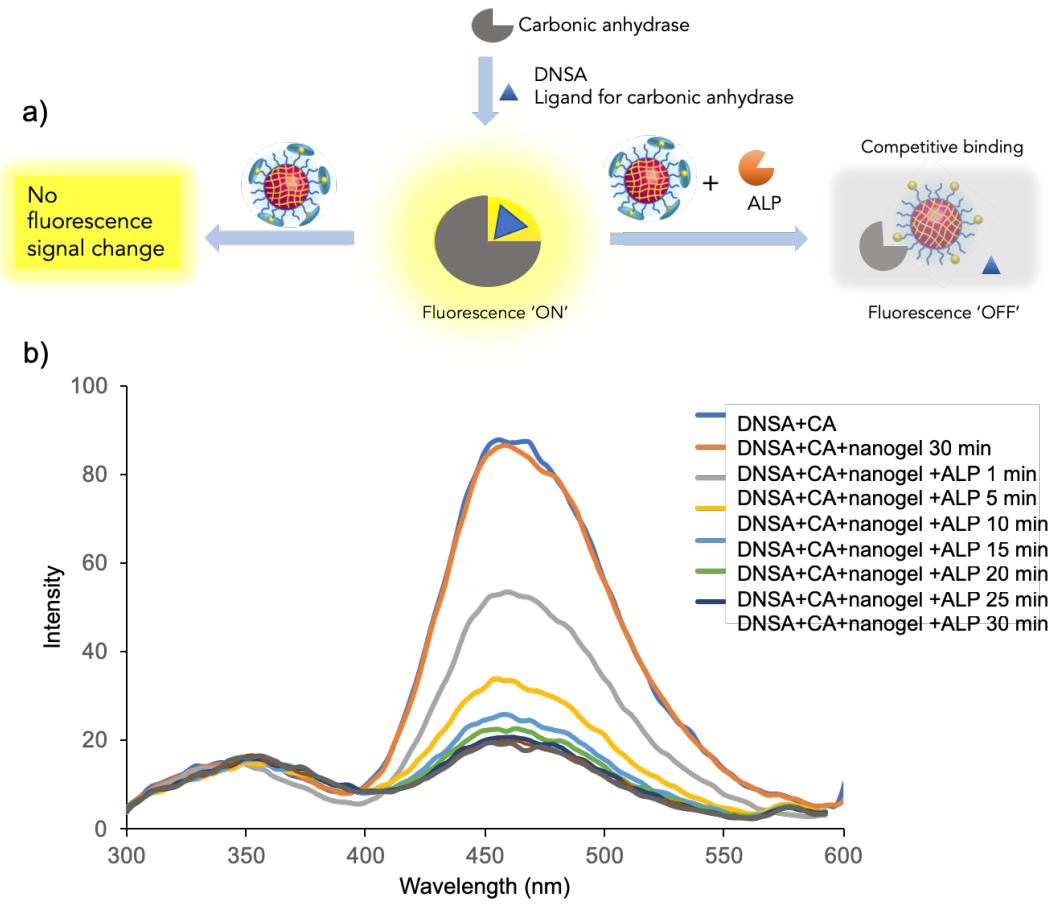

Figure 5.5 a) Schematic representation of competitive binding assay; b) Emission spectrum of DNSA-bCA complex after treating with nanogel and ALP.

5.2.4 Intracelluar uptake of nanogels gated by ALP and CA9 in SAOS-2 cells

Following this exciting finding, we then want to further test this nanogel system in vitro. SAOS-2 is a human osteosarcoma cell line which overexpresses both ALP and CA9. We designed a set of experiments listed in table 5.1, by treating the SAOS-2 cells with ALP inhibitor or CA9 inhibitor or the combination of these two, we are able to design experiments to test whether the cellular uptake of the designed nanogels follows the AND gate.

Table 5.1. Experimental variations to create AND gated conditons

SAOS-2 cell line	Treated with ALP inhibitor	Treated with CA9 inhibitor
a	✅	❎
b	❎	✅
c	✅	✅
d	❎	❎

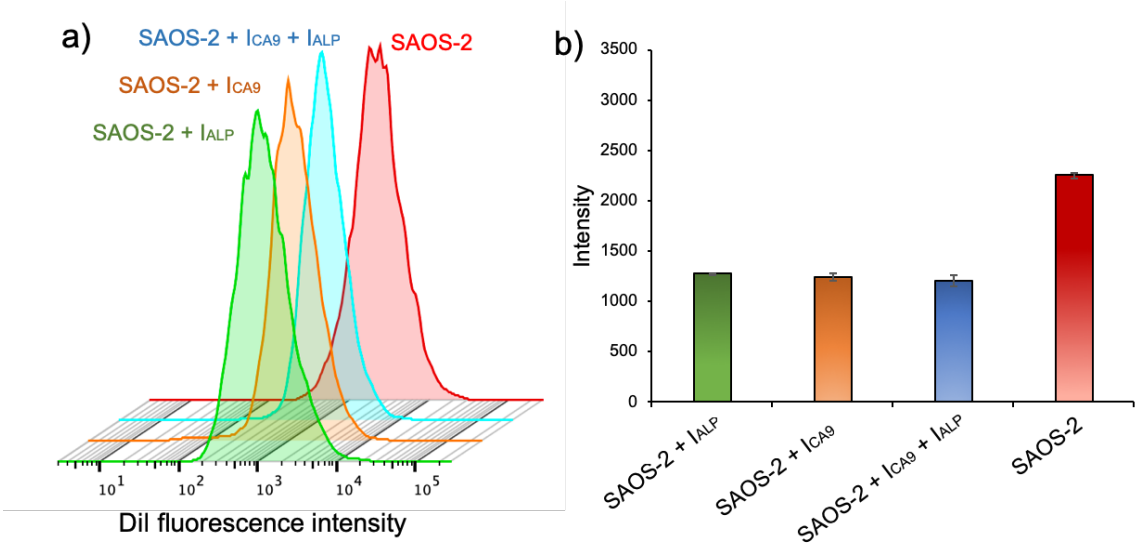

Figure 5.6 a) Flow cytometry histograms of SAOS-2 cells (with/without inhibitor treatment) after 2 hours incubation with DiI loaded nanogels, b) statistic data showing the DiI loaded nanogel accumulation in SAOS-2 cells.

We hypothesized that SAOS-2 cells treated with either one of the enzyme inhibitors or the combination of these two would not uptake the nanogels efficiently, only the control cells without any inhibitor treatments would be observed significant nanogel accumulation. To test this hypothesis, we loaded the nanogel with a hydrophobic dye, 1,1'-dioctadecyl-3,3,3'3'-tetramethyl-indocarbocyanine perchlorate (DiI), to track and quantify the cellular uptake using flow cytometry and confocal laser scanning microscopy. We were excited to find that nanogel accumulation in non-treated cells is significantly higher than cells treated

with either ALP or CA IX inhibitors (Figure 5.6). These findings supported our hypothesis that ALP and CA IX need to be concurrently present for the nanogels to be uptaken efficiently.

We are then excited to evaluate the selectivity of nanogels over four different cell lines. If proposed AND gate mechanism is operating in this case, the accumulation of nanogels will be only observed in the human osteosarcoma Saos-2 cells, where ALP and CA9 are concurrently overexpressed. The absence of either protein expression in the other cell lines will suppress the accumulation of nanogels. This possibility was tested using Saos-2 (ALP+, CA9+), MDA-MB-231(ALP+, CA9-), HT-1080 (ALP-, CA9+) and MCF-7 (ALP-, CA9-) cell lines. Indeed, DiI loaded nanogels are readily taken up by SAOS-2 (ALP+, CA+) cells, but not by MDA-MB-231 (ALP+), MCF-7 (ALP-, CA-), or HT-1080 (CA+) cells, as shown in Figure 5.7.

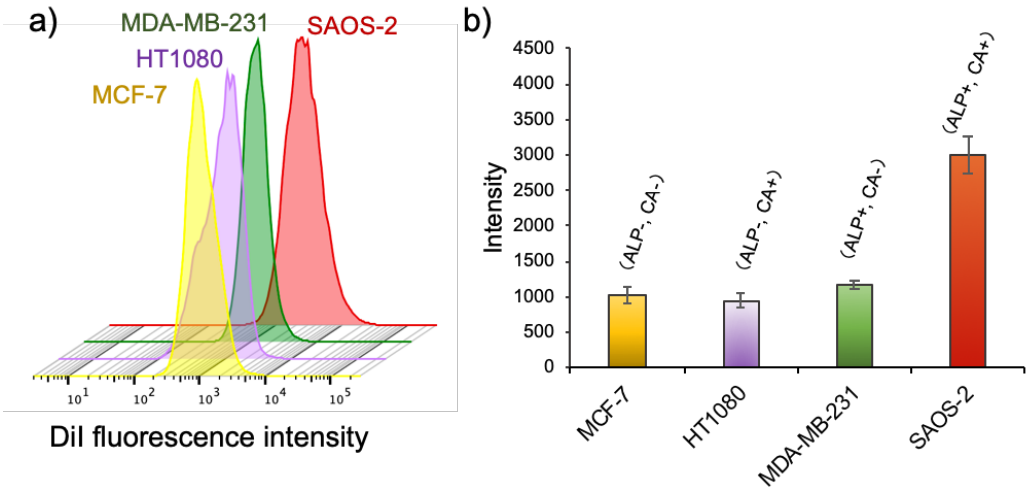

Figure 5.7 a) Flow cytometry histograms of SAOS-2 cells, MCF-7, HT1080, MDA-MB-231 cells after 2 hours incubation with DiI loaded nanogels, b) statistic data showing the DiI loaded nanogel accumulation in four cell lines.

5.2.5 Enhanced nanogel cellular uptake regulated by a second cell line

Membrane vesicle trafficking plays an important role in intercellular communication so that multitypes of cells could work together to maintain the biofunctions. Inspired by this, we have tried to coculture HT-1080 (CA+) and MDA-MB-231 (ALP+) cells and then incubated with DiI loaded nanogels. Although these assemblies do not readily enter HT-1080 (CA+) cells or MDA-MB-231 (ALP+) cells when they were cultured separately, we have observed a significant nanogel accumulation in HT-1080 (CA+) cells when they are cocultured with MDA-MB-231 (ALP+), where the cell surface ALP in the latter cell line processes the nanogels to be taken up by the former cells after binding to the carbonic anhydrase. These results were displayed in Figure 5.8.

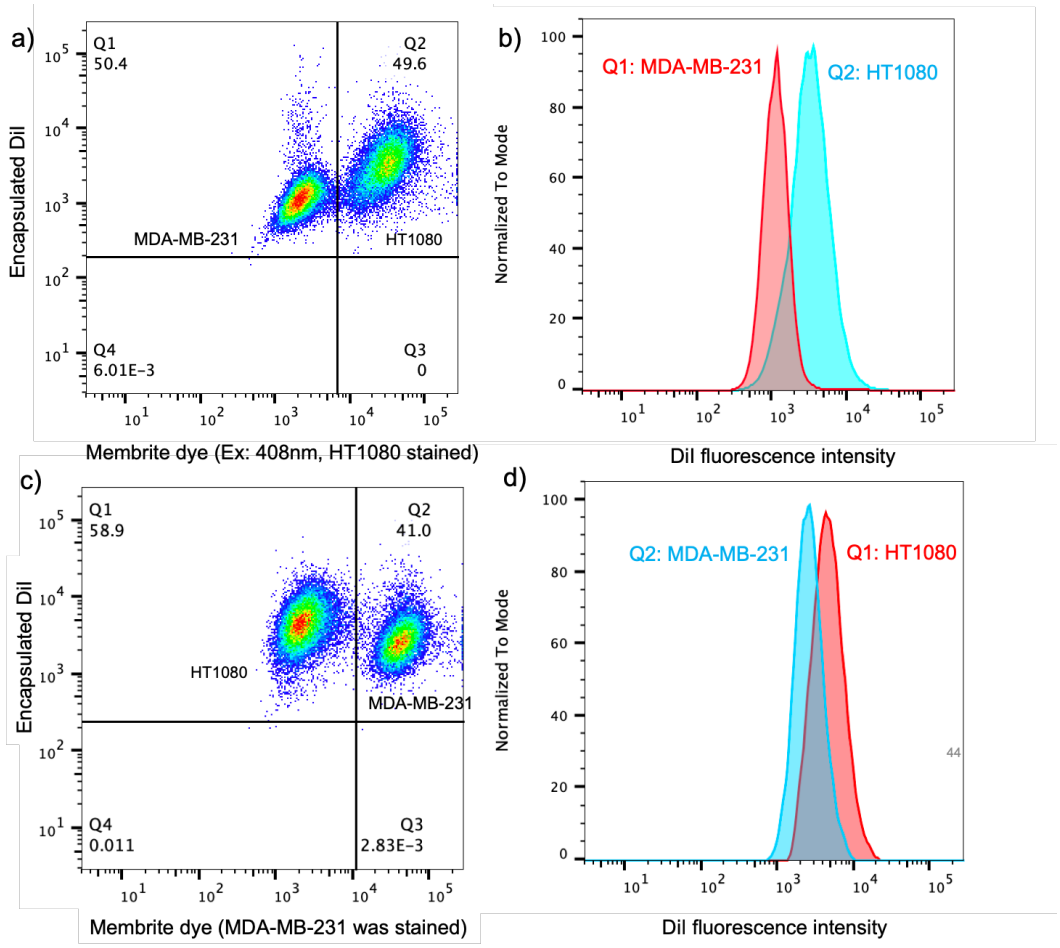

Figure 5.8 Flow cytometry dual fluorescence density plot histograms of HT1080 and MDA-MB-231 coculture (nanogel was loaded with DiI dye, one of the cell lines was stained with membrite dye), a) MDA-MB-231 and stained HT1080, b) Histogram of nanogel uptake in these two cell lines, c) MDA-MB-231 and stained HT1080 coculture, d) Histogram of nanogel uptake in two cell lines.

5.3 Summary

In summary, we have demonstrated a set of cellular logic gates that exhibit efficient nanogel uptake in target cells in the presence of two different proteins. Stable nanogels with dye loading property have been designed and utilized to evaluate the cellular logic gates. We outline molecular designs that can be uptaken selectively by SAOS-2 cells overexpress both ALP and CA IX, as well as enhanced uptake in HT1080 cells promoted by cocultured MDA-MB-231 cells. The nanogel system was developed by caging a carbonic anhydrase-specific ligand with an ALP cleavable phosphate group that masks the ligand from being available for protein binding and following cellular accumulation. For the programmed single cellular AND gate, it requires the concurrent presence of both ALP and CA IX for selective accumulatin only in SAOS-2 cells. Enhanced nanogel uptake into HT1080 cells was further promoted by cocultured MDA-MB-231 cells following the intercellular AND gate where MDA-MB-231 cells firstly process the nanogels by romoving the phosphate mask and reveal the ligands so that they can bind with CA IX in HT1080 cells and get uptaken. The design insights and the concept of cellular AND gates provided here will find use in the design of novel protein-responsive drug delivery and highly selective tumor imaging.

5.4 Experimental

5.4.1 General Methods

All the reagents were from commercial source and used as received. ^{1}H NMR and ^{13}C NMR spectra were recorded on a Bruker DPX-400 MHz NMR spectrometer using the residual proton resonance of the solvent as the internal standard. Molecular weight of the polymers was measured by gel permeation chromatography (GPC, Agilent) using a PMMA standard with a refractive index detector. THF was used as eluent with a flow rate of 1mL/min. UV-vis absorption spectra were obtained by a Carry 100 Scan spectrometer. Fluorescence spectra were recorded on a PerkinElmer LS 55 spectrofluorimeter. Dynamic Light Scattering (DLS) data were recorded by a Malvern Nanozetasizer ZS90 with a 637-nm laser source with non-invasive backscattering technology detected at 173^{o} using disposable sizing cuvette. For Transmission Electron Microscope (TEM) Study: The same sample for DLS measurement was dropped onto carbon-coated copper grid. The grid was dried by slow evaporation in air, and then dry separately in a vacuum overnight. Images were recorded on a JEOL-2000FX electron microscopy operated at 200 kV and at a nominal magnification of 5000X. At least 10 locations on the TEM grid were examined.

5.4.2 Polymer synthesis

Synthesis of **L0**: small molecule a and b were synthesized according to previously reported procedures. Molecule **a** (298 mg, 1 mmol) was dissolved in dry THF at 0 ^{o}C and then molecule **b** (536 mg, 1.2 mmol) and triethylamine (203 mg, 2 mmol) was added dropwise and kept at room temperature for 8 hours, solvent was removed and then redissolved in 20 mL dichloromethane, the organic phase was then washed by brine (3*30 mL). The organic layer was then evaporated to dryness and purified by silica gel column chromatography (0-

30% ethyl acetate in hexanes) to afford 318 mg (45 % yield) of **L0**. ^{1}H NMR (400 MHz, CDCl3) δ 8.21-8.19 (d, *J* = 8.8 Hz, 2H), δ 8.12-8.10 (d, *J* = 8.4 Hz, 2H), δ 7.32 (m, 10H), δ 7.17-7.15 (d, *J* = 8.4 Hz, 2H), δ 5.12-5.10 (d, *J* = 8.4 Hz, 4H), δ 5.02 (s, 2H), δ 2.9 (s, 4H). ESI-MS (expected: $[m+H]^+$= 709.1179, obtained: $[m+Na]^+$= 731.6345)

Scheme 5.1 synthesis route for phosphate ligand and target polymer

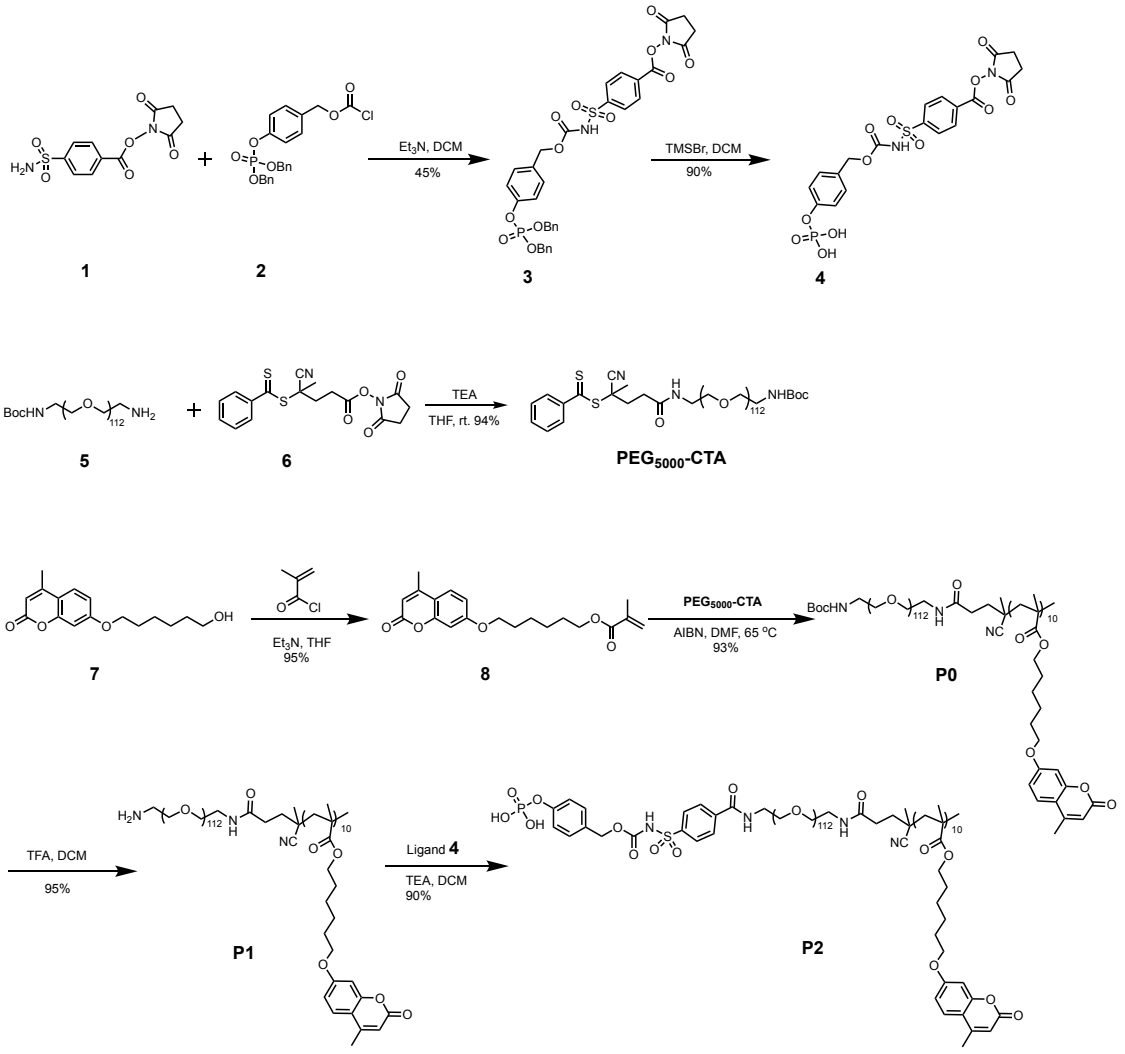

Synthesis of **L1**: Molecule **L0** (300 mg, 1 mmol) was dissolved in anhydrous dicholoromethane at 0 °C under argon protection and then TMSBr (130 mg, 2 mmol) was added dropwise and kept at room temperature for 1 hour, 2 drops of water was added to

the reaction mixture and let it stir for another two hours, white precipate was collected through filtration and washed three times with cold DCM. The prodcut was collected as white powder and generated 201 mg (90 % yield) of **L0**. ^{1}H NMR (400 MHz, CDCl3) δ 8.33-8.31 (d, *J* = 8 Hz, 2H), δ 8.18-8.16 (d, *J* = 8.4 Hz, 2H), δ 7.32-7.30 (d, *J* = 8.4 Hz, 2H), δ 7.21-7.19 (d, *J* = 8.4 Hz, 2H), δ 5.07 (s, 2H), δ 2.94 (s, 4H). ESI-MS (expected: $[m+H]^{+}$= 529.0240, obtained: $[m+Na]^{+}$= 551.3352)

Synthesis of **P0**: A solution of **M** (103 mg, 0.3 mmol), PEG-CTA (150 mg, 0.03 mmol) and AIBN (0.984 mg, 0.006 mmol), in THF (400 uL) was degassed by three freeze-pump-thaw cycles before being sealed off under argon protection and vaccum. After 6 h at 65 °C, the polymerization media was diluted in dichloromethane and condensed using rotavap, precipitated in diethyl ether for 3 times to remove unreacted monomers. The precipitate was collected and dried under vacuum to yield 233 mg (93% yield) of **P0**. GPC (THF): Mn= 8.8 K Da, Đ= 1.02. ^{1}H NMR (400 MHz, $CDCl_3$) δ 7.45, 6.80, 6.79, 6.07, 3.97, 3.83, 3.66, 3.48, 2.36, 1.96, 1.82, 1.67, 1.50, 1.46, 1.26, 1.06, 0.89. From ^{1}H NMR, integration of peak at δ 6.07 and δ 3.83 provided the molar ratio of PEG/PDS to be 1:10.

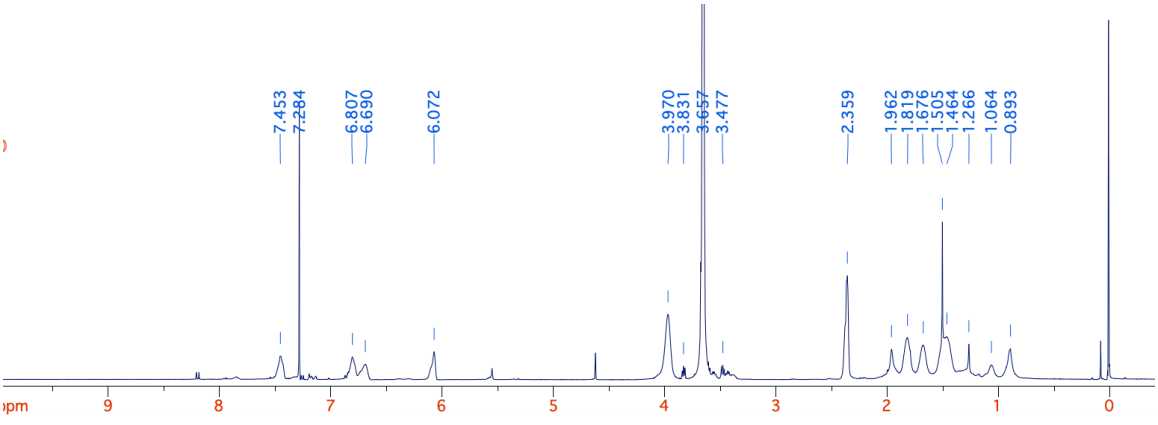

Synthesis of polymer **P1**: **P0** was dissolved in DCM/TFA (1mL/1mL) mixture and stirred overnight at room temperature. The solvent was evaporated and redissolved in DCM, the

solution was then dialyzed against DCM/MeOH to get purified **P1** (95% yield). GPC (THF): Mn= 8.2 K Da, Đ= 1.05. ^{1}H NMR (400MHz, CDCl3) δ 7.43, 6.78, 6.67, 6.05, 3.95, 3.81, 3.63, 3.45, 2.34, 1.97, 1.80, 1.66, 1.43, 1.24, 1.04, 0.87. Disapperance of peak i at 1.50 ppm confirmed the successful deprotection.

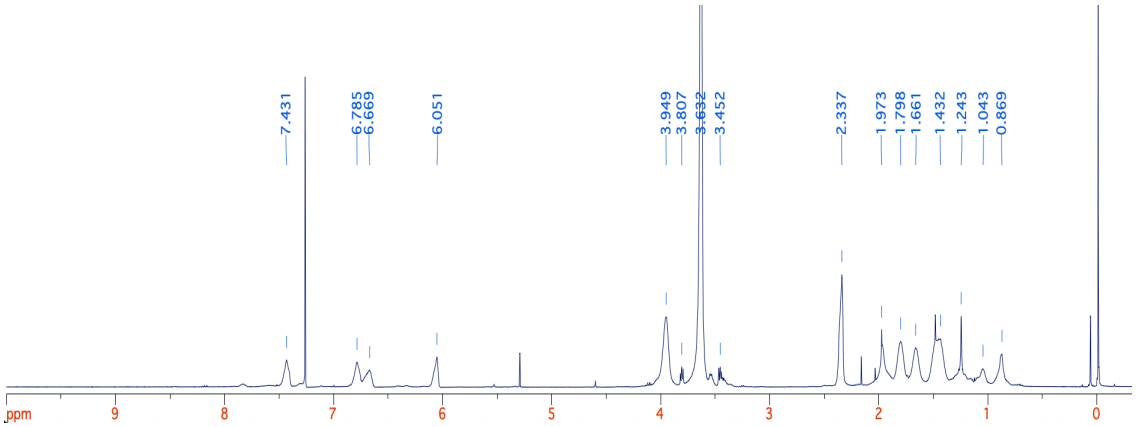

Synthesis of polymer **P2**: **P1** (100 mg)**,** triethylamine (5 uL) and ligand **L1** (8.8 mg, 10 eq.) was dissolved in DCM and stirred overnight at room temperature. The solvent was evaporated and redissolved in DCM, the solution was then dialyzed against DCM/MeOH to get purified **P2** (95% yield). GPC (THF): Mn= 9 K Da, Đ= 1.05. ^{1}H NMR (400MHz, CDCl3) δ 8.22-8.15, 7.45-7.41, 6.78, 6.67, 6.05, 5.13, 3.95, 3.81-3.45, 2.92, 2.33, 1.80, 1.65, 1.45, 1.27, 1.05, 0.87. New peaks at δ 8.22-8.15, δ 7.45-7.41 and δ 5.13 ppm confirmed the ligand modification.

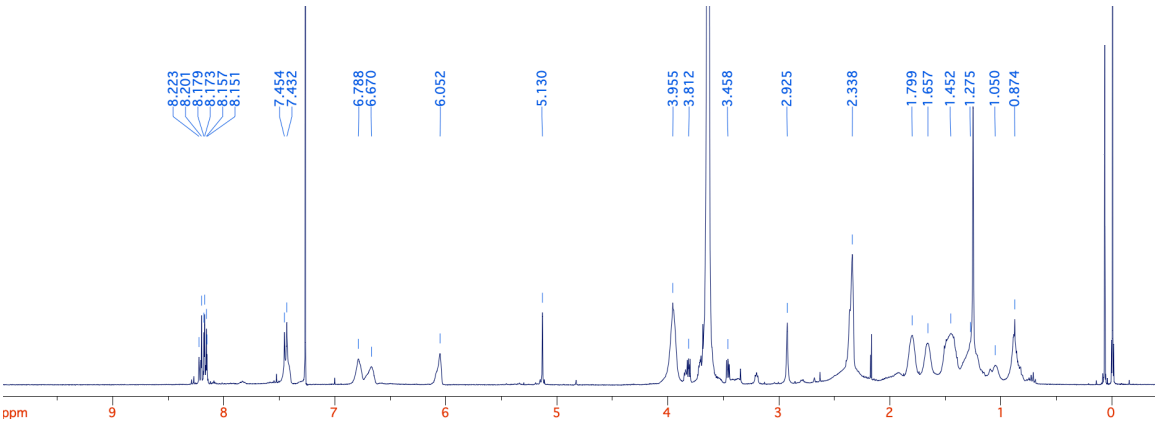

5.4.3 Nanogel preparation and characterization

DiI loaded nanogel: Polymer solutions (5 mg/mL) in deionized water were stirred at room temperature and DiI stock solution (5 mg/mL in acetone) was added according to designated feeding ratio 5 wt%. The solutions were stirred for 8 h in room temperature and filtered with 0.45 um PTFE filter to remove unencapsulated dye molecules. Cross-linking was done by exposing polymer solutions to UV irradiation (365 nm) for 2 minutes. The size of these nanogel samples were then measured by dynamic light scattering at 0.2 mg/ml.

5.4.4 Cellular uptake

Human breast cancer cell lines MDA-MB-231 and MCF-7, a fibrosarcoma cell line HT1080, a human osteosarcoma cell line SAOS-2 were grown in DMEM supplemented with 10% (FBS), 1% l-glutamine, and 1% antibiotic-antimycotic (comprised of 100 units/mL penicillin and 100 µg/mL of streptomycin). All cells were grown at 5% CO_2 and 37 °C. Digestion of cells for culture was performed according to protocols from ATCC.

a) Confocal imaging: Cells were seeded at 30–50% confluency in 8-well ibidi chamber glass bottom dishes and incubated 12 hours at 37 °C in 5% CO_2 before performing uptake. Culture media was removed, cells were washed with PBS one time before adding new culture media containing DiI loaded nanogels diluted to 0.0375 mg/mL in DMEM. Samples were incubated for 1 h. Nuclear staining (NucBlue, 80 µL/mL of media) was added in the final 30 min of incubation. Medium was removed from cells, which were washed with PBS three times; then, live cell imaging buffer was added for confocal imaging. Assessment of nanogel intracellular uptake was recorded using 560 nm laser, and nuclear stain was detecting using a 405 nm wavelength laser. Confocal

microscopy was performed on a Nikon Yokogawa spinning disk confocal microscope equipped with 40× oil or 60× oil objectives and an Andor EMCCD camera.

b) Flow cytometry: For single cellular uptake experiments, each cell type was seeded at the following density in a 12-well glass bottom dish and maintained at 37 °C overnight in 5% CO_2 for 12 hours before performing uptake: MDA-MB-231 at 15K cells/mL, HT1080 at 10K cells/mL, MCF-7 at 15K cells/mL, SAOS-2 at 30K cells/mL. Culture medium was removed, and cells were washed with PBS one time before adding new culture medium containing DiI loaded nanogels diluted to 0.0375 mg/mL in DMEM (10Å~ , diluted to 1Å~ with PBS). Samples were incubated for 1h, then washed with PBS, trypsinized, and collected by centrifugation. The cells were resuspended in 200 μL of PBS buffer and stored at 4°C. A minimum of 100,000 cells were analyzed for each sample using a BD LSRFortessa.

   For cocultured cellular uptake experiments, coculture of stained MDA-MB-231 and unstained HT1080 cells at a seeding ratio of 3:2 were seeded in 6-well glass bottom dish for 12 hours and then following same procedures as above. Similar procedures also applied to the coculture of unstained MDA-MB-231 and stained HT1080 cells.

5.5 References

1. Prabhakar, U.; Maeda, H.; Jain, R.K.; Sevick-Muraca, E.M.; Zamboni, W.; Farokhzad, O. C.; Barry, S.T.; Gabizon, A.; Grodzinski, P.; Blakey, D.C. *Cancer Res.* **2013**, *73*, 2412-2417.
2. Maeda, H.; Bharate, G.Y.; Daruwalla. *J. Eur. J. Pharm. Biopharm*. 2009, 71, 409-419.
3. Bae, Y. H.; Park, K. *J Control Release*, **2011**, 153, 198-205.
4. Yuan, F.; Salehi, H.A.; Boucher, Y.; Vasthare, U.S.; Tuma, R.F.; Jain, R.K. Cancer Res. **1994**, *54*, 4564-4568.
5. Maeda, H.; *Adv. Drug Deliv. Rev*. **2015**, *91*, 3-6.
6. Kobayashi H.; Watanabe, R.; Choyke, P.L. *Theranostics*, **2014**, *4*, 81-89.
7. Shi, J.; Xiao, Z.; Kamaly, N. Farokhzad, O.C. *Acc. Chem. Res.* **2011**, *44*, 1123-1134.
8. Cheng, Y.; Morshed, R.A.; Auffinger B.; Tobias, A.L. Lesniak, M.S. *Adv. Drug Deliv. Rev.* **2014**, *66*, 42-57.
9. Byrne, J.D.; Betancourt, T.; Brannon-Peppas, L. *Adv. Drug Deliv. Rev.* **2008**, *60*, 1615-1626.
10. Low, P.S. Henne W.A.; Doorneweerd, D.D., *Acc. Chem. Res.* **2008**, *41*, 120-129.
11. Yuan, C.; Raghupathi, K.; Popere, B. C.; Ventura, J.; Dai, L.; Thayumanavan, S. *Chem. Sci.* **2014**, 5, 229-234.
12. Li, L.; Raghupathi, K.; Yuan, C.; Thayumanavan, S. Chem. Sci. **2013**, 4, 3654-3660.
13. Crayton, S.H.; Tsourkas, A. *ACS Nano*, **2011**, *5*, 9592-9601.

14. Reshetnyak, Y. K.; Andreev, O.A.; Segala, M.; Markin, V.S.; Engelman, D.M. *Proc. Natl. Acad. Sci.* **2008**, *105*, 15340-15345.

15. Romberg, B.; Hennink, W.E.; Storm. G. *Pharm. Res*. **2008**, *25*, 55-71.

16. Quan, C.Y.; Chen, J.X.; Wang, H.Y.; Li, C.; Chang, C.; Zhang, X.Z.; Zhuo, R.X. *ACS Nano*, **2010**, *4*, 4211-4219.

17. Zhao, R.; Han, X.; Li, Y.; Wang, H.; Ji, T.; Zhao, Y.; Nie, G. *ACS Nano*, **2017**, *11*, 8103-8113.

18. Harris T.J.; von Maltzahn, G.; Lord, M.E.; Park, J.-H.; Agrawal, A.; Min, D.-H.; Sailor, M.J.; Bhatia, S.N. *Small*, **2008**, 4, 1307-1312.

19. Hatakeyama, H.; Akita, H. ; Kogure, K. ; Oishi, M. ; Nagasaki, Y.; Kihira, Y.; Ueno, M.; Kobayashi, H. ; Kikuchi, H. Harashima, ; H.; *Gene Therapy*, **2007**,14, 68-77.

20. Zhang, J. X. ; Zalipsky,S. ; Mullah,N. ; Pechar,M. ; Allen,T. M. *Pharmacol. Res*. **2004,** *49*, 185-198.

21. Jiang,T. ; Olson, E. S.; Nguyen,Q. T.; Roy, M. ; Jennings, P. A. ; Tsien, R. Y. *Proc. Nat. Acad. Sci. U. S. A.* **2004**, *101*, 17867-17872.

22. Zhang, Y.; So, M. K. ; Rao, J. H. ; *Nano Lett.* **2006**, *6*, 1988-1992.

23. Suresh, A.K.; Weng, Y.; Li, Z.; Zerda, R.; Haute, D.V.; Williams, J.C.; Berlin, J.M. *J. Mater. Chem. B*, **2013**, *1*, 2341-2349.

24. Sharma U, Pal D, Prasad R. *Indian Journal of Clinical Biochemistry*. **2014** , 29(3):269-78.

25. Ooi, K., Shiraki, K., Morishita, Y. and Nobori, T., *Journal of clinical laboratory analysis*, **2007,** 21(3), 133-139.

26. Bui, M.H., Seligson, D., Han, K.R., Pantuck, A.J., Dorey, F.J., Huang, Y., Horvath, S., Leibovich, B.C., Chopra, S., Liao, S.Y. and Stanbridge, E., *Clinical cancer research*, **2003**, 9(2), 802-811.

27. Thiry, A., Dogne, J.M., Masereel, B. and Supuran, C.T., *Trends in pharmacological sciences*, **2006,** 27(11), 566-573.

28. Mal, N.K., Fujiwara, M. and Tanaka, Y., *Nature*, **2003,** 421(6921), 350.

29. Trenor, S.R., Shultz, A.R., Love, B.J. and Long, T.E., *Chemical Reviews*, **2004**. 104(6), 3059-3078.

CHAPTER 6

SUPRAMOLECULAR ASSEMBLIES FOR PROTEIN TRANSPORT ACROSS SOLVENT INTERFACE

Adapted with permission from Gao, J.; Zhao, B.; Wang, M.; Serrano, M. A. C.; Zhuang, J.; Ray, M.; Rotello, V.; Vachet, R. W.; Thayumanavan, S. "Supramolecular Assemblies for Transporting Proteins Across an Immiscible Solvent Interface" *J. Am. Chem. Soc.,* **2018**, 140, 2421–2425.

6.1 Introduction

Transporting molecules across incompatible interfaces is a significant challenge, especially for macromolecules. A striking example of an interfacial barrier is the cellular membrane, where an organized presentation of hydrophilic and hydrophobic functional groups provides a formidable barrier for molecular transport.[1] While small hydrophobic molecules can passively transport across this membrane barrier and small ionic molecules can be transported through natural or artificial ion channels, globular proteins with large hydrophilic surfaces offer no easy access. [2,3] Nonetheless, cells do transport proteins when necessary for inter-cellular communication, often using nanoscopic vesicular compartments called exosomes.[4,5] Inspired by these cell-derived vesicles, we became interested in exploring the possibility of transporting proteins into a nanoscopic compartment across a solvent interface. While simply transporting proteins across interfaces has many implications, selective transport, while retaining structure and function, could be transformative in applications such as sensing, delivery, and diagnostics. Supramolecular assemblies have already shown great potential in these areas[6-8] and

supramolecular protein transport would add to this armor. Reverse micelle systems from small molecule surfactants have shown the potential to solubilize proteins in organic solvent, however, the stability can be easily affected by a lot of factors such as salt and pH.[9-11] Also, the selectivity of these systems is quite limited. Herein, we report a simple supramolecular approach based polymeric platform that selectively transports water-soluble globular proteins from an aqueous phase to the water-pool of a reverse micelle in an apolar organic phase (Figure 6.1).

We outline two strategies to selectively shuttle protein molecules from an aqueous phase. In the first approach, we rely on complementary electrostatic interactions to bind proteins in an aqueous phase and ferry them over to the interior of a reverse micelle in an apolar solvent such as toluene. In a second approach, we explore the use of specific ligand-protein interactions to selectively transport proteins from an aqueous phase into an apolar phase.

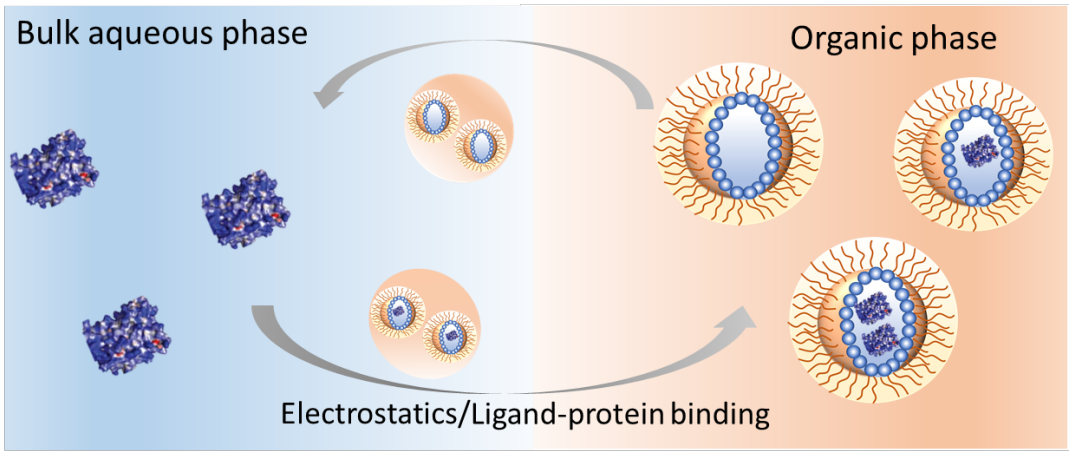

Figure 6.1. Schematic representation of reverse micelle driven protein transportation.

6.2 Results and discussion

6.2.1 Molecular design and synthesis

For the initial proof-of-concept, we first synthesized a polystyrene-based amphiphilic random copolymer **P1** (M_n= 11 kDa, Đ=1.09) (Figure 6.2a). This anionic polymer, achieved using nitroxide-mediated polymerization, comprises of 40% *p*-decyloxystyrene as the hydrophobic monomer and 60% of *p*-oxyacetyl-styrene as the hydrophilic monomer. A corresponding cationic polymer, **P2**, was obtained by coupling the carboxylate acid moiety in **P1** with *N,N*-dimethylethylenediamine under EDC-coupling conditions, followed by quaternization of the tertiary amine with methyl trifluoromethanesulfonate (Figure 6.2b).

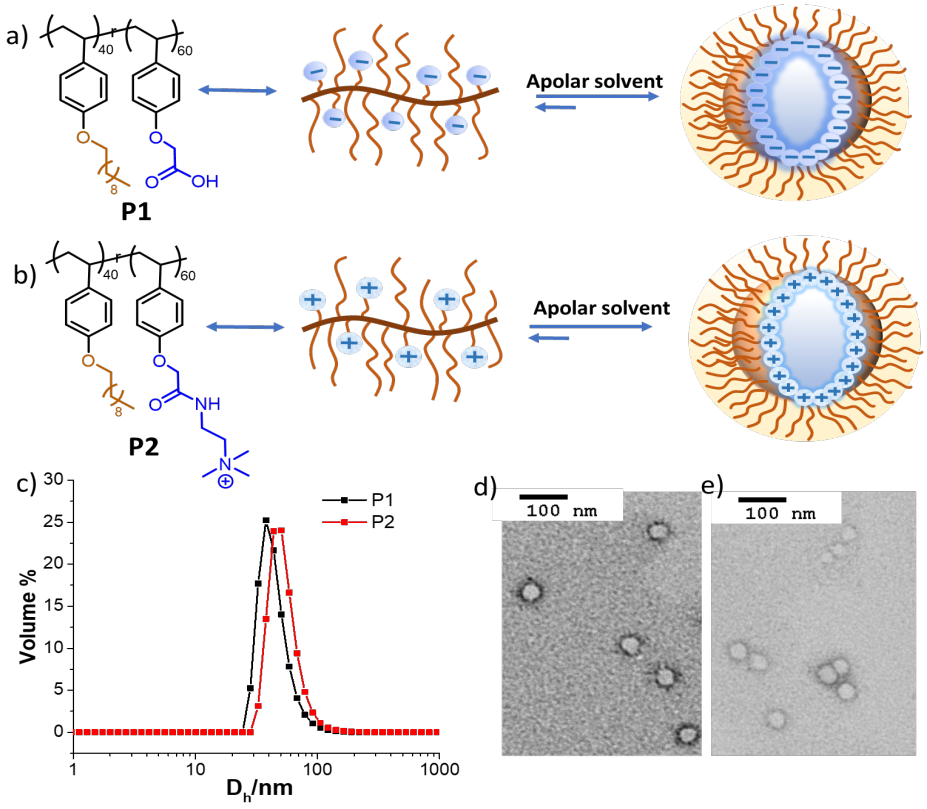

Figure 6.2. Structural features of polymeric reverse micelles. Molecular structure of polymer **P1** (M_n= 11 kDa, Đ= 1.09) a) and **P2** b) (M_n= 12 kDa, Đ= 1.15), c) DLS profile of **P1** and **P2** in toluene, TEM of **P1**(d) and **P2**(e).

6.2.2 Reverse micelle preparation and characterization

The possibility of these polymers forming a reverse micelle assembly was tested by distributing these polymers in toluene along with two equivalents of water per carboxylate or quaternary ammonium moiety. The water molecules are added to provide a 'water pool' for the reverse micelles. Assemblies with a fairly homogeneous size distribution of 50 nm for **P1** and 37 nm for **P2** were observed, as discerned by both dynamic light scattering (DLS) (Figure 6.2c) and transmission electron microscopy (TEM) (Figure 6.2d-e).

6.2.3 Electrostatic interaction driven protein transport

The key premise for the work here is that the polymers would self-assemble in apolar solvents, bind to complementarily charged proteins in the aqueous phase, and ferry them across the interface to the interior of the reverse micelles in toluene. To test this possibility, porcine liver esterase (plE, MW = 168 kDa) was used as the model protein, because this protein is negatively charged enzyme at pH 8.0 (isoelectric point pI = 5.3). We used reverse micelles based on the cationic polymer **P2**. Upon equilibrating an aqueous solution containing plE with a toluene solution containing **P2** (1 mg/mL) reverse micelles, the presence of proteins in both phases was detected using matrix assisted laser desorption/ionization mass spectrometry (MALDI-MS). Figures 6.3a and 6.3b show the

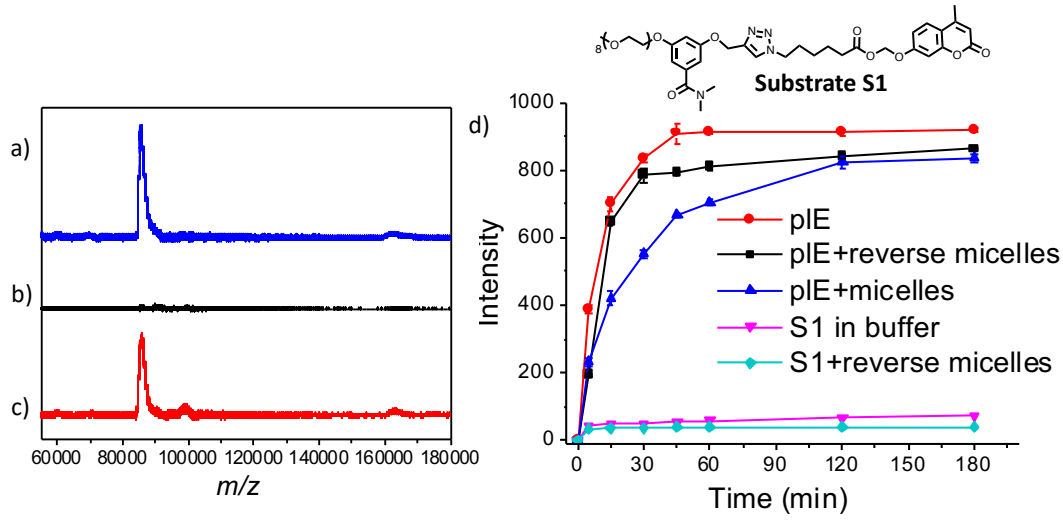

Figure 6.3. MALDI-MS analysis of a) aqueous phase before equilibration, b) organic phase before equilibration, and c) the organic phase after equilibration. d) Activity of esterase (based on substrate cleavage) inside reverse micelles compared with esterase activity in bulk aqueous phase.

mass spectrum of the aqueous and organic phases, respectively, before equilibration. After equilibration, we were gratified to observe the presence of a peak corresponding to plE in the organic phase (Figure 6.3c), suggesting that plE was successfully transported into interior of the reverse micelles.

In order to quantify the extent of protein that was encapsulated within the reverse micelles, we analyzed the organic phase for proteins using the bicinchoninic acid (BCA) assay. This analysis showed that 1 mg of polymer is capable of transporting and binding to 0.05 mg of plE, an equivalent of 5 wt% loading capacity. This capacity compares much more favorably

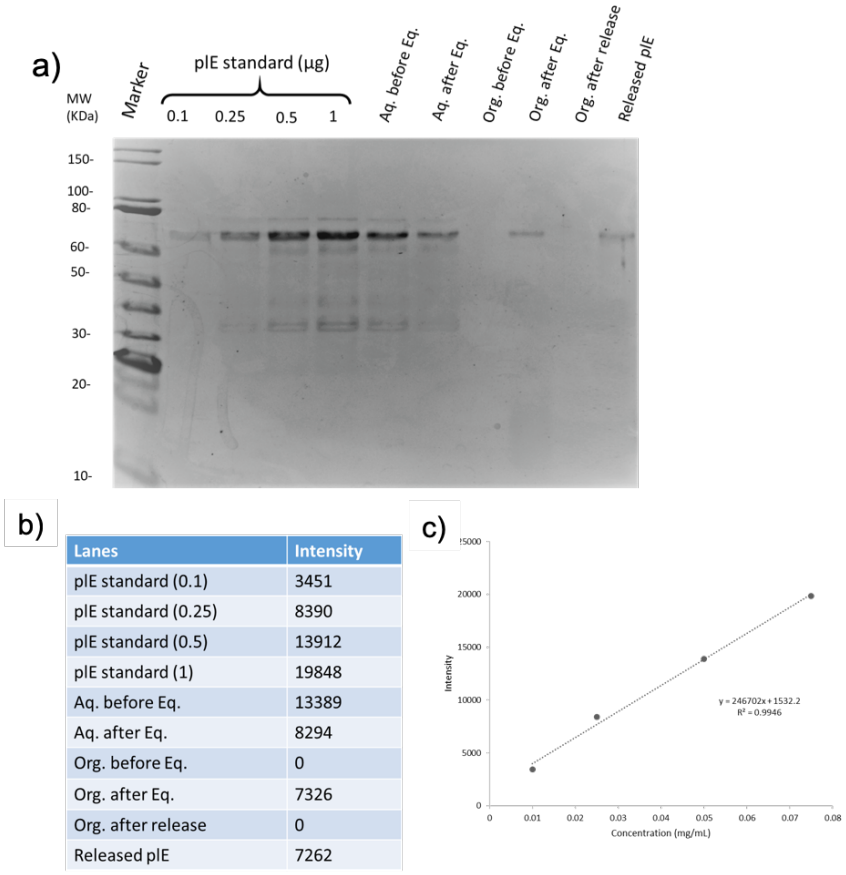

Lanes	Intensity
pIE standard (0.1)	3451
pIE standard (0.25)	8390
pIE standard (0.5)	13912
pIE standard (1)	19848
Aq. before Eq.	13389
Aq. after Eq.	8294
Org. before Eq.	0
Org. after Eq.	7326
Org. after release	0
Released pIE	7262

Figure 6.4. a) SDS-PAGE for transport and release of plE from reverse micelles; b) Intensity value for each band of SDS-PAGE; c) Standard curve of plE based on SDS-PAGE.

than the typical loading capacity of proteins in liposomes.[15] When treated the organic phase with THF and acidic solution, we found that the plE can be released into the aqueous phase, as shown in the SDS-PAGE analysis of organic phase and aqueous phase before and after equilibration (Figure 6.4).

A more compelling analysis is to identify whether the enzyme molecules, which were extracted into the organic phase, remain active. To investigate this possibility, we synthesized a substrate for plE that is amenable for use both in organic and aqueous phases (Scheme 6.1). If we were to use water-soluble substrates and investigate the activity in the reverse micelles using an apolar solvent, we would likely get a solvophobically driven concentration increase of the substrate, which could be interpreted as an increase in

enzymatic activity in the reverse micelle. Instead, we were interested in truly estimating the activity of the enzyme. Therefore, we designed and synthesized an amphiphilic coumarin-based profluorophore **S1**. The alkylated phenolic state of this substrate causes this molecule to be non-fluorescent. When the ester bond of **S1** is cleaved by the enzyme, the resultant hemiacetal rapidly degrades to generate umbelliferone, a fluorescent coumarin molecule.

Scheme 6.1. Substrate cleavage in present of esterase

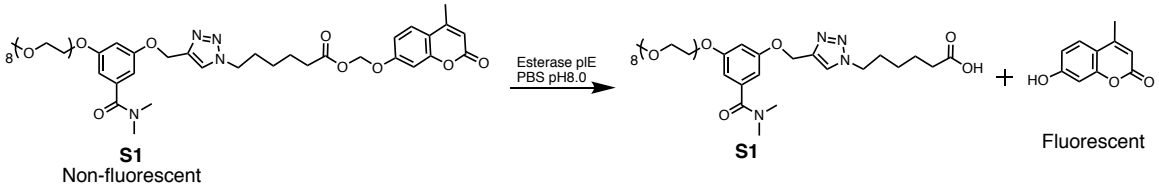

The substrate itself was quite stable in PBS buffer as well as after equilibration with toluene solution containing **P2**. In the presence of plE, however, a rapid hydrolysis of **S1** to generate the fluorescent umbelliferone was observed (Figure 6.3d). We then analyzed the possibility of this reaction in toluene in the presence of reverse micelles loaded with plE. Interestingly, the hydrolysis rate was found to be quite similar to that of the free enzyme. As the estimated concentration of the enzyme inside the reverse micelle and the free plE in the aqueous phase in the two experiments above are the same, these results were taken to suggest that the activity of plE is maintained inside the reverse micelles. As another control experiment, we were interested in finding whether the electrostatic complex between **P2** and plE has any inherent effects upon the activity of the latter. To test this, we mixed plE and **P2** in aqueous phase and found that the activity of the enzyme was slightly lower, suggesting that interactions between **P2** and plE have little effect on plE activity.

When considering the pathway by which these polymers could transport proteins across the interface, two limiting possibilities can be proposed. Note that these polymers can form

micelle-like assemblies in the aqueous phase and reverse-micelle-like assemblies in the apolar toluene phase. Therefore, it is possible that the polymers equilibrate themselves between the two phases. The resultant thermodynamic equilibrium between the two solvent phases, combined with the complementary binding affinity to the proteins, cause proteins to be extracted to the organic phase. Alternately, the exchange of water molecules between the interior of the reverse micelle and the bulk water (in the biphasic mixture) ferry proteins into the interior of the reverse micelles. If there is an affinity between the protein and the functional groups within the interior of the assembly, then the proteins would stay in the reverse micelle. In this latter scenario, the polymer assemblies remain kinetically trapped as reverse micelles in the organic phase. To differentiate these two pathways, we equilibrated the reverse micelle assemblies of polymers **P1** and **P2** with water. UV-visible absorption spectra of both phases indicate that these polymers fully remain in the apolar phase (Figure 6.5). While this suggests that the polymers might be kinetically trapped in the organic phase, it is also possible that these polymers thermodynamically prefer the apolar phase. To delineate this possibility, these polymers were initially assembled as micelles in the aqueous phase and equilibrated with toluene (Figure 6.6). The exclusive presence of these polymers in the aqueous phase, this time, shows that these supramolecular assemblies are kinetically trapped in the solvent that they are initially assembled. Overall, these results suggest protein molecules can exchange between phases, but only remain in the apolar phase if they have favorable interactions with the reverse micelle interiors.

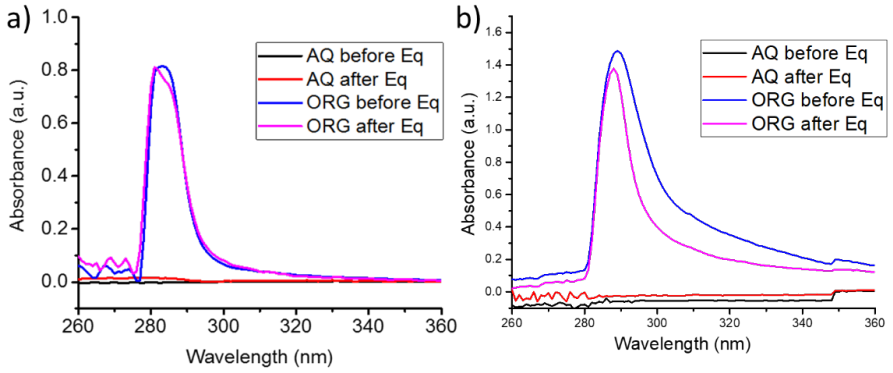

Figure 6.5. UV-Vis measurements with reverse micelles of a) polymer P1 (1×10^{-4} M), b) polymer P2 (1×10^{-4} M starting in toluene (ORG), before and after equilibration with aqueous phase (AQ).

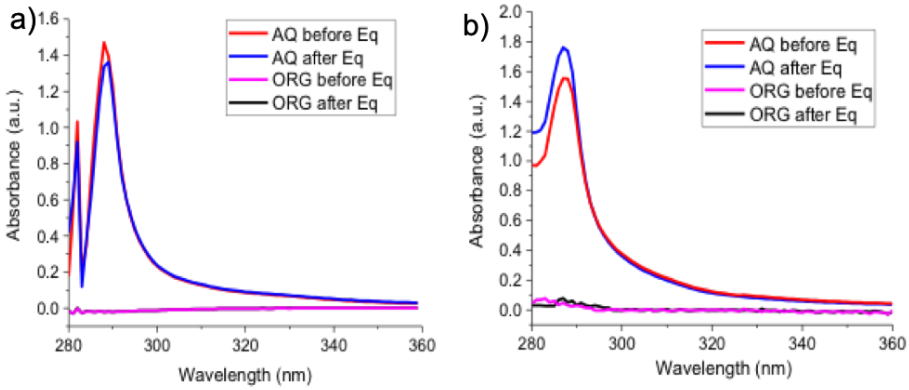

Figure 6.6. UV-Vis measurements with micelles of a) polymer P1 (1×10^{-4} M), b) polymer P2 (1×10^{-4} M starting in water (AQ), before and after equilibration with apolar phase toluene (ORG).

Following these observations, we were interested in exploring the applicability of this approach to other non-enzymatic proteins. Green fluorescent protein (GFP) was used as the first model protein, not only because it can be readily monitored using fluorescence, but also because the fluorescence itself is a good indicator of whether the protein maintains its tertiary structure. Since wild-type GFP (pI 6.2) has a net charge of -7 at pH 7.4, we hypothesized that positively-charged reverse micelles from **P2** should be able to move GFP (-7) from aqueous phase to organic phase. To test this possibility, an aqueous solution of GFP was equilibrated with the **P2** reverse micelle solution in toluene. We were gratified to find that the emission spectrum of the organic phase clearly showed the presence of GFP. To further confirm the presence of GFP in the organic phase, samples of both phases were analyzed by MALDI-MS and a peak with a *m/z* ratio of 28,432 Da was indeed observed in both phases (Figure 6.7).

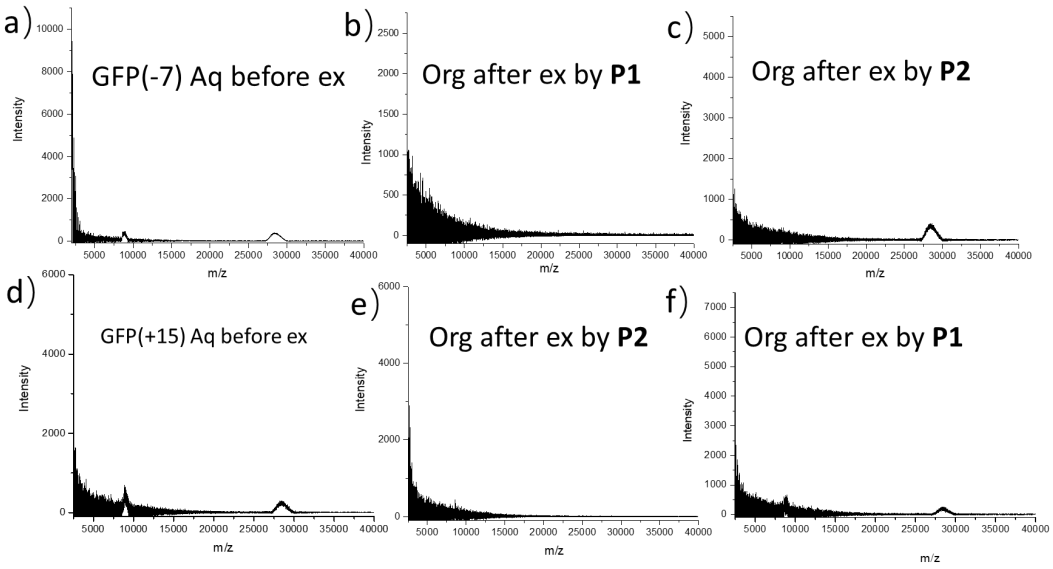

Figure 6.7 MALDI-MS analysis of GFP before and after transportation a) GFP (-7) before transportation, b) organic phase after transportation GFP (-7) using P1, c) organic phase after transportation GFP (-7) using P2, d) GFP (+15) before transportation, b) organic phase after transportation GFP (+15) using P2, c) organic phase after transportation GFP (+15) using P1.

Note that the extent of extraction was not optimized to be quantitative, because the incomplete extraction provides an important insight into the nature of the GFP inside the reverse micelles. The combination of emission intensities in the aqueous and the organic phases equal that of the pre-equilibrated emission intensity in the aqueous phase (Figure 6.8a). This observation suggests that GFP maintains its tertiary structure, responsible for the fluorophore preservation in the protein, during the transport process across the solvent interface. To confirm that this transport is indeed due to electrostatic complementarity, a control experiment using the anionic reverse micelle from **P1** was carried out. Indeed, there was no discernible change in the emission intensity of the aqueous phase (Figure 6.8b).

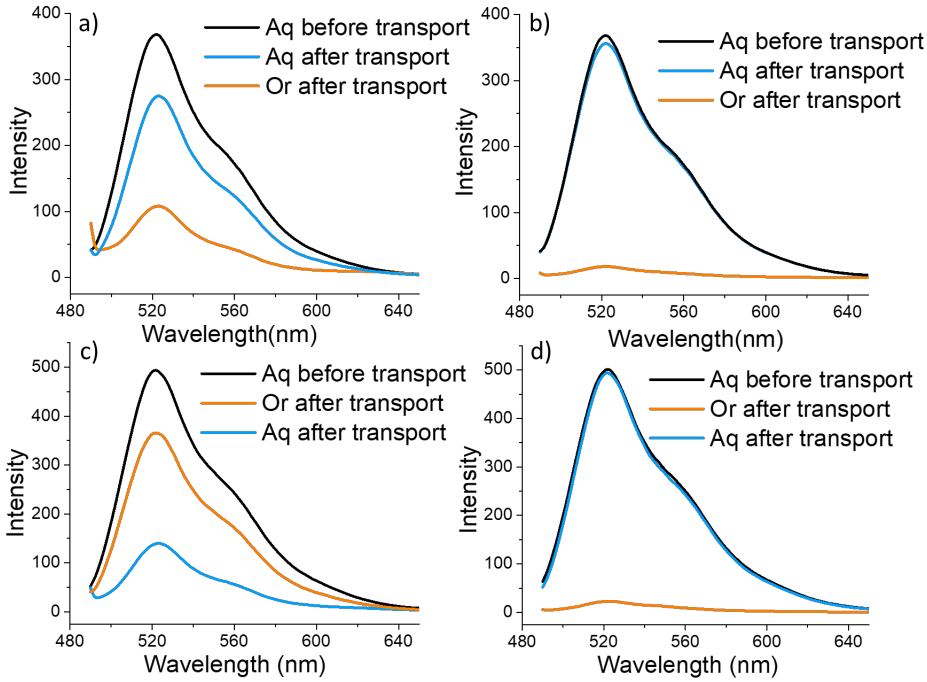

Figure 6.8. Emission spectrum of GFP showing whether it was transported to the organic phase, a) GFP (-7) transport by **P2**, b) GFP (-7) transported by **P1**, c) GFP (+15) transported by **P1**, d) GFP (+15) transported by **P2**.

To further test this idea, we utilized cationic GFP protein, the so-called supercharged GFP (+15).[16] Indeed here, the anionic polymeric reverse micelle from **P1** is able to transport the protein across the interface, while the cationic reverse micelle from **P2** does not affect the

protein in the aqueous phase (Figures 6.8c and 6.8d). The results from these studies show that: (*i*) transport of proteins across the interface is due to electrostatic complementarity, not due to spurious differences in inherent binding abilities of **P1** and **P2**; (*ii*) the tertiary structure of the proteins can be preserved upon transport across the interface as indicated by the roughly equal emission intensities before and after equilibration; (*iii*) at similar polymer and protein concentrations, the extent of protein extraction in GFP (+15) is considerably higher than GFP (-7), showing that binding affinity can influence the extent of proteins transported across the interface.

6.2.4 Protein transport driven by ligand-protein binding

While electrostatic complementarity can be utilized to simplify protein mixtures and enable identification of the presence of specific proteins, this ability will be even more greatly enhanced if proteins can be transported across an interface in response to a specific ligand-protein interaction. To investigate this possibility, we used bovine carbonic anhydrase (bCA) as the model protein, because aryl sulfonamides are well-established as small molecule ligands for this protein.[15,18] The design hypothesis here is that if this ligand was installed in the polymeric reverse micelles, it should be able to selectively transport bCA to the organic phase due to specific binding.

We designed a zwitterionic amphiphilic polymer for this purpose, as the charge-neutral zwitterionic polymer avoids any electrostatics-based non-specific interactions. Accordingly, a random copolymer **P3** (Figure 6.9a), containing 40% decyl chain as the hydrophobic moiety, 40% zwitterionic sulphobetain group as the hydrophilic moiety and 20% benzene sulfonamide as the ligand moiety, was prepared through post-modification of polymer **P1**. **P3** forms a similarly sized assembly in apolar solvents. To test the capability

of **P3** in transporting proteins, we first labeled bCA with tetramethylrhodamine-5-isothiocyanate (TRITC) to monitor the location of proteins using fluorescence. Indeed, after equilibration of an aqueous phase containing TRITC-bCA with the organic phase containing **P3** micelles, we observed a strong emission peak in organic phase, indicating the transportation of TRITC-bCA conjugates. Concurrently, there is a dramatic decrease in the fluorescence intensity in the aqueous phase, indicating bCA is successfully transported across the interface.

To investigate whether this is driven by the ligand-protein binding, we designed a control experiment in which a structurally similar amphiphilic polymer, **P4**, which forms reverse micelles but lacks the sulfonamide functional group, was equilibrated with an aqueous solution containing TRITC-bCA. No change is observed in the emission spectrum of both organic and aqueous phases, when using **P4** as the transporter (Figure 6.9b). To further test whether the specific ligand-protein interaction is responsible for the observed transport across the interface, we designed another control experiment. For a ligand to bind to the active site of the protein, the structural integrity of the protein must be maintained. Before attempting to transport the protein, we disrupted the structure of the protein by denaturing the protein with acetonitrile and heat. The denatured bCA should not be able to bind the sulfonamide ligands and thus would not be transported into the organic phase. Indeed, we find that no fluorescence changes in the aqueous or organic phase are observed, showing that no bCA was transported into the organic phase (Figure 6.9b). These results confirm that transportation occurs only when bCA's native structure is maintained in such a way to preserve its ability to bind the sulfonamide ligand. Overall, these results suggest that

specific ligand-protein interactions can be utilized to bind and transport proteins across the solvent interface.

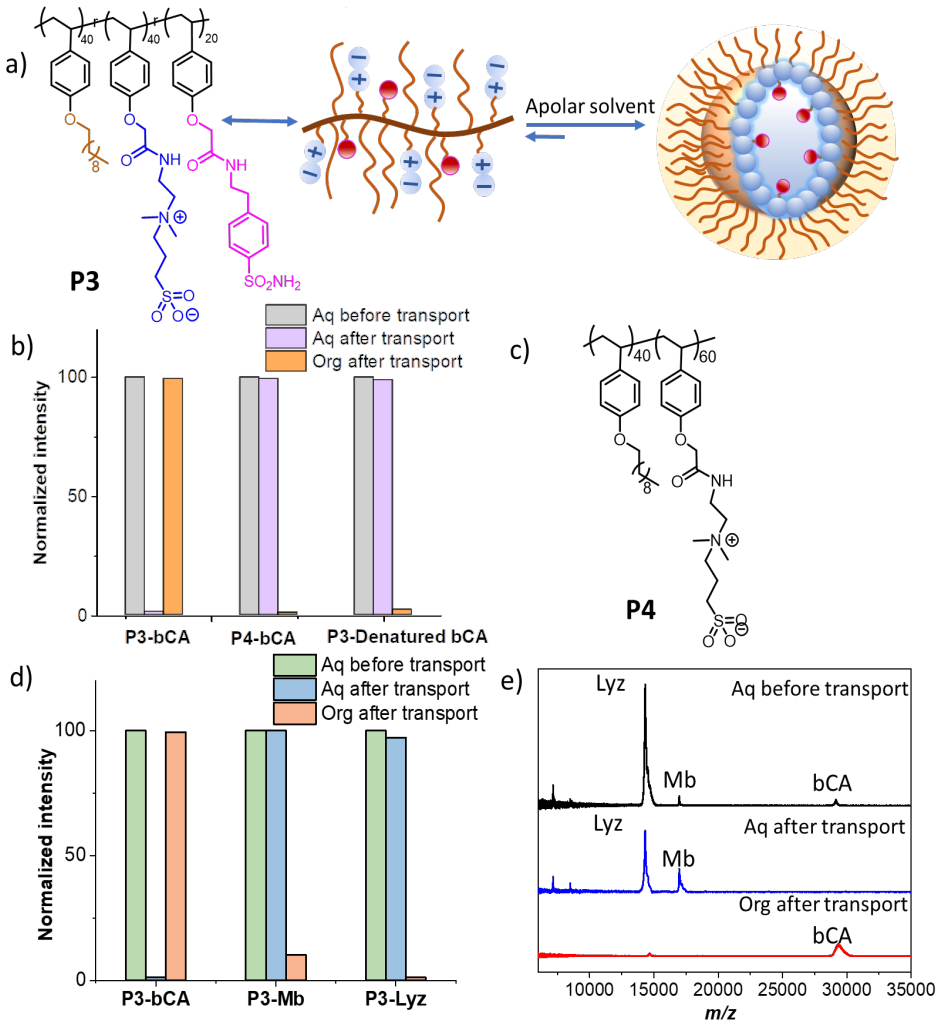

Figure 6.9. a) Molecular structure of P3, b) Fluorescence change of aqueous/organic phase using P3 or P4 to transport bCA, c) Molecular structure of P4, d) Fluorescence change of aqueous/organic phase of P3 to transport bCA, Myb or Lyz, e) MALDI-MS analysis of protein mixture before and after transportation.

Next, to test the ligand-protein binding based selectivity associated with this process, we performed another set of control experiments using myoglobin (Mb) and fluorescently labelled lysozyme (Lyz). Myoglobin was chosen because it has absorption at 409 nm, while lysozyme was labelled as TRITC-lysozyme conjugates, in order to independently monitor the movement of these proteins by fluorescence change. Since benzene sulfonamide

ligands have little to no binding affinity to these proteins, we predicted that Mb and Lyz would remain in the aqueous phase. Indeed, no discernible fluorescence change was observed in both aqueous and organic phases for these two proteins, suggesting that the ligand attached reverse micelles are specific for the target protein bCA (Figure 6.9d). These experiments were initially done separately due to the possible bleeding of fluorescence emission. Selective transport from a mixture of these proteins was tested using MS. In this experiment, Mb, Lyz and bCA were prepared as a protein mixture at the same concentration, and then **P3** was used to transport bCA from the aqueous phase to the organic phase. We were gratified to find that only bCA is transported to the organic phase, while Mb and Lyz remained in the aqueous phase as indicated by the mass spectra before and after equilibration (Figure 6.9e). These data strongly support the idea that ligand-attached reverse micelle systems are specific for target proteins.

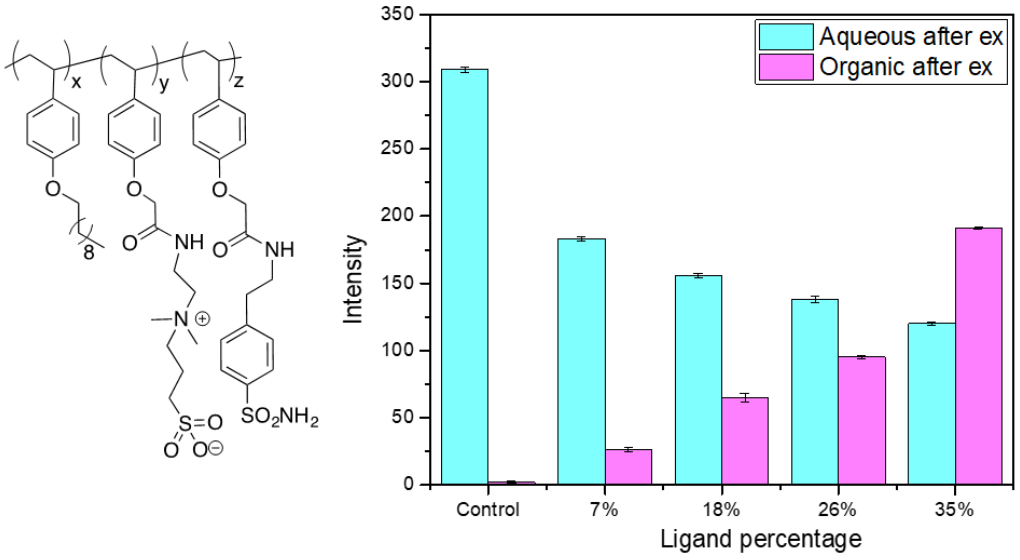

Figure 6.10. Increase in the ligand intensity (z value) can transport more bCA from aqueous phase to organic phase.

6.3 Summary

In conclusion, we have demonstrated a set of supramolecular assemblies, based on

amphiphilic polymers, that can transport proteins across a solvent interface. We have shown here that: (*i*) simple electrostatic complementarity in polymeric reverse micelle systems can transport proteins from bulk aqueous phase into the interior of a reverse micelle assembly in the apolar organic phase; (*ii*) the activity of the transported proteins is retained in the process; (*iii*) the efficiency of protein binding is dependent on the charge density presented on the protein surface; (*iv*) the kinetically trapped nature of the assemblies suggest that the polymers do not ferry the proteins but instead transport likely occurs during the solvent exchange within the interior of the assembly, when these assemblies transiently find themselves at the aqueous/organic phase interface during equilibration, as illustrated in Figure 6.1; (*v*) specific ligand-receptor interactions can be used to selectively extract proteins from the aqueous phase. Overall, the most gratifying finding here is that whole proteins can be moved across a solvent interface into the interior of a supramolecular assembly, even though the resident location of the assembly is in an incompatible solvent for the protein. The preliminary findings here have implications in many areas, especially in sensing, diagnostics, and catalysis. For example, these systems can be further developed to detect biomarkers in more complex mixtures of proteins.[17-23] Similarly, facile incorporation of active proteins in organic solvents could facilitate enzyme-based catalysis for a broader range of organic substrates.[24-29] These constitute examples of future directions for this research in our own laboratories.

6.4 Experimental procedures

6.4.1 General methods

All reagents were commercially available and used as received unless stated otherwise. ^{1}H-NMR spectra were recorded on a 400 MHz or a 500 MHz NMR spectrometer using residual

proton resonance of the solvents as internal standard. Chemical shifts are reported in parts per million (ppm). Mass spectra were obtained by a Bruker AmaZon quadrupole ion trap mass spectrometer coupled with electrospray ionization source. Gel permeation chromatography (GPC) was used to estimate the molecular weight of polymers using THF/DMF as eluent and 1 μL of toluene was added as the internal reference. Polystyrene standards were used for calibration and data analysis.

For the DLS measurements, the polymers were dissolved in toluene, and one equivalent of water per hydrophilic unit was added to form the water pool inside the reverse micelles. The samples were sonicated until clear solutions were formed. DLS measurements were carried out in a quartz cuvette at room temperature. The sizes of each solution were recorded overtime by a Malvern Nanozetasizer ZS90 with a 637-nm laser source with non-invasive backscattering technology detected at 173^{o} using quartz cuvette. Standard operating procedures (SOP) are set up including following parameters: the sample was equilibrated for 120 s at 25 ^{o}C before each measurement; the sizes were reported as the hydrodynamic diameter (D_H) and each measurement average 16 runs were repeated three times.

For TEM measurement, the same sample for DLS measurement was dropped onto carbon-coated copper grid. The grid was dried by slow evaporation in air, and then dry separately in a vacuum overnight. Images were recorded on a JEOL-2000FX electron microscopy operated at 200 kV and at a nominal magnification of 5000X. At least 10 locations on the TEM grid were examined. The assembly diameter was calculated using ImageJ software.

Matrix Assisted Laser Desorption/Ionization Mass Spectrometry (MALDI-MS): MALDI-MS analysis of samples before and after transport were performed with Bruker Autoflex

III time-of-flight mass spectrometer. The matrix was prepared with a solvent mixture of acetonitrile, water and trifluoroacetic acid (with a ratio 50:47.5:2.5) containing 10 mg/mL sinapic acid. The matrix and samples from aqueous or organic phase were mixed at 1:1 ratio and spotted on the MALDI target for analysis.

Protein transport and release experiments: For protein transport with reverse micelles, 500 uL of a toluene solution of polymers (1 mg/mL) with 1 mL of protein in 10 mM PBS buffer at pH 7.4. The mixture is vortexed for 30 min and centrifuged at 10,000 rpm for 1 h to separate the organic and aqueous layers. The organic phase and aqueous phase is then analyzed by MALDI-MS or fluorimeter.

For the release of proteins back into the aqueous phase, the 500 uL organic phase contains proteins was treated with 100 uL THF and then equilibrated with 400 uL 1 M HCl for 30 minutes. After centrifugation for 30 minutes, the phase was separated. The pH of aqueous phase was adjusted to 7.4 for further analysis.

Quantification of porcine liver esterase in reverse micelles: 1) Through the BCA method: The standard curve was made using Pierce BCA assay kit[S3] as following the protocols. Pipette 0.1 mL of each standard sample (0.005, 0.025, 0.05, 0.125, 0.25, mg/mL, three replicates for each sample) and the unknown plE sample into test tube and then add 2.0 mL of the working reagent to each tube and mix well. Cover and incubate tubes at 60 ^{o}C for 30 minutes and then cooled to room temperature. Then took the readings from UV-Vis at 562 nm. The standard curve was prepared plotting the average 562 nm measurement for each standard sample vs. its concentration. Then the plE concentration of aqueous phase after transport was determined using the standard curve. The difference of aqueous phase before and after the equilibration provide the loading capacity of reverse micelles.

2) Through SDS-PAGE method: Standard curves were generated from the known concentrations of protein samples loaded into the gel lanes. Then the samples of aqueous phase before and after the equilibration were loaded to the gel lane. For the organic phase, the samples for gel lanes were dried with air and dissolved in THF/H_2O. The intensities for the band will be used to calculate the protein concentration of each phase. The concentration of protein for the organic phase after equilibration can provide how much proteins have been transported into the organic phase.

SDS-PAGE Analysis: For the transport and release of plE studies: 20 μL of different samples containing plE were mixed with 20 μL of loading buffer (3% DTT), then incubated 95 ºC for 10 minutes before subjecting 10 μL of each sample to acrylamide gel electrophoresis. Standard curves were generated from the known concentrations of pure protein samples loaded into the gel lanes. The gel image analysis and quantification were performed with Bio-Rad Image LabTM software.

Evaluation of PlE activity in reverse micelles: First, the amount of plE that got transported into the organic phase was calculated based on the SDS-PAGE or BCA assay. The organic phase containing plE was then equilibrated with an aqueous phase of substrate S1 (100 μM) for 30 minutes. After centrifugation for 30 minutes, the fluorescence of aqueous phase was measured over time. The control experiments with the same amount of plE were performed in aqueous phase.

Protein denaturation: bCA was dissolved in 10 mM PBS (pH 7.4) buffer at a concentration of 1mg/mL, 10% by volume of acetonitrile was added to the solution and stirred at room temperature for 10 minutes. After that, the mixture was heated at 100ºC for 2 minutes and then a buffer exchange was performed using 3 k Da Amicon Ultra Centrifugal Filters to

remove acetonitrile. Then the sample was diluted to 0.1 mg/mL in 10 mM PBS (pH 7.4) for CD measurement.

Circular dichroism (CD) spectra: CD spectra bCA and denatured bCA were recorded on JASCO J-1500 spectrophotometer. For recording the spectra, 200 μL 0.1 mg/mL protein solution was injected into a quartz cuvette of 1-mm path length, equilibrated at 25 ºC for 10 min and scanned from 190 to 250 nm (scan rate: 20 nm/min, interval: 0.2 nm, average of three spectra).

Fluorescent labeling proteins: Labeling of proteins (lysozyme (Lyz), bovine serum albumin (BSA) and bovine carbonic anhydrase (bCA)) with Tetramethylrhodamine-5-Isothiocyanate (TRITC) or Fluorescein Isothiocyanate (FITC). In a typical labelling procedure, proteins (4 mg) were dissolved separately in 2 mL of 0.1 M $NaHCO_3$ buffer (pH 8.5) and stirred for 15 min at 4 ºC. TRITC/FITC (5 eq. of each protein, 10 mg/mL in DMSO) was added dropwise to each protein solution and stirred at 4 ºC for 2 h protected from light. The labelled-proteins were purified by extensive dialysis with 50 mM PBS pH 7.4 and 50 mM NaCl mixture to remove excess dye and concentrated using 3 kDa Amicon Ultra Centrifugal Filters. Protein concentrations in each labelled conjugate were calculated using UV-Vis spectroscopy.

6.4.2 Polymer synthesis

Synthesis of compound 1: According to previous procedure[S1], to a solution of acetone mixed with K_2CO_3 (11.84 g, 85.65 mmol) and 18-crown-6 (1.13 g, 4.28 mmol), 4-hydroxybenzaldehyde (5.23 g, 42.83 mmol) was added and stirred for 5 min. To this mixture, 1-bromodecane (14.21 g, 64.24 mmol) was added and stirred while refluxing for 20 h. The reaction mixture was then cooled to room temperature and filtered to afford the

crude product in acetone solution. The solvent was evaporated to dryness and purified by silica gel column chromatography (8-10% ethyl acetate in hexanes) to obtain 8.8 g (79% yield) of **1**. ^{1}H NMR (400 MHz, $CDCl_3$) δ 9.80 (s, 1H), δ 7.83-7.81 (d, *J* = 8.0 Hz, 2H), δ 7.00-6.98 (d, *J* = 8.0 Hz, 2H), δ 4.02-4.05 (t, *J* = 6.6 Hz, 2H), δ 1.76-1.83 (quint, 2H), δ 1.47-1.26 (m, 14H), δ 0.87-0.91 (t, *J* = 6.8 Hz, 3H). ^{13}C NMR (100 MHz, $CDCl_3$) δ 190.7, 164.2, 131.9, 129.7, 114.7, 68.4, 31.9, 29.5, 29.63, 29.32, 29.31, 29.1, 25.9, 22.7, 14.1. ESI-MS (expected: $[m+H]^+$= 263.19, obtained: $[m+Na]^+$= 285.2)

Scheme 6.2. Synthetic route for polymer **P1**

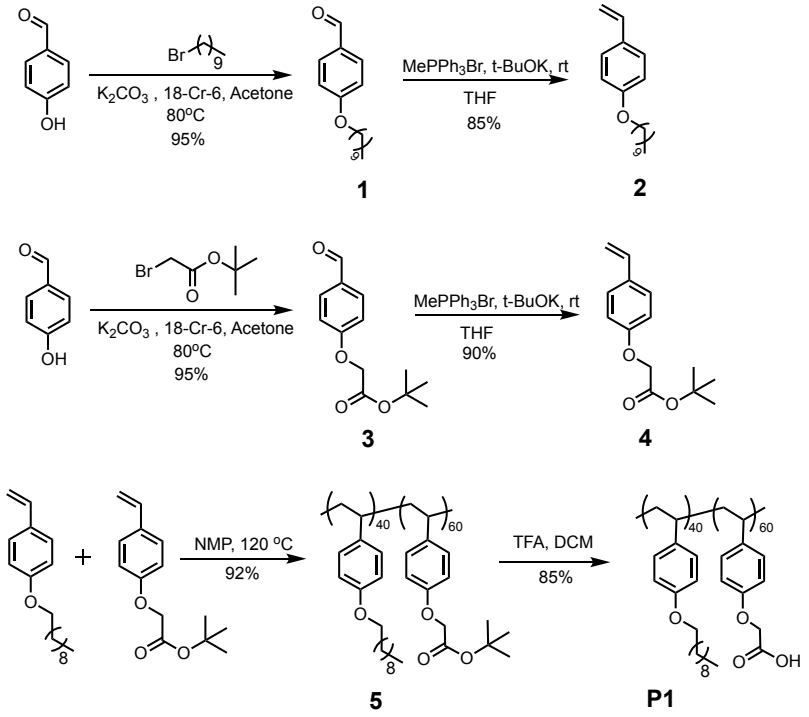

Synthesis of compound 2: Methyltriphenylphosphonium bromide (6.58 g, 25.11 mmol) and potassium tert-butoxide (3.94 g, 35.15 mmol) were mixed in a round bottom flask, and dry THF (20 mL) was added to the mixture. The mixture was stirred under argon atmosphere in an ice bath for 15 min to yield a bright yellow solution. **1** (6.58 g, 25.11 mmol) was slowly added to the mixture. The reaction mixture was further stirred for 5 h.

After the reaction, saline and ethyl acetate were added for extraction. The combined organic layer was separated and washed with saline (3 times). The organic layer was evaporated to dryness and purified by silica gel column chromatography (3-5% ethyl acetate in hexanes) to afford 5.7 g (88% yield) of **2**. ^{1}H NMR (400 MHz, $CDCl_3$) δ 7.31-7.33 (d, J = 8.0 Hz, 2H), δ 6.83-6.85 (d, J = 3.4 Hz, 2H), δ 6.61-6.68 (q, 1H), δ 5.57-5.61 (d, J = 7.2 Hz, 1H), δ 5.09-5.12 (d, J = 4.4 Hz, 1H), δ 3.93-3.96 (t, J = 5.4 Hz, 3H), δ 1.73-1.80 (quint, 2H), δ 1.27-1.46 (m, 14H), δ 0.86-0.89 (t, J = 6.8 Hz, 3H). ^{13}C NMR (125 MHz, $CDCl_3$) δ 159.1, 136.4, 130.3, 127.4, 114.6, 111.5, 68.1, 32.1, 29.7, 29.7, 29.5, 29.4, 29.4, 26.1, 22.8, 14.2. ESI-MS (expected: $[m+H]^+$= 261.21, obtained: $[m+Na]^+$= 283.2).

Scheme 6.3. Synthetic route for polymer **P2**, **P3** and **P4**

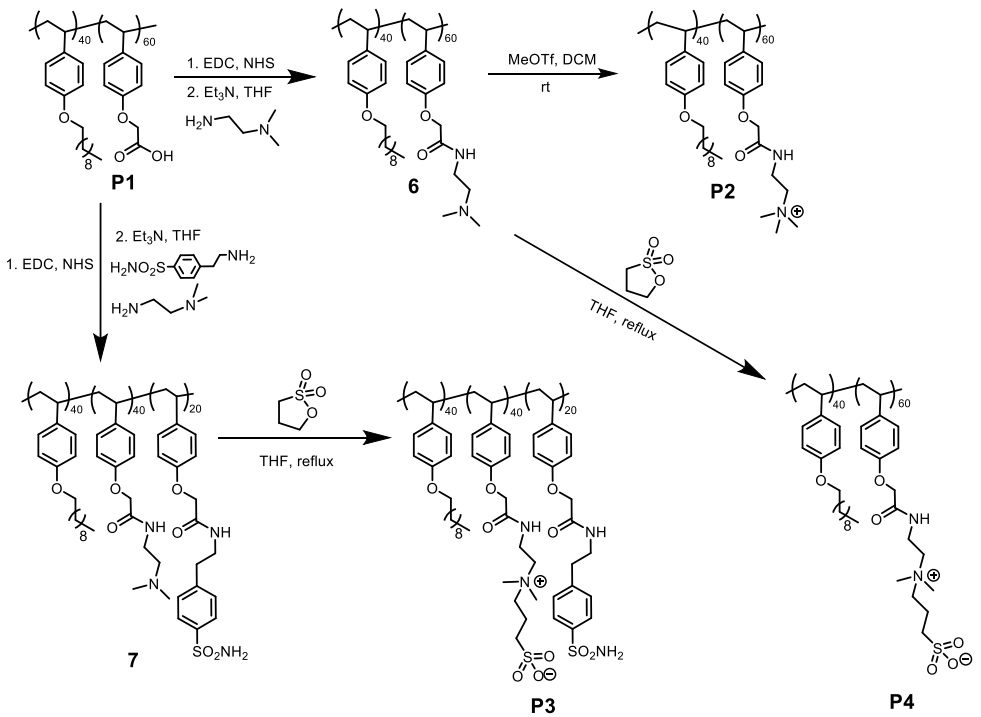

Synthesis of compound 3: To a solution of acetone mixed with K_2CO_3 (6.79 g, 49.13 mmol), NaI (7.36 g, 49.13 mmol) and 18-crown-6 (0.65 g, 2.46 mmol), 4-hydroxybenzaldehyde (3.00 g, 24.57 mmol) was added and stirred for 5 min. To this mixture, tert-butyl

bromoacetate (9.58 g, 49.13 mmol) was added and stirred while refluxing for 20 h. The reaction mixture was then cooled to room temperature and filtered to afford the crude product in acetone solution. The solvent was evaporated to dryness and purified by silica gel column chromatography (10-13% ethyl acetate in hexanes) to obtain 5.3 g (91% yield) of **3**. ^{1}H NMR (400MHz, $CDCl_3$) δ 9.88 (s, 1H), δ 7.82-7.84 (d, *J* = 4.2 Hz, 2H), δ 6.97-6.99 (d, *J* = 4.4 Hz, 2H), δ 4.59 (s, 2H), δ 1.47 (s, 9H). ^{13}C NMR (100 MHz, $CDCl_3$) δ 190.8, 167.2, 162.8, 132.0, 130.7, 114.9, 83.0, 65.6, 28.1. ESI-MS (expected: $[m+H]^+$= 237.1, obtained: $[m+Na]^+$= 259.1)

Synthesis of compound 4: Methyltriphenylphosphonium bromide (7.94 g, 22.24 mmol) and potassium tert-butoxide (2.50 g, 22.24 mmol) were mixed in a round bottom flask, and dry THF (15 mL) was added to the mixture. The mixture was stirred under argon atmosphere in an ice bath for 15 min to yield the bright yellow solution. **3** (3.5 g, 14.83 mmol) was slowly added to the mixture. The reaction mixture was further stirred for 5 h. After the reaction, saline and ethyl acetate were added for extraction. The combined organic layer was separated and washed with saline (3 times). The organic layer was evaporated to dryness and purified by silica gel column chromatography (3-5% ethyl acetate in hexanes) to afford 3.3 g (95% yield) of **4**. ^{1}H NMR (400MHz, $CDCl_3$) δ 7.33-7.35 (d, *J* = 1.0 Hz, 2H), δ 6.84-6.87 (d, *J* = 1.0 Hz, 2H), δ 6.63-6.68 (dd, *J* = 17.6, 10.9 Hz, 1H), δ 5.60-5.64 (dd, *J* = 17.6, 0.9 Hz, 1H), δ 5.13-5.15 (dd, *J* = 10.9, 0.8 Hz,), δ 4.51 (s, 2H), δ 1.49 (s, 9H). ^{13}C NMR (100MHz, $CDCl_3$) δ 168.0, δ 157.7, δ 136.2, δ 131.3, δ 127.48, δ 114.7, δ 112.1, δ 82.4, δ 65.8, δ 28.1. ESI-MS (expected: $[m+H]^+$= 235.1, obtained: $[m+Na]^+$= 257.1)

Synthesis of random copolymer 5: A mixture of the compound **1** (500 mg, 1.92 mmol), **2** (675 mg, 2.88 mmol) and *N*-*tert*-butyl-*N*-(2-methyl-1-phenylpropyl)-*O*-(1-phenylethyl) hydroxylamine (NMP initiator, 25 mg, 0.077 mmol) were degassed by three freeze/thaw cycles, sealed under argon, and heated at 120 °C under argon for 12 h. After the reaction cooled down to room temperature, the reaction mixture was dissolved in minimal amount of DCM, and precipitated 3 times in MeOH. The precipitate was collected and dried under vacuum to yield 988 mg (84% yield) of **5**. GPC (THF): M_n= 11 K Da, Đ= 1.09. ^{1}H NMR (400MHz, $CDCl_3$) δ 6.59-6.25, 4.42, 3.85, 1.75, 1.48-1.21, 0.88. From ^{1}H NMR, integration of methylene proton next to the phenol in both alkyl unit (f) and carboxylate unit (g) provided the molar ratio of monomers to be 4:6 (decyl/carboxylate).

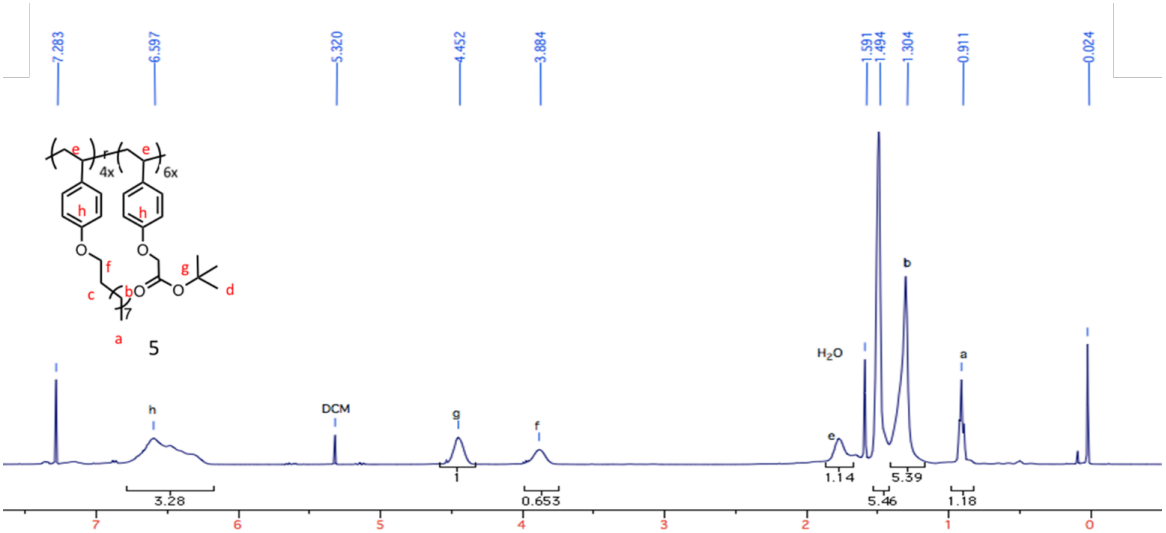

Synthesis of random copolymer P1: Dichloromethane (2 mL) was added to dissolve the dried random copolymer **P1** (200 mg). Trifluoroacetic acid (0.5 mL) was added to the mixture and stirred for 12 h at room temperature. The reaction mixture was evaporated and dried under vacuum to obtain **P1** (95% yield). ^{1}H NMR (400MHz, $CDCl_3$) δ 6.59, 4.65, 3.90, 1.75, 1.48-1.21, 0.88. ^{13}C NMR (100MHz, $CDCl_3$) δ 174.2, 156.6, 154.8, 128.7, 114.2, 68.1, 65.1, 39.9, 31.9, 29.6, 29.3, 26.1, 22.7, 14.1. GPC (DMF): M_n= 11 K Da, Đ= 1.12.

From ^{1}H NMR, a sharp decrease in integration at δ 1.48 suggested the successful deprotection of tert-butyl group. From ^{1}H NMR, integration of proton a and f again confirmed the molar ratio of monomers to be 4:6 (decyl/carboxylate)

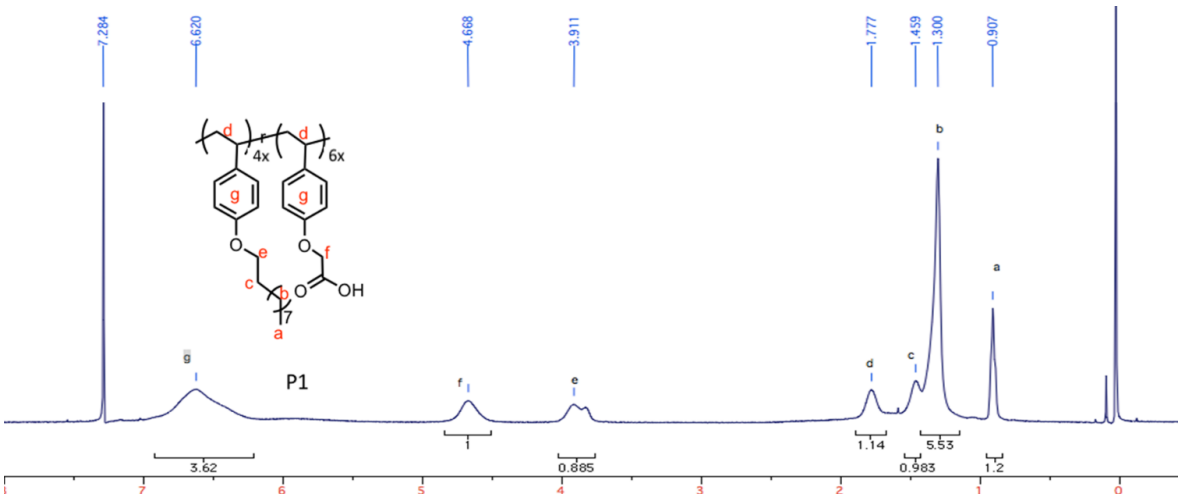

Synthesis of random copolymer 6: Carboxylate polymer **P1** (100 mg, 0.22 mmol carboxylic acid repeat unit) and N-Hydroxysuccinimide (38 mg, 0.33 mmol) was weighed in a 20 mL glass vial and dissolved in 5 mL dry THF and stirred at 0 ºC. N-(3-Dimethylaminopropyl)-N'-ethylcarbodiimide hydrochloride (EDC) (63 mg, 0.33 mmol) was added to the mixture and stirred for 4 hours. Afterwards, triethylamine (92 uL, 0.66 mmol) and N, N-dimethylethylenediamine (29 mg, 0.33 mmol) were added dropwise to the reaction mixture and the solution was stirred for 24 h at room temperature. After that, the modified polymer was purified by dialyzing against dichloromethane/methanol using a membrane of MWCO: 3.5 kDa. After dialysis, the solvent was evaporated and the polymer was dried under vacuum for 24 h. Yield: 90%, GPC (THF) Mn: 12 K. Đ: 1.15. ^{1}H NMR (400 MHz, $CDCl_3$): δ 7.15, 6.57-6.2, 4.39, 3.84, 3.42, 2.44, 2.22, 1.74, 1.43-1.26,

0.88. From ^{1}H NMR, integration of proton a and e again confirmed the molar ratio of these two monomers to be 4:6.

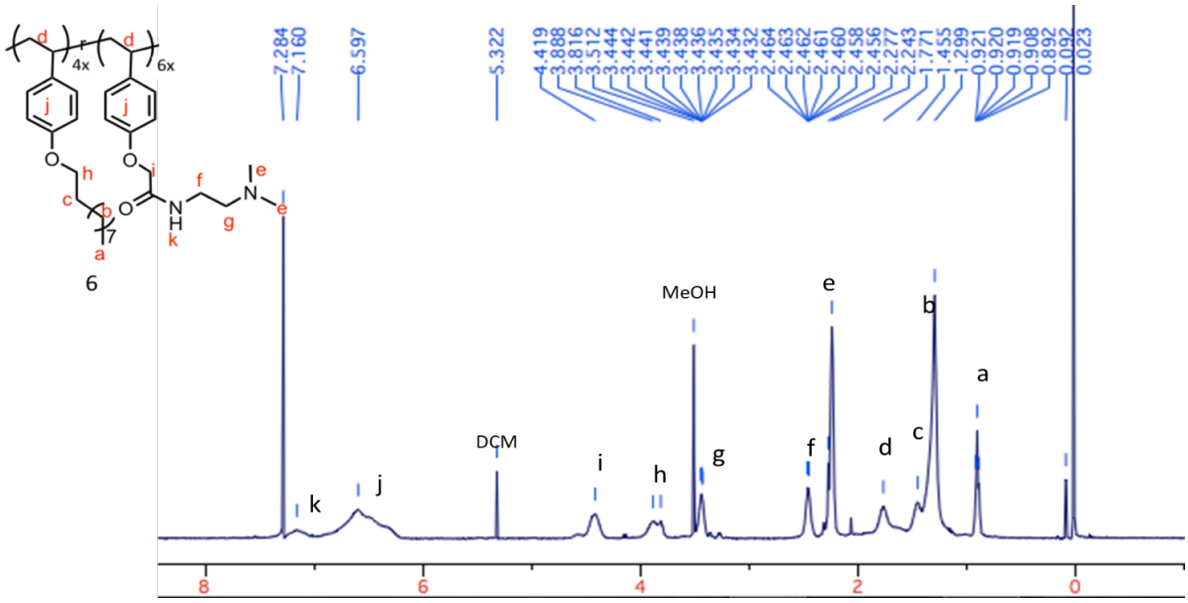

Synthesis of random copolymer P2: Random copolymer **6** (80 mg, 0.16 mmol tertiary amine repeat unit) was weighed in a 20 mL glass vial and dissolved in 5 mL dry THF and stirred at 0 °C under argon protection. Methyl trifluoromethanesulfonate (56 mg, 0.33 mmol) was added to the solution dropwise and stirred for 2 hours. Afterwards, the solvent was evaporated and the polymer was dried under vacuum for 24 h. Yield: 90%, GPC (THF) Mn: 12 K. Đ: 1.15. ^{1}H NMR (400 MHz, acetone-d6): δ 8.24, 6.7-6.3, 4.49, 3.92, 3.77, 3.40, 1.78, 1.48-1.26, 0.88. ^{13}C NMR (100 MHz, $CDCl_3$) δ 173.5, 156.6, 122.7, 53.5, 49.8, 31.9, 29.6, 29.35, 29.33, 26.1, 22.7, 14.1. From ^{1}H NMR, proton peak of e shifting downfield suggested the successful conversion of tertiary amine to quaternary ammonium. Ratios of two monomers were calculated based on integration of a and h.

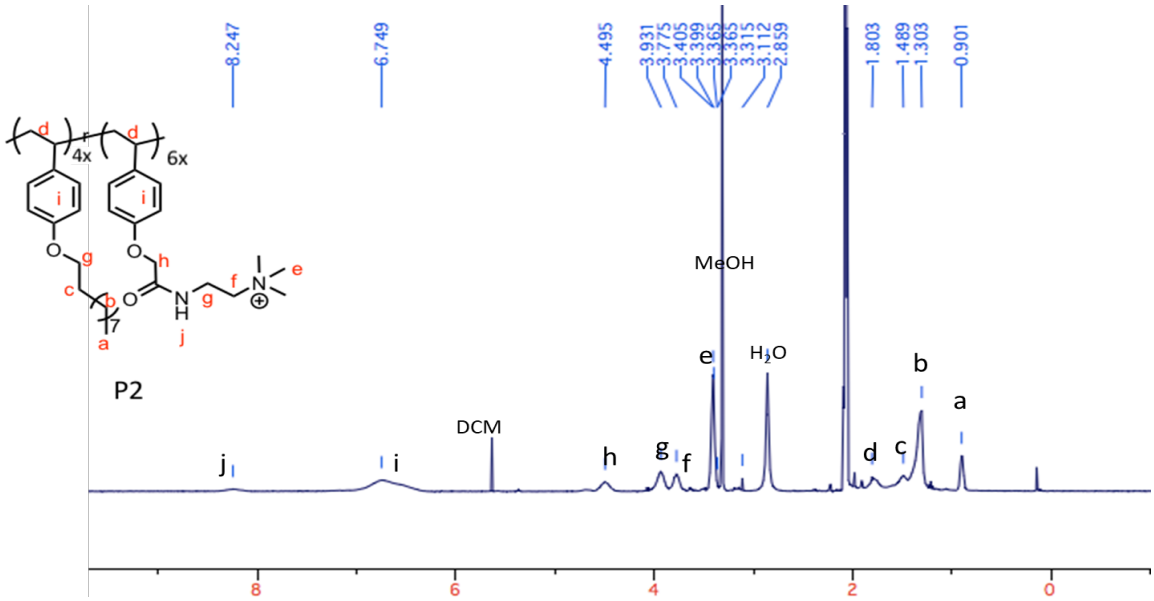

Synthesis of random copolymer 7: **P1** (100 mg, 0.22 mmol carboxylic acid repeat unit) and N-hydroxysuccinimide (38 mg, 0.33 mmol) was dissolved in 5 mL dry THF and stirred at 0 °C. EDC (63 mg, 0.33 mmol) was added and stirred for 4 hours. Afterwards, triethylamine (92 uL, 0.66 mmol) was added and stirred for 30 minutes. Then a mixture of 4-(2-aminoethyl) benzenesulfonamide (22 mg, 0.11 mmol) and N, N-dimethylethylenediamine (19.3 mg, 0.22 mmol) in 1 mL DMF were added dropwise and the solution was stirred for 24 h at room temperature. After that, the modified polymer was

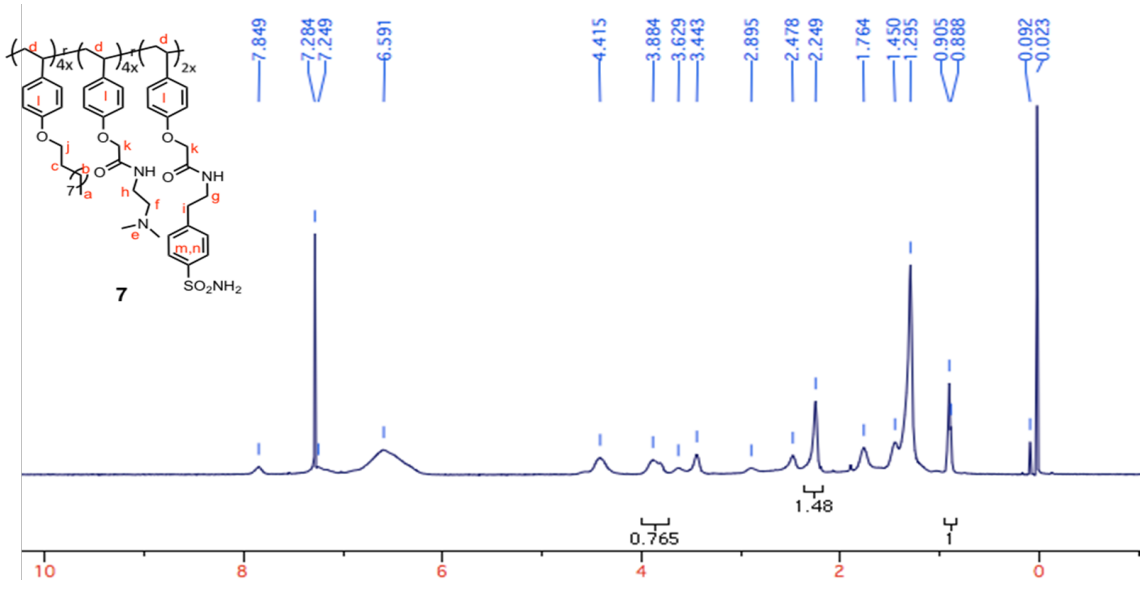

purified by dialyzing against DCM/methanol using a membrane of MWCO: 3.5 kDa. After dialysis, the solvent was evaporated and the polymer was dried under vacuum for 24 h. Yield: 93%, GPC (THF) Mn: 12 K. Đ: 1.2. ^{1}H NMR (400 MHz, $CDCl_3$): δ 7.82, 7.15, 6.57-6.2, 4.56-4.2, 3.87-3.78, 3.42, 2.44, 2.22, 1.74, 1.43-1.26, 0.88. Ratios of three components were calculated based on integration of a, e and m.

Synthesis of random copolymer P3: Random copolymer **7** (80 mg, 0.09 mmol tertiary amine repeat unit) was dissolved in 5 mL dry THF, 1,3-propane sultone (39 uL, 0.45 mmol) was added to the solution and the mixture was refluxed at 80 ºC overinight. Then the modified polymer was purified by dialyzing against aacetone using a membrane of MWCO: 3.5 kDa. After dialysis, the solvent was evaporated and the polymer was dried under vacuum for 24 h. Yield: 95%, GPC (DMF) Mn: 12 K. Đ: 1.2. ^{1}H NMR (400 MHz, $CDCl_3$): δ 7.8, 7.15, 6.57-6.2, 4.52-4.2, 4.05-3.42, 2.78, 1.98, 1.74, 1.43-1.26, 0.88. ^{13}C NMR (100 MHz, $CDCl_3$) δ 181.6, 172.8, 170.4, 156.3, 128.8, 114.2, 100.5, 67.9 43.4, 39.6, 31.9, 29.6, 29.3, 26.15, 26.13, 22.7, 14.1. Ratios of three components were calculated based on copolymer **7**.

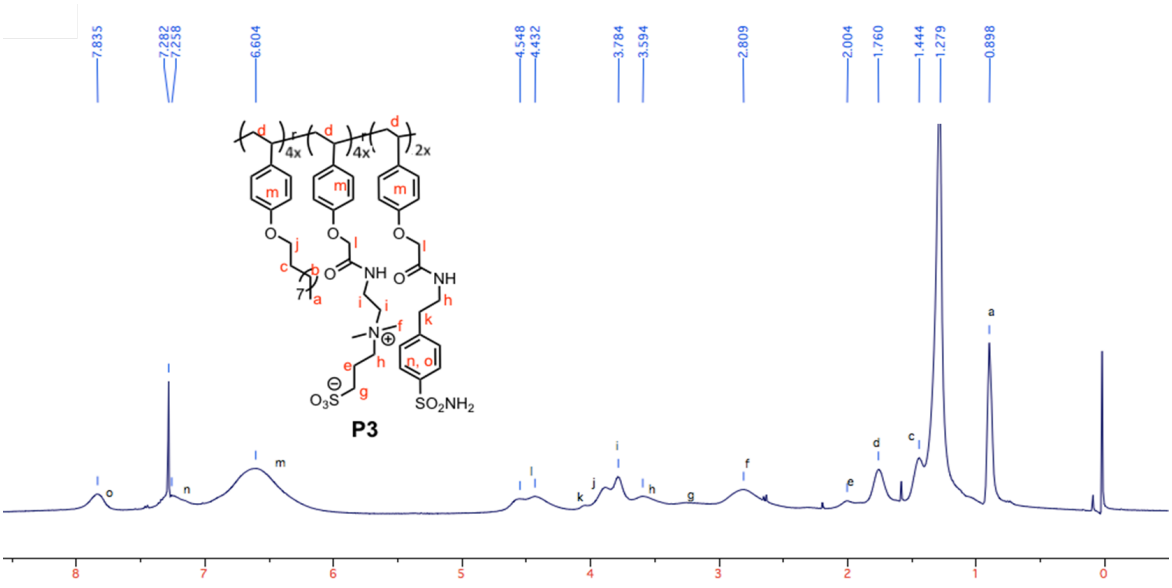

Synthesis of random copolymer P4: Random copolymer **6** (80 mg, 0.16 mmol tertiary amine repeat unit) was dissolved in 5 mL dry THF, 1,3-propane sultone (71 uL, 0.80 mmol) was added to the solution and the mixture was refluxed at 80 °C overinight. Then the modified polymer was purified by dialyzing against aacetone using a membrane of MWCO: 3.5 kDa. After dialysis, the solvent was evaporated and the polymer was dried under vacuum for 24 h. Yield: 95%, GPC (DMF) Mn: 11 K. Đ: 1.1. ^{1}H NMR (400 MHz, $CDCl_3$): δ 8.30, 6.2-6.61, 4.64−4.29, 3.97-2.65, 1.76, 1.54-1.1, 0.87. ^{13}C NMR (100 MHz, $CDCl_3$) δ 170.7, 157.8, 129.0, 114.8, 107.9, 68.2, 50.9, 42.8, 31.9, 29.6, 29.3, 26.2, 22.7, 14.1. Ratios of two components were calculated based on polymer **P1**.

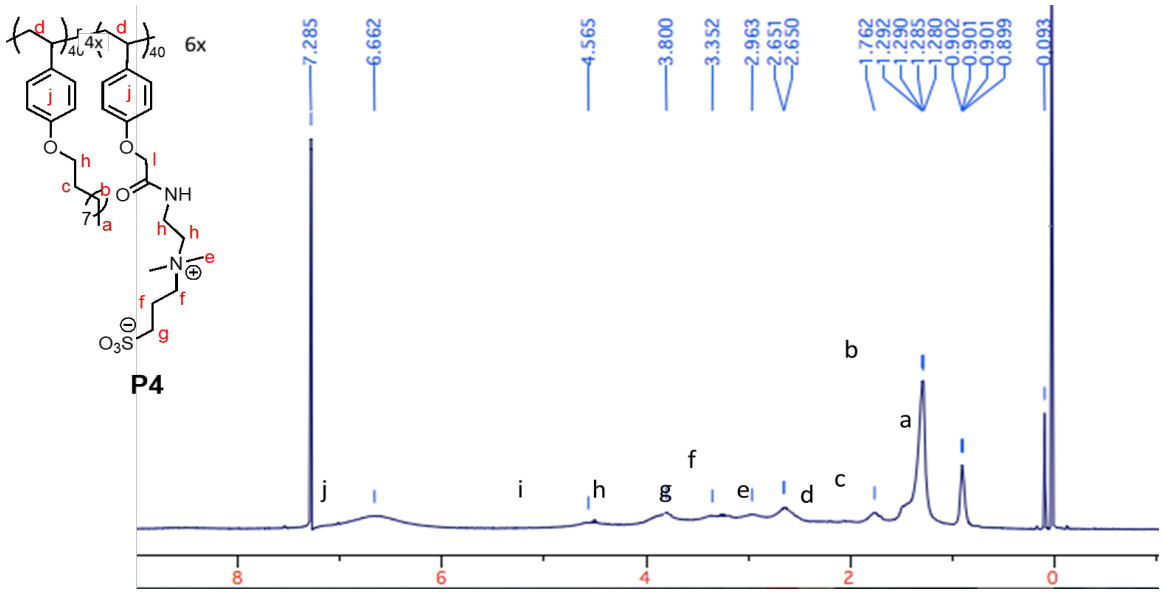

Synthesis of substrate S1: Compound **8** and **9** were synthesized according to previous reported procedures.[S2] The mixture of compound **8** (1.0 eq), compound **9** (2 eq), $CuSO_4{\cdot}5H_2O$ (0.5 equiv.) and sodium ascorbate (0.5 eq.) in MeOH/H_2O (1:1) solvent mixture was heated at 50 °C for 24 h. The reaction progress was monitored by TLC. After completion of the reaction, the reaction mixture was partitioned between ethyl acetate and saturated aqueous NH_4Cl solution. The aqueous layer was extracted twice with ethyl

acetate and the combined organic layer was dried over Na_2SO_4 and evaporated to dryness. The crude product was purified by silica gel column chromatography. Yield: 93%, ^{1}H NMR (400 MHz, $CDCl_3$) δ 7.61 (s, 1H), δ 7.53 (d, *J* = 4.4 Hz, 1H), δ 6.95 (m, 2H), δ 6.61-6.52 (m, 2H), δ 6.18 (s, 1H), δ 5.80 (s, 2H), δ 5.15 (s, 2H), 4.32 (t, *J* = 3.6 Hz, 2H), δ 4.12 (t, *J* = 4.8 Hz, 2H), δ 3.85 (t, J = 4.6 Hz, 2H), δ 3.75-3.62 (m, 26H), δ 3.55 (m, 2H), δ 3.36 (s, 3H), δ 3.10 (s, 3H), δ 2.95 (s, 3H), δ 2.4 (m, 4H), δ 1.92 (m, 2H), δ 1.65 (m, 4H), δ 1.35 (m, 2H); ^{13}C NMR (100 MHz, $CDCl_3$) δ 171.9, 160.9, 160.0, 159.4, 159.2, 154.9, 152.3, 138.4, 125.9, 115.2, 113.2, 113.0, 106.2, 106.0, 103.4, 84.8, 71.9, 70.8, 70.6, 70.58, 70.50, 69.6, 59.1, 40.1, 35.4, 33.7, 29.3, 26.2, 23.9, 18.7. HR-ESI-MS (calculated: $[m+H]^+$= 931.45, obtained: $[m+Na]^+$= 953.3553).

6.5 References

1. Yang, N. J.; Hinner, M. J. *Methods Mol. Biol.* **2015**, *1266*, 29–53.
2. Huang, J.; Lein, M.; Gunderson, C.; Holden, M. A. *J. Am. Chem. Soc.* **2011**, *133*, 15818–15821.
3. Orozco, J.; Cortés, A.; Cheng, G.; Sattayasamitsathit, S.; Gao, W.; Feng, X.; Shen, Y.; Wang, J. *J. Am. Chem. Soc.* **2013**, *135*, 5336–5339.
4. Denzer, K.; Kleijmeer, M. J.; Heijnen, H. F.; Stoorvogel, W.; Geuze, H. J. *J. Cell Sci.* **2000**, *113*, 3365–3374.
5. Skog, J.; Wurdinger, T.; Van Rijn, S.; Meijer, D.; Sena-Esteves, M.; Curry Jr, W. T.; Carter, R. S.; Krichevsky, A. M.; Breakefield, X. O. *Nat. Cell Biol.* **2008**, *10*, 1470.
6. Yu, G.; Jie, K.; Huang, F. *Chem. Rev.* **2015**, *115*, 7240–7303.
7. Ma, X. Zhao, Y. *Chem. Rev.* **2015**, *115*, 7794-7839.
8. Cui, H.; Xu, B. *Chem. Soc. Rev.* **2017**, *46*, 6430–6432.
9. Oldfield, C. Biotechnol. Genet. *Eng. Rev.* **1994,** 12, 255-327.
10. Leser, M. E., Mrkoci, K. & Luisi, P. L. *Biotechnol. Bioeng.* **1993,** 41, 489-492.
11. Nicot, C.; Waks, M. Biotechnol. Genet. *Eng. Rev.* **1996,** 13, 267-314.
12. Valdez, D.; Le Huerou, J. Y.; Gindre, M.; Urbach, W.; Waks, M. *Biophys. J.* **2001**, 80, 2751-2760.
13. Du, X., Song, N., Yang, Y.W., Wu, G., Ma, J. and Gao, H.. *Polym. Chem.* **2014,** 5, 5300–5309.
14. Cöklen, K. E. & Hatton, T. A. *Biotechnol. Prog.* **1985,** 1, 69–74.
15. Colletier, J.-P.; Chaize, B.; Winterhalter, M.; Fournier, D. *BMC Biotechnol.* **2002**, *2*, 9.
16. Lawrence, M. S.; Phillips, K. J.; Liu, D. R. *J. Am. Chem. Soc.* **2007**, *129*, 10110–10112.

17. Alterio, V.; Di Fiore, A.; D'Ambrosio, K.; Supuran, C. T.; De Simone, G. *Chem. Rev.* **2012**, *112*, 4421–4468.

18. Whitcombe, M. J.; Chianella, I.; Larcombe, L.; Piletsky, S. A.; Noble, J.; Porter, R.; Horgan, A. *Chem. Soc. Rev.* **2011**, *40*, 1547–1571.

19. Rodthongkum, N.; Ramireddy, R.; Thayumanavan, S.; Richard, W. V. *Analyst* **2012**, *137*, 1024–1030.

20. Santra, S.; Zhang, P.; Wang, K.; Tapec, R.; Tan, W. *Anal. Chem.* **2001**, *73*, 4988–4993.

21. Wang, M.; Gao, J.; Zhao, B.; Thayumanavan, S. Vachet, R.W. Analyst ,**2019** , 144, 6321-6326.

22. Serrano, M. A. C.; Gao, J.; Kelly, K. A.; Thayumanavan, S.; Vachet, R. W. *ACS Appl. Mater. Interfaces* **2018**, *10,* 40443–40451.

23. Zhao, B.; Serrano, M. A. C.; Gao, J.; Zhuang, J.; Vachet, R. W.; Thayumanavan, S. *Polym. Chem.* **2018**, *9,* 1066-1071.

24. Nam, J.-M.; Thaxton, C. S.; Mirkin, C. A. *Science.* **2003**, *301*, 1884–1886.

25. Zhang, H.; Piacham, T.; Drew, M.; Patek, M.; Mosbach, K.; Ye, L. *J. Am. Chem. Soc.* **2006**, *128*, 4178–4179.

26. Vriezema, D. M.; Comellas Aragonès, M.; Elemans, J. A. A. W.; Cornelissen, J. J. L. M.; Rowan, A. E.; Nolte, R. J. M. *Chem. Rev.* **2005**, *105*, 1445–1490.

27. Bruns, N.; Tiller, J. C. *Nano Lett.* **2005**, *5*, 45–48.

28. Grzelakowski, M.; Onaca, O.; Rigler, P.; Kumar, M.; Meier, W. *Small* **2009**, *5*, 2545–2548.

29. Broz, P.; Driamov, S.; Ziegler, J.; Ben-Haim, N.; Marsch, S.; Meier, W.; Hunziker, P. *Nano Lett.* **2006**, *6*, 2349–2353.

CHAPTER 7

ENZYME NANOREACTOR FOR CATALYSIS IN APOLAR SOLVENT

7.1 Introduction

Despite many decades of research to match the catalytic fidelity of nature's macromolecules, enzymes still remain the hallmark of excellence for activity, selectivity, and turnover numbers.[1,2] Nature had billion years of evolutionary pressure as the driving force to arrive at these efficient catalysts. Achieving such fidelity, using synthetic molecules, on a reasonable human time scale is difficult.[3–7] Therefore, it is useful to capture the essence of biological catalysts themselves in abiological processes. This goal is complicated by the fact that practical utility of enzymes is quite limited in most abiological processes, because these catalysts are evolved to only operate in their native environment.[8–11] Endowing proteins with the ability to operate in non-native environments is clearly a challenge, which has been recognized for several decades.[12–14] A promising solution to this challenge would involve the ability to encapsulate proteins in a compatible local nano-environment, although the global environment of the reaction media might be incompatible with the protein.[15–18] Although this is easy to imagine, implementation of such a possibility is cumbersome, because this requires proteins to be transported across the incompatible solvent interface.

Reverse micelles or water-in-oil microemulsions, stabilized by amphiphilic molecules, can form the basis for distributing enzymes in apolar organic solvents.[19–24] In this approach, the enzymes can be directly encapsulated inside without the need of any functional group modification. With the presence of surfactants at the interface of water and organic solvents,

enzymes are protected against potential denaturation by the bulk organic solvents. This scenario allows for organic substrate molecules to be conveniently distributed in the bulk solvent. We have shown a simple polymeric platform that selectively transports water-soluble proteins from an aqueous phase to the water-pool of a reverse micelle in an apolar organic phase based on complementary electrostatic interactions or specific ligand-protein binding interactions.[25] Such a capability provides a great opportunity for performing and modulating enzymatic catalysts in organic solvents. Controlling substrate accessibility to the core of the nanoreactor can expand the system to function in a more complex environment, where a mixture of substrates is present. In this chapter, we will build enzyme nanoreactors for catalysis in apolar solvent, and then introduce crosslinks in the molecular assemblies to control substrate permeability into the assembly to engineer unnatural selectivity in enzymes that are known to be inherently promiscuous in substrate selectivity (Figure 7.1).

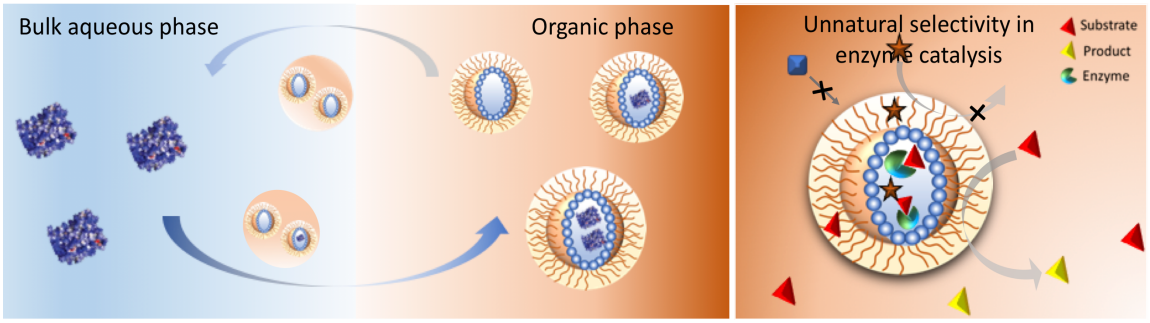

Figure 7.1. Schematic representation of enzyme nanoreactor in organic phase and introduce unnatural substrate selectivity to the enzymes for catalysis in apolar solvent.

7.2 Results and discussion

7.2.1 Molecular design and synthesis

We are interested in engineering the reverse micelle scaffold to introduce new substrate selectivity in enzymes, which are known to be inherently promiscuous. We hypothesize

that crosslinking the reverse micelles in the organic phase would affect the substrate permeability into this aggregate, which should introduce size-based selectivity. For this purpose, we propose a polymer design, achieved using nitroxide-mediated polymerization, comprises of 50% p-decyloxystyrene as the hydrophobic monomer and 50% of N-methylpyridyldisulfide-styrene as the hydrophilic monomer. The hydrophilic side chain functionalities also can be readily crosslinked in presence of dithiolthreitol (DTT). The polymer was prepared following scheme 7.1.

Scheme 7.1 Synthesis route for target polymer

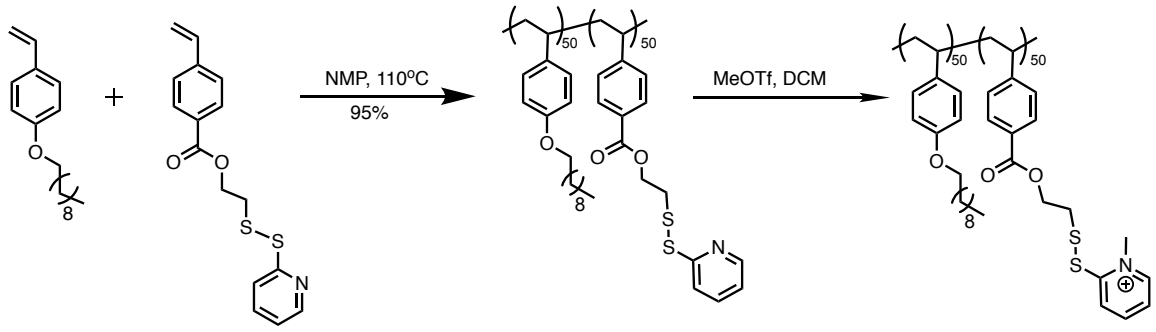

7.2.2 Reverse micelle preparation and characterization

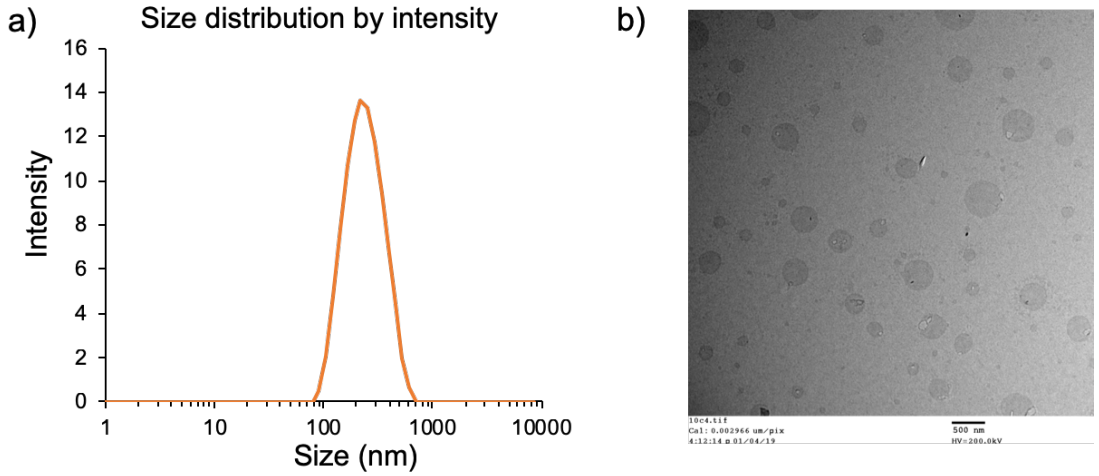

Figure 7.2. a) DLS profile of target polymer in DCM at 1 mg/mL; b) TEM images of reverse micelle solutions.

We firstly tested whether this polymer would self-assemble in apolar solvent. By distributing it in different organic solvents such as toluene, dichloromethane, chloroform and ethylacetate at a concentration of 1 mg/mL (2 eq. water per charged group), we have observed aggregate formation in DCM and chloroform. Assemblies with a fairly homogeneous size distribution of 500 nm was found for designed polymer, as discerned by both dynamic light scattering (DLS) (Figure 7.2a) and transmission electron microscopy (TEM) (Figure 7.2b). The water molecules are added here to provide a 'water pool' for the reverse micelles, which is quite critical for the enzyme entrapment and retainment of enzyme activity in the following experiments. Therefore, we have tried to vary the water content of the reverse micelle assemblies from 0.5 uL to 5 uL per mL reverse micelle solution. We have figured out that if water is more than 2 uL per mL reverse micelle solution, the assemblies were no longer stable because we didn't see a peak from DLS. Only when water addition is lower than 2 uL/mL could we see peaks from DLS. Also, with the increasing amount of water, the size of reverse micelles also increased (Figure 7.3).

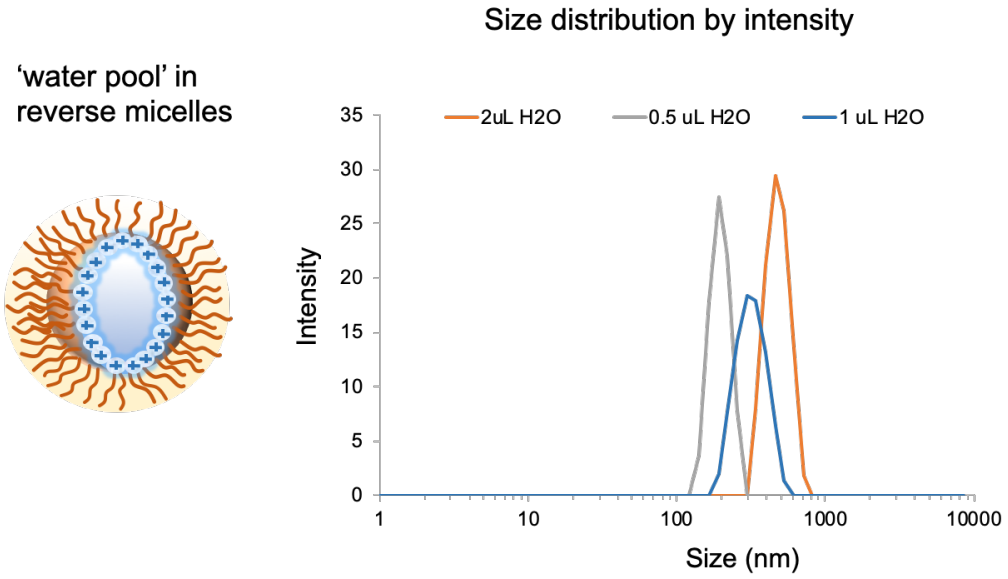

Figure 7.3. DLS profiles for reverse micelles with varied amount of water added.

Next, we are curious to see whether we could crosslink the reverse micelles and control the crosslinking density. In addition to increasing thermodynamic stability to the reverse micelle assemblies, this process should also offer selective permeability of substrate molecules. For this purpose, we added different amount of DTT to induce the disulfide crosslinking. As shown in Figure 7.4, we firstly quantified the maximum amount of the PDS group in 1 mg/ml polymer solution based on the absorbance of cleaved PDS at 350 nm. Then varied amount of DTT from 0.1 eq. to 0.3 eq. of PDS group was added to the reverse micelle solution to get desired crosslinking density (Figure 7.4).

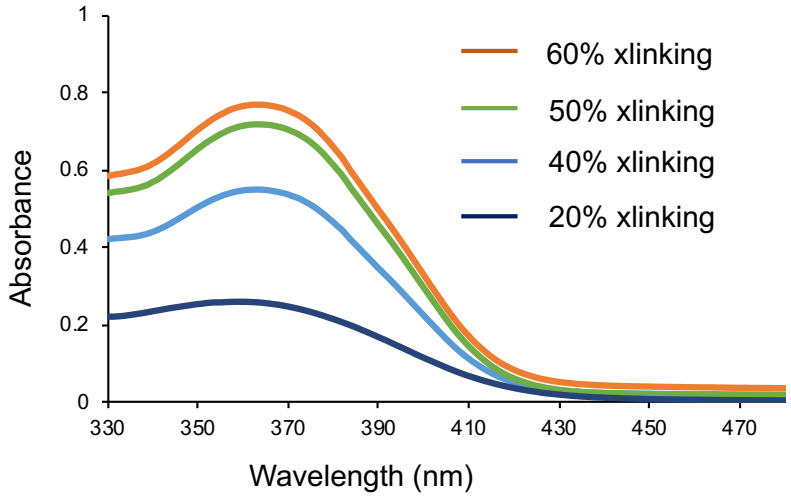

Figure 7.4 Crosslinking of reverse micelles with varied amount of DTT

7.2.3 Enzyme encapsulation and quantification

We envisaged that our reverse micelles would bind to complementarily charged proteins in the aqueous phase and ferry them over to the organic phase and remain active based on our previous findings. To test this possibility, we used GFP as the model protein because we can easily monitor the encapsulation and speculate their structural integrity using fluorescence. As shown in Figure 7.5a, with increased polymer concentration from 0.25

mg/mL to 1 mg/mL, we observed increased encapsulation in organic phase, suggested from the increase in fluorescence signal of GFP.

We were then excited to test this system with an enzymatic protein, porcine liver esterase (plE), which would be the model enzyme to build nanoreactor due to its catalytic efficiency in a variety of ester substrates. To monitor and quantify the enzyme encapsulation by reverse micelles, we labeled plE with a fluorescent dye, Cy3. Herein we have tried two different approaches for enzyme encapsulation: 1) liquid-liquid extraction between reverse micelle in DCM and enzyme solution in PBS buffer; 2) directly add 1uL of plE aqueous solution into the organic phase and sonicate. We found that two approaches offered same loading capacity based on the same polymer concentration. The loading capacity for 1mg/mL polymer was found to be 2.75 nM.

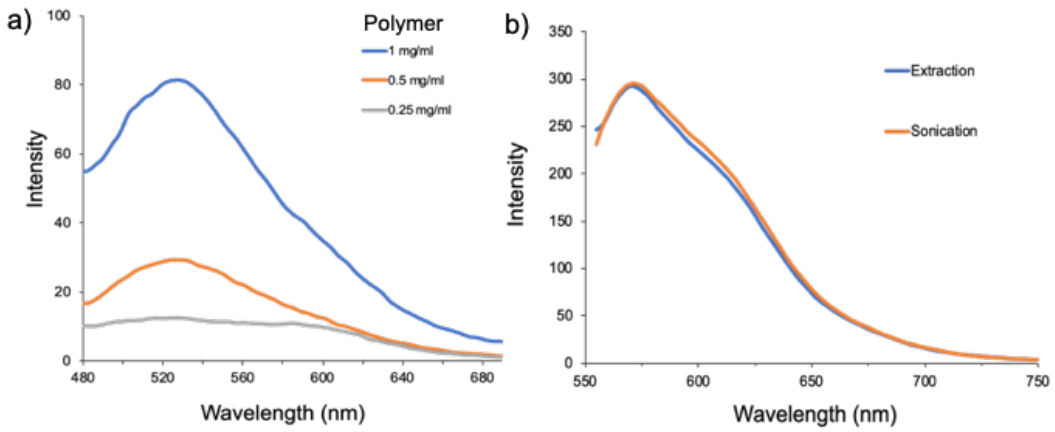

Figure 7.5. a) GFP encapsulation by reverse micelles with varied concentration; b) Cy3 labeled plE encapsulation in reverse micelles through extraction approach (blue) or sonication approach (orange).

7.3 Summary and future directions

In this chapter, we have investigated the use of amphiphilic polymer based reverse micelles to transport enzymes across an immiscible solvent interface in order to perform

enzymatic catalysis in organic solvents. Using random cationic amphiphilic polymer, we have shown the preparation of reverse micelles, enzyme encapsulation in apolar solvent and controlled crosslinking density of these nanoassemblies. We found that the micelle size can be tuned by the amount of water added. Crosslinking of reverse micelles from the hydrophilic core can be achieved using disulfide chemistry but the DTT might affect the protein activity in the following studies. Future work will need to use different crosslinking chemistry to minimize the implications in the encapsulated enzyme. Also, studying the enzyme catalysis over a range of different substrates will be done to figure out whether there can be a threshold for the molecules to diffuse into the reactor.

7.4 Experimental procedures

7.4.1 General methods

All reagents were commercially available and used as received unless stated otherwise. ^{1}H-NMR spectra were recorded on a 400 MHz or a 500 MHz NMR spectrometer using residual proton resonance of the solvents as internal standard. Chemical shifts are reported in parts per million (ppm). Mass spectra were obtained by a Bruker AmaZon quadrupole ion trap mass spectrometer coupled with electrospray ionization source. Gel permeation chromatography (GPC) was used to estimate the molecular weight of polymers using THF/DMF as eluent and 1 μL of toluene was added as the internal reference. Polystyrene standards were used for calibration and data analysis.

Dynamic Light Scattering (DLS): For the DLS measurements, the polymers were dissolved in toluene/dichromethane/chloroform, and two equivalent of water per hydrophilic unit was added to form the water pool inside the reverse micelles. The samples were sonicated until clear solutions were formed. DLS measurements were carried out in a quartz cuvette

at room temperature. The sizes of each solution were recorded overtime by a Malvern Nanozetasizer ZS90.

Transmission Electron Microscope (TEM): The same sample for DLS measurement was dropped onto carbon-coated copper grid. The grid was dried by slow evaporation in air overnight. Images were recorded on a JEOL-2000FX electron microscopy operated at 200 kV and at a nominal magnification of 5000X. At least 10 locations on the TEM grid were examined. The assembly diameter was calculated using ImageJ software.

Protein encapsulation by reverse micelles: 600 uL of a DCM solution of polymers (1 mg/mL) with 200 uL of enzyme in 10 mM PBS buffer at pH 7.4. The mixture is vortexed for 30 min and centrifuged at 10,000 rpm for 1 h to separate the organic and aqueous layers. The organic phase and aqueous phase are then separated for analysis.

Evaluation of PlE activity in reverse micelles: First, the amount of plE that got transported into the organic phase was calculated based on the SDS-PAGE or BCA assay. The organic phase containing plE was then equilibrated with an aqueous phase of substrate S1 (100 μM) for 30 minutes. After centrifugation for 30 minutes, the fluorescence of aqueous phase was measured over time. The control experiments with the same amount of plE were performed in aqueous phase.

7.4.2 Synthesis

Synthesis of molecule **2**: Methyltriphenylphosphonium bromide (7.94 g, 22.24 mmol) and potassium tert-butoxide (2.50 g, 22.24 mmol) were mixed in a round bottom flask, and dry THF (30 mL) was added to the mixture. The mixture was stirred under argon atmosphere in an ice bath for 15 min to yield the bright yellow solution. Molecule **1** (2.2 g, 14.83 mmol) was slowly added to the mixture. The reaction mixture was further stirred overnight. After

the reaction, THF was evaporated, saline and ethyl acetate were then added for extraction. The organic layer was washed with saline (3 times) and then evaporated to dryness and purified by silica gel column chromatography (3-5% ethyl acetate in hexanes) to afford 1.3 g (65% yield) of **2**. ^{1}H NMR (400MHz, $CDCl_3$) δ 7.97-7.99 (d, J = 8.0 Hz, 2H), δ 7.46-7.44 (d, J =8 Hz, 2H), δ 6.78-6.71 (dd, J = 11.2, 11.2 Hz,), δ 5.88-5.84 (d, J =16 Hz, 1H), δ 5.40-5.37 (d, J =12 Hz, 1H). ESI-MS (expected: $[m+H]^+$= 149.05, obtained: $[m+Na]^+$= 171.1)

Scheme 7.2 Synthesis route for monomers and target polymer

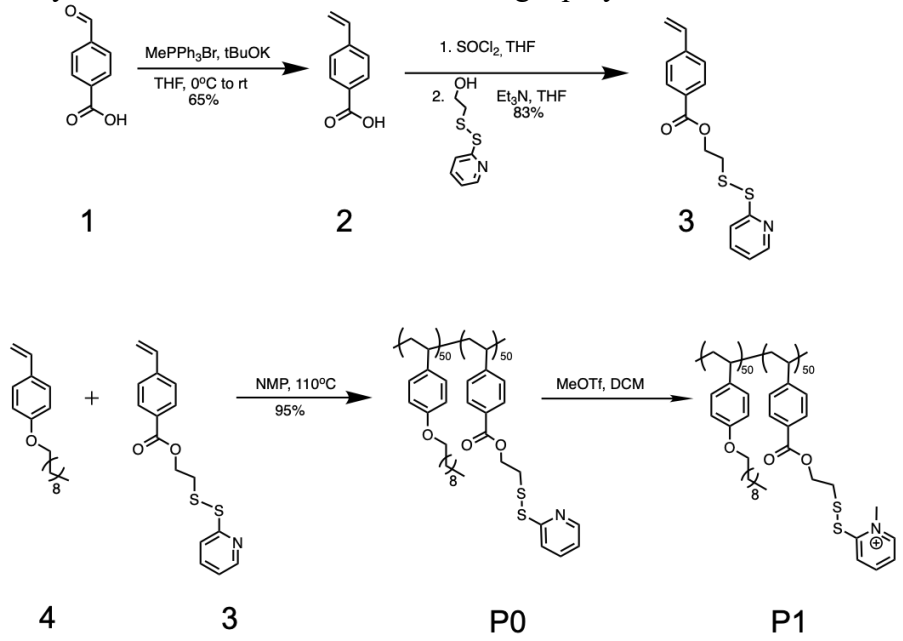

Synthesis of molecule **3**: Molecule **2** (1.3 g, 8.7 mmol), $SOCl_2$ (1.2g, 10.4 mmol) and THF (20 mL) were kept under reflux for overnight. The mixture was then evaporated to dryness and redissolved in fresh and dry THF (20 mL). 2-Hydroxyethylpyridyldisulfide (1.63g, 8.7 mmol) and triethylamine (1.77g, 17.4 mmol) with 5mL THF was then added to this solution and stirred at room temperature for 12 hours. Solvent was evaporated and the residue was further purified by silica gel column chromatography (3-5% ethyl acetate in hexanes) to

afford 2.2 g (83% yield) of **3.** ^{1}H NMR (400 MHz, $CDCl_3$) δ 8.45-8.44 (d, *J* = 4.0 Hz, 1H) 7.97-7.99 (d, *J* = 8.0 Hz, 2H), δ 7.70-7.68 (d, *J* = 8.0 Hz, 1H), δ 7.58-7.53 (m, 1H), δ 7.46-7.44 (d, *J* =8 Hz, 2H), δ 7.07-7.04 (m, 1H), δ 6.78-6.71 (dd, *J* = 11.2, 11.2 Hz,), δ 5.88-5.84 (d, *J* =16 Hz, 1H), δ 5.40-5.37 (d, *J* =12 Hz, 1H), δ 4.56 (t, 2H), δ 3.18 (t, 2H). ESI-MS (expected: $[m+H]^+$= 318.05, obtained: $[m+Na]^+$= 340.13)

Synthesis of polymer **P0**: A mixture of the compound **3** (610 mg, 1.92 mmol), **4** (499 mg, 1.92 mmol) and *N*-*tert*-butyl-*N*-(2-methyl-1-phenylpropyl)-*O*-(1-phenylethyl)hydroxyl amine (NMP initiator, 25 mg, 0.077 mmol) were degassed by three freeze/thaw cycles, sealed under argon and heated at 120 °C for 10 h. After the reaction cooled down to room temperature, the reaction mixture was dissolved in minimal amount of DCM and precipitated 3 times in MeOH. The precipitate was collected and dried under vacuum to yield 1045 mg (95% yield) of **5**. GPC (THF): M_n= 14.5 K Da, Đ= 1.09. ^{1}H NMR (400

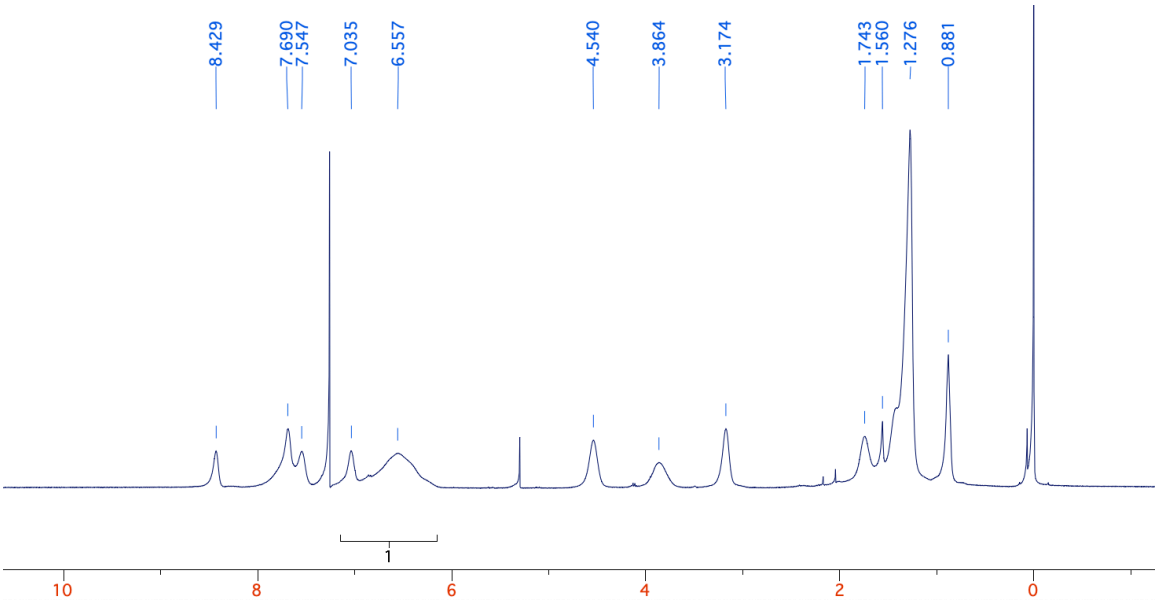

MHz, $CDCl_3$) δ 8.43, 7.69, 7.55, 7.04, 6.56, 4.54, 3.86, 3.17, 1.74-1.21, 0.88. From ^{1}H NMR, integration of peak at δ 4.54 and peak at δ 3.86 provided the molar ratio of monomers to be 1:1 (decyl/PDS).

Synthesis of polymer **P1**: Random copolymer **P0** (200 mg, 0.35 mmol PDS repeat unit) was weighed in a 20 mL glass vial and dissolved in 5 mL dry dichoromethane and stirred at 0 °C under argon protection. Methyl trifluoromethanesulfonate (118 mg, 0.7 mmol) was added to the solution dropwise and stirred for 2 hours. Afterwards, the solvent was evaporated, the polymer was dried under vacuum for 24 h. Yield: 90%, GPC (THF) Mn: 15 K. Đ: 1.15. ^{1}H NMR (400 MHz, acetone-d6): δ 9.03, 8.77, 8.54, 7.93, 7.76, 6.71, 4.67, 4.66, 3.94, 3.52, 3.40, 1.78-1.26, 0.88. From ^{1}H NMR, proton peak of δ 4.46 suggested the successful conversion of tertiary amine to quaternary ammonium.

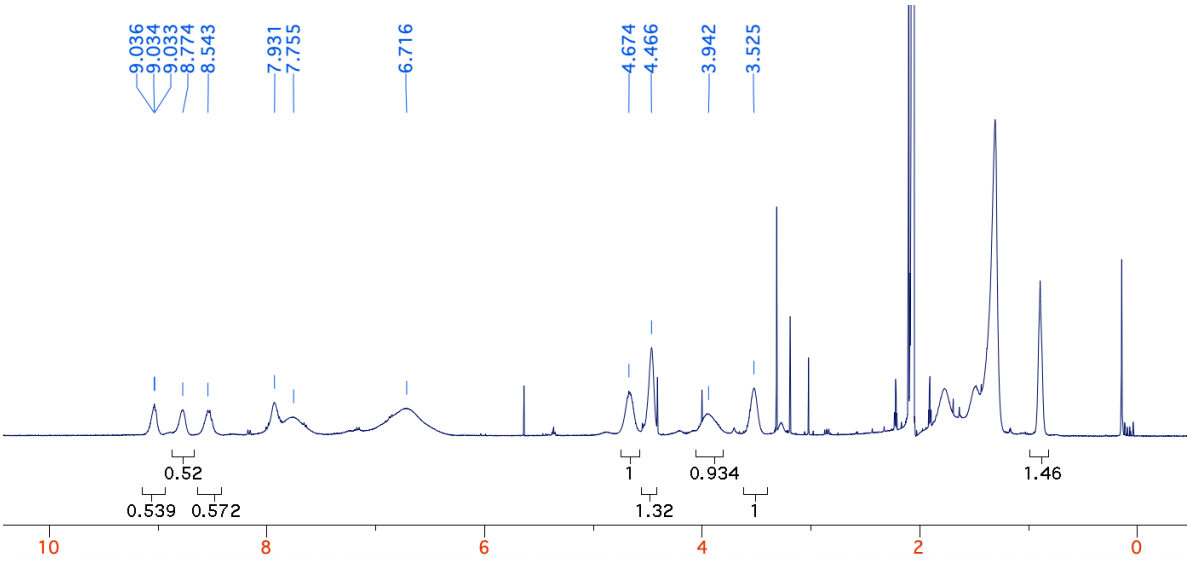

7.5 References

1. Cornish-Bowden, A.; Cornish-Bowden, A. Wiley-Blackwell Weinheim, Germany, 2012; Vol. 510.
2. Fersht, A. WH Freeman, 1985; Vol. 99.
3. Grondal, C.; Jeanty, M.; Enders, D. *Nat. Chem.* **2010**, *2* (3), 167.
4. Silva, G. A. *Ann. N. Y. Acad. Sci.* **2010**, *1199* (1), 221–230.
5. Schoffelen, S.; van Hest, J. C. M. *Curr. Opin. Struct. Biol.* **2013**, *23* (4), 613–621.
6. Wang, Y.; Lu, H.; Xu, P.-F. *Acc. Chem. Res.* **2015**, *48* (7), 1832–1844.
7. Chen, D.-F.; Zhao, F.; Hu, Y.; Gong, L.-Z. *Angew. Chemie Int. Ed.* **2014**, *53* (40), 10763–10767.
8. Atkinson, D. E. *Annu. Rev. Microbiol.* **1969**, *23* (1), 47–68.
9. Iyer, P. V; Ananthanarayan, L. *Process Biochem.* **2008**, *43* (10), 1019–1032.
10. Parkin, G. *Chem. Rev.* **2004**, *104* (2), 699–768.
11. Duetz, W. A.; Van Beilen, J. B.; Witholt, B. *Curr. Opin. Biotechnol.* **2001**, *12* (4), 419–425.
12. Asuri, P.; Karajanagi, S. S.; Yang, H.; Yim, T.-J.; Kane, R. S.; Dordick, J. S. *Langmuir* **2006**, *22* (13), 5833–5836.
13. Dill, K. A. Dominant Forces in Protein Folding. *Biochemistry* **1990**, *29* (31), 7133–7155.
14. Gupta, M. N.; Roy, I. *Eur. J. Biochem.* **2004**, *271* (13), 2575–2583.
15. Chen, K.; Arnold, F. H. *Proc. Natl. Acad. Sci.* **1993**, *90* (12), 5618–5622.
16. Gupta, M. N. *Eur. J. Biochem.* **1992**, *203* (1–2), 25–32.
17. Karajanagi, S. S.; Vertegel, A. A.; Kane, R. S.; Dordick, J. S. *Langmuir* **2004**, *20* (26),

11594–11599.

18. Avnir, D.; Braun, S.; Lev, O.; Ottolenghi, M. *Chem. Mater.* **1994**, *6* (10), 1605–1614.
19. Zoumpanioti, M.; Karali, M.; Xenakis, A.; Stamatis, H. *Enzyme Microb. Technol.* **2006**, *39* (4), 531–539.
20. Mitsou, E.; Xenakis, A.; Zoumpanioti, M. *Catalysts* **2017**, *7* (2), 52.
21. Shipovskov, S.; Trofimova, D.; Saprykin, E.; Christenson, A.; Ruzgas, T.; Levashov, A. V; Ferapontova, E. E. *Anal. Chem.* **2005**, *77* (21), 7074–7079.
22. KHMELNITSKY, Y. L.; HILHORST, R.; VERGER, C. Detergentless *Eur. J. Biochem.* **1988**, *176* (2), 265–271.
23. Pavlidis, I. V; Gournis, D.; Papadopoulos, G. K.; Stamatis, H. *J. Mol. Catal. B Enzym.* **2009**, *60* (1–2), 50–56.
24. Moniruzzaman, M.; Kamiya, N.; Nakashima, K.; Goto, M. *Green Chem.* **2008**, *10* (5), 497–500.
25. Gao, J., Zhao, B., Wang, M., Serrano, M.A., Zhuang, J., Ray, M., Rotello, V.M., Vachet, R.W. and Thayumanavan, S.,. *J. Am. Chem. Soc*, **2018**, 140(7), 2421-2425.

CHAPTER 8

SUMMARY AND FUTURE DIRECTIONS

8.1 Summary of the dissertation

Through the use of modern synthetic organic chemistry, we have built interesting, novel and smart Nanoassemblies with tunable responses and potential applications such as sensing, diagnostics and drug delivery. We have synthesized a variety of amphiphiles to understand the structural factors that program molecules to self-assemble into functional materials. Furthermore, by addressing the design challenge to prepare smart materials with desired functionalities, controlled molecular weight and the ability to respond to a broad range of stimuli, we have developed different applications based on these materials.

The primary challenge for design of novel stimuli-responsive materials concerns stimulus and response. In chapter 2, taking different stimulus as inputs and response as outputs, I successfully achieved logic control over the designed materials. Notably, a combination of an intrinsic trigger and an extrinsic trigger was introduced to this system for the first time. A photocaged ligand activation method was designed that nanoassembly would disassemble only to the concurrent presence of two inputs (AND gate). Similarly, molecular designs for OR gate and NOT gate were also developed and demonstrated. This set of materials offer the possibility of substantially increasing specificity in responses, which could find use in many applications, including drug delivery and diagnostics.

Enzyme as a stimulus to trigger the response of nanomaterials is an exciting finding from our group and has shown great potential for developing rapid response materials for sensing. In chapter 3, rrom the chemistry perspective, I have a strong desire to dig the structural factors that tailor the molecules to self-assemble into enzyme responsive materials. By

synthesizing two series of 12 new oligomers with varied structures, I systematically investigated how molecular weight and hydrophilic-hydrophobic balance affects the materials' response towards enzyme. The fundamental insights generated from these findings are impacting the new materials design in our group and will also benefit areas of enzyme-sensitive materials.

In chapter 4, I designed a self-immolative nanogel platform based on block-copolymers, which aims to minimize the implications associated with currently reported systems such as stability loss and limited efficiency for post-modification. The new material design involves simple synthesis and accessible reactive group present on the surface, which can be easily functionalized with ligand functionalities. The easy preparation and capabilities for post-modification provide great potential to be used as delivery vehicles.

When translating nanoparticle-based biomedical imaging and therapy, one big obstacle is the poor selectivity of these materials in vivo due to off-target localization. To address this issue, In chapter 5 we come up with a simple material design that are available to mask cell interactive functionalities on nanogel during circulation and then restore nanogel-cell interaction by revealing the presence of these surface functionalities at a target site. These nanogels with triggerable variational properties can function as imaging agents, my success on this project will push our work on step closer to industrial applications.

Transporting molecules across incompatible interfaces is a significant challenge, especially for globular proteins with large hydrophilic surfaces. If we could transport enzymes into an organic phase without disrupting the structure and functions of these enzymes, it would raise up a broad range of applications such as catalysis and sensing. To combat this problem, I developed a novel and simple supramolecular approach in chapter 6, with which we were

gratifying to find that not only the proteins can be easily shuttled from aqueous phase to organic phase, their structures and functions are well maintained. Another achievement is that specific protein from mixtures can be selectively extracted by introducing ligand into the materials. These exciting findings from my project open up new possibilities for application of supramolecular assemblies in sensing, diagnostics and catalysis.

Following the findings in chapter 6, we use specifically engineered interactions between a polymer assembly in the apolar organic phase and a protein as the driving force to transport the protein that was originally present in the aqueous phase in chapter 7. By crosslinking the reverse micelles in the organic phase, we could introduce new size-based selectivity in enzymes. Controlling substrate accessibility to the core of the nanoreactor can expand the system to function in a more complex environment, where a mixture of substrates is present.

8.2 Future directions

8.2.1 Unnatural silectivity in enzyme nanoreactor

Controlling substrate accessibility to the core of the nanoreactor can expand the system to function in a more complex environment, where a mixture of substrates is present. With this reverse micelle scaffold, we can introduce new substrate selectivity in enzymes, which are known to be inherently promiscuous. We hypothesize that crosslinking the reverse micelles in the organic phase would affect the substrate permeability into this aggregate, which should introduce size-based selectivity. We will test this permeability using a series of substrate molecules that contain the same enzyme-sensitive functional group, but with systematic variations in molecular weights of the substrate molecules (Scheme 8.1a).

Scheme 8.1 Structures of substrates with varied molecular weight for enzyme nanoreactors

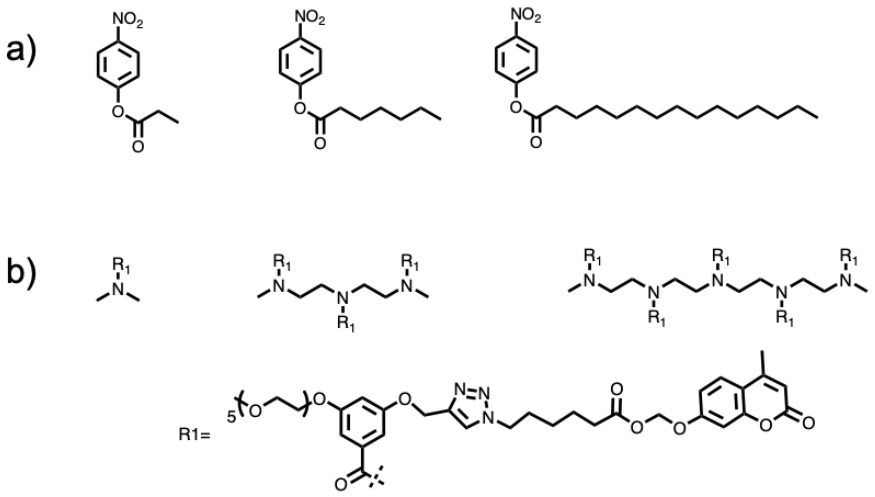

To further investigate the impact of the crosslinking-based selectivity in these assemblies, we will also test the catalytic function using amphiphilic substrates to delineate the effect of hydrophobicity that could affect the inherent accessibility to the interior of nanoreactors. The proposed structures are shown in Scheme 8.1 b.

It is also reasonable to expect that crosslinking density of the reverse micelles would alter the substrate selectivity. To investigate this possibility, we will systematically vary the extent of DTT crosslinker addition and assess change in substrate selectivities in these assemblies.

Unifying the lessons from these Aims will provide robust design guidelines for the next generation of enzyme nanoreactors for performing biocatalysis in apolar solvent, with capabilities that do not exist at this time. In addition to bringing the high catalytic fidelity of nature's catalysts as an enabler in organic synthesis, these design guidelines will also open up new possibilities for versatile applications such as on-demand release, point-of-care catalysis, sensing and drug delivery.

8.2.2 Switchable catalytic reactions in the reverse micelles

Triggerable materials have been extensively explored for various applications such as controlled release and sensing, because their response can be turned 'on' by certain stimulus.[1-6] Inspired by the opportunities such triggerable materials offer, we are interested in identifying opportunities to effectively regulate reaction processes and behaviors with external stimuli by simply controlling the timepoint to switch the nanoreactors 'on' and 'off'. For this purpose, we design a light triggerable enzyme nanoreactor that can perform on-demand catalytic function in apolar organic solvents. Light as the catalysis-controlling agent is particularly appealing, since it offers a non-contact, extrinsic control and can be delivered instantaneously to the whole system without any diffusion limitations that are inherent to chemical and thermal deliveries. Additionally, its operational convenience and temporal control over the light irradiation time and intensity can improve the practical potential of the light-responsive catalytic system enormously.

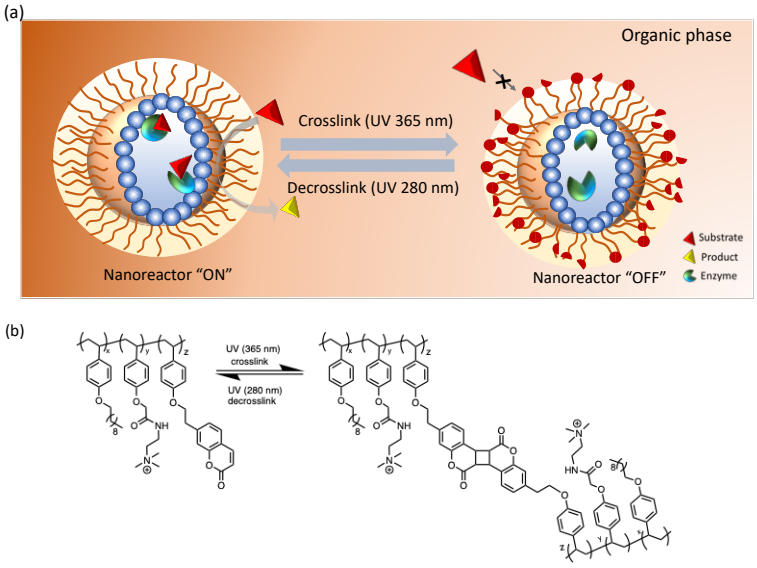

Figure 8.1 (a) Schematic representation shows triggerable switch for turn 'on' and 'off' of the nanoreactor. (b) molecular design and reversible crosslinking chemistry reaction using coumarin.

Here we choose coumarin as the hydrophobic moiety, which is also crosslinkable. Coumarins can undergo a 2+2 photo-dimerization upon irradiations at $\lambda > 300$ nm, whereas the reverse photo-scission reaction occurs under irradiation at $\lambda < 300$ nm.[7-8] We will choose the crosslink densities, using the lessons learnt from the sub-Aims above, such that these assemblies do not allow substrate molecules to enter the lumen of the assembly when crosslinked. In this scenario, we can indeed regulate the accessibility of certain substrate to enzyme and thus control the reaction by crosslinking or decrosslinking the reverse micelle systems (Figure 8.1).

8.3 References

1. Hu, J.; Liu, S. *Macromolecules* **2010**, *43*, 8315–8330.
2. Zhuang, J.; Gordon, M. R.; Ventura, J.; Li, L.; Thayumanavan, S. *Chem. Soc. Rev.* **2013**, *42* (17), 7421–7435.
3. Blum, A. P.; Kammeyer, J. K.; Rush, A. M.; Callmann, C. E.; Hahn, M. E.; Gianneschi, N. C. *J. Am. Chem. Soc.* **2015**, *137* (6), 2140–2154.
4. Molina, M.; Asadian-Birjand, M.; Balach, J.; Bergueiro, J.; Miceli, E.; Calderón, M. *Chem. Soc. Rev.* **2015**, *44* (17), 6161–6186.
5. Gao, J.; Wang, H.; Zhuang, J.; Thayumanavan, S. *Chem. Sci.* **2019**, *10,* 3018-3024.
6. Chujo, Y.; Sada, K.; Saegusa, T. *Macromolecules* **1990**, *23* (10), 2693–2697.
7. Li, W.; Lynch, V.; Thompson, H.; Fox, M. *J. Am. Chem. Soc.* **1997**, *119* (31), 7211–7217.

BIBLIOGRAPHY

1. Aathimanikandan, S. V.; Savariar, E. N.; Thayumanavan, S. *J. Am. Chem. Soc.* **2005**, 127, 14922-14929
2. Akhtar M. J., Kumar S.. et al, *Clin. Chim. Acta* **2014**, *436*, 78–92.
3. Alterio V., A. Di Fiore, K. D'Ambrosio, C. T. Supuran, G. De Simone, *Chem. Rev.* **2012**, 112, 4421-4468.
4. Alterio, V.; Di Fiore, A.; D'Ambrosio, K.; Supuran, C. T.; De Simone, G. *Chem. Rev.* **2012**, *112*, 4421–4468.
5. Amir R. J., Pessah N., Shamis M., Shabat D., *Angew. Chemie* **2003**, 115, 4632-4637.
6. Amir R. J., Shabat D., *Chem. Commun.* **2004**, 1614-1615.
7. André N., Braguer D., Brasseur G., Gonçalves A., Lemesle-Meunier D., Guise S., Jordan M. A., Briand C., *Cancer Res.* **2000**, *60*, 5349–5353.
8. Appiah Kubi G., Z. Qian, S. Amiar, A. Sahni, R. V Stahelin, D. Pei, *Angew. Chemie* **2018**, *130*, 17429–17434.
9. Asuri, P.; Karajanagi, S. S.; Yang, H.; Yim, T.-J.; Kane, R. S.; Dordick, J. S. *Langmuir* **2006**, *22* (13), 5833–5836.
10. Atkinson, D. E. *Annu. Rev. Microbiol.* **1969**, *23* (1), 47–68.
11. Avnir, D.; Braun, S.; Lev, O.; Ottolenghi, M. *Chem. Mater.* **1994**, *6* (10), 1605–1614.
12. Azagarsamy M. A., Sokkalingam P. and S. Thayumanavan, *J. Am. Chem. Soc.*, 2009, **131**, 14184–14185.
13. Azagarsamy, M. A.; Yesilyurt, V.; Thayumanavan, S. *J. Am. Chem. Soc.* **2010**, *132*, 4550-4551.
14. Bae, Y. H.; Park, K. *J Control Release*, **2011**, 153, 198-205.

15. Bernardos A., E. Aznar, M. D. Marcos, R. Mart'inez-Máñez, F. Sancenón, J. Soto, J. M. Barat and P. Amorós, *Angew. Chemie*, 2009, **121**, 5998–6001.

16. Blanco E., H. Shen, M. Ferrari, *Nat. Biotechnol.* **2015**, *33*, 941–951.

17. Blum A. P., Kammeyer J. K., Rush A. M., Callmann C. E., Hahn M. E., Gianneschi N. C.*, J. Am. Chem. Soc.***2015**, 137, 2140-2154.

18. Broz, P.; Driamov, S.; Ziegler, J.; Ben-Haim, N.; Marsch, S.; Meier, W.; Hunziker, P. *Nano Lett.* **2006**, *6*, 2349–2353.

19. Bruns, N.; Tiller, J. C. *Nano Lett.* **2005**, *5*, 45–48.

20. Bui, M.H., Seligson, D., Han, K.R., Pantuck, A.J., Dorey, F.J., Huang, Y., Horvath, S., Leibovich, B.C., Chopra, S., Liao, S.Y. and Stanbridge, E. *Clinical cancer research*, **2003**, 9(2), 802-811.

21. Byrne, J.D.; Betancourt, T.; Brannon-Peppas, L. *Adv. Drug Deliv. Rev.* **2008**, *60*, 1615-1626.

22. Collier C. P., Wong E. W., Belohradský M., Raymo F. M., Stoddart J. F., Kuekes P. J., R. Williams S., Heath J. R., *Science,* **1999**, 285, 391-394.

23. Cabral H., Nishiyama N., Kataoka K.*, Acc. Chem. Res*. **2011**, 44, 999-1008.

24. Chacko R. T., Ventura J., Zhuang J., Thayumanavan S., *Adv. Drug Deliv. Rev.* **2012**, *64*, 836–851.

25. Chaudhuri T. K., Paul S., *FEBS J.* **2006**, 273, 1331-1349.

26. Chen J., Fang Z., Lie P., Zeng L., *Anal Chem.* **2012**, 84, 6321.

27. Chen T., Hu Y., Cen Y., Chu X., Lu Y., *J. Am. Chem. Soc.* **2013**, 135, 11595-11602.

28. Chen, D.-F.; Zhao, F.; Hu, Y.; Gong, L.-Z. *Angew. Chemie Int. Ed.* **2014**, *53* (40), 10763–10767.

29. Chen, K.; Arnold, F. H. *Proc. Natl. Acad. Sci.* **1993**, *90* (12), 5618–5622.

30. Cheng, Y.; Morshed, R.A.; Auffinger B.; Tobias, A.L. Lesniak, M.S. *Adv. Drug Deliv. Rev.* **2014**, *66*, 42-57.

31. Chiti F., Dobson C. M., *Annu. Rev. Biochem.* **2006**, 75, 333-366

32. Cöklen, K. E. & Hatton, T. A. *Biotechnol. Prog.* **1985,** 1, 69–74.

33. Colletier, J.-P.; Chaize, B.; Winterhalter, M.; Fournier, D. *BMC Biotechnol.* **2002**, *2*, 9.

34. Cornish-Bowden, A.; Cornish-Bowden, Wiley-Blackwell Weinheim, Germany, **2012**; 510.

35. Crayton, S.H.; Tsourkas, A. *ACS Nano*, **2011**, *5*, 9592-9601.

36. Cui, H.; Xu, B. *Chem. Soc. Rev.* **2017**, *46*, 6430–6432

37. De Silva A. P., James M. R., McKinney B. O. F., Pears D. A., Weir S. M., *Nat. Mater*. **200**6, 5, 787.

38. De Silva A. P., *Nat. Mater.* **2005**, 4(1), 15.

39. De Silva A. P., Uchiyama, S. *Nat. Nanotech.* **2007**, 2(7), 399-410.

40. De Silva P. A., Gunaratne N. H. Q., McCoy C. P., *Nature* **1993**, 364, 42-44.

41. De Vries W. C., D. Grill, M. Tesch, A. Ricker, H. Nüsse, J. Klingauf, A. Studer, V. Gerke. Aviram A., *J. Am. Chem. Soc*. **1988**, 110, 5687-5692.

42. Deng Z., Qian Y., Yu Y., Liu G., Hu J., Zhang G., Liu S*., J. Am. Chem. Soc* **2016**, 138, 10452-10466.

43. Denzer, K.; Kleijmeer, M. J.; Heijnen, H. F.; Stoorvogel, W.; Geuze, H. J. *J. Cell Sci.* **2000**, *113*, 3365–3374.

44. Dhanasekaran S. M., Barrette T. R., Ghosh D., Shah R., Varambally S., Kurachi K., Pienta K. J., Rubin M. A. and Chinnaiyan A. M., *Nature*, 2001, **412**, 822.

45. Dill, K. A. *Biochemistry* **1990**, *29* (31), 7133–7155.

46. Dobson C.M., *Nature* **2002**, 418, 729-730.

47. Du J., Tang Y., Lewis A. L., Armes S. P., *J. Am. Chem. Soc.* **2005**, 127, 17982-17983.

48. Du, X., Song, N., Yang, Y.W., Wu, G., Ma, J. and Gao, H.. *Polym. Chem.* **2014,** 5, 5300–5309.

49. Duetz, W. A.; Van Beilen, J. B.; Witholt, B. *Curr. Opin. Biotechnol.* **2001**, *12* (4), 419–425.

50. Ellis G. A., M. J. Palte, R. T. Raines, *J. Am. Chem. Soc.* **2012**, *134*, 3631–3634.

51. Erbas S. Cakmak, E.U. Akkaya, *Angew. Chem., Int. Ed.* **2013**, 52, 11364-11368.

52. Evans C.-O., P. Reddy, D. J. Brat, E. B. O'Neill, B. Craige, V. L. Stevens, N. M. Oyesiku, *Cancer Res.* **2003**, *63*, 4218–4224.

53. Ferris D. P., Zhao Y.-L., Khashab N. M., Khatib H. A., Stoddart J. F., Zink J. I., *J. Am. Chem. Soc.* **2009**, 131, 1686-1688.

54. Fersht, A. *Enzyme Structure and Mechanism*; WH Freeman, 1985; Vol. 99.

55. Fleischer G., *J. Phys. Chem.*, 1993, **97**, 517–521.

56. Fulda S., L. Galluzzi, G. Kroemer, *Nat. Rev. Drug Discov.* **2010**, *9*, 447.

57. Gao, J., Zhao, B., Wang, M., Serrano, M.A., Zhuang, J., Ray, M., Rotello, V.M., Vachet, R.W. and Thayumanavan, S. *J. Am. Chem. Soc.*, **2018**, 140, 2421-2425.

58. Gao, J.; Wang, H.; Zhuang, J.; Thayumanavan, S. *Chem. Sci.* **2019**, *10,* 3018-3024.

59. Gao, J.; Liu, X.; Secinti, H.; Jiang, Z.; Munkhbat, O.; Xu, Y.; Guo, X.; Thayumanavan, S. *Chem. Eur. J.* **2018**, 24, 1789–1794.

60. Gelperina S., K. Kisich, M. D. Iseman, L. Heifets, *Am. J. Respir. Crit. Care Med.***2005**, *172*, 1487–1490.

61. Ghosh P., Han G., De M., Kim C. K., Rotello V. M., *Adv. Drug Deliv. Rev.* **2008**, *60*, 1307–1315.

62. Gillies E. R., Frechet J. M. J., *Drug Discov. Today* **2005**, *10*, 35–43.

63. Gillies E. R., Jonsson T. B., Fréchet J. M., *J. Am. Chem. Soc.* **2004**, 126, 11936-11943.

64. Goggins S., B. J. Marsh, A. T. Lubben and C. G. Frost, *Chem. Sci.*, **2015**, 6, 4978–4985.

65. Goodwin A. P., Mynar J. L., Ma Y., Fleming G. R., Fréchet J. M., *J. Am. Chem. Soc.* **2005**, 127, 9952-9953.

66. Gordon M. R., Zhao B., Fernandez A., Canakci M., Anson F., Homyak C., Singh K., Vachet R. W., Thayumanavan S., *Biomacromolecules* **2018**, *19*, 860–871.

67. Grondal, C.; Jeanty, M.; Enders, D. *Nat. Chem.* **2010**, *2* (3), 167.

68. Grzelakowski, M.; Onaca, O.; Rigler, P.; Kumar, M.; Meier, W. *Small* **2009**, *5*, 2545–2548.

69. Gupta, M. N. *Eur. J. Biochem.* **1992**, *203* (1–2), 25–32.

70. Gupta, M. N.; Roy, I. *Eur. J. Biochem.* **2004**, *271* (13), 2575–2583.

71. Hamachi I., *Nat. Chem.* **2009**, 1, 557-561.

72. Hamblin M. R., *J. Am. Chem. Soc*. **2017**, 139, 4584-4610.

73. Harnoy A. J., Rosenbaum I., Tirosh E., Ebenstein Y., Shaharabani R., Beck R. and Amir R. J., *J. Am. Chem. Soc.*, **2014**, 136, 7531–7534.

74. Harris T.J.; von Maltzahn, G.; Lord, M.E.; Park, J.-H.; Agrawal, A.; Min, D.-H.; Sailor, M.J.; Bhatia, S.N. *Small*, **2008**, 4, 1307-1312.

75. Hartgerink J. D., Beniash E., Stupp S. I., *Science* **2001**, 294, 1684-1688.

76. Hartmann L. C., *Gynecol. Oncol.* **2008**, *108*, 619–626.

77. Hatakeyama, H.; Akita, H.; Kogure, K.; Oishi, M.; Nagasaki, Y.; Kihira, Y.; Ueno, M.; Kobayashi, H.; Kikuchi, H. Harashima; H.; *Gene Therapy*, **2007**,14, 68-77.

78. Hawker C. J., Wooley K. L. and Frechet J. M. J., *J. Chem. Soc. Perkin Trans. 1*, 1993, 1287–1297.

79. Hu, J.; Liu, S. *Macromolecules* **2010**, *43*, 8315–8330.

80. Hu X., Zhang Y., Xie Z., Jing X., Bellotti A., Gu Z., *Biomacromolecules* **2017**, 18, 649-673.

81. Huang, J.; Lein, M.; Gunderson, C.; Holden, M. A. *J. Am. Chem. Soc.* **2011**, *133*, 15818–15821.

82. Imming P., C. Sinning and A. Meyer, *Nat. Rev. Drug Discov.*, **2006,** 5, 821.

83. Israelachvili J. N., D. J. Mitchell, B. W. Ninham, *J. Chem. Soc*., Faraday Trans. **1976**, 72, 1525−1568.

84. Iyer, P. V; Ananthanarayan, L. *Process Biochem.* **2008**, *43* (10), 1019–1032.

85. Jiang,T. ; Olson, E. S.; Nguyen,Q. T.; Roy, M. ; Jennings, P. A. ; Tsien, R. Y. *Proc. Nat. Acad. Sci. U. S. A.* **2004**, *101*, 17867-17872.

86. Kang J.-H., D. Asai, J.-H. Kim, T. Mori, R. Toita, T. Tomiyama, Y. Asami, J. Oishi, Y. T. Sato, T. Niidome and others, *J. Am. Chem. Soc.*, **2008**, 130, 14906–14907.

87. Karajanagi, S. S.; Vertegel, A. A.; Kane, R. S.; Dordick, J. S. *Langmuir* **2004**, *20* (26), 11594–11599.

88. Karimi M., Sahandi P., Zangabad, Baghaee-Ravari S., Ghazadeh M., Mirshekari H., Khmelnitsky,Y. L.; Hilhorst, R.; Verger, C. *Eur. J. Biochem.* **1988**, *176* (2), 265–271.

89. Kobayashi H.; Watanabe, R.; Choyke, P.L. *Theranostics*, **2014**, *4*, 81-89.

90. Kolakowski R. V, Haelsig K. T., Emmerton K. K., Leiske C. I., Miyamoto J. B., Cochran J. H., Lyon R. P., Senter P. D., Jeffrey S. C., *Angew. Chemie Int. Ed.* **2016**, *55*, 7948–7951.

91. Kostiainen M. A., Kotimaa J., Laukkanen M.-L., Pavan G. M., *Chem.-A Eur. J.* **2010,** 16, 6912-6918.

92. Kostiainen M. A., Smith D. K., Ikkala O., *Angew. Chemie Int. Ed.* **2007**, 46, 7600–7604.

93. Kou S., Lee H.N., Noort D. van, Swamy K.E.E., Kim S.H., Soh J.H., Park S., *Angew. Chem., Int. Ed.* **2008**, 47, 872-876.c

94. Krishnamurthy V. M., Kaufman G. K., Urbach A. R., I. Gitlin, Gudiksen K. L., Weibel D. B., Whitesides G. M., *Chem. Rev.* **2008**, 108, 946- 1051.

95. Langer R., others, *NATURE-LONDON*- **1998**, 5–10.

96. Lawrence, M. S.; Phillips, K. J.; Liu, D. R. *J. Am. Chem. Soc.* **2007**, *129*, 10110–10112.

97. Ledermann J. A., Canevari S., Thigpen T., *Ann. Oncol.* **2015**, *26*, 2034–2043.

98. Lee D.-E., H. Koo, I.-C. Sun, J. H. Ryu, K. Kim and I. C. Kwon, *Chem. Soc. Rev.*, **2012**, 41, 2656–2672.

99. Lee S. M., Nguyen S. T., *Macromolecules* **2013**, 46, 9169-9180.

100. Leser, M. E., Mrkoci, K. & Luisi, P. L. *Biotechnol. Bioeng.* **1993,** 41, 489-492.

101. Li C., Madsen J., Armes S. P., Lewis A.L., *Angew. Chem., Int. Ed*. **2006**, 45, 3510-3513.

102. Li H. N., Ci Y. X., *Analytica chimica acta* **1995**, 317, 353-357.

103. Li Y., Du W., Sun G., Wooley K. L., *Macromolecules* **2008**, 41, 6605-6607.

104. Li Y., Liu G., Wang X., Hu J. and Liu S., *Angew. Chemie Int. Ed.*, **2016**, 55, 1760–1764.

105. Li Y., Zhao T., Wang C., Lin Z., Huang G., Sumer B. D., Gao J., *Nat. Commun.* **2016**, 7, 13214.

106. Li, L.; Raghupathi, K.; Yuan, C.; Thayumanavan, S. Surface Charge Generation in Nanogels for Activated Cellular Uptake at Tumor-Relevant pH. Chem. Sci. **2013**, 4, 3654-3660.

107. Liu G., X. Wang, J. Hu, G. Zhang, S. Liu, *J. Am. Chem. Soc.* **2014**, *136*, 7492–7497.

108. Liu, G.; Zhang, G.; Hu, J.; Wang X.; Zhu M.; Liu S. *J. Am. Chem. Soc.* **2015**, *137*,

109. Low, P.S. Henne W.A.; Doorneweerd, D.D., *Acc. Chem. Res.* **2008**, *41*, 120-129.

110. Lowe A. B., *Polymer (Guildf).*, 2014, **55**, 5517–5549.

111. Lu L., Chen W., Liu J., Wang Y., Jiang C., Yu B., Sun Z., *Angew. Chemie Int. Ed.* **2019.**

112. Ma, X. Zhao, Y. *Chem. Rev.* **2015**, *115*, 7794-7839.

113. Maeda, H. *Adv. Drug Deliv. Rev*. **2015**, *91*, 3-6.

114. Maeda, H.; Bharate, G.Y.; Daruwalla. *J. Eur. J. Pharm. Biopharm*. **2009**, 71, 409-419.

115. Mahoney K. M., Goswami P. P., Winter A. H., *J. Org. Chem.* **2013**, *78*, 702–705.

116. Mal N. K., Fujiwara M., Tanaka Y., *Nature* **2003,** 421, 350.

117. Margulies D., G. Melman, C.E. Felder, R. Arad-Yellin, A. Shanzer, *J. Am. Chem. Soc.* **2004**, 126, 15400-15401.

118. Margulies D., Hamilton A. D., *J. Am. Chem. Soc.* **2009**, 131, 9142.

119. Miller K., Wang M., Gralow J., Dickler M., Cobleigh M., Perez E. A., Shenkier T., Cella D., Davidson N. E., *N. Engl. J. Med.* **2007**, *357*, 2666–2676.

120. Mitsou, E.; Xenakis, A.; Zoumpanioti, M. *Catalysts* **2017**, *7* (2), 52.

121. Molina M., Asadian-Birjand M., Balach J., Bergueiro J., Miceli E. and Calderón M., *Chem. Soc. Rev.*, **2015**, 44, 6161–6186.

122. Moniruzzaman, M.; Kamiya, N.; Nakashima, K.; Goto, M. *Green Chem.* **2008**, *10* (5), 497–500.

123. Munkhbat, O.; Garzoni, M.; Raghupathi, K. R.; Pavan, G. M., S. Thayumanavan, *Langmuir*, **2016**, 32, 2874-2881.

124. Mura S., J. Nicolas and P. Couvreur, *Nat. Mater.*, **2013**, 12, 991.

125. Nam, J.-M.; Thaxton, C. S.; Mirkin, C. A. *Science.* **2003**, *301*, 1884–1886.

126. Napoli A., Valentini M., Tirelli N., Muller M., Hubbell J. A., *Nat. Mater.* **2004**, 3, 183.

127. Nazemi A., Gillies E. R., *Chem. Commun.* **2014**, 50, 11122-11125.

128. Nazemi A., Schon T. B., Gillies E. R., *Org. Lett.* **2013**, 15, 1830-1833.

129. Newkome G. R., C. N. Moorefield, G. R. Baker, A. L. Johnson and R. K. Behera, *Angew. Chemie Int. Ed. English*, **1991**, 30, 1176–1178.

130. Nicot, C.; Waks, M. Biotechnol. Genet. *Eng. Rev.* **1996,** 13, 267-314.

131. Nikitin, M. P., Shipunova, V. O., Deyev, S. M., & Nikitin, P. I. *Nat. Nanotech,* **2014**, 9, 716-722.

132. Oldfield, C. Biotechnol. Genet. *Eng. Rev.* **1994,** 12, 255-327.

133. Ooi, K., Shiraki, K., Morishita, Y. and Nobori, T., *Journal of clinical laboratory analysis*, **2007,** 21, 133-139.

134. Orozco, J.; Cortés, A.; Cheng, G.; Sattayasamitsathit, S.; Gao, W.; Feng, X.; Shen, Y.; Wang, J. *J. Am. Chem. Soc.* **2013**, *135*, 5336–5339.

135. Parkin, G. *Chem. Rev.* **2004**, *104*, 699–768.

136. Pavlidis, I. V; Gournis, D.; Papadopoulos, G. K.; Stamatis, H. *J. Mol. Catal. B Enzym.* **2009**, *60*, 50–56.

137. Peng H. S., Stolwijk J. A., Sun L. N., Wegener J., Wolfbeis O. S., *Angew. Chem., Int. Ed.* **2010**, 122, 4342-4345.

138. Peterson G. I., Larsen M. B., Boydston A. J., *Macromolecules* **2012**, *45*, 7317–7328.

139. Prabhakar, U.; Maeda, H.; Jain, R.K.; Sevick-Muraca, E.M.; Zamboni, W.; Farokhzad, O. C.; Barry, S.T.; Gabizon, A.; Grodzinski, P.; Blakey, D.C. *Cancer Res.* **2013**, *73*, 2412-2417.

140. Quan, C.Y.; Chen, J.X.; Wang, H.Y.; Li, C.; Chang, C.; Zhang, X.Z.; Zhuo, R.X *ACS Nano*, **2010**, *4*, 4211-4219.

141. Raghupathi K. R., Azagarsamy M. A. and Thayumanavan S., *Chem. Eur. J.*, 2011, **17**, 11752–11760.

142. Raghupathi K. R., Guo J., Munkhbat O., Rangadurai P., S. Thayumanavan, *Acc. Chem. Res*. **2014**, 47, 2200-2211.

143. Raghupathi K. R., Sridhar U., Byrne K., Raghupathi K. and Thayumanavan S., *J. Am. Chem. Soc.*, **2015**, 137, 5308–5311.

144. Randolph L. M., Chien M.-P. and Gianneschi N. C., *Chem. Sci.*, **2012**, 3, 1363–1380.

145. Ravoo B. J., *Angew. Chem., Int. Ed.* **2017**, 56, 9603-9607.

146. Reshetnyak, Y. K.; Andreev, O.A.; Segala, M.; Markin, V.S.; Engelman, D.M. *Proc. Natl. Acad. Sci.* **2008**, *105*, 15340-15345.

147. Rodthongkum, N.; Ramireddy, R.; Thayumanavan, S.; Richard, W. V. *Analyst* **2012**, *137*, 1024–1030.

148. Romberg, B.; Hennink, W.E.; Storm. G. *Pharm. Res*. **2008**, *25*, 55-71.

149. Ross C. A., M.A. Poirier*, Nat. Med.* **2004**, 10, S10-S17.

150. Ryu J.-H., Chacko R. T., Jiwpanich S., Bickerton S., Babu R. P., Thayumanavan S., *J. Am. Chem. Soc.* **2010**, *3*, 2–10.

151. Ryu J.-H., Jiwpanich S., Chacko R., Bickerton S., Thayumanavan S., *J. Am. Chem. Soc.* **2010**, *132*, 8246–8247.

152. Ryu J., Chacko R.T., Jiwpanich S., Bickerton S., Babu R.P., Thayumanavan S., *J. Am. Chem. Soc.* **2010**, 132, 17227-17235.

153. Sagi A., R. Weinstain, N. Karton, D. Shabat, *J. Am. Chem. Soc.* **2008**, *130*, 5434–5435.

154. Santra, S.; Zhang, P.; Wang, K.; Tapec, R.; Tan, W. *Anal. Chem.* **2001**, *73*, 4988–4993.

155. Sato H., T. Takino, Y. Okada, J. Cao, A. Shinagawa, E. Yamamoto and M. Seiki, *Nature*, **1994**, 370, 61.

156. Savariar E. N., Aathimanikandan S. V and Thayumanavan S., *J. Am. Chem. Soc.*, **2006**, 128, 16224–16230.

157. Schmitt S., Zischka H., *Dtsch. Zeitschrift fur Onkol.* **2018**, *50*, 124–130.

158. Schoffelen, S.; van Hest, J. C. M. *Curr. Opin. Struct. Biol.* **2013**, *23* (4), 613–621.

159. Schomburg I., A. Chang, S. Placzek, C. Söhngen, M. Rother, M. Lang, C. Munaretto, S. Ulas, M. Stelzer, A. Grote, M. Scheer and D. Schomburg, *Nucleic Acids Res.*, **2013**, 41, 764–772.

160. Sharma U, Pal D, Prasad R. Alkaline phosphatase: an overview. *Indian Journal of Clinical Biochemistry*. **2014**, 29, 269-78.

161. Shi B., M. Zheng, T. Jiang, W. Yang, Y. Zou, H. Wu, X. Liu, K. McDonald, D. Ling, J. Shi, et al., *Angew. Chemie Int. Ed.* **2019**.

162. Shi J., O. C. Farokhzad. et al, *Nat. Rev. Cancer* **2017**, *17*, 20–37.

163. Shi, J.; Xiao, Z.; Kamaly, N. Farokhzad, O.C. *Acc. Chem. Res.* **2011**, *44*, 1123-1134.

164. Shipovskov, S.; Trofimova, D.; Saprykin, E.; Christenson, A.; Ruzgas, T.; Levashov, A. V; Ferapontova, E. E. *Anal. Chem.* **2005**, *77* , 7074–7079.

165. Silva, G. A. *Ann. N. Y. Acad. Sci.* **2010**, *1199*, 221–230.

166. Skog, J.; Wurdinger, T.; Van Rijn, S.; Meijer, D.; Gainche, L.; Sena-Esteves, M.; Curry Jr, W. T.; Carter, R. S.; Krichevsky, A. M.; Breakefield, X. O. *Nat. Cell Biol.* **2008**, *10*, 1470.

167. Slowing I. I., J. L. Vivero-Escoto, C.-W. Wu, V. S.-Y. Lin, *Adv. Drug Deliv. Rev.* **2008**, *60*, 1278–1288.

168. Soussan E., Cassel S., Blanzat M., Rico-Lattes I., *Angew. Chem., Int. Ed.* **2009**, 48, 274-288.

169. Suresh, A.K.; Weng, Y.; Li, Z.; Zerda, R.; Haute, D.V.; Williams, J.C.; Berlin, J.M. *J. Mater. Chem. B*, **2013**, *1*, 2341-2349.

170. Takaoka Y., T. Sakamoto, S. Tsukiji, M. Narazaki, T. Matsuda, H. Tochio, M. Shirakawa, *Nature chemistry*, **2009**, *1*, 557.

171. Tan X., Li B. B., Lu X., Jia F., Santori C., Menon P., Li H., Zhang B., Zhao J. J., Zhang K., *J. Am. Chem. Soc.* **2015**, *137*, 6112–6115.

172. Tanford C., C. 2nd ed.; *J. Wiley and Sons: New York*, **1980**.

173. Tang R., Wang M., Ray M., Jiang Y., Jiang Z., Xu Q., V. M. Rotello, *J. Am. Chem. Soc.* **2017**, *139*, 8547–8551.

174. Thiry, A., Dogne, J.M., Masereel, B. and Supuran, C.T., *Trends in pharmacological sciences*, **2006,** 27(11), 566-573.

175. Tibbitt M. W., J. E. Dahlman, R. Langer, *J. Am. Chem. Soc.* **2016**, *138*, 704–717.

176. Torchilin V. P., *J. Controlled Release* **2001**, 73, 137-172.

177. Trenor, S.R., Shultz, A.R., Love, B.J. and Long, T.E., *Chemical Reviews*, **2004**. 104, 3059-3078.

178. Ulijn R. V, *J. Mater. Chem.*, **2006**, 16, 2217–2225.

179. Valdez, D.; Le Huerou, J. Y.; Gindre, M.; Urbach, W.; Waks, M. *Biophys. J.* **2001**, 80, 2751-2760.

180. Vriezema, D. M.; Comellas Aragonès, M.; Elemans, J. A. A. W.; Cornelissen, J. J. L. M.; Rowan, A. E.; Nolte, R. J. M. *Chem. Rev.* **2005**, *105*, 1445–1490.

181. Wang, M.; Zhao, B.; Gao, J.; He, H.; Castellanos, L. J.; Thayumanavan, S.; Vachet, R. W. *Langmuir* **2017**, 33, 14004–14010.

182. Wang, M.; Gao, J.; Zhao, B.; Thayumanavan, S. Vachet, R.W. Analyst ,**2019** , 144, 6321-6326.

183. Wang F., Klaikherd A. and Thayumanavan S., *J. Am. Chem. Soc.*, **2011**, 133, 13496–13503.

184. Wang Y., K. Zhou, G. Huang, C. Hensley, X. Huang, X. Ma, T. Zhao, B. D. Sumer, R. J. DeBerardinis and J. Gao, *Nat. Mater.*, **2013**, 13, 204.

185. Wang Z., W. Guo, X. Kuang, S. Hou, H. Liu, *Asian J. Pharm. Sci.* **2017**, *12*, 498–508.

186. Wang, Y.; Lu, H.; Xu, P.-F. *Acc. Chem. Res.* **2015**, *48*, 1832–1844.

187. Weitman S. D., A. G. Weinberg, L. R. Coney, V. R. Zurawski, D. S. Jennings, B. A. Kamen, *Cancer Res.* **1992**, *52*, 6708–6711.

188. Whitcombe, M. J.; Chianella, I.; Larcombe, L.; Piletsky, S. A.; Noble, J.; Porter, R.; Horgan, A. *Chem. Soc. Rev.* **2011**, *40*, 1547–1571.

189. Xiao Y., F. Patolsky, E. Katz, J. F. Hainfeld and I. Willner, *Science (80-.).*, 2003, **299**,

1877–1881.

190. Xu X., M. S. Han and C. A. Mirkin, *Angew. Chemie*, 2007, **119**, 3538–3540.

191. Yang Z., M. Lin, C. Ren, J. Liu, L. Dai, Y. Shi, J. Gao, H. Shen, J. Zhan, Y. Cai, *J. Am. Chem. Soc.* **2017**, *139*, 2876–2879.

192. Yang, N. J.; Hinner, M. J. *Methods Mol. Biol.* **2015**, *1266*, 29–53.

193. Yao Y., Wang Y., Huang F., *Chem. Sci*., **2014**, 4312-4316.

194. Yesilyurt V., Ramireddy R., Thayumanavan S., *Angew. Chem., Int. Ed.* **2011**, 50, 3038-3042

195. You L., D. Zha and E. V Anslyn, *Chem. Rev.*, 2015, **115**, 7840–7892.

196. You M., L. Peng, N. Shao, L. Zhang, L. Qiu, C. Cui, W. Tan, *J. Am. Chem. Soc.* **2014**, *136*, 1256–1259.

197. Yu G., Jie K., Huang F*., Chem. Rev.* **2015**, 115, 7240-7303.

198. Yu G., Yu W., Mao Z., Gao C., Huang F., *Small*, **2015**, 11, 919-925.

199. Yu, G.; Jie, K.; Huang, F. *Chem. Rev.* **2015**, *115*, 7240–7303.

200. Yuan, C.; Raghupathi, K.; Popere, B. C.; Ventura, J.; Dai, L.; Thayumanavan, S. *Chem. Sci.* **2014**, 5, 229-234.

201. Yuan, F.; Salehi, H.A.; Boucher, Y.; Vasthare, U.S.; Tuma, R.F.; Jain, R.K. Cancer Res. **1994**, *54*, 4564-4568.

202. Zelzer M., Todd S. J., Hirst A. R., McDonald T. O. and Ulijn R. V, *Biomater. Sci.*, **2013**, 1, 11–39.

203. Zhang S., Liu X., Bawa-Khalfe T., Lu L.-S., Lyu Y. L., Liu L. F., Yeh E. T. H., *Nat. Med.* **2012**, *18*, 1639.

204. Zhang, H.; Piacham, T.; Drew, M.; Patek, M.; Mosbach, K.; Ye, L. *J. Am. Chem. Soc.*

2006, *128*, 4178–4179

205. Zhang, Y.; So, M. K.; Rao, J. H.; *Nano Lett.* **2006**, *6*, 1988-1992.

206. Zhang J. X.; Zalipsky S.; Mullah N.; Pechar M.; Allen T. M. *Pharmacol. Res*. **2004,** *49*, 185-198.

207. Zhao, R.; Han, X.; Li, Y.; Wang, H.; Ji, T.; Zhao, Y.; Nie, G. *ACS Nano*, **2017**, *11*, 8103-8113.

208. Zhou J., G. Yu and F. Huang, *Chem. Soc. Rev.*, 2017, **46**, 7021–7053.

209. Zhuang J., Gordon M. R., Ventura J., Li L., Thayumanavan S., *Chem. Soc. Rev.* **2013**, 42, 7421-7435.

210. Zhuang J., S. Jiwpanich, V. D. Deepak, S. Thayumanavan, *ACS Macro Lett.* **2012**, *1*, 175–179.

211. Zoumpanioti, M.; Karali, M.; Xenakis, A.; Stamatis, H. *Enzyme Microb. Technol.* **2006**, *39* (4), 531–533.